
On the Role of Fluctuations in Evolutionary Dynamics and Transport on Microtubules

Anna Tatjana Melbinger



München 2011

On the Role of Fluctuations in Evolutionary Dynamics and Transport on Microtubules

Anna Tatjana Melbinger

Dissertation
an der Fakultät für Physik
der Ludwig-Maximilians-Universität
München

vorgelegt von
Anna Tatjana Melbinger
aus München

München, den 27. Mai 2011

Erstgutachter: Prof. E. Frey

Zweitgutachter: Prof. H. Stark

Tag der mündlichen Prüfung: 11. Juli 2011

Zusammenfassung

Leben weist eine unermessliche Vielfalt und Komplexität auf. Die ihm zugrunde liegenden biologischen Prozesse sind daran angepasst die unterschiedlichsten Aufgaben akkurat zu erfüllen. Dass dies mit einer derartigen Präzision geschieht, ist umso erstaunlicher, wenn man bedenkt, dass Fluktuationen in der Natur allgegenwärtig sind. Diese intrinsische Stochastizität vieler Abläufe entsteht durch das diskrete Vorkommen der an dynamischen Prozessen beteiligten Substanzen, und durch thermische Fluktuationen. In vorliegender Arbeit soll der Einfluss von derartigen Fluktuationen an zwei spezifischen Beispielen erläutert werden. Der erste Teil widmet sich evolutionären Prozessen, während im zweiten Teil Transport entlang von intrazellulären Filamenten, sogenannten Mikrotubuli, untersucht wird.

Evolution beschäftigt sich mit der zeitlichen Entwicklung von verschiedenen Merkmalen in einer Population unter dem Einfluss von Selektion. Die dieser Dynamik zu Grunde liegenden Prozesse sind Geburt und Tod einzelner Individuen in einer Population. Damit besteht eine enge Verbindung zwischen evolutionärer Dynamik und der zeitlichen Entwicklung von Populationsgrößen, der sogenannten Populationsdynamik. Ein wichtiger Aspekt dieser Arbeit ist das Zusammenspiel dieser beiden Dynamiken. Hierzu wird ein stochastisches Modell verwendet, das die zeitliche Entwicklung sowohl der Zusammensetzung als auch der Größe einer Population berücksichtigt. Um diesen Ansatz zu validieren, wird ein spezielles, aber wesentliches Beispiel analysiert: Es handelt sich um Bakterien, bei welchen das Kooperationsdilemma auftritt. Kooperierende Bakterien produzieren ein Protein, das für die Gemeinschaft von Vorteil ist, ein sogenanntes öffentliches Gut. Durch die damit verbundenen metabolischen Kosten, haben Kooperatoren einen Nachteil gegenüber jenen Bakterien, die sich nicht an der Produktion des öffentlichen Guts beteiligen, aber von dessen Präsenz profitieren. Anhand dieses Beispiels stellt sich heraus, dass demographische Fluktuationen eine bemerkenswerte Rolle spielen. Durch sie können die Nachteile von Kooperatoren unter gewissen Umständen überwunden werden. Dadurch kann der relative Anteil von Kooperatoren in der Gesamtpopulation sogar zeitweise zunehmen. Obwohl dieser Anstieg nur transient ist, kann ein ähnlicher Mechanismus in strukturierten Populationen auch auf längeren Zeitskalen Kooperation aufrechterhalten. In Populationen, die in Gruppen eingeteilt sind, welche immer wieder neu gemischt werden, lassen sich zwei Mechanismen identifizieren, die kooperatives Verhalten bevorzugen. Der „group-growth“-Mechanismus ermöglicht Evolution von Kooperation, d.h. eine einzelne kooperierende Mutante kann sich solange ausbreiten bis es zu einer stabilen Koexistenz zwischen Kooperatoren und nicht-kooperierenden Individuen kommt. Der „group-fixation“-Mechanismus führt indes dazu, dass sich rein kooperative Populationen bilden können, wenn zuvor ein gewisser Schwellwert im Anteil der Kooperatoren überschritten wurde.

Der zweite Teil dieser Arbeit beschäftigt sich mit molekularen Motoren, welche sich entlang von intrazellulären Filamenten, sogenannten Mikrotubuli, bewegen. Diese Motoren transportieren zum einen große Makromoleküle durch die Zelle, zum anderen können sie am Ende

der Mikrotubuli als Polymerase oder Depolymerase wirken und somit deren Länge regulieren. Besonders wichtig wird diese Regulation während der Zellteilung, für die eine dynamische Längenanpassung der Mikrotubuli essentiell ist. Untersucht wurde die Interaktion von depolymerisierenden Motoren mit Mikrotubuli in einem stochastischen Modell, das insbesondere Stauphänomene berücksichtigt. Durch jüngst durchgeführte Experimente lässt sich dieses Modell qualitativ validieren, ohne dass freie Fitparameter verwendet werden. Außerdem gibt das Modell Aufschluß über die Rolle von molekularen Staus entlang der Filamente. Sie können das Depolymerisationsverhalten entscheidend verändern. Die Folge ist die Ausbildung von zwei unterschiedlichen Regimen. Im ersten hängt die Depolymerisationsgeschwindigkeit ausschließlich von der mikroskopischen Abbaurate ab, während im zweiten Regime nur die Motorendichte auf dem Mikrotubulus von Belang ist. Da diese Motorendichte abhängig von der Länge des Filaments ist, ändert sich auch die Depolymerisationsgeschwindigkeit mit eben dieser Länge. In Kombination mit Polymerisation, die zum Wachsen der Mikrotubuli führt, kann diese längenabhängige Depolymerisation zu einer wohldefinierten Länge des Mikrotubulus führen, die sich von selbst adjustiert. Unter Berücksichtigung zweier unterschiedlicher Polymerisationsszenarien, wurden insbesondere jene Regime untersucht, in denen sich diese stabile Länge einstellt. Im *exklusiven Szenario* findet Polymerisation nur statt, wenn sich kein depolymerisierender Motor am Ende des Filaments befindet, wohingegen Abbauvorgänge unabhängig von dieser Besetzung im *nicht-exklusiven Szenario* möglich sind. Die dabei herausgearbeiteten Unterschiede sollen in zukünftigen Experimenten dazu beitragen, das tatsächliche Polymerisationsverhalten aufzuklären.

Die vorliegende Arbeit gliedert sich in zwei Teile. Nach einer kurzen Einleitung (Kapitel 1) werden in Teil I die Grundlagen von evolutionärer Dynamik erklärt (Kapitel 2). In Kapitel 3 liegt der Fokus auf dem Kooperationsdilemma in Population, die in Subpopulationen eingeteilt sind. In Teil II werden die Interaktionen von molekularen Motoren mit Mikrotubuli analysiert. Dabei beschäftigt sich Kapitel 4 mit deren Transporteigenschaften, während sich Kapitel 5 hauptsächlich der Längenregulation durch polymerisierende und depolymerisierende Motoren widmet.

Abstract

Life shows an astonishing diversity and complexity. Its underlying biological processes are adapted to fulfill various specific tasks with remarkable accuracy. The enormous precision, with which life operates, is even more impressive considering the ubiquitous fluctuations in nature. Fluctuations in diverse biological quantities arise due to intrinsic randomness of biological processes caused by the discrete nature of the involved substances and thermal influences. In this thesis, the impact of such fluctuations is discussed for two specific examples. The first part is concerned with evolutionary dynamics, while the second part focusses on transport on intracellular filaments.

The driving force of evolution is selection. It favors fitter individuals and thereby changes the composition of a population. The origins of such evolutionary dynamics are varying birth and death events of single individuals. Hence, evolutionary dynamics of a population is closely related to population dynamics describing the time evolution of the population size. The interplay of these two types of dynamics is an important aspect of this thesis. As such, we propose a full stochastic model considering the evolution of both a population's composition and its size. To validate our approach, an important example is analyzed, namely the dilemma of cooperation in bacterial populations. Cooperating bacteria produce a certain protein which is beneficial for the population as a whole. As the production of this public good is metabolically costly, cooperators have an evolutionary disadvantage compared to non-contributing free-riders. This example illustrates the crucial role of demographic fluctuations, the importance of which increases with decreasing population size. In particular, during population bottlenecks these fluctuations may be strong enough to overcome the selection disadvantage of cooperators. For this reason, we find that the level of cooperation increases transiently. To explain cooperative behavior also in the long run, we further study the repetitive fragmentation of a population into small subcolonies. In such a model, two distinct mechanisms favor cooperative behavior. The group-growth mechanism facilitates the evolution of cooperation from a single mutant to coexistence between cooperators and free-riders. In contrast, the group-fixation mechanism can lead to a purely cooperative population under the condition that a certain threshold level of cooperation is already present.

The second part of this thesis is concerned with molecular motor proteins walking along microtubule filaments which are constituents of the cytoskeleton. These motors transport large macromolecules through the crowded cytosol. Furthermore, they can act as polymerases or depolymerases at the microtubule tip and thereby regulate its length. This length-regulation is especially important for cell division as a dynamic length adaptation of the filaments is essential there. We investigate the interaction between depolymerizing motors and microtubules in a stochastic model accounting for crowding phenomena. Importantly, our model can be validated by comparison with recent experiments without employing any fit parameters. Our model provides insight into the role of molecular jams along the track. These jams result in

two regimes of qualitatively different behavior. In the first regime, the depolymerization speed depends solely on the microscopic depolymerization rate, while in the second regime the density of molecular motors on the filament regulates the speed. As the motor density depends on the length of the microtubules, the depolymerization speed also varies with length. In combination with polymerization a certain length can be adjusted. We investigate the regimes where such a well-defined length can be achieved by analyzing two distinct polymerization scenarios. In the exclusive scenario, the microtubule only polymerizes if the tip is unoccupied by a depolymerizing motor. In the non-exclusive scenario, by contrast, polymerization always happens at a certain rate. Our analysis reveals differences between these scenarios which may help to clarify the actual depolymerization behavior in future experiments.

The outline of this thesis is as follows. In Chapter 1, a short introduction focussing on the role of fluctuations is provided. Part I is concerned with evolutionary dynamics. In Chapter 2 the basic mathematical concepts are introduced while in Chapter 3 the dilemma of cooperation for individuals divided into subcolonies is investigated. Part II focusses on transport along microtubules. Chapter 4 mainly deals with the transport properties of molecular motors. Finally, in Chapter 5 length-regulation due to polymerization and depolymerization is discussed.

Contents

1	Fluctuations in Biological Systems	1
I	Evolutionary Dynamics	7
2	Ecology and Evolution	9
2.1	Ecology	9
2.2	Evolution	11
2.3	Mathematical Formulation of Evolutionary Dynamics	14
2.3.1	Price Equation	14
2.3.2	Replicator Equation	15
2.3.3	Evolutionary Game Theory	16
2.3.4	The Role of Fluctuations	18
2.4	The Mutual Interaction of Evolutionary and Population Dynamics	19
2.5	Manuscripts and Papers	21
2.5.1	Evolutionary Game Theory in Growing Populations	21
2.5.2	Evolutionary and Populations Dynamics - A Coupled Approach	22
2.5.3	Conclusion and Outlook	22
	A. Melbinger, J. Cremer, E. Frey, Evolutionary game theory in growing populations, Phys. Rev. Lett. 105 , 178101 (2010)	24
	J. Cremer, A. Melbinger, E. Frey, Evolutionary dynamics and population size: A coupled approach, Phys. Rev. E 84 , 051921 (2011)	34
3	The Dilemma of Cooperation in Structured Populations	45
3.1	The Dilemma of Cooperation	45
3.1.1	Social Bacteria	46
3.1.2	Dicrocoelium Dentrificum - the Small Liver Fluke	47
3.2	Possible Solutions Solving the Dilemma	50
3.2.1	Multilevel Selection	50
3.2.2	Hamilton's Rule	51
3.2.3	Group and Kin Selection	53
3.3	On the Role of Dynamics and Fluctuations	55
3.4	Papers and Manuscripts	56
3.4.1	Growth dynamics and the evolution of cooperation in microbial populations	56
3.4.2	Conclusion and Outlook	56
	J. Cremer, A. Melbinger, E. Frey, Growth dynamics and the evolution of cooperation in bacterial populations, Scientific Reports 2 , 281 (2012)	58

II	Molecular Motors and their Interaction with Microtubules	75
4	Transport on Microtubules	77
4.1	Cytoskeleton	77
4.2	Molecular Motors	80
4.3	Driven Exclusion Processes	81
4.3.1	Totally Asymmetric Simple Exclusion Process	81
4.3.2	TASEP/LK	83
4.3.3	Extensions of these Models	85
4.4	Papers and Manuscripts	85
4.4.1	Two Lanes with Particle Exclusion and Obstruction	85
4.4.2	Conclusion and Outlook	86
A.	Melbinger, T. Reichenbach, T. Franosch, E. Frey, Driven Transport on Parallel Lanes with Particle Exclusion and Obstruction, <i>Phys. Rev. E</i> 83 , 031923 (2011)	87
5	Length-Dependent Regulation	97
5.1	Experimental Findings	97
5.2	Depolymerization	99
5.3	Depolymerization and Polymerization	101
5.3.1	The Exclusive Scenario	102
5.3.2	The Non-Exclusive Scenario	107
5.3.3	Length-Regulation	111
5.3.4	Comparison of the Exclusive and Non-Exclusive Scenario	113
5.3.5	Discussion	115
5.4	Papers and Manuscripts	117
5.4.1	Crowding of Molecular Motors Determines Microtubule Depolymerization	117
5.4.2	Conclusion and Outlook	117
L.	Reese, A. Melbinger, E. Frey, Crowding of Molecular Motors determines Microtubule Depolymerization, <i>Biophys. J.</i> 101 , 9, 2190 (2011)	118

1 Fluctuations in Biological Systems

Life's complexity and beauty raises many biological issues. Much progress was done in identifying the functional building blocks of living organisms. Higher, multicellular life forms are composed of cells highly adapted to specific tasks as they build the nervous system, skin or other organs. The cells in turn are structured and consist of a membrane which is stabilized by its scaffolding, the cytoskeleton, and includes functional entities, the organelles [1]. The information for this astonishingly complex construction plan is stored in DNA or RNA [2] which encode for proteins [3] regulating the dynamic sequences accommodating life. These dynamic sequences operate with a remarkable precision. This foreshadows an important aspect which is considered in this thesis, namely the role of fluctuations. Fluctuations are ubiquitous in nature and thereby influence biological processes in various ways. Fluctuations arise from intrinsic randomness in biological processes due to thermal fluctuations, as well as the discreteness of relevant factors, such as chemical substances. Hence, they are inextricably linked to biological functionality. In general, fluctuations result in distributions around the mean which may alter the outcome of biological processes in two ways. First, they may result in deviations from the optimum or cause rare events which are not tolerated by a living organisms. Second, fluctuations are not necessarily detrimental, but however, may result in functional noise [4]. For example fluctuations can switch between the states of a bistable system [5] and thereby lead to beneficial heterogeneity. All in all, the role of fluctuations in biological processes varies and has to be understood in more detail to clarify the mechanisms underlying biological functionality.

One important example highlighting the accuracy at which dynamic behavior in nature is achieved is cell division. A complex sequence of dynamic steps has to be performed to divide a mother cell into two daughter cells. In eukaryotic cells, the nucleus (mitosis or meiosis) as well as the whole cell must divide [1]. This division consists of several consecutive steps: During interphase the genetic material is doubled. In the ensuing phases, prophase, metaphase and anaphase, chromosomes are condensed and distributed to both cell poles. This separation is achieved by the mitotic spindle, which consists of thin filaments, namely microtubules [6]. These microtubules attach to the chromosomes and pull them apart such that a copy of each chromosome is located at both poles. In the last stage of mitoses, the telophase, chromosomes decondense and the nucleus wall reforms. The division of the cell itself mainly occurs during the late stages of nucleus division. Each of these steps is highly dynamic and requires complex regulatory machinery [7]. Most dynamic processes in living organisms involve gene regulation [8]. In its simplest form, the transcription of DNA to RNA is influenced (transcriptional regulation). This can, for example, be achieved by binding of different proteins to sites on the DNA close to the operon where transcription starts. These proteins may have either an inhibiting or a catalyzing effect and thereby hamper or stimulate the transcription of the respective gene sequence. Gene regulation may also be accomplished by influencing the ensuing translation (translational regulation), where the RNA sequence is

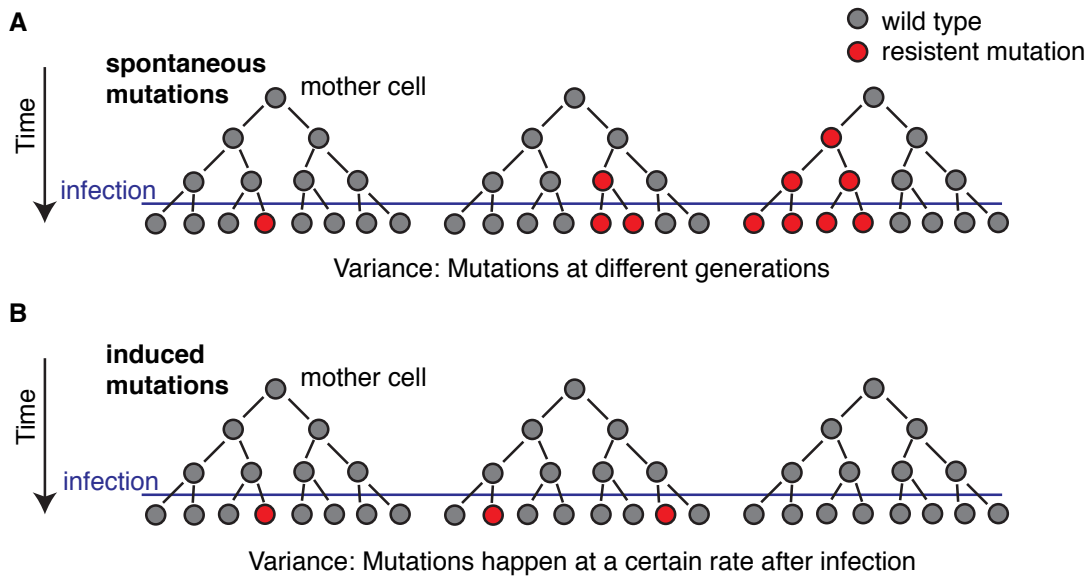


Figure 1.1: Illustration of the basic idea behind the Luria-Delbrück experiment. **A** Spontaneous mutations may arise any time. They can then be enhanced through exponential growth of the bacterial population. After infection, non-resistant wild types die. Therefore the variance of the number of surviving bacteria is much higher than in the induced mutation scenario (**B**). There, mutations arise as a consequence of the infection and the variance is created solely by the intrinsic randomness of mutations.

read out and transferred into a chain of amino acids, forming a protein. Importantly, the proteins produced in this process may, in turn, regulate genes and create feedback loops. In total, this leads to a complex gene regulatory network. These networks are constantly subject to fluctuations [9, 10, 11]. In fact the concentrations of the regulating enzymes and proteins are not stable, but variable due to the discreteness of the relevant substances and temperature. From this point of view, the precise functionality of gene regulation is even more remarkable.

One of the most important experiments in modern biology also highlighting the role of fluctuations was the Luria-Delbrück experiment [12]. Designed by the microbiologist Salvador Edward Luria with theory from the physicist Max Delbrück, it was also one of the first collaborations between physics and biology in modern science. The question which was addressed relates to bacteria subject to stress from a viral infection. After the infection most of the bacteria die. But due to a few mutations, leading to resistant individuals, the population can recover afterwards. The issue is whether these mutations occur as a consequence of the exposure to the virus or whether they occur regularly but only gain functionality by ensuring the survival when the virus is added. This question can also be associated with a more general context, namely to decide whether Lamarck's or Darwin's theories on the evolution of species hold. In Lamarckian theory [13], individuals acquire some needed characteristics, *e.g.* the resistance against the virus when exposed to it, during life time and pass them to their offspring. In contrast, variation is always present in Darwinian theory [14], but selection only favors it if the new characteristics leads to a fitness advantage. For the bacteria

investigated in the Luria-Delbrück experiment, mutations causing resistance are of minor importance until infection; after this point they become immensely beneficial. It was Salvador Luria who realized that fluctuations are the key to decide which of these theories is true. When he watched a colleague gambling, he noticed that fluctuations can have an enormous impact, *i.e.* winning the jackpot. According to this idea he designed an experiment, also called fluctuation test, which is depicted in Fig. 1.1. Observing a set of bacterial cultures (an ensemble), the variance in the outcome differs depending on whether mutations are induced or spontaneous. In the latter scenario, mutations can spread exponentially in the population depending on how long before the infection they emerged. Therefore, subpopulations where mutations happened early contain more resistant individuals than other ones. After infection, non-resistant bacteria die and the number of surviving individuals is given by the number of resistant ones. Thus, the variance in the population size is comparably large. In contrast with induced mutations, resistance arises in response to the viral infection. Therefore, mutations emerge more or less simultaneously after infection corresponding to a Poisson process. Hence, the variance in the number of individuals is smaller than in the scenario discussed above. As the Luria-Delbrück and many following experiments [15] confirmed, mutations arise spontaneously in many examples. Modern research further investigated the emergence of these mutations. It was shown that bacteria are able to increase their mutation rate in response to stress but no evidence for directional mutations were found [16]. Recent studies also confirmed the existence of epigenetics [17], *i.e.* individuals achieve adaptations during the life span by changing genetic regulation which can be passed over a few generations at least. The achievements of Luria and Delbrück was honored in 1969 with the nobel price in physiology or medicine.

The Luria-Delbrück experiment is also a paradigm for the progress possible through the mutual enrichment of biology and physics. Since pioneers like Max Delbrück and Erwin Schrödinger [18, 19], physicists have become more and more interested in the question at how life operates and have formed a large community within physics. Biology, which has made enormous achievements in understanding the building blocks and processes facilitating life, is more and more turning to quantitative measurements in modern research. Physics, which has always been a quantitative science, can accelerate this progress which is one of the keys for a mechanistic understanding of the underlying processes. In this context theoretical modeling is also important as it affords the reduction of a complex system to its most important components, the influence of which can then be investigated. Combining experimental results with such models may lead to a deeper understanding of biological phenomena. Furthermore, concerning the topic of this thesis, fluctuations, physicists have gained much experience in this field. In analogy to fluctuations arising from non-zero temperatures in many-body systems, finite size fluctuations can be also handled. Combined with the know-how of biology this may result in a broader knowledge concerning the role of fluctuations and how they promote and jeopardize biological functionality.

The focus of this thesis lies in two particular examples highlighting the importance of fluctuations in two different fields of biology, evolutionary dynamics and transport along microtubules. A short overview on the role of fluctuations in these fields is provided in the following.

Evolutionary Dynamics

One central question in the field of evolution is how the abundance of a certain trait evolves over time. Darwin's famous idea [14], based on reproduction, variation and heredity, was the key to understand this: Individuals reproduce and mutations or recombinations lead to variation in their phenotype. Different phenotypes have different success rates in reproduction and survival, measured by their fitness. Selection, the driving force of evolution, favors fitter individuals which then outcompete less adapted ones [20, 21]. Demographic fluctuations, whose strength scales with the population size [22, 23], arise due to discrete birth and death events of the individuals. Therefore, by chance, traits corresponding to a comparably small fitness can also be augmented. As the size of populations is highly dynamic, the role of fluctuations is even more pronounced as already indicated by the Luria-Delbrück experiment. In the field of evolution another question also arises. While in many examples from cell biology mainly robustness against fluctuations is important, here fluctuations can also be functional. For example, a variable phenotype caused by noise can be advantageous if environmental conditions change repeatedly [4, 24, 25].

Intracellular Transport

As mentioned above a cell is not a disordered accumulation of molecular building blocks but a highly functional and organized entity. As transport through the crowded cytosol would often be too slow, active transport mechanisms must be employed. For example, molecular motors 'walking' along intracellular filaments are used to accelerate the transport of metabolically important substances [26]. As this transport is a non-equilibrium stochastic process fluctuations are especially important. In addition, molecular motors not only transport cargos, they also play a crucial role in cell division [27, 28, 29, 30]. The mitotic spindle, which distributes chromosomes to the cell poles, consists of microtubules whose length has to be regulated. By growth and shrinkage, these filaments search for chromosomes in the cytosol and bind to them [6]. Afterwards, the microtubules shrink and thereby pull the chromosomes apart. Recent experiments support the crucial role of molecular motors serving as polymerases and depolymerases for length-regulation [31, 32, 33, 34]. But the exact mechanisms are not fully resolved. Again, the robustness against fluctuations is of major interest, as a failure in the length-regulation of microtubules would lead to the lethal inability to divide.

Outline

Part I of this thesis is concerned with evolutionary processes. In Chapter 2, we introduce the basic ideas of evolutionary and population dynamics which are two closely related fields in biology. We combine both views in a mathematical model which highlights the role of fluctuations as they can change the evolutionary outcome drastically. In Chapter 3, we focus on evolutionary dynamics in structured populations. We explain and study the dilemma of cooperation as an example, a problem which is ubiquitous in nature. Hence, we introduce a model describing the interaction of cooperating and free-riding individuals in group-structured populations. Part II of this thesis deals with the interaction of molecular motors and microtubules. In Chapter 4, we give an overview on the cytoskeleton including microtubules and

motor proteins. Furthermore, we discuss driven exclusive transport as a model system for molecular motors moving on cellular filaments. In Chapter 5, we focus on length-regulation of microtubules, an essential mechanism for cell division. Finally, we discuss the influence of depolymerizing motors on the microtubule in combination with its polymerization.

Part I

Evolutionary Dynamics

2 Ecology and Evolution

Ecology and evolution are two intertwined fields in biology. A major aspect of ecology is population dynamics which describes the time evolution of the number of individuals living in a population. Evolutionary theory in its simplest form focusses on the change in the composition of populations under the pressure of selection. Since both dynamics are based on birth and death events, their coupling seems to be natural. One of the main issues of this thesis is to investigate the interdependence of these two fields. Therefore, we introduce the key concepts of both, population and evolutionary dynamics, in the following. In particular, we focus on different scenarios of population growth. Further, we review mathematical models describing evolutionary dynamics: the Price equation, the replicator equation, evolutionary game theory, and approaches accounting for demographic fluctuations. Finally, we introduce a stochastic model which takes the coupling of evolutionary and populations dynamics into account.

2.1 Ecology

Ecology (greek: *oikos*, house, and *logos*, study) is concerned with the question how individuals interact among each other and with their environment [35]. Populations do not evolve independently of their surrounding, as their dynamics depends on various internal and external factors. For example, nutrient supply plays an essential role. Depletion and replenishment of nutrients and the number of individuals with which those have to be shared are crucial for population dynamics. Thereby, this *scramble competition* engenders density-dependent dynamics [36]. Moreover, there exist food-webs interrelating various different species living in the same ecosystem in a complex way [37]. Its simplest form, a food-web consisting of just two species: prey and predator, is discussed in the following [38, 39]. But different species cannot only interact detrimentally, *e.g.* by preying or competing for nutrients. There also exist purely beneficial relationships as mutualism or symbiosis [40]. Furthermore, also external factors, which do not depend on the species living in a population, strongly influence population dynamics. Examples are seasons subsequently changing the ecological conditions or environmental catastrophes causing population bottlenecks. How all these factors collectively govern the state of a population, is the main question tackled in ecology.

A major theme in ecology is population dynamics where the time evolution of the number of individuals in a population is considered [41, 42]. One of the first theoretical approaches in this field was proposed by Malthus in 1798 [43]. Neglecting other possible influences, he assumed that individuals reproduce at a constant rate r_1 while they die at a rate r_2 . Thereby, Malthus arrived at the well-known formula of exponential growth,

$$N(t) = N_0 e^{rt}. \tag{2.1}$$

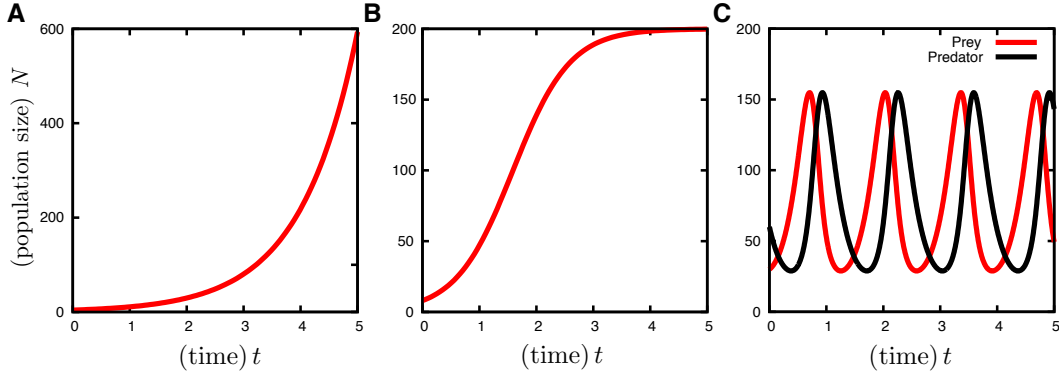


Figure 2.1: Three typical examples for population dynamics. **A** Malthusian or exponential growth of an unbounded population. **B** Logistic growth (Verhulst): Initially a population grows exponentially while due to limited resources it later saturates at a fixed value, the carrying capacity, K . **C** Predator-prey dynamics (Lotka-Volterra): The number of prey and the number of predators oscillate showing a relative phase shift.

Here, $N(t)$ denotes the number of individuals at a certain time, t , and $r := r_1 - r_2$ is the net growth rate. For an illustration, see Fig. 2.1A. If individuals live in a nutrient rich environment and therefore do not compete for resources, population growth can be successfully described by this equation.

In contrast, if resources are limited, nutrients have to be shared and reproduction and viability depend on the number of individuals in a population. This effect can be modeled by making the birth rates or death rates decreasing or increasing functions of total population size respectively. The first scenario might be more suitable for bacterial populations which go into a dormant state, *i.e.* they stop reproduction if nutrients are rare, while the second one holds for organisms dying due to starvation. Without taking fluctuations into account, both scenarios are mathematically equivalent. The ensuing population dynamics is given by the well-known equation of logistic growth which was proposed by Verhulst in 1838 [44],

$$\dot{N} = r(1 - N/K)N, \quad (2.2)$$

where the carrying capacity, K , corresponds to the maximal number of individuals which may live in a population. For small initial population sizes $N(0) \ll K$ the solution of Eq. (2.2) first grows exponentially and later saturates at K , cf. Fig. 2.1B.

In general, growth dynamics can be described mathematically by differential equations of the form $\dot{N}(t) = \mathcal{F}(N(t), \mathbf{v}, t)$. Here, $\mathcal{F}(N(t), \mathbf{v}, t)$ incorporates factors as birth, death, and migration and depends on the size of a population $N(t)$, a set of external factors \mathbf{v} and time t [42]. As the dynamics can have different time scales, varying results depending on the temporal observation window may be found [45]. Further generalizations include for example age-dependent reproduction rates or delayed interactions [46].

Important biological examples, where population dynamics is especially pronounced, are bacterial cultures. In Fig. 2.2 the typical growth behavior of such a bacterial colony is depicted [47]. After inoculating some bacteria into a growth medium, bacteria only increase in

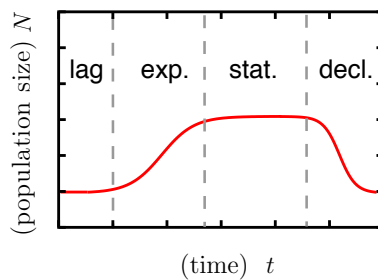


Figure 2.2: Illustration of typical growth phases of bacterial populations. A detailed description of the phases can be found in the main text.

cell size but do not divide. In this *lag phase* the number of individuals remains relatively constant over time. Then, bacteria start to divide and grow exponentially (*exponential phase*¹). In the ensuing *stationary phase* the number of bacteria saturates at the carrying capacity of the medium. In this regime birth and death balance each other, either because bacteria go into a metabolically dormant state or die more frequently (lysis) [48]. As mentioned before, the latter two phases can be well described mathematically by logistic growth or its extension, the generalized logistic function [49]. Finally, without adding additional nutrients to the cell culture, the population shrinks as bacteria die due to starvation (*phase of decline*).

In the example of bacterial growth as well as in the more general equations discussed above only one species was considered. But in ecology also the interplay of several interacting types of individuals is studied. To exemplify this aspect, let us briefly review the predator prey model. It consists of only two species: a predator $P(t)$, subsisting on its prey, $R(t)$. Such an interdependence can be described by the well-known Lotka-Volterra equations,

$$\begin{aligned}\dot{R}(t) &= R(t)(a - bR(t)), \\ \dot{P}(t) &= P(t)(cR(t) - d).\end{aligned}\tag{2.3}$$

Here, the death rate of prey is increased by the presence of predators. As the predator feeds on prey to gain energy for reproduction, its birth rate depends on the number of prey in a population. The actual strength of these interactions is set by the parameters $a, b, c, d > 0$. For specific sets of parameters the resultant dynamics is oscillatory with the populations of each species showing a relative phase shift, see Fig. 2.1C. The phase shift arises due to the positive and negative coupling, respectively. This example of a food-web highlights that often the abundance of a species cannot be described reasonably without considering other interacting species.

2.2 Evolution

The tree of life as shown in Fig. 2.3 visualizes the enormous variety and specification of living species. Adapted to various different environmental conditions, a plethora of unique

¹In biological literature, this phase is also called *log phase* as the growth curve is a straight line in a semi-logarithmic plot.

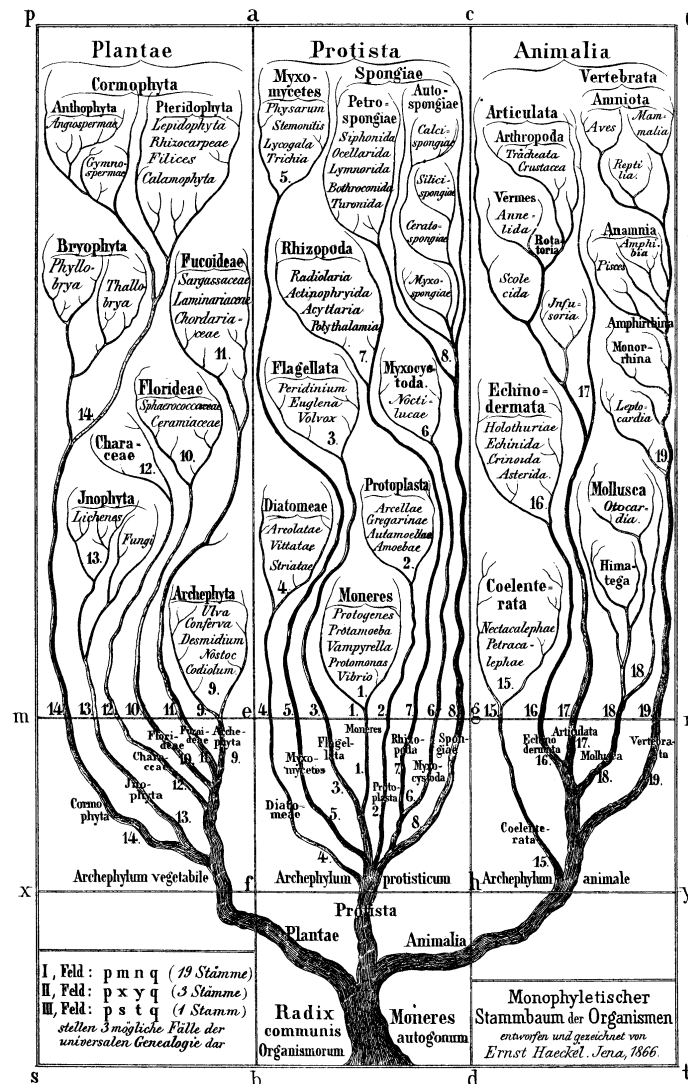


Figure 2.3: A simplified version of the tree of life. Adapted from [63]

species has evolved. From bacteria which can survive in almost every environment, via species with remarkably varied life cycles, through to such sophisticated organisms as mammals, biodiversity is truly remarkable. The question evolutionary biologists struggle with is why and how life could yield such sophisticated organisms. This issue has many different aspects, starting from the origin of life [50, 51, 52, 53, 54] to the evolution of multicellularity [55, 56, 57].

Since its foundation by Darwin and Wallace [58, 59] evolutionary theory has become one of the most important fields in modern biology. The main idea behind this theory is a combination of reproduction, variation, and selection [58, 59, 14, 60, 61, 62]: Individuals reproduce and mutations or recombination cause variations in their characteristics. If these variations are beneficial and thereby provoke a higher fitness, selection, the driving force of evolution, favors them. Actually, the fitness of an individual is a measure for its adaptedness to the circumstances it is living in.

Proposed in 1859, Darwin's theory of evolution did not include knowledge about modern genetics. Namely, the DNA, as the storage of the genetic code, and the mechanisms of heredity were not discovered yet. Only in 1865, Mendel shed light in this field by discovering the famous Mendelian rules which describe how traits are passed in a predictable way [64]. Much progress was made in the 20th century, starting from the discovery of the genetic code to its decryption [2]. Another crucial point for further development in this field was the genotype to phenotype mapping. While the genotype is defined by the genetic code, the phenotype is basically the sum of observable properties of an individual. Thereby, individuals with a distinct genotype, can possess exactly the same phenotype and vice versa. Importantly, selection acts on the phenotype level, while hard-wired variation is generated by mutation and recombination of the genotype. Nowadays, population genetics and the modern synthesis Neo-Darwinism [20, 65] have filled the gap between the originally proposed theory of Darwin and the progress in the field of heredity. Thereby they became powerful tools to study genetic variance in the genotype under the influence of selection acting on the phenotype.

Before elaborating on the theoretical aspects of evolutionary dynamics in more detail, let us discuss briefly the concept of fitness. Depending on a multitude of factors, the origin of fitness is not fully resolved [66, 67]. As mentioned above, fitness is a measure for the successfulness of an individual of a certain type interacting with other species and its environment. To get a deeper understanding, this fitness must not be taken as an abstract quantity but the underlying mechanisms have to be considered. The fitness of an individual basically relies on its reproduction and survival chances which in turn can depend on various factors. For example the environment plays a crucial role: Nutrients, climate and the presence of deleterious substances depend on the habitat an organism is living in. This idea is incorporated in the niche theory [68]. Therein a niche is defined by a typical set of environmental conditions. As these conditions and thus the ensuing fitness terms may vary dramatically in different niches, this theory is a possible explanation for the observed biodiversity. Especially life under very extreme conditions, *e.g.* if light or oxygen is rare [69], can be linked to such theories. Depending on various factors, which can change over time, fitness may also vary temporally. In this context, the concept of static fitness landscapes can be replaced by fitness seascares [70, 71] accounting for dynamic changes in the fitness. Further, the reproduction success or survival chances of species may depend on the presence of other species in the habitat. One famous example, already discussed in the context of ecology, are food-webs [38, 39] or symbiotic relationships [40]. To incorporate this, fitness can be generalized through fitness terms depending on the frequencies² of all other traits in a populations. This so-called frequency-dependent fitness is the key concept of evolutionary game theory [72] which we summarize in Sec. 2.3.3. A related idea, which originated from the question why social behavior pays off, is inclusive fitness theory [73]. At first glance, a high fitness can only be caused by large reproduction rates or a high viability, which are directly compared to the corresponding rates of competing individuals. Besides these direct fitness terms, inclusive fitness also accounts for indirect factors which favor an individual under the force of selection. For example, benefits arising in social populations can be taken into account with such indirect fitness terms which build the inclusive fitness in combination with the direct terms. A more detailed description of the advantages and disadvantages associated with cooperative behavior can be found in Chapter 3. Sometimes the fitness also depends on, at the first sight, non-reasonable factors and therefore selection favors disadvantageous traits, *e.g.* a peacock has an enormous tail resulting in its

²In evolutionary dynamics the term frequency corresponds to the fraction of a certain trait in the population.

inability to fly. This question already puzzled Darwin, who proposed the theory of sexual selection [74] to resolve this question. Therein, fitness depends on the reproduction success which in turn is given by the mating success for species which reproduce sexually. Some traits, like a long tail of peacocks, are selected because the mating partners choose accordingly to these traits. The questions why some disadvantageous traits, as the tail of a peacock or the dark mane of a lion³, have evolved can be summarized under the name Lek paradox [75].

2.3 Mathematical Formulation of Evolutionary Dynamics

In the following a short overview on the basic mathematical concepts describing evolution under the pressure of selection is provided. We here focus on works which are important in the context of this thesis and skip theories which do not support the understanding of our papers. Some important examples of the latter are coalescence theory [76] and the Eigen model [77, 78]. First, the Price equation, which is more or less a mathematical identity, is explained. Then, the replicator equation, which compares fitness differences to determine the evolutionary outcome, is considered. Between both exists a mapping, which is also discussed in the following. Finally, we focus on the role of demographic fluctuations in evolutionary processes.

2.3.1 Price Equation

In 1970, Price proposed his famous equation to describe evolution including mutation and selection [79, 21, 80, 81]. To this day, the Price equation plays an important role, especially in the context of kin selection, see Sec. 3.2.3. Therefore, we provide a short derivation following Ref. [82]. Let us consider a population containing N individuals at time t . The individuals are labeled by an index $i \in \{1, 2, \dots, N\}$. In the population a certain trait is observed, for example the body height or the weight, and each individual has assigned a certain value of this trait z_i . Initially, each individual has the abundance $h_i = 1/N$ in the population⁴. The average value of the trait is therefore given by $\langle z_i \rangle := \sum_i h_i z_i = 1/N \sum_i z_i$ ⁵. We are now interested in how this average value of the trait changes in a time interval Δt ,

$$\langle \Delta z_i \rangle = \langle z'_i \rangle - \langle z_i \rangle, \quad (2.4)$$

where $\langle z'_i \rangle$ is the average trait value at time $t' = t + \Delta t$. Again this average value can be calculated by $\langle z'_i \rangle = \sum_i h'_i z'_i$, but both the values of the trait, z'_i , as well as the abundances, h'_i , might have changed during the time interval. The new trait can be rewritten as $z'_i = z_i + \Delta z_i$. The new abundance follows from the underlying dynamics whose influence is summarized into a growth factor w_i of an individual i . For instance, this growth factor is given by 2 for an individual which reproduces once during the time interval, while it is zero for an individual which dies. The new abundance of an individual i can then be derived by dividing its growth

³In a lion's typical hot environment, such a dark mane is clearly disadvantageous.

⁴The index i can also be chosen to label the traits instead of the individuals. In this equivalent notation the abundance h_i corresponds to the probability to find the trait z_i in the population.

⁵We choose the notation $\langle z_i \rangle$ instead of $\langle z \rangle_i$. As it will turn out in the following chapter, this notation has some advantages when deriving Hamilton's rule, see Sec. 3.2.2.

factor, w_i , which corresponds to the number of individuals of type i at time $t + \Delta t$, by the new population size, N' . The new population size can be calculated by multiplying N with the average growth factor in the population, $\langle w_i \rangle = \sum_i w_i / N$. Taken together, the abundance at time $t + \Delta t$ is given by $h'_i = \frac{w_i}{N'} = \frac{w_i}{\langle w_i \rangle N} = \frac{w_i}{\langle w_i \rangle} h_i$. To derive the famous Price equation, we now have to combine all considerations above. Plugging them in Eq. (2.4) leads to,

$$\begin{aligned} \langle \Delta z_i \rangle \langle w_i \rangle &= \langle z_i w_i \rangle - \langle z_i \rangle \langle w_i \rangle + \langle \Delta z_i w_i \rangle \\ &= \text{Cov}[z_i w_i] + \langle \Delta z_i w_i \rangle. \end{aligned} \quad (2.5)$$

The Price equation can be interpreted intuitively: Traits which are positively correlated to the growth factors increase, while other ones decline.

2.3.2 Replicator Equation

Another standard description for different competing species is the replicator equation [72, 83, 84]. While the Price equation describes the mean value of a certain trait, the replicator equation focusses on the fraction of individuals with the same trait or the abundance of a certain species. The state of a population with d different traits (species) can be described by the fraction of the population with the same trait, $x_k \in \{x_1, x_2, \dots, x_d\}$. The traits differ in their fitness which are given by $f_k \in \{f_1, f_2, \dots, f_d\}$. The replicator equation then reads,

$$\dot{x}_k = (f_k - \bar{f})x_k \quad \text{or} \quad \dot{x}_k = \frac{f_k - \bar{f}}{\bar{f}}x_k \quad \text{in its adjusted form.} \quad (2.6)$$

On the right-hand side of the equation the fitness of a certain trait, f_k , is compared with the average fitness in the population, $\bar{f} = \sum_k x_k f_k$. Depending on whether the fitness of this trait, f_k , is smaller or larger than the average fitness, x_k decreases or increases, respectively. The division by \bar{f} in the adjusted form corresponds to a rescaling of time and does not alter the evolutionary outcome. The replicator equation captures the essence of selection without considering mutations. This can be resolved by employing the replicator-mutator equation which has an additional term on the right hand side incorporating mutations from species k to species l at rate $\mu_{k \rightarrow l}$. In a simple two species scenario it reads,

$$\dot{x}_k = (f_k - \bar{f})x_k - x_k \mu_{k \rightarrow l} + x_l \mu_{l \rightarrow k}. \quad (2.7)$$

Between the Price equation discussed above and the replicator equation there exists a mapping which is briefly sketched in the following. As mentioned above, in the replicator equation the fractions of certain traits, x_k , instead of the values of the traits, z_i , themselves are considered. To achieve a mapping, the more general quantity, z_i , has to be chosen appropriately: The trait z_i now marks the belonging of an individual, i , to a certain species, k . Each species, k , can be distinguished by its typical value of the trait z_k . We therefore define new traits whose values are $\tilde{z}_i^{(k)} = 1$ if the individual i is of type k and $\tilde{z}_i^{(k)} = 0$ if it belongs to any other species. This can be summarized to $\tilde{z}_i^{(k)} = \delta_{z_i, z_k}$. The fraction of species k is then given by $x_k = \langle \tilde{z}_i^{(k)} \rangle = \sum_i h_i \delta_{z_i, z_k}$. The growth factor, w_i , in the Price equation corresponds to the fitness of an individual and therefore solely depends on the species the considered individual belongs to. Therefore, it is given by $w_i = \sum_l \delta_{z_i, z_l} f_l$. For example an individual, i , belonging

to species k has the growth factor $w_i = f_k$. The average growth factors is then given by the average fitness in the population, $\langle w_i \rangle = \bar{f}$. As mutations are not included, $\tilde{z}_i^{(k)}$ does not change and $\Delta \tilde{z}_i^{(k)} = 0$ holds. Taken together, this yields the following modification of the Price equation (2.5),

$$\Delta x_k \bar{f} = \sum_i h_i \tilde{z}_i^{(k)} w_i - \bar{f} x_k. \quad (2.8)$$

The term $\sum_i h_i \tilde{z}_i^{(k)} w_i = \sum_{i,l} h_i \delta_{z_i, z_k} \delta_{z_i, z_l} f_l$ is only nonzero, if the considered species is of type k . Then its fitness is always given by f_k . Therefore, $\sum_i h_i \tilde{z}_i^{(k)} w_i = f_k \sum_i h_i \delta_{z_i, z_k} = f_k x_k$ holds and Eq. (2.8) simplifies to,

$$\Delta x_k \bar{f} = (f_k - \bar{f}) x_k. \quad (2.9)$$

This expression is equivalent to the adjusted replicator equation for discrete time steps. Performing the limit $\Delta t \rightarrow 0$ then leads exactly to Eq. (2.6).

2.3.3 Evolutionary Game Theory

Evolutionary game theory (EGT) is a prominent extension of standard evolutionary models and was introduced in 1973 by Price and Maynard-Smith [72, 85]. It employs the ideas and concepts developed in game theory to describe evolutionary dynamics [86]. Namely, the quality of a certain strategy depends on the strategies of all others participants in the game. Applied to evolution this means that the fitness of a species depends on the composition of the whole population (frequency-dependent fitness). Employing such frequency-dependent fitness functions instead of constant ones in replicator dynamics is the main idea of EGT [72, 83, 84, 87].

To understand this in more detail, let us consider a population consisting of d species whose composition is described by the vector $\mathbf{x} = (x_1, x_2, \dots, x_d)$ where x_k is the fraction of species k . The interactions between species result in different payoffs measuring the advantages and disadvantages of these interactions. All these payoffs are summarized in the payoff matrix, P , where the entry P_{lm} gives the payoff an individual belonging to species l gains if it interacts with species m . The fitness, f_k , then follows from averaging over all possible interactions with other individual and is given by,

$$f_k = (1 + sP\mathbf{x})_k, \quad (2.10)$$

where s is the selection strength weighting the summand 1 with the frequency-dependent part, $P\mathbf{x}$. For purely deterministic models this distinction is not necessary and s just leads to a rescaling of time. In contrast, for approaches including fluctuations the dynamics may be considerably influenced by the interplay of the frequency-independent and frequency-dependent part as discussed in Sec. 2.3.4.

To understand the consequences of frequency-dependence in more detail we examine two-player games of social dilemmas in the following. Such two-player games are described by 2×2 payoff matrices where the rows and columns correspond to the strategies cooperation and defection, respectively,

$$P = \begin{pmatrix} \mathcal{R} & \mathcal{S} \\ \mathcal{T} & \mathcal{P} \end{pmatrix}. \quad (2.11)$$

Game	Payoff	Characteristics
Coordination game	$\mathcal{S} - \mathcal{P} < 0, \mathcal{T} - \mathcal{R} < 0$	Coexistence unstable
Prisoner's dilemma	$\mathcal{S} - \mathcal{P} < 0, \mathcal{T} - \mathcal{R} > 0$	Defection stable
Mutualism	$\mathcal{S} - \mathcal{P} > 0, \mathcal{T} - \mathcal{R} < 0$	Cooperation stable
Snowdrift game	$\mathcal{S} - \mathcal{P} > 0, \mathcal{T} - \mathcal{R} > 0$	Coexistence stable

Table 2.1: Classification of standard two-player games. Depending on the entries of the payoff matrix, different scenarios with distinct evolutionary stable strategies emerge.

Here \mathcal{T} stands for *Temptation to defect*, \mathcal{R} for *Reward for mutual cooperation*, \mathcal{P} for *Punishment for mutual defection*, and \mathcal{S} for *Sucker's payoff*. The favored strategy whose frequency increases in terms of EGT depends on these values. Therefore, four different games can be classified depending on \mathcal{T} , \mathcal{R} , \mathcal{P} , \mathcal{S} [87, 88], see Table 2.1. As the principles governing the ensuing dynamics are the same for all games, we restrict our discussion to the prisoner's dilemma defined by $\mathcal{T} > \mathcal{R} > \mathcal{P} > \mathcal{S}$. As it deals with the question if it is beneficial to cooperate, it finds applications not only in biology, but also in sociology and economics. The game can be explained by the following story which is also responsible for its name. Let us consider a crime two imprisoned men have committed. Both are interrogated separately and can decide whether they testify and thereby betray the other one or not. The authorities do not have enough evidence to send somebody to jail for a long time without the testimonial of the other prisoner. Therefore such a testimonial can be rewarded by a reduction in prison sentence. It would be optimal, if both cooperated and did not testify. Then both would gain \mathcal{R} , the second largest value. But, if the players do not trust each other, their payoff is always larger, *i.e.* less years in prison, when defecting as $\mathcal{T} > \mathcal{R}$ and $\mathcal{S} > \mathcal{P}$ hold. Hence, from the point of view of a single prisoner, the optimal strategy is to defect. Another equivalent interpretation of the dilemma of cooperation is the public goods game. There, a cooperator provides a benefit b to other individuals. For providing the benefit, the cooperator has to pay the cost c which is smaller than b ⁶. In this context, defectors are often called free-riders. The resulting payoff matrix is given by,

$$P = \begin{pmatrix} b - c & -c \\ b & 0 \end{pmatrix}. \quad (2.12)$$

In an evolutionary setup, where cooperating individuals compete with free-riding ones, the ensuing fitness terms of cooperators and free-riders directly follow from Eq. (2.10), $f_C = 1 + s(bx - c)$ and $f_D = 1 + sbx$. Thus, the following replicator equation describes the dynamics,

$$\dot{x} = -scx(1 - x) < 0, \quad (2.13)$$

where x is the fraction of cooperators. As the fitness difference is always negative, cooperators go extinct even though it would be optimal if everyone cooperated. This so-called dilemma of cooperation is ubiquitous in nature and we turn to it in more detail in Chapter 3.

Of course, evolutionary dynamics can also be applied to more than two species. Especially, by considering three cyclic competing species [89, 90, 91] interesting results concerning the dynamics in combination with spatial structure and/or fluctuations have been found [92, 93, 94, 95, 94, 96, 97, 98].

⁶For $b < c$ the dilemma would not exist because then cooperation would never be a beneficial strategy.

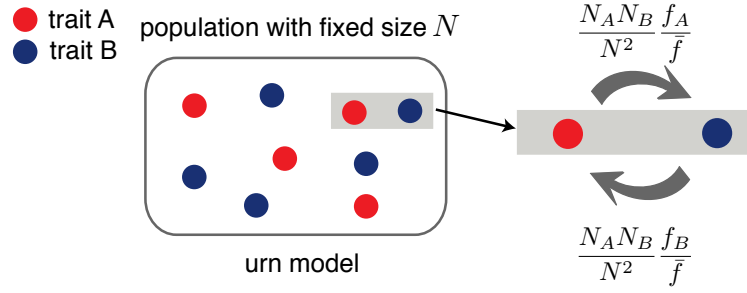


Figure 2.4: Illustration of the Moran process. An individual is chosen according to its fitness to replace a randomly chosen individual.

2.3.4 The Role of Fluctuations

The so far, discussed approaches were purely deterministic, *i.e.* fluctuations in the number of individuals were completely neglected. But in realistic populations fluctuations, causing stochastic deviations from the mean, are present. One of the pioneers in this field was Wright who emphasized the role of fluctuations in evolutionary dynamics [99]. To account for these demographic fluctuations, individual-based modeling has to be employed. In the simplest version, the total number of individuals in a population, N , is fixed. A prominent example is the Fisher-Wright model [100, 101, 102, 103]. It assumes discrete generations each containing N individuals. In every generation, the individuals reproduce with a probability proportional to their abundance and their fitness. To additionally include continuous time instead of fixed generations, rate-based modeling has to be employed. In standard urn models, transition rates for an individual of type A to replace an individual of type B describe the dynamics. The exact form of these rates depends on the specific update-rule, *e.g.* Moran process [104] or local-update rule [105]. Since results do not depend qualitatively on these microscopic details for weak selection, we restrict our discussion to the Moran process in the following. For a more general overview on stochastic models in this field see Ref. [106] for example.

As illustrated in Fig. 2.4, the Moran process is an urn model and the transition rates are given by,

$$\Gamma_{A \rightarrow B} = \frac{f_A}{\bar{f}} \frac{N_A N_B}{N^2}. \quad (2.14)$$

An individual A is chosen to replace an individual B according to its fitness, f_A/\bar{f} , and its abundance in the population, N_A/N . In contrast, the probability that an individual B is replaced only depends on its abundance N_B/N . The full stochastic dynamics can be described by a master equation,

$$\partial_t P(N_A, t) = \sum_S [(\mathbb{E}_A^- - 1)\Gamma_{S \rightarrow A} + (\mathbb{E}_A^+ - 1)\Gamma_{A \rightarrow S}] P(N_A, t), \quad (2.15)$$

where \mathbb{E}_A^\pm are step operators increasing/decreasing the number of individuals of species S by one [107], *i.e.* $\mathbb{E}_A^\pm f(N_A) = f(N_A \pm 1)$. Solving such a master equation is almost never feasible. Therefore, simplifications have to be made. As a first approach, the deterministic limit neglecting all correlations and fluctuations can be studied. For a Moran process this mean-field approximation just leads to the adjusted replicator equation, Eq. (2.6). To account for

fluctuations, typically approximations like the Kramers-Moyal expansion [108] or the Omega expansion proposed by van Kampen [107] have to be employed. While the first one works well for a constant population size the second one is suitable for problems where this assumption is skipped⁷. Performing a Kramers-Moyal expansion of Eq. (2.15) leads to the following Fokker-Planck equation,

$$\partial_t P(\mathbf{x}, t) = - \underbrace{\partial_x \alpha(\mathbf{x}) P(x, t)}_{\text{selection}} + \underbrace{\frac{1}{2N} \partial_x^2 \beta(\mathbf{x}) P(\mathbf{x}, t)}_{\text{fluctuations}}. \quad (2.16)$$

The first part is the deterministic drift shifting the probability distribution according to the coefficient $\alpha(\mathbf{x})$. The second term accounts for fluctuations and is often referred to as random drift. The details of this random drift are reflected by the coefficient $\beta(\mathbf{x})$ which is weighted by N . The ensuing scaling of fluctuations as $1/\sqrt{N}$ is especially important: The smaller a population is, the more pronounced is the role of fluctuations. Therefore, as we highlight in the following chapter fluctuations can be enhanced by population bottlenecks. If individuals occupy new habitats or undergo external catastrophes decimating their number, fluctuations gain importance and may alter the evolutionary outcome drastically. Another example for the importance of fluctuations are propagating fronts. At these front only a few individuals enter a new environment and fluctuations gain special importance [109, 110, 111]. Due to fluctuations also the speed at which populations move in the fitness landscape may be altered, *e.g.* trapped in a local maximum, fluctuations enable a population to find the global maximum faster if the population size is small [112].

The Model of Neutral Evolution

Besides these Neo-Darwinian models, another field focussing on the role of fluctuations and random drift evolved. Both, Hubbell [22] and Kimura [23], introduced neutral models where no fitness differences are included and the evolutionary outcome solely depends on random walks of the abundances of different species through the species state simplex [113]. Note, that even though Kimura took an ansatz neglecting fitness differences he never thought Darwinian evolution was wrong. He just stated that there are regimes where stochastic effects are dominant and thereby become the main driving force for evolution. This is also well-reflected by his condition for neutral evolution [23, 65, 88],

$$sN \approx 1, \quad (2.17)$$

which describes the crossover between selection and fluctuation driven evolution. For $sN \ll 1$, evolution is effectively neutral, *i.e.* fluctuations determine the evolutionary outcome, while for $sN \gg 1$ selection is the dominant driving force.

2.4 The Mutual Interaction of Evolutionary and Population Dynamics

As we have learned by now, ecology and evolution are closely related [114, 115]. While some specific examples of this coupling, *e.g.* density-dependent selection [116, 117], have already

⁷This situation is considered in Sec. 2.4.

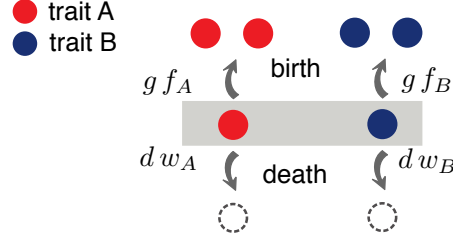


Figure 2.5: The per capita birth and death rates for two different traits, A and B . Each rate depends on a global, trait-independent and a relative, trait-dependent part. While the global and relative fitness terms, g and $f_{A/B}$ affect the birth rates, the global and relative weakness terms d and $w_{A/B}$ determine the death rates.

been considered, we go beyond this and include also demographic fluctuations in a general model. Up to now fluctuations have been mostly studied in models like the Moran process which do not include population dynamics. But when thinking about the microscopic driving forces of population and evolutionary dynamics, their linkage becomes obvious as they are both based on reproduction and death events of single individuals.

The Model

In contrast to the Moran process, where an individual always replaces another individual, here decoupled birth and death events are considered [118, 119],

$$\Gamma_{S \rightarrow 2S} = G_S N_S, \quad \Gamma_{S \rightarrow \emptyset} = D_S N_S. \quad (2.18)$$

The total reproduction rate of species S depends on its per capita reproduction rate, G_S , and the number of individuals of this species, N_S . Analogously, the death rates are decomposed in the per capita death rate, D_S , and N_S . Without losing generality, the birth and death rates can be factorized in global and relative parts, see Fig. 2.5,

$$G_S = g(\mathbf{x}, N) f_S(\mathbf{x}), \quad D_S = d(\mathbf{x}, N) w_S(\mathbf{x}). \quad (2.19)$$

Here, the global parts, the global birth $g(\mathbf{x}, N)$ and death functions $d(\mathbf{x}, N)$, account for factors which influence all individuals in the same way, *e.g.* limited resources or changing environmental conditions. In contrast, the relative parts, namely the relative birth fitness $f_S(\mathbf{x})$ and the weakness $w_S(\mathbf{x})$, describe species-specific factors. They mainly determine the internal evolution of different species, *i.e.* the change in the composition of population. This becomes obvious by examining the deterministic equations following from the master equation with transition rates according to Eq. (2.19),

$$\partial_t N = [g(\mathbf{x}, N) - d(\mathbf{x}, N)] N \quad (2.20a)$$

$$\partial_t x_S = g(\mathbf{x}, N) [f_S(\mathbf{x}) - 1] x_S - d(\mathbf{x}, N) [w_S(\mathbf{x}) - 1] x_S, \quad (2.20b)$$

where $\bar{f} = \bar{w} = 1$ is assumed without loss of generality. The first equation, which describes the evolution of the population as a whole, does solely depend on the global parts. In contrast, the second equation resembling the replicator equation, Eq. (2.6), describes the internal evolution

of different traits. It compares the fitness (weakness) of an individual with the average fitness (weakness). Both terms are weighted with the corresponding global functions. Note that the fitness terms dominate the population in growth phases, while the weakness terms are more important, if the population shrinks. Thus, by accounting for population dynamics and by distinguishing between birth fitness and weakness, which is not possible in standard approaches, a more complex picture of evolutionary dynamics can be obtained.

Van Kampen Approximation

Analogously to the results obtained in Sec. 2.3.4, fluctuations can also be described by a Fokker-Planck equation in this model. But in contrast to the Moran process, the Kramers-Moyal expansion fails, since it assumes a constant population size. Therefore, one has to apply a van Kampen approximation [107]. The basic idea is to separate the influence of the deterministic solution from the one of fluctuations. This is achieved by the following ansatz,

$$N_S = \Omega n_S(t) + \sqrt{\Omega} \xi_S, \quad (2.21)$$

where the stochastic variable N_S , *i.e.* the number of individuals of type S , is rewritten in terms of the deterministic solution, $n_S(t)$, and the stochastic variable, ξ_S , which describes fluctuations in N_S . The latter term is weighted by $\sqrt{\Omega}$, where Ω scales the impact of fluctuations and is proportional to the system size. Expanding the resulting master equation in $\sqrt{\Omega}$, leads to a Fokker-Planck equation in the variables $\xi = (\xi_1, \xi_2, \dots, \xi_d)$ with the deterministic solutions as time dependent parameters, $\mathbf{n}(t) = (n_1(t), n_2(t), \dots, n_d(t))$,

$$\partial_t P(\xi, t) = -\partial_\xi \alpha(\xi, \mathbf{n}(t)) P(\xi; t) + \partial_x^2 \beta(\xi, \mathbf{n}(t), \Omega) P(\xi; t). \quad (2.22)$$

Since this Fokker-Planck equation depends on the fluctuation variables, ξ , instead of N_S or \mathbf{x} , its interpretation is different from Eq. (2.16). Here, the drift term determines whether fluctuations decay or are amplified and thereby alter the evolutionary outcome. An example of the latter scenario is studied in [118, 119]. The second term of the Fokker-Planck equation accounts for intrinsic noise due to birth and death events.

2.5 Manuscripts and Papers

2.5.1 Evolutionary Game Theory in Growing Populations

The letter “Evolutionary game theory in growing population”, Phys. Rev. Lett. **105**, 178101 (2010), by Anna Melbinger, Jonas Cremer and Erwin Frey introduces the model presented in Sec. 2.4. By applying it to the dilemma of cooperation in growing bacterial populations, the influence of population dynamics on the internal evolution is exemplified. Therein our assumptions are minimal: Cooperators reproduce slower than free-riders and more cooperative populations grow faster. Based on asymmetric amplification of fluctuations a transient increase in the level of cooperation can be found. In detail, this means that fluctuations towards more cooperators enforce population growth, while the opposite ones hamper it.

Thereby the weights in the probability distributions are shifted and, for weak enough selection, the fraction of cooperators increases. We complete our analyses by calculations of the boundary between the regime of transient increase and immediate decrease by employing a van Kampen approximation. This boundary is given by,

$$s = \frac{p}{2N_0(1 + px_0)}. \quad (2.23)$$

Here, p scales the growth advantage of more cooperative populations, s is the strength of selection and N_0 and x_0 are the initial population size and level of cooperators, respectively. The boundary compares the growth advantage of more cooperative populations which arises due to fluctuations scaling with \sqrt{N} , with the selection disadvantage of cooperators, s . It resembles the condition of neutral evolution, Eq. (2.17).

2.5.2 Evolutionary and Populations Dynamics - A Coupled Approach

In the paper “Evolutionary and population dynamics - A coupled approach”, Phys. Rev. E **84**, 051921 (2011), by Jonas Cremer, Anna Melbinger and Erwin Frey, the model introduced in Sec. 2.4 is thoroughly discussed and analyzed. Especially, its mapping to standard approaches, as the Moran processes, is pointed out. Further, we study the dilemma of cooperation in growing bacterial populations. Here, two distinct growth scenarios are distinguished. In the dormancy scenario bacteria stop growing if the population size reaches its carrying capacity. In contrast, in the balanced growth scenario, a constant population size is reached due to birth and death events happening at the same frequency. For both scenarios, we find a transient increase of cooperation. We analyze this increase, depending on the growth advantage of cooperative groups p , the initial fraction of cooperators x_0 , the strength of selection s , and the initial population size N_0 . This is achieved by stochastic simulations and analytic calculations employing van Kampen’s approximation. Thereby, we are able to find an analytic expression for the boundary of the regime of transiently increasing cooperation depending on arbitrary global growth functions $g(x)$,

$$s = \frac{\partial_x \ln[g(x)]|_{x_0}}{N(1/g(x))|_{x_0}} = \frac{\partial_x g(x)|_{x_0}}{N(1/g(x))g(x)|_{x_0}}. \quad (2.24)$$

The regime, where the transient increase is present, therefore increases with a larger derivative of the global growth function, $\partial_x g(x)|_{x_0}$, and decreases with its actual value, $g(x_0)$.

2.5.3 Conclusion and Outlook

Both, evolutionary and population dynamics, rely on birth and death events as the microscopic origin of their dynamics. Therefore, a combined description is highly reasonable. In contrast to standard approaches as the Fisher-Wright or Moran model, the model introduced above decouples birth and death events and thereby offers the possibility to study the interdependence of evolutionary and population dynamics. By investigating the dilemma of cooperation in growing bacterial populations, we found that this coupling can lead to a transient increase of cooperation. This increase is mainly caused by fluctuations which are

asymmetrically amplified. Thus, the population size has to be sufficiently small, *i.e.* a population bottleneck is present. An interesting extension of this approach would be to test how repeated population bottlenecks affect the system. One example employing group structure is discussed in Chapter 3. But these bottlenecks can also be modeled by time dependent global growth and death functions. The repeatedly reoccurring small population numbers might increase the influence of fluctuations also on larger time scales. Thereby cooperation might be favored also in the long run.

Additionally, the distinction between birth fitness and weakness offers the possibility to study their influence separately. As mentioned above, fitness terms dominate during growth phases, while weakness terms do so in shrinkage phases. The consequently arising question is how the interplay between both leads to an effective fitness. A further interesting scenario is to consider two species which have exactly the same fitness, but reproduce and die on two completely different time scales. Do these different time scales influence the evolutionary outcome, when considering fluctuations? Furthermore, the model can be extended to account for age-dependent reproduction rates, *i.e.* these rates change during the life-span of an individual. Thereby, insights on age-structured populations [46] can be obtained.

Evolutionary Game Theory in Growing Populations

Anna Melbinger, Jonas Cremer, and Erwin Frey

*Arnold Sommerfeld Center for Theoretical Physics (ASC) and Center for NanoScience (CeNS), Department of Physics,
Ludwig-Maximilians-Universität München, Theresienstrasse 37, D-80333 München, Germany*
(Received 16 April 2010; revised manuscript received 21 July 2010; published 18 October 2010)

Existing theoretical models of evolution focus on the relative fitness advantages of different mutants in a population while the dynamic behavior of the population size is mostly left unconsidered. We present here a generic stochastic model which combines the growth dynamics of the population and its internal evolution. Our model thereby accounts for the fact that both evolutionary and growth dynamics are based on individual reproduction events and hence are highly coupled and stochastic in nature. We exemplify our approach by studying the dilemma of cooperation in growing populations and show that genuinely stochastic events can ease the dilemma by leading to a transient but robust increase in cooperation.

DOI: 10.1103/PhysRevLett.105.178101

PACS numbers: 87.23.Kg, 05.40.-a, 87.10.Mn

Commonly, Darwinian evolution in terms of reproduction, selection, and variation is described in frameworks of population genetics and evolutionary game theory [1–3]. These approaches model the internal evolutionary dynamics of a species' different strategies (or traits) in a relative perspective. Namely, they compare fitness terms and focus on the relative advantage and abundance of different traits. In such a setup, the time evolution of the relative abundance x of a certain strategy is frequently described by a replicator equation,

$$\partial_t x = (f - \langle f \rangle)x. \quad (1)$$

A trait's relative abundance will increase if its fitness f exceeds the average fitness $\langle f \rangle$ in the population.

While in these evolutionary approaches the dynamics of the population size N is mostly left unconsidered or assumed to be fixed [3], in population ecology the dynamical behavior of a species' population size is studied. Models of population dynamics [4,5] usually describe the time development of the total number of individuals N by equations of the form

$$\partial_t N = \mathcal{F}(N, t). \quad (2)$$

$\mathcal{F}(N, t)$ is in general a nonlinear function which includes the influence of the environment on the population, such as the impact of restricted resources or the presence of other species. By explicitly depending on time, a changing environment such as, for example, the seasonal variation of resources can be taken into account.

The internal evolution of different traits and the dynamics of a species' population size are, however, not independent [6]. Actually, species typically coevolve with other species in a changing environment, and a separate description of both evolutionary and population dynamics is in general not appropriate. Not only population dynamics affects the internal evolution (as considered, for example, by models of density-dependent selection [7]), but also vice versa. Illustrative examples of the coupling are

biofilms which permanently grow and shrink. In these microbial structures diverse strains live, interact, and out-compete each other while simultaneously affecting the population size [8]. So far, specific examples of this coupling have been considered by deterministic approaches only, e.g., [9,10]. However, classical and recent work have emphasized the importance of fluctuations for internal evolution which are only accounted for by stochastic, individual-based models, e.g., [11–14].

In this Letter, we introduce a class of stochastic models which consider the interplay between population growth and its internal dynamics. Both processes are based on reproduction events. A proper combined description should therefore be solely based on isolated birth and death events. Such an approach also offers a more biological interpretation of evolutionary dynamics than common formulations like the Fisher-Wright or Moran process [1,3,12,15]. That is to say, fitter individuals prevail due to higher birth rates and not by winning a tooth-and-claw struggle where the birth of one individual directly results in the death of another one. The advantage of our formulation is illustrated by the dilemma of cooperation where a transient increase in cooperation can be found [which does not exist in standard approaches, Eq. (1)].

In the following, we consider two different traits, A and B , in a well-mixed population; however, generalizing the model to more traits is straightforward. The state of the population is then described by the total number of individuals $N = N_A + N_B$ and the fraction of one trait within the population $x = N_A/N$. The stochastic evolutionary dynamics is fully specified by stochastic birth and death events with rates

$$\Gamma_{\emptyset \rightarrow S} = G_S(x, N)N_S, \quad \Gamma_{S \rightarrow \emptyset} = D_S(x, N)N_S, \quad (3)$$

where $G_S(x, N)$ and $D_S(x, N)$ are per capita reproduction and death rates for an individual of type $S \in \{A, B\}$, respectively. We consider these rates to be separable into

a global and relative part, meaning a trait-independent and trait-dependent part:

$$G_S = g(x, N)f_S(x), \quad D_S = d(x, N)w_S(x). \quad (4)$$

The global population fitness $g(x, N)$ and the global population weakness $d(x, N)$ affect the population dynamics of all traits in the same manner. For example, they account for constraints imposed by limited resources or how one strategy impacts the whole population. In contrast, the relative fitness $f_S(x)$ and the relative weakness $w_S(x)$ characterize the relative advantage of one strategy compared to the other. They are different for each trait and depend, in a first approach, only on the relative abundance x [16]. The relative fitness terms $f_S(x)$ affect the corresponding birth rates, and the relative weakness functions $w_S(x)$ describe the chances for survival of distinct traits.

While in evolutionary game theory only the relative fitness is considered [2], and common models of population dynamics take only the global functions into account, we consider here both global and relative fitness and show how their interplay determines the evolutionary outcome of a system. In the following, we set $w_A(x) = w_B(x) = 1$ in order to compare our unifying approach with standard formulations [2]. Though the full stochastic dynamics are given by a master equation, it is instructive to disregard fluctuations for now and examine the corresponding set of deterministic rate equations:

$$\partial_t x = g(x, N)(f_A(x) - \langle f \rangle)x, \quad (5a)$$

$$\partial_t N = [g(x, N)\langle f \rangle - d(x, N)]N, \quad (5b)$$

where $\langle f \rangle = xf_A + (1-x)f_B$ denotes the average fitness. Equation (5a) has the form of a replicator equation [2]. However, in Eq. (5a) there is an additional factor, namely, the global population fitness $g(x, N)$. This leads to a coupling of x and N whose implications we will discuss later on. Similarly, Eq. (5b) describing population growth is coupled to the internal evolution, Eq. (5a). Note that for frequency-independent global functions, $g(x, N) \equiv g(N)$ and $d(x, N) \equiv d(N)$, Eqs. (5) resemble Eqs. (1) and (2). Only then, the deterministic dynamics reduces to the common scenario [12,13,15], where a changing population size is immaterial to the evolutionary outcome of the dynamics [3]. For the full stochastic dynamics the strength of fluctuations scales as $\sqrt{1/N}$ [3,11,14] and thereby is strongly affected by population growth.

In more realistic settings, the global fitness and weakness functions, $g(x, N)$ and $d(x, N)$, can also depend on the relative abundance x . This implies an interdependence of population growth and internal evolution. In the following, we focus on one particular but very important example: the dilemma of cooperation in a growing population. There is an ongoing debate in sociobiology regarding how cooperation within a population emerges in the first place and how it is maintained in the long run [8,17]. Microbial biofilms serve as versatile model systems [8,18–20].

There, cooperators are producers of a common good, usually a metabolically expensive biochemical product. For example, for the proteobacteria *Pseudomonas aeruginosa*, cooperators produce iron-scavenging molecules (siderophores). Released into the environment, these molecules strongly support the iron uptake of each individual in the population [20]. Cooperators thereby clearly increase the global fitness of the population as a whole, leading to a faster growth rate and a higher maximum population size [20]. In such a setting, however, nonproducers (“cheaters”) have a relative advantage over cooperators as they save the cost of providing the common good, e.g., the production of siderophores. Hence, their relative fraction is expected to increase within the population, implying that the global fitness of the population declines. Surprisingly, as we show in the following, a coupling between growth and internal evolution can overcome this dilemma transiently, and the average level of cooperators can increase despite a disadvantage in relative fitness.

We model the internal evolutionary dynamics by the prisoner’s dilemma game [2,17]. Within this standard approach, individuals are either cooperators (A) or cheaters (B). While cooperators provide a benefit b to all players at the expense of a (metabolic) cost $c < b$, a cheater saves the cost by not providing the benefit. The relative fitness of these traits is given by $f_A(x) = 1 + s[(b-c)x - c(1-x)]$ and $f_B(x) = 1 + sbx$, respectively, where the frequency-independent and dependent parts are weighted by the strength of selection s [12]. Analyzing the prisoner’s dilemma *per se*, defectors are always better off than cooperators because of their advantage in relative fitness, $f_A(x) < f_B(x)$ [17]. In the following, we choose for specificity $b = 3$ and $c = 1$; however, our conclusions are independent of the exact values.

Importantly, cooperation positively affects the whole population by increasing its global fitness, e.g., by production of a common good such as siderophores. Here, we consider bounded population growth with a growth rate increasing with the cooperator fraction x . In detail, we choose an x -dependent global fitness, $g(x) = 1 + px$, and an N -dependent global weakness, $d(x, N) = N/K$, accounting for limited resources. For $p = 0$, one obtains the well-known dynamics of logistic growth [21] with a carrying capacity K . For $p > 0$, the carrying capacity, $K(1 + px)$, depends on the fraction of cooperators. For instance, for *P. aeruginosa* [20], the iron uptake, and hence the birth rates, increase with a higher siderophore density and therefore with a higher fraction of cooperators.

To analyze the evolutionary behavior of our model we performed extensive simulations of the stochastic dynamics given by the master equation determined by the birth and death rates, Eq. (3). All ensemble averages were performed over a set of 10^4 realizations. In Fig. 1 the average population size N and the average fraction of cooperators x are shown for different initial population sizes N_0 . The influence of a frequency-dependent growth on the population is twofold. First, starting in the regime of

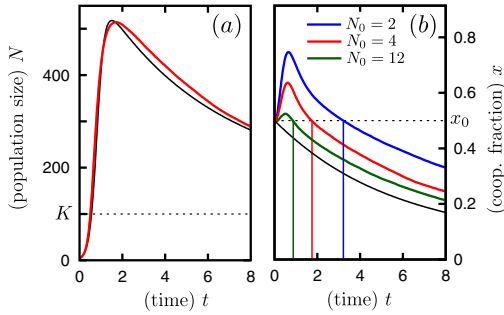


FIG. 1 (color online). The dilemma of cooperation in growing populations. (a) Average population size over time. Because of a cooperation-mediated growth advantage, it can show an overshoot. The gray (red) line corresponds to simulation results while the black line is obtained by evaluating Eqs. (6). (b) The average level of cooperation increases transiently for times $t < t_c$, especially if the initial population size is small meaning fluctuations are large. The parameters are given by $x_0 = 0.5$, $b = 3$, $c = 1$, $s = 0.05$, $K = 100$, and $p = 10$. In (a), N_0 is 4. In (b), the gray lines correspond to $N_0 = 2$ (blue), 4 (red), and 12 (green), from top to bottom. The black line is obtained by evaluating Eqs. (6) for $N_0 = 4$. Cooperation times t_c are denoted by thin lines.

exponential growth, the frequency-dependent global fitness may cause an overshoot in the population size [Fig. 1(a)]. Second, and more strikingly, the selection disadvantage of cooperators can be overcome and a transient increase of cooperation emerges [Fig. 1(b)]. It is maintained until a time t_c , which we term as the cooperation time.

Both phenomena rely on a subtle interplay between internal evolution, with a selection pressure towards more defectors, and population growth, with a growth rate increasing with the fraction of cooperators. While the overshoot in population size can already be understood on the basis of the rate equations,

$$\partial_t x = -s(1 + px)x(1 - x), \quad (6a)$$

$$\partial_t N = [(1 + px)\langle f \rangle - N/K]N, \quad (6b)$$

the transient increase of cooperation is a genuinely stochastic event as discussed in detail below. A first impression of the antagonism between selection pressure and growth can already be obtained by examining the characteristic time scales. While the fraction of cooperators changes on a time scale $\tau_x \propto 1/s$, the population size evolves on a time scale $\tau_N \propto 1$. Hence, the strength of selection s regulates the competition between population growth and internal dynamics. For $s \gg 1$, selection is much faster than growth dynamics. Therefore, the rapid ensuing extinction of cooperators cannot be compensated for by the growth advantage of populations with a larger fraction of cooperators. In contrast, in the limit of weak selection ($s \ll 1$), growth dynamics dominates selection and both an overshoot in the population size and a transient increase of cooperation become possible (see below). In the following we focus on this latter, more interesting, scenario of weak selection ($\tau_N < \tau_x$).

Let us first consider the overshoot in the population size [Fig. 1(a)]. It is caused by a growth rate and a carrying capacity which are increasing functions of the fraction of cooperators (here we use $p = 10$ as observed in microbial experiments [19]). For $t < \tau_x$, a small population [$N \ll K(1 + px_0)$] with an initial fraction of cooperators x_0 grows exponentially towards its comparatively large carrying capacity $K(1 + px_0)$. During this initial time period the fraction of cooperators evolves only slowly and can be considered as constant. On a longer time scale, $t > \tau_x$, however, selection pressure drives the fraction of cooperators substantially below its initial value x_0 , leading to a smaller carrying capacity, $K(1 + px)$. Finally, cooperators go extinct and the population size decreases to K . This functional form of $N(t)$ is well described by the rate equations (6); see black line in Fig. 1(a).

In contrast, the transient increase of cooperation, cf. Fig. 1(b), cannot be understood on the basis of a simple deterministic approach, where $\partial_t x \leq 0$ holds strictly [see black line in Fig. 1(b)]. It is a genuinely stochastic effect, which relies on the amplification of stochastic fluctuations generated during the initial phase of the dynamics where the population is still small. In more detail, for small populations, the fraction of cooperators is subject to strong fluctuations and differs significantly from one realization to another. Crucially, due to the coupling between the growth of a population and its internal composition, these fluctuations are amplified asymmetrically, favoring a more cooperative population; i.e., growth, set by the global fitness $g(x)$, is amplified by an additional cooperator while it is hampered by an additional defector. This implies that the ensemble of realizations becomes strongly skewed towards realizations with more cooperators. If this effect is strong enough the ensemble average $x(t) = \sum_i N_{A,i}(t) / \sum_i N_i(t)$, which describes the mean fraction of cooperators when averaging over different realizations i , increases with time. Because of a subsequent antagonism between selection pressure towards more defectors and asymmetric exponential amplification of fluctuations during growth phase, there is only a transient increase of cooperation in a finite time window, $t \in [0, t_c]$. These findings are illustrated in a movie in [22] showing the time evolution of the probability distribution for an ensemble of stochastic realizations.

Additional qualitative and quantitative insights can be gained from analytic calculations via a van Kampen approximation [23]; see the supplementary material [22]. Thereby starting with a master equation given by Eq. (3), first and higher moments of the fluctuations can be obtained. They show that fluctuations during the first generation (i.e., doubling the initial population size on average) are by far the dominant source for the variance in the composition of the population. In addition (see below), these calculations give a strictly lower bound on the parameter regime where the cooperation time is finite and thus quantify the magnitude of fluctuations necessary to overcome the strength of selection acting against cooperators.

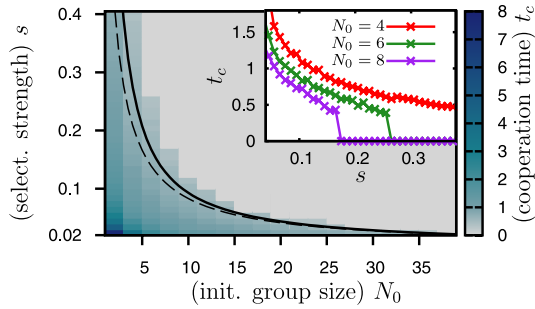


FIG. 2 (color online). Dependence of the cooperation time t_c on the strength of selection s and the initial population size N_0 . There exist two distinct phases: the phase of transient maintained cooperation (where $t_c > 0$ holds) and the phase of extinction of cooperation (where $t_c = 0$). The boundary of both phases (solid line) is approximately given by $sN_0 \approx p/(1 + px_0)$ (dashed line). The cooperation time t_c is shown for varying s but fixed N_0 in the inset. See text and [22].

Figure 2 shows the cooperation time t_c with varying selection strength s and initial population size N_0 . For large s and N_0 (light gray area), t_c is identical to zero; i.e., the fraction of cooperators always decreases as predicted by the deterministic replicator dynamics, Eq. (6a). In contrast, if s and N_0 are sufficiently small, t_c is finite. The transition between these regimes is discontinuous and is marked by a steep drop in the cooperation time from a finite value to zero; see Fig. 2 (inset). A strictly lower bound for the phase boundary (Fig. 2, solid line) can be derived analytically by comparing the antagonistic effects of drift and fluctuations; see [22]. Its asymptotic behavior for large N_0 is given by $sN_0 \approx p/(1 + px_0)$ (Fig. 2, dashed line). This behavior resembles the condition for neutral evolution [11,14]. Indeed, for $sN_0 < p/(1 + px_0)$, fluctuations dominate and the system evolves neutrally. It is this neutral evolution leading to sufficiently large fluctuations which in turn—by asymmetric amplification—result in a transient increase of cooperation.

In summary, we introduced a general approach, which couples the internal evolution of a population to its growth dynamics. Both processes originate from birth and death events and are therefore naturally described by a unifying stochastic model. The standard formulations of evolutionary game theory and population dynamics emerge as special cases. Importantly, by including the coupling, our model offers the opportunity to investigate a broad range of phenomena which cannot be studied by standard approaches. We have demonstrated this for the prisoners' dilemma in growing populations. Here, a transient regime of increasing cooperation can emerge by a fluctuation-induced effect. For this effect, the positive correlation between global population fitness and the level of cooperation is essential. Similar to the Luria-Delbrück experiment [24], initial fluctuations in the fraction of cooperators are exponentially amplified. Here, this renders it possible for cooperators to overcome the selection advantage of defectors.

In biological settings, growth is ubiquitous: populations regularly explore new habitats, or almost go extinct by external catastrophes and rebuild afterwards. For a realistic description, it is therefore necessary to relax the assumption of a decoupled population size. Especially for bacterial populations undergoing a life cycle with a repeated change between dispersal and maturation phases [8,18–20], a transient increase in cooperation may be sufficient to overcome the dilemma of cooperation.

Financial support by the Deutsche Forschungsgemeinschaft through the SFB TR12 “Symmetries and Universalities in Mesoscopic Systems” is gratefully acknowledged.

- [1] W. J. Ewens, *Mathematical Population Genetics* (Springer, New York, 2004).
- [2] J. Maynard Smith, *Evolution and the Theory of Games* (Cambridge University Press, Cambridge, England, 1982).
- [3] R. A. Blythe and A. J. McKane, *J. Stat. Mech.* (2007) P07018.
- [4] J. Murray, *Mathematical Biology* (Springer, New York, 2002), Vol. 1.
- [5] A. Hastings, *Population Biology: Concepts and Models* (Springer, New York, 1997).
- [6] M. E. Hibbing, C. Fuqua, M. R. Parsek, and S. B. Peterson, *Nat. Rev. Microbiol.* **8**, 15 (2010).
- [7] J. Roughgarden, *Ecology* **52**, 453 (1971).
- [8] S. A. West, A. S. Griffin, A. Gardner, and S. P. Diggle, *Nat. Rev. Microbiol.* **4**, 597 (2006).
- [9] C. Hauert, M. Holmes, and M. Doebeli, *Proc. R. Soc. B* **273**, 2565 (2006).
- [10] R. Cressman and G. Vickers, *J. Theor. Biol.* **184**, 359 (1997).
- [11] M. Kimura, *The Neutral Theory of Molecular Evolution* (Cambridge University Press, Cambridge, England, 1983).
- [12] M. A. Nowak, A. Sasaki, C. Taylor, and D. Fudenberg, *Nature (London)* **428**, 646 (2004).
- [13] A. Traulsen, J. C. Claussen, and C. Hauert, *Phys. Rev. Lett.* **95**, 238701 (2005).
- [14] J. Cremer, T. Reichenbach, and E. Frey, *New J. Phys.* **11**, 093029 (2009).
- [15] P. A. Moran, *The Statistical Processes of Evolutionary Theory* (Clarendon, Oxford, 1964).
- [16] By incorporating an N dependence in f_S and w_S , one can extend our model to other forms of density dependence.
- [17] M. A. Nowak, *Science* **314**, 1560 (2006).
- [18] J. Gore, H. Youk, and A. van Oudenaarden, *Nature (London)* **459**, 253 (2009).
- [19] J. S. Chuang, O. Rivoire, and S. Leibler, *Science* **323**, 272 (2009).
- [20] A. S. Griffin, S. A. West, and A. Buckling, *Nature (London)* **430**, 1024 (2004).
- [21] P. F. Verhulst, *Corresp. Math. Phys.* **10**, 113 (1838).
- [22] See supplementary material at <http://link.aps.org/supplemental/10.1103/PhysRevLett.105.178101> for details of analytical calculations and a movie.
- [23] N. V. Kampen, *Stochastic Processes in Physics and Chemistry* (Elsevier, Amsterdam, 2007), 3rd ed.
- [24] S. E. Luria and M. Delbrück, *Genetics* **28**, 491 (1943).

Evolutionary game theory in growing populations

Anna Melbinger, Jonas Cremer, and Erwin Frey

Supplementary EPAPS document: conditions for the transient increase of cooperation

The transient increase of cooperation emerges if initial fluctuations in the evolutionary dynamics are sufficiently large such that the asymmetrical amplification of those can overcome the selection advantage of cheaters. In this Supplementary Material we derive the conditions for the transient increase. In particular, we give an analytical expression for the phase boundary in Fig. 2 (black line).

The full stochastic dynamics is given by the master equation determined by the birth and death rates, Eq. (3),

$$\begin{aligned} \frac{dP(A, B)}{dt} = & \Gamma_{\emptyset \rightarrow A}(A-1, B)(A-1)P(A-1, B) + \Gamma_{\emptyset \rightarrow B}(A, B-1)(B-1)P(A, B-1) \\ & + \Gamma_{A \rightarrow \emptyset}(A+1, B)(A+1)P(A+1, B) + \Gamma_{B \rightarrow \emptyset}(A, B+1)(B+1)P(A, B+1) \\ & - [\Gamma_{\emptyset \rightarrow A}(A, B)A + \Gamma_{\emptyset \rightarrow B}(A, B)B + \Gamma_{A \rightarrow \emptyset}(A, B)A + \Gamma_{B \rightarrow \emptyset}(A, B)B] P(A, B). \end{aligned} \tag{7}$$

Here, $A \equiv N_A$ and $B \equiv N_B$ stand for the number of individuals of both traits. We approximate the master equation upon performing a van Kampen expansion [1]. To this end, we consider A and B as extensive variables which we write as

$$\begin{aligned} A &= \Omega a(t) + \sqrt{\Omega} \xi, \\ B &= \Omega b(t) + \sqrt{\Omega} \mu. \end{aligned} \tag{8}$$

Here, Ω is of the order of the actual system size, and deterministically evolving densities $a(t)$ and $b(t)$ are corrected by fluctuations $\xi(t)$ and $\mu(t)$. By this Ansatz the strength

of fluctuations is correctly considered; their relative impact decreases like $1/\sqrt{\Omega}$ with increasing system size. In the following, we consider the initial dynamics of the population when starting with a small population size N_0 . Then, Ω is of the order $\Omega \approx N_0$. Death events can be neglected as the initial population size is far below the carrying capacity, $N_0/K \approx 0$.

To proceed, we expand Eq. (7) in orders of $1/\sqrt{\Omega}$. The deterministic equations follow to leading order, $\mathcal{O}(\sqrt{\Omega})$, see Eqs. (6) with $N/K \rightarrow 0$ and $x(t) = a(t)/[a(t) + b(t)]$. The next leading order, $\mathcal{O}(\Omega^0)$, results in a Fokker-Planck equation for the probability distribution of the fluctuations, $\Pi(\xi, \mu)$. The dynamics in $\Pi(\xi, \mu)$ is coupled to the deterministic equations and can be extended to include higher orders, $\mathcal{O}(1/\sqrt{\Omega})$. From the Fokker-Planck equation for $\Pi(\xi, \mu)$, differential equations for the first moments of ξ and μ can be obtained. They have the following functional form,

$$\begin{aligned}\partial_t \langle \xi \rangle &= C_1 \langle \xi \rangle + C_2 \langle \mu \rangle + \frac{1}{\sqrt{\Omega}} (C_3 \langle \xi^2 \rangle + C_4 \langle \xi \mu \rangle + C_5 \langle \mu^2 \rangle) + \mathcal{O}\left(\frac{1}{\Omega}\right), \\ \partial_t \langle \mu \rangle &= D_1 \langle \xi \rangle + D_2 \langle \mu \rangle + \frac{1}{\sqrt{\Omega}} (D_3 \langle \xi^2 \rangle + D_4 \langle \xi \mu \rangle + D_5 \langle \mu^2 \rangle) + \mathcal{O}\left(\frac{1}{\Omega}\right).\end{aligned}\quad (9)$$

The constants C_i and D_i with $i \in \{1, 2, 3, 4, 5\}$, depend on the parameters s, b, c, p , the *deterministic* parts of the composition of the population, $x(t) = a(t)/[a(t) + b(t)]$, and the population size $n(t) = a(t) + b(t)$ (in units of Ω), respectively. Importantly, the second moments couple into the dynamics only through $\mathcal{O}(1/\sqrt{\Omega})$ corrections.

Neglecting these second and higher order moments, the ensuing linear equation has an unstable fixed point at $(\langle \xi \rangle, \langle \mu \rangle)^* = (0, 0)$. The eigendirection with the larger (positive) eigenvalue has a component in the ξ -direction which is significantly larger than its component in the μ -direction. As a consequence, the fluctuations in the number of coop-

erators (ξ) are amplified more strongly than those of the defectors (μ); fluctuations are asymmetrically amplified.

Next, we analyze the effect of the second moments on the dynamics. Consider a single initial state without any variance (and all other higher moments identically zero), starting the dynamics in the fixed point, $(\langle \xi \rangle, \langle \mu \rangle)^* = (0, 0)$. Then, since the first moments are zero, only higher orders in Eq. (9) lead to deviations from the (linearly unstable) fixed point. Once such deviations are generated these are amplified *exponentially* by the (linearly) unstable dynamics, i.e. the first moments in Eq. (9). In more detail, consider the differential equations of the second moments which, for $t \rightarrow 0$, have the following asymptotic form:

$$\begin{aligned}\partial_t \langle \xi^2 \rangle &= n(1 + px) [1 + s(bx - c)] x, \\ \partial_t \langle \xi \mu \rangle &= 0, \\ \partial_t \langle \mu^2 \rangle &= n(1 + px)(1 + sbx)(1 - x).\end{aligned}\tag{10}$$

Starting with zero at $t = 0$, both, $\langle \xi^2 \rangle$ and $\langle \mu^2 \rangle$ increase linearly in time (note that the fitness of a cooperator $1 + s(bx - c) > 0$ since otherwise the birth rate would be negative). Within one generation, $t_g = 1/[(1 + px)(1 + s(b - c)x)]$ (compare Eq. (6b)), i.e. doubling the population size on average, finite variances $\langle \xi^2 \rangle_g$ and $\langle \mu^2 \rangle_g$ are generated. This variance can be taken as a *lower bound*. We even expect this lower bound to be a reasonable estimate for the actual value since the impact of the variance created in following generations on Eqs. 9 is strongly suppressed by the exponential increase in population size.

Upon inserting the values $\langle \xi^2 \rangle_g$ and $\langle \mu^2 \rangle_g$ into Eq. (9) one can now calculate the time

evolution of the first moments, $\langle \xi \rangle$ and $\langle \mu \rangle$. This allows to determine the conditions necessary for a transient increase of cooperation by analyzing the fraction of cooperators $\langle \frac{A}{A+B} \rangle$; see Eqs. (8). The phase boundary separating the regimes of transient increase and immediate decrease of cooperation is defined by the condition of an initially stationary fraction of cooperators: $\partial_t \langle \frac{A}{A+B} \rangle = 0$ at $t \approx 0$.

The ensuing phase boundary is plotted in Fig. 2 (black line). The deviation from the actual (numerically determined) transition line is small for intermediate Ω and goes to zero for larger Ω . By evaluating the expression in orders of s/p , the lower bound of the transition line can be further simplified. To first order one finds

$$s = \frac{p}{n\Omega(1+px)}, \quad (11)$$

with $\Omega n = N_0$; see Fig. 2, dashed line. Note that this expression gives the asymptotically correct results for large Ω .

It is instructive to compare this result with the theory of neutral evolution [2] where a condition $sN_0 \propto 1$ separates regimes of neutral and selection-dominated evolution [2, 3]. In the present case, for the transient increase of cooperation to occur, the system has to evolve neutrally in the initial phase to create a large enough variation in the fraction of cooperators. Then, after being asymmetricly amplified, these fluctuations can overcome the selection pressure towards more defectors. This is mathematically reflected in Eqs. (9) and (10). Initially, the second moments increase, Eqs. (10), which then feed into Eqs. (9) and lead to an increase in the first moments. Finally, the good agreement of the phase boundary with its lower bound, reassures that the variation in cooperators fraction is mainly generated at the beginning of the dynamics.

References

- [1] N.G. Van Kampen. *Stochastic Processes in Physics and Chemistry (North-Holland Personal Library)*. North Holland, 2nd edition, 2001.
- [2] M. Kimura. *The Neutral Theory of Molecular Evolution*. Cambridge University Press, Cambridge, 1983.
- [3] J. Cremer, T. Reichenbach, and E. Frey. The edge of neutral evolution in social dilemmas. *New J. Phys.*, 11:093029, 2009.

Evolutionary and population dynamics: A coupled approach

Jonas Cremer, Anna Melbinger, and Erwin Frey

Arnold Sommerfeld Center for Theoretical Physics (ASC) and Center for NanoScience (CeNS), Department of Physics,
Ludwig-Maximilians-Universität München, Theresienstrasse 37, D-80333 Munich, Germany

(Received 10 August 2011; revised manuscript received 8 October 2011; published 28 November 2011)

We study the interplay of population growth and evolutionary dynamics using a stochastic model based on birth and death events. In contrast to the common assumption of an independent population size, evolution can be strongly affected by population dynamics in general. Especially for fast reproducing microbes which are subject to selection, both types of dynamics are often closely intertwined. We illustrate this by considering different growth scenarios. Depending on whether microbes die or stop to reproduce (dormancy), qualitatively different behaviors emerge. For cooperating bacteria, a permanent increase of costly cooperation can occur. Even if not permanent, cooperation can still increase transiently due to demographic fluctuations. We validate our analysis via stochastic simulations and analytic calculations. In particular, we derive a condition for an increase in the level of cooperation.

DOI: [10.1103/PhysRevE.84.051921](https://doi.org/10.1103/PhysRevE.84.051921)

PACS number(s): 87.23.Kg, 87.10.Mn, 05.40.-a, 02.50.Le

I. INTRODUCTION

The time evolution of size and internal composition of a population are both driven by discrete birth and death events. As a consequence, population dynamics and internal evolutionary dynamics are intricately linked. The biological significance of this coupling has previously been emphasized [1–9]. Those studies mostly employ density-dependent fitness functions to phenomenologically derive sets of coupled deterministic equations for the size and composition of populations in various ecological contexts. While those studies correctly describe the evolutionary dynamics of large population sizes, they do not account for stochastic effects arising at low population sizes. These demographic fluctuations are naturally described in the theoretical framework of stochastic processes based on elementary birth and death events as recently introduced [10]. In particular, this approach allows one to explore the role of fluctuations in populations with a time-varying population size.

To understand such interdependence of population and evolutionary dynamics, it is instructive to first review the decoupled and deterministic formulations of both. *Evolutionary game theory* is a well-defined framework to describe the temporal development of different interacting traits or strategies [11,12]. It has been established as a standard approach to describe evolutionary dynamics if the fitness is frequency-dependent (i.e., if the fitness of a certain strategy depends on the abundance of other strategies within the population). Within the most basic setup, well-mixed populations are assumed and the evolution of strategies is solely determined by fitness advantages. The temporal development of the abundance x_S of a trait S follows a *replicator dynamics* [11–13],

$$\partial_t x_S = (\phi_S - \bar{\phi})x_S. \quad (1)$$

A trait's abundance increases if its fitness ϕ_S exceeds the average fitness $\bar{\phi}$ of the population. The frequency-dependence, with ϕ_S a function of the abundances \vec{x} of all strategies, provoke nonlinearities in Eq. (1). Starting from this standard approach, many specific examples and extensions thereof have been studied [12–14]. This comprises, for example, the prisoner's

dilemma, the snowdrift game and other games in well-mixed populations [11–13,15]. It further ranges from the role of spatial arrangements and network interactions [16–25] via cyclic dominance [7,26–33], structured populations [34,35], modified update rules [36,37], multiplayer games [38], and evolutionary algorithms [39] to the influence of internal and external fluctuations [40–45]. While these models consider a wide range of evolutionary aspects, they mostly rely on one key assumption, a decoupled, constant population size.

In contrast, *population dynamics* focuses on the time evolution of the population size and how it is determined by environmental impacts like limited resources or seasonal variations. The dynamics is typically described by differential equations of the form [46–48],

$$\partial_t N = \mathcal{F}(N; t), \quad (2)$$

where $\mathcal{F}(N; t)$ may explicitly depend on time [46]. The most prominent example is logistic growth [49]. While a small population grows exponentially, the growth rate decreases with increasing population size due to limitations of resources and the population size is bounded below a maximum carrying capacity.

Illustrative examples of dynamical changes in the population size comprise bacterial and other microbial populations [50–52]: A surplus in nutrients or other metabolism-related factors, can lead to an immediate and strong growth of the population while resource limitations or antibiotics and other detrimental factors can imply a stop in growth or even an abrupt death of single individuals. Even for only slightly varying environmental conditions, a fixed population size is thus rather the exception than the rule.

But microbes not only show rich population dynamics, they are also subject to diverse evolutionary forces [53–57]. Microbes live in interacting collectives of different traits. Evolution is ubiquitous and strong forms of frequency dependence can be observed. Public good scenarios where a metabolically costly biochemical product is shared among individuals are of particular interest from an evolutionary perspective (see, e.g., [51,55,58–60]). This includes, for example, nutrient uptake, like disaccharides in yeast [61–63], collective

fruiting body formation [64,65], or the active formation of biofilms [52,57,66,67]. An example regarding iron uptake is considered below in more detail [68–70]. Furthermore, synthetical microbial systems have been considered [71,72].

Motivated by these recent studies of microbial systems, we here investigate the consequences of such an interdependence between evolutionary and population dynamics. Employing a previously introduced theoretical approach [10], we study the influence of different growth scenarios in combination with demographic fluctuations.

The outline of this article is the following. In Sec. II we discuss the stochastic dynamics and its deterministic approximation. Furthermore, we consider the limits in which the model maps to standard (deterministic and stochastic) formulations of evolutionary dynamics. In Sec. III we consider the dilemma of cooperation in growing populations. Here, an increase of cooperation can be observed which is analyzed in detail. In particular, we discuss the outcomes for two different growth scenarios (i.e., a reproduction dynamics which either is balanced by death events or simply arrests in the stationary case). Finally, we close with a short conclusion in Sec. IV.

II. COUPLING OF EVOLUTIONARY AND POPULATION DYNAMICS

A. Microscopic model

We consider a population of M different traits. Each trait S is represented by N_S individuals, such that the state of the population is given by $\vec{N} = (N_1, N_2, \dots, N_M)$. We further denote the frequencies of all different traits by $\vec{x} = \vec{N}/N$ with $N = \sum_S N_S$ being the total population size. The stochastic evolutionary dynamics is formulated in terms of per capita birth and death rates, G_S and D_S , respectively. The total rate for the abundance of trait S to increase or decrease by one individual is given by

$$\Gamma_{S \rightarrow 2S} = G_S N_S, \quad \Gamma_{S \rightarrow \emptyset} = D_S N_S. \quad (3)$$

The various biological factors determining each rate can be split up into two parts, a global and a relative contribution. While the global term is trait-independent and affects all traits in the same manner the relative term is trait-dependent and sets the differences between traits. We write

$$G_S = g(\vec{x}, N) f_S(\vec{x}), \quad D_S = d(\vec{x}, N) w_S(\vec{x}), \quad (4)$$

and refer to $g(\vec{x}, N)$ and $d(\vec{x}, N)$ as *global birth-fitness* and *global weakness*, respectively. The trait-dependent terms are the *relative birth-fitness* $f_S(\vec{x})$ and the *relative weakness* $w_S(\vec{x})$.¹ While birth-fitness terms affect the birth rates, weakness terms determine the expected survival times of individuals and hence their viability. A short illustration of the stochastic processes is given in Fig. 1 for the case of two different traits.

To specify the relative fitness terms, we follow the standard approach of evolutionary game theory [11], and assume them to depend linearly on the frequencies \vec{x} . Let \mathcal{P} be the payoff

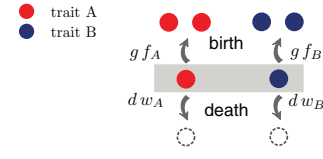


FIG. 1. (Color online) The per capita birth and death rates for two different traits, A [light gray (red)] and B [dark gray (blue)]. Each rate depends on a global, trait-independent and a relative, trait-dependent part. While the global and relative fitness terms g and $f_{A/B}$ affect the birth rates, the global and relative weakness terms d and $w_{A/B}$ determine the death rates.

matrix for birth events. Then, the corresponding fitness vector for all traits is defined as

$$\vec{\phi} = 1 + s\mathcal{P}\vec{x}. \quad (5)$$

Following standard formulations, the *selection strength* s defines the relative weight of a frequency-dependent part with respect to a background-fitness set to 1 [40,43]. As will become clear in the following, it is convenient to make use of normalized fitness values,

$$\vec{f} = \vec{\phi}/\bar{\phi}, \quad (6)$$

where $\bar{\phi} = \sum_S \phi_S x_S$ such that $\vec{f} = \sum_S f_S x_S = 1$. Without loss of generality, this choice separates global and relative parts in such a way that the dynamics of the population size depends only on the global functions g and d ; see also the following Eq. (8a). An analogous approach with a payoff matrix \mathcal{V} for death events can be used to obtain the frequency-dependent weakness functions w_S , which are also taken as normalized, $\sum_S w_S x_S = 1$. Of course, a more general, nonlinear frequency dependence for both relative functions can readily be taken into account. For example, in microbial systems the fitness of an individual or the whole community depends in an intricate way on a plethora of factors (e.g., the abundance of individuals, secretion, and detection of signaling molecules, toxin secretion leading to interstrain competition, and changes in environmental conditions). Nonlinear frequency-dependent fitness functions might help to account for such factors (see, e.g., [58,62]).

In general, the global terms $g(\vec{x}, N)$ and $d(\vec{x}, N)$ depend on the population size and are frequency dependent. Limited growth is one example of size dependence. In such a setting, small populations start to grow exponentially but growth is bounded due to limited resources [e.g., $d(\vec{x}, N)$ increases with N]. Frequency-dependent terms can, for example, occur in public good situations, as discussed in Sec. III.

B. Dynamics

The per-capita birth and death rates Eq. (4) define a continuous-time Markov process [73,74]. It is described by a master equation for the probability density $P(\vec{N}; t)$ to find the population in state \vec{N} at time t :

$$\frac{dP(\vec{N}; t)}{dt} = \sum_S [(\mathbb{E}_S^- - 1)G_S N_S + (\mathbb{E}_S^+ - 1)D_S N_S] P(\vec{N}; t). \quad (7)$$

¹In this work, we assume the relative parts to be independent of the system size. However, including a density-dependent part also in the relative terms is straightforward.

Here, \mathbb{E}_S^\pm are step operators increasing or decreasing the number of individuals of trait S by one [74], for example,

$$\mathbb{E}_S^\pm P(\vec{N}; t) = P(N_1, \dots, N_S \pm 1, \dots, N_M; t).$$

For a reference it is instructive to first consider a deterministic limit where both fluctuations and correlations can be neglected. Then, upon factorizing higher moments of the probability density [73,74], one finds a closed set of equations for the expected frequencies x_S and the total population size N :

$$\partial_t N = [g(\vec{x}, N)\bar{f} - d(\vec{x}, N)\bar{w}]N, \quad (8a)$$

$$\partial_t x_S = g(\vec{x}, N)[f_S(\vec{x}) - \bar{f}]x_S - d(\vec{x}, N)[w_S(\vec{x}) - \bar{w}]x_S, \quad (8b)$$

where $\bar{f} = \bar{w} = 1$ according to Eq. (6). To unclutter notation, we have not explicitly marked the expectation values in Eq. (8) but use the same notation as for the stochastic variables.

This set of coupled nonlinear equations resembles other deterministic approaches [1–4,6–8] and has a simple interpretation. Equation (8a) describes the population dynamics. As is typical for a deterministic approach, the dynamics does not depend on the global birth–fitness g and the global weakness d separately, but only on their difference. Equation (8b) describes the internal evolution of the population: The time evolution of the frequency of a strategy S is given by the interplay between a growth and a death term. Each of them consists of a relative term measuring the surplus of the fitness or weakness relative to the corresponding population average. The weight of these terms are given by the respective global fitness functions g and d . During phases of population growth, where $g > d$ holds [see Eq. (8a)], the growth term and hence differences in relative birth–fitness dominate the internal evolution of the population. Similarly, weakness differences are the main evolutionary driving forces during population decline.

From these considerations it follows that both the time scale of population and evolutionary dynamics have a crucial impact on the dynamics. This is obvious if the time scales are similar. Such biological situations have been observed in many examples (see, e.g., [75–78]). But also if evolution happens on longer time scales than ecology this coupling can affect the evolutionary outcome as we show in the following.

Importantly, fluctuation cannot be ignored in general but can change evolutionary dynamics dramatically. Then, the deterministic approach given by Eq. (8) is not adequate. This regards, for example, fixation and extinction events but also the evolution of first and higher moments of a trait’s abundance. For a proper description, one has to take the full stochastic dynamics and master equation Eq. (7) into account. One example where fluctuations drastically change the outcome is given in the following Sec. III.

C. Mapping to standard approaches: replicator dynamics and the Moran process

We now consider in which limits and to what extent our stochastic approach resembles the standard approaches of evolutionary dynamics. Let us first consider the special case where the global rates $g(\vec{x}, N) \equiv g(N)$ and $d(\vec{x}, N) \equiv d(N)$ are frequency-independent and the ensuing deterministic

dynamics exhibits a stable fixed point N^* in the population size. Then, birth and death events exactly balance each other, $g(N^*) = d(N^*)$, such that N^* is fixed, $\partial_t N^* = 0$. This is, for example, the case if the population size evolves according to a logistic growth law and the carrying capacity has been reached. In the deterministic limit, the internal dynamics, Eq. (8b), simplifies to

$$\partial_t x_S = g(N^*)[f_S(\vec{x}) - \bar{f} - w_S(\vec{x}) + \bar{w}]x_S. \quad (9)$$

The fraction x_S evolves like in a standard replicator equation, similar to Eq. (1). It is the difference of both relative terms, the effective fitness $f_S - w_S$, which determines internal evolution. Compared to Eq. (1), the additional constant prefactor $g(N^*)$ in Eq. (9) just rescales the time scale on which internal evolution occurs [41].

Furthermore, also the full stochastic formulations of our model and the standard stochastic approaches with a fixed population size resemble each other. In those standard approaches, the birth of one individual is directly coupled to the death of another one. The dynamics is described by *update rules*. For example, for the time-continuous formulation used here, the stochastic dynamics can be described by the Moran process [40,41,43,44,79–81].² In our formulation, this process holds in the limit where the fixed point of the population size N^* is linearly stable with a large stability coefficient.³ Then, a birth event is directly followed by a death event and vice versa. The effective rate for such a combined birth–death event is given by

$$\tilde{\Gamma}_{S \rightarrow S'} = \Gamma_{S' \rightarrow 2S'} \Gamma_{S \rightarrow \emptyset} + \Gamma_{S \rightarrow \emptyset} \Gamma_{S' \rightarrow 2S'}. \quad (10)$$

The strength of fluctuations in the fraction of a certain species is of the order $1/\sqrt{N^*}$ and the transition rate $\tilde{\Gamma}_{S \rightarrow S'}$ follows by the logic of an urn model, where fitness-dependent individuals reproduce to substitute other, randomly chosen, individuals [40,41,43,79,80].

Beyond the Moran process, however, if N^* is not linearly stable with sufficiently high stability coefficients, then birth and death events do not strictly follow each other. Depending on the stability of the fixed point, evolutionary paths deviating from N^* by more than one individual have to be taken into account to derive an effective rate for a combined birth–death event.

In general, the population size changes with time, $N = N(t)$. For frequency-independent global rates, the deterministic limit of the internal evolutionary dynamics resembles the form of a replicator equation,

$$\partial_t N = [g(N) - d(N)]N, \quad (11a)$$

$$\partial_t x_S = \{g(N)[f_S(\vec{x}) - \bar{f}] \quad (11b)$$

$$- d(N)[w_S(\vec{x}) - \bar{w}]\}x_S. \quad (11c)$$

²Similarly, the stochastic dynamics is described by a Fisher–Wright process for discrete time steps. Other update rules are based on other fitness functions or the way one individual replaces another one.

³To strictly ensure N to vary around N^* with ± 1 , the fixed point has to be linear stable with additional higher orders supporting the stability.

However, in contrast to Eq. (1), both relative fitness terms f and w are now weighted by the global rates. This has important implications. While in growth phases with $g > d$ the relative birth-fitness f_S dominates the dynamics, the relative weakness functions w_S dominate during population decline, $g < d$. Moreover, the time-varying population size also leads to a changing strength of fluctuations $\sim 1/\sqrt{N(t)}$. In particular, when fitness differences are weak and the dynamics is close to neutral evolution, such a change might have strong consequences [41,43,45,82,83].

III. THE DILEMMA OF COOPERATION IN GROWING POPULATIONS

To exemplify the importance of coupling and fluctuations offered by our approach, we here study the dilemma of cooperation in growing populations. This is motivated by the dynamics observed in microbial biofilms where strong forms of cooperation can be observed [51,55,57,59,60,67]. Single individuals produce metabolically costly products which they release into the environment to support, for example, biofilm formation or nutrient depletion. As these products are available for other bacteria in the colony, the cooperating individuals are producers of a public good, and, by having the extra load of production, permanently run the risk to be undermined by nonproducing free-riding strains. An example is provided by the proteobacterium *Pseudomonas aeruginosa* [68–70]. To facilitate the metabolically important iron uptake, these microbes produce siderophores which they release into the environment. Given the high binding affinity to iron, these proteins are capable of scavenging single iron atoms from larger iron clusters. The iron-siderophore complex can then be taken up by the bacteria, ensuring their iron supply. However, as every bacterium, not only the producing ones, can take advantage of the released siderophores there is a dilemma of cooperation: While it would be optimal for the whole population to cooperate, cooperators are endangered due to their reproduction disadvantage.

In addition to the evolutionary dynamics, microbial colonies are also subject to strong changes in population size [50–52,84]. While in the presence of nutrients, small colonies grow exponentially, growth is bounded due to limitations in resources or deteriorating environmental conditions. This includes insufficient amounts of nutrients, a lack of oxygen or a poisoning by metabolites. Eventually the colony size remains constant or even declines again [50]. Given the exact interplay of these detrimental and other environmental factors, and differing from species to species, growth dynamics varies between two scenarios [85,86]. First, bacteria can switch into a dormant state where individuals stay alive but regulate reproduction rates and metabolic activity toward zero (*dormancy scenario*). Depending on environmental conditions dormancy can increase survival chances. For example, in the presence of antibiotics, this downgraded metabolism can make bacteria less vulnerable leading to persistence [87–90], or dormancy might hedge a population against strongly fluctuating environments [86,90,91]. Second, environmental conditions can lead to death rates increasing with the population size N while birth rates are only slightly affected [92]. The population, therefore, reaches a state of dynamical maintained

population size with the death rates exactly balancing the birth rates (*scenario of balanced growth*). In many populations, a situation in between both scenarios is observed. In pathogens like *P. aeruginosa*, the fraction of individuals transferring to the dormancy state varies between 20% and 80% [93]. In the following we consider both scenarios and their impact on internal evolution separately.

A. The balanced growth scenario

Let us first study the balanced growth dynamics where, in the stationary state, birth and death events are both present, but exactly balance each other such that the population size is about constant. We consider a population which consists of two traits, cooperators (C) and free-riders (F). The total number of individuals in the population is given by $N = N_C + N_F$ and the fraction of cooperators by $x \equiv x_C = N_C/N$. The relative birth-fitness f_S (ϕ_S , if not normalized) accounts for the reproduction disadvantage of cooperating individuals. We study the well-known prisoner’s dilemma [11]:⁴

$$\phi_C = 1 + s(\bar{b}x - \bar{c}), \quad \phi_F = 1 + s\bar{b}x, \quad \bar{\phi} = 1 + s(\bar{b} - \bar{c})x. \quad (12)$$

As introduced in Sec. II, the frequency-dependent part is weighted with the strength of selection s . Individuals obtain a benefit \bar{b} from direct interaction with cooperators, while only cooperating individuals have to pay the cost \bar{c} for producing the public good. For the resulting normalized fitness functions, $f_S = \phi_S/\bar{\phi}$, the inequality $f_C < f_F$ always holds; within the same population, the reproduction rate of cooperators is always smaller than the one of free-riders.

In the following, we take the payoff parameters to be constant, $\bar{c} = 1$ and $\bar{b} = 3$. Then, s directly sets the time scale of the internal evolution. The relative weakness is assumed to be trait-independent and constant, $w_C = w_F = 1$; free-riders and cooperators have equal survival chances.

Furthermore, because cooperators are the producers of a public good, the overall growth condition of a population improves with a higher level of cooperation. We here choose the global birth-fitness to increase linearly with the level of cooperation,

$$g(x) = 1 + px. \quad (13)$$

The parameter p scales the positive impact of the presence of public good on the population. In the scenario of balanced growth, we consider death rates increasing with the population size. For specificity, we assume logistic growth [49] and set

$$d(N) = N/K. \quad (14)$$

K scales the maximal size a population can reach (carrying capacity) as discussed in detail below.

⁴More generally we could also study other types of interactions like the snowdrift game. However, as we want to show the importance of population dynamics for supporting cooperation we chose the worst-case scenario for cooperation, the prisoner’s dilemma.

The master equation (7) describing the full stochastic dynamics then takes the form,

$$\frac{dP(N_C, N_F)}{dt} = [(\mathbb{E}_C^- - 1)gf_C N_C + ((\mathbb{E}_F^- - 1)gf_F N_F + (\mathbb{E}_C^+ - 1)d N_C + (\mathbb{E}_F^+ - 1)d N_C]P(N_C, N_F). \quad (15)$$

To explore the dynamics, we performed extensive stochastic simulations. They were obtained by simulating $i = 1, \dots, R$ different realizations with the Gillespie algorithm [94], according to the master equation (15). In Fig. 2, we show the ensemble averages of the population size $\langle N \rangle$ and the fraction of cooperators (x) given by

$$\langle N \rangle = \sum_i N_i(t)/R, \quad (16a)$$

$$\langle x \rangle = \sum_i N_{C,i}(t) / \sum_i N_i(t). \quad (16b)$$

This choice for the average naturally accounts for the fact that realizations with a larger population size have a larger weight. It is especially important for biological situations where several realizations exist at the same time (e.g., [72]). In such an ensemble cooperation can increase in principle if there is a positive correlation between population size and the fraction of cooperators. The existence of this effect, also known as Simpson's paradox, has been shown recently by Chuang *et al.* for microbial populations [72]. Here we want to understand the dynamics underlying this correlation underlying cooperation.

Starting with a small population, the system size grows exponentially (*exponential phase*), reaches a maximum size, and then declines again. Furthermore, and more strikingly, the disadvantage of cooperators can be overcome and a transient increase of cooperation can emerge. Even though the transient increase is caused by demographic fluctuations, it is instructive to examine the deterministic equations first. They not only describe the overshoot in the population size well, but also give insights into the relevant time scales of the dynamics:

$$\partial_t x = -s(1 + px)x(1 - x), \quad (17a)$$

$$\partial_t N = \left(1 + px - \frac{N}{K}\right)N. \quad (17b)$$

The first equation describes the change in the average fraction of cooperators. The dynamics occurs on the time scale $\tau_x \sim 1/s$ (i.e., the strength of selection sets the time scale of internal evolution). Note that $\partial_t x \leq 0$ always holds and therefore the deterministic approximation cannot give rise to any transient increase of cooperation. In contrast, the dynamics of the total population size is well described deterministically [see Fig. 2(a)]. It resembles the well-known equation of logistic growth [49] with a frequency-dependent maximal population size $K(1 + px)$ (carrying capacity). During growth, changes in the population size occur on a time scale $\tau_N \sim 1 + px$ [cf. Eq. (17b)]. In the limit of weak selection, τ_N is comparably

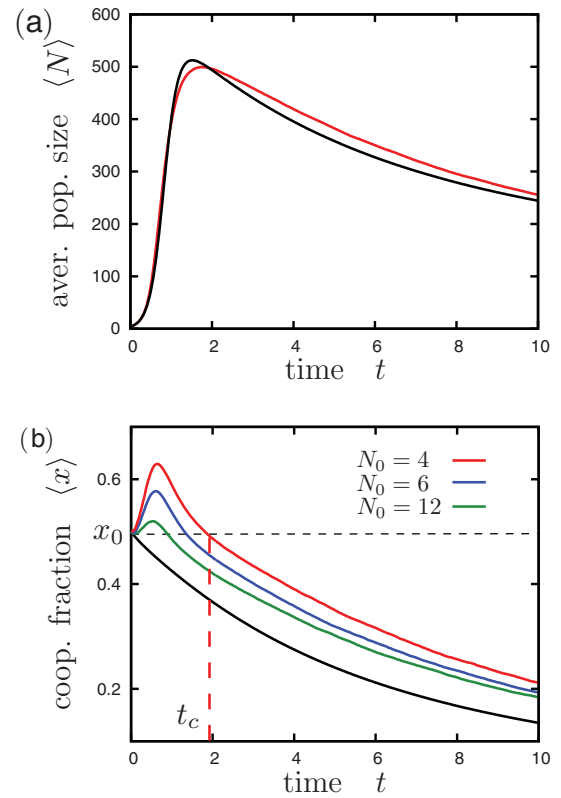


FIG. 2. (Color online) Cooperation in growing populations. Temporal development of ensemble averages. (a) The population size. Starting with $N_0 = 4$, the system grows exponentially until the carrying capacity is reached. It then falls again due to selection and a decreasing carrying capacity; see text. The full stochastic solution, gray (red) line, is described well by the deterministic approximation, black line. (b) The fraction of cooperators. It initially increases due to asymmetric amplification of fluctuations, and then falls again due to selection; see text. The level of cooperation x falls below its initial value x_0 at the cooperation time t_c . The transient increase is stronger for larger fluctuations and thus is stronger with a smaller initial population size N_0 ; see gray (colored) lines. The deterministic approximations do not account for this behavior (cf. black line). Parameters are $s = 0.1$ and $p = 10$.

smaller than the time scale τ_x on which selection occurs. This and the frequency-dependent carrying capacity are the reason for the overshoot: At the beginning the maximal population size is given by $K(1 + px_0)$. Because cooperators go extinct, the size decreases with time. As this reduction is happening on a faster time scale than selection, $\tau_N < \tau_x$, the population size grows toward a larger carrying capacity, and then subsequently drops with decreasing carrying capacity due to a decline in cooperation.

B. A transient increase of cooperation

The stochastic dynamics of the average fraction of cooperators $\langle x \rangle$ is qualitatively different from its deterministic limit. We observe a transient increase in the level of cooperation during a time window $(0, t_c)$. The magnitude of the *cooperation time* t_c strongly depends on the initial population size N_0 (cf. Fig. 2). The origin of this transient increase in cooperation

is a genuine stochastic effect: Demographic fluctuations during the initial phase are subsequently asymmetrically amplified by the population dynamics. Heuristically, this can be understood as follows; for a detailed mathematical analysis employing a van Kampen expansion see the next section.

For a small initial population size N_0 demographic fluctuations are effectively symmetric (i.e., the occurrence of an additional cooperator or an additional free-rider are equally likely). However, the consequences of these two directions of demographic fluctuations differ strongly: In the exponential phase, an additional cooperator amplifies the growth of the population, while an additional free-rider hampers it. In other words, fluctuations toward more cooperators imply a larger growth rate and hence a larger population size. Therefore, those realizations of the stochastic dynamics have a larger weight in the ensemble average Eq. (16b) and enable an increase in the overall fraction of cooperators. With these considerations, a criterion for the transient increase of cooperation can be obtained: Demographic fluctuations, which are of size \sqrt{N} [41], have to be large enough to overcome the selection pressure toward free-riders. This can already be inferred from Fig. 2(b), where curves for three different values of the initial population size are shown. For the smallest N_0 the effect is the strongest because fluctuations are large at the beginning. In summary, a population bottleneck which corresponds to a small initial population size can favor cooperation transiently. Furthermore, if populations repeatedly undergo population bottlenecks, the increase in cooperation can be manifested also permanently.

C. Van Kampen expansion

As discussed above the transient increase of cooperation is caused by fluctuations which are asymmetrically amplified. In order to quantify these findings analytically, we employ an Omega expansion in the system size according to van Kampen [74] of the master equation (15). For generality, we perform these calculations for arbitrary global growth function $g(x)$. The deterministic solutions are separated from fluctuations by the following ansatz:

$$N_C = \Omega c(t) + \sqrt{\Omega} \xi, \quad N_F = \Omega f(t) + \sqrt{\Omega} \mu. \quad (18)$$

$c(t)$ and $f(t)$ correspond to the deterministic solutions, as shown below. ξ and μ are fluctuations in the number of cooperators and free-riders. The relative strength of fluctuations and the deterministic parts are weighted by powers of Ω which scales with the current system size. For instance, to describe the transient increase which is generated by fluctuations at the beginning, Ω is given by N_0 . Hence, this ansatz accounts for the fact that fluctuations scale as $1/\sqrt{N}$ [73]. Equation (15) is expanded in orders of $1/\sqrt{\Omega}$. With Eq. (18), the step operators $\mathbb{E}_S^+, \mathbb{E}_S^-$ are given by

$$\begin{aligned} \mathbb{E}_C^\pm &= 1 \pm \frac{1}{\sqrt{\Omega}} \partial_\xi + \frac{1}{2\Omega} \partial_\xi^2 + \mathcal{O}(\Omega^{3/2}), \\ \mathbb{E}_F^\pm &= 1 \pm \frac{1}{\sqrt{\Omega}} \partial_\mu + \frac{1}{2\Omega} \partial_\mu^2 + \mathcal{O}(\Omega^{3/2}). \end{aligned} \quad (19)$$

Employing these and Eq. (18) in Eq. (15) leads to

$$\begin{aligned} \partial_t P(\xi, \mu) - \sqrt{\Omega} (\dot{c} \partial_\xi + \dot{f} \partial_\mu) \\ = \left[-\sqrt{\Omega} g \left(\frac{\phi_C}{\phi} c \partial_\xi + \frac{\phi_F}{\phi} f \partial_\mu \right) \right. \\ \left. + \Omega^0 (\dots) + \frac{1}{\sqrt{\Omega}} (\dots) + \mathcal{O}(\Omega^{-3/2}) \right] P(\xi, \mu), \end{aligned} \quad (20)$$

where terms of the order Ω/K and higher are neglected. Initially, starting with a small population, these higher orders are very small because $\Omega \approx N_0$ and $N_0 \ll K$ holds. The orders Ω^0 and $1/\sqrt{\Omega}$ depend on $c, f, s, \bar{b}, \bar{c}, g, \partial_\xi, \partial_\mu, \xi, \mu$ and are not written out in this equation for clarity. By collecting terms of order $\sqrt{\Omega}$ and using the identities $n = c(t) + f(t)$ and $x = c(t)/[c(t) + f(t)]$ the deterministic equations (17) are obtained (for $K \rightarrow \infty$). Higher orders of Eq. (20) lead to a Fokker-Planck equation for $P(\xi, \mu)$. From this Fokker-Planck equation, differential equations for the first and second moments of the fluctuations can be obtained. The first moments are given by

$$\begin{aligned} \langle \dot{\xi} \rangle &= \left[\frac{g\phi_C}{\phi} + x(1-x) \partial_x \frac{g\phi_C}{\phi} \right] \langle \xi \rangle \\ &\quad - x^2 \partial_x \frac{g(x)\phi_C}{\phi} \langle \mu \rangle + \frac{1}{2n\sqrt{\Omega}} [(1-x)^2 \langle \xi^2 \rangle \\ &\quad - 2x(1-x) \langle \xi \mu \rangle + x^2 \langle \mu^2 \rangle] \partial_x^2 \frac{g\phi_C x}{\phi}, \\ \langle \dot{\mu} \rangle &= (1-x)^2 \partial_x \frac{g\phi_F}{\phi} \langle \xi \rangle + \left[\frac{g\phi_F}{\phi} - x(1-x) \partial_x \frac{g\phi_F}{\phi} \right] \langle \mu \rangle \\ &\quad + \frac{1}{2n\sqrt{\Omega}} [(1-x)^2 \langle \xi^2 \rangle - 2x(1-x) \langle \xi \mu \rangle + x^2 \langle \mu^2 \rangle] \\ &\quad \times \partial_x^2 \frac{g\phi_F(1-x)}{\phi}. \end{aligned} \quad (21)$$

Note that the second moments only couple at order $1/\sqrt{\Omega}$. Neglecting these higher orders, Eq. (21) is linear and has an unstable fixed point at $(\xi, \mu)^* = (0, 0)$.

Next, we analyze the impact of the second moments on the dynamics. Their coupling into Eq. (21) is only important for small times, when the first moments are still at the initial condition, the unstable fixed point $(\xi, \mu)^* = (0, 0)$. Therefore, it is appropriate to examine the second moments for small times, $t \rightarrow 0$. They then have the asymptotic form,

$$\partial_t \langle \xi^2 \rangle = 2ng \frac{\phi_C}{\phi} x, \quad \partial_t \langle \xi \mu \rangle = 0, \quad \partial_t \langle \mu^2 \rangle = 2ng \frac{\phi_F}{\phi} (1-x). \quad (22)$$

Due to the inhomogeneity of the differential equations, the second moments $\langle \xi^2 \rangle$ and $\langle \mu^2 \rangle$ immediately start to grow. These nonzero second moments now couple back into the first moments Eq. (21), and push them out of the unstable fixed point. To quantify this, the solution of Eq. (22) is employed in Eq. (21). The resulting equations are solved for small but finite times. As the increase of cooperation is caused by fluctuations, fluctuations have to establish first. As fixed time we here consider the doubling time of the initial population $t_d = 1/g(x)$. Within the time window $[0, t_d]$ evolution is neutral ($s \ll g(x)$) and thus $x = x_0$ holds. The

approximation leads to a lower bound for the strength of fluctuations. Furthermore, the initial conditions are given by $\langle \xi_0 \rangle = \langle \mu_0 \rangle = \langle \xi_0^2 \rangle = \langle \mu_0^2 \rangle = 0$. If the initially generated and asymmetrically enhanced fluctuations are large enough to overcome the selection disadvantage, the transient increase of cooperation arises. To quantify this, the total fraction of cooperators in the system has to be examined:

$$\frac{d}{dt} \langle x \rangle = \frac{\langle N_C \rangle}{\langle N_C + N_F \rangle} = \frac{\dot{x} + 1/\sqrt{\Omega} \langle \dot{\xi} \rangle}{n + 1/\sqrt{\Omega} (\langle \xi \rangle + \langle \mu \rangle)} - \frac{(xn + 1/\sqrt{\Omega}) (\langle \dot{\xi} \rangle + \langle \dot{\mu} \rangle)}{(n\sqrt{\Omega} + 1/\Omega (\langle \xi \rangle + \langle \mu \rangle))^2}. \quad (23)$$

For $\frac{d}{dt} \langle x \rangle > 0$ the transient increase of cooperation is present. The condition $\frac{d}{dt} \langle x \rangle = 0$ leads, to first order in s , to the transition line,

$$s = \frac{\partial_x \ln[g(x)]}{n(1/g(x))\Omega} \Big|_{x_0} = \frac{\partial_x g(x)}{n(1/g(x))\Omega g(x)} \Big|_{x_0}. \quad (24)$$

Here, Ω is given by the initial population size N_0 . For smaller s there is a transient increase in cooperation, while for larger s the level of cooperation decreases immediately. This resembles the condition for neutral evolution (e.g., [45,82]); evolution is only neutral for $sN \lesssim \text{const}$. Thus, only if fluctuations are strong during the initial phase of the dynamics, such that the system behaves neutrally, are they sufficient to overcome the selection pressure toward free-riders. The phase boundary and thereby the strength of the transient increase depends on $\partial_x g(x)|_{x_0}$ and $g(x_0)$. Both terms have antagonistic impacts on the transition line. The reason for this behavior is that the initial doubling time (i.e., the time during which fluctuations are the most pronounced) decreases with increasing $g(x_0)$. The positive enhancement relies on the growth advantage of more cooperative realizations, which depends on $\partial_x g(x)|_{x_0}$ at the beginning. Note that for nonlinear growth functions, where $\partial_x g(x)|_{x_0}$ also depends on x_0 , the transient increase can even be reduced by accounting for higher orders. This behavior was also experimentally observed in recent studies with microbes, where the growth advantage of cooperators was tuned [72]. In the next paragraph, we show that the calculated phase boundaries match our simulation results very well for several distinct global growth functions.

D. Phase diagrams

In the following we consider how the duration t_c of the transient increase in cooperation depends on the system parameters for the specific global growth function $g(x) = 1 + px$ (cf. Fig. 3). Then, the transition line between a transient increase $t_c > 0$, and an immediate decrease $t_c = 0$, given by Eq. (24), now reads

$$s = \frac{p}{n\Omega(1 + px_0)}, \quad (25)$$

where $n\Omega = 2N_0$. For smaller selection strength, $s < \frac{p}{n\Omega(1+px_0)}$, the asymmetric amplification of fluctuations is sufficient to overcome the selection disadvantage of cooperators while for larger selection strength, $s > \frac{p}{n\Omega(1+px_0)}$, free-riders prevail.

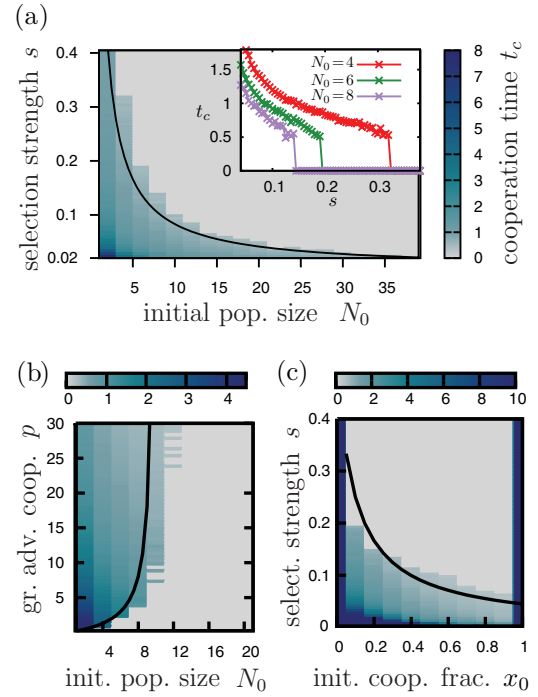


FIG. 3. (Color online) The transient increase of cooperation and its dependence on parameters. Encoded in gray (colored) scale, the cooperation time t_c is plotted for three different pairs of parameters: $\{N_0, s\}$, $\{N_0, p\}$, and $\{x_0, s\}$ in (a), (b), and (c), respectively. The boundary between the regimes of transient increase and immediate decrease are in good agreement given by Eq. (24), plotted as black lines. In the inset of (a), the cooperation time is shown for varying selection strength s : t_c sharply drops at the boundary. Not varied parameters are given by $p = 10, x_0 = 0.5$ in (a); $s = 0.05$ and $x_0 = 0.5$ in (b); $p = 10, N_0 = 6$ in (c).

In Fig. 3, we compare this result of the analytical calculations with the stochastic simulations. We observe that upon increasing the strength of selection s , which sets the advantage of free-riders, the cooperation time t_c decreases. In contrast, stronger demographic fluctuations, their strength scales as $1/\sqrt{N_0}$, prolong the duration of the transient increase [i.e., t_c increases with decreasing N_0 ; cf. Fig. 3(a)]. These two antagonistic effects lead to a sharp phase boundary between the regimes of transient increase ($t_c > 0$) and immediate decrease ($t_c = 0$); see inset of Fig. 3(a). Here, the cooperation time steeply drops to zero if the strength of selection exceeds a critical value. The boundary line is in good agreement with Eq. (25); cf. black line in Fig. 3(a).

In Fig. 3(b), the cooperation time is shown for varying initial population size N_0 and strength of the global fitness advantage due to cooperators p . Now, the phase boundary is determined by the interplay between the size of demographic fluctuations and its amplification due to the global fitness advantage of more cooperative populations. N_0 has to be small enough for the asymmetric amplification mechanism to be effective. Again, the phase boundary is in good agreement with Eq. (24); see solid black line in Fig. 3(b).

In Fig. 3(c), the cooperation time is plotted for varying initial cooperators fraction x_0 and selection strength s . We find that the cooperation time decreases with increasing x_0 .

Remarkably, for small x_0 , the amplification mechanism is especially pronounced and therefore able to compensate comparably large selection strengths s . This is again well described by Eq. (25) [see Fig. 3(c), solid black line]. The observation is of possible relevance for the evolution of cooperation since it allows a small initial fraction of cooperators to proliferate in the population.

Taken together, our analytical calculations provide a mechanistic understanding for the transient increase of cooperation and its dependence on the system parameters s , p , x_0 , and N_0 . We have quantitatively calculated the phase boundary and gained insights into the basic nature of the transient increase: First, the probability distribution in the cooperator fraction $\langle x \rangle$ is broadened due to neutral evolution; note that Eq. (25) resembles the condition for neutral evolution [45,82]. Second, these initially generated fluctuations are asymmetrically amplified and can, therefore, cause an increase in the level of cooperation.

E. The dormancy scenario

Let us now consider the dormancy scenario where the ability to reproduce decreases with increasing population size. For specificity, we assume the global birth and death functions to be given by

$$g(x, N) = 1 + px - \frac{N}{K}, \quad \text{and} \quad d = 0. \quad (26)$$

In this scenario individuals do not die but the birth rates decrease toward zero as the population size reaches its carrying capacity. The relative functions, f_S and w_S , are the same as before; the weakness terms are constant and the fitness terms given by Eq. (12).

To understand the differences in the evolutionary outcome, we again study the deterministic rate equations first. They are given by

$$\partial_t N = \left(1 + px - \frac{N}{K}\right) N, \quad (27a)$$

$$\partial_t x = -s \left(1 + px - \frac{N}{K}\right) x(1-x). \quad (27b)$$

The equation describing population growth is formally identical to the corresponding equation in the balanced growth scenario Eq. (17b). Differences arise because in the present case there is mutual feedback between internal and population dynamics. This coupling implies that both arrest once the population size reaches its carrying capacity. In the arrested state there is a relation between population size N^* and composition x^* : $1 + px^* = N^*/K$. Thus, the reached stationary state (x^*, N^*) depends on the initial values x_0 and N_0 . The precise mapping depends on the selection strength s . For weak selection (small s), the population dynamics is much faster than the internal dynamics and hence the population size reaches a stationary state while the composition is still at its initial value x_0 [i.e., $N^* = K(1 + px_0)$]. In contrast, for strong selection, cooperators go extinct quickly with $x^* = 0$ such that the stationary population size becomes $N^* = K$. An example for the deterministic dynamics is shown as a solid black line in Fig. 4. As for balanced growth, the deterministic dynamics

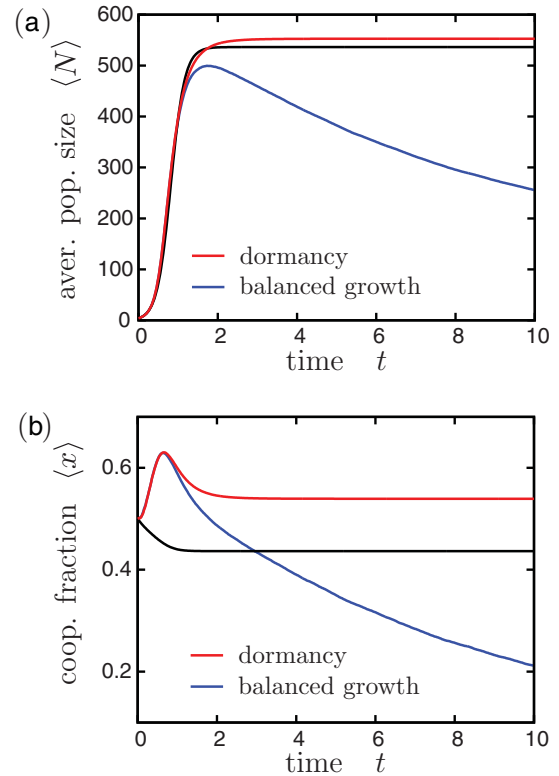


FIG. 4. (Color online) The dilemma of cooperation in the dormancy scenario. (a) The growth dynamics. Initially, the small population grows exponentially until growth is stopped [cf. light gray (red) line]. This behavior is well described by the deterministic equation (27a); see black line. In contrast, for the balanced growth scenario, the dynamics continue and, due to selection, the population size falls again; see dark gray (blue) line. (b) The fraction of cooperators. Equal to the balanced growth scenario, dark gray (blue) line, there is an initial increase of cooperation due to asymmetric amplification within the dormancy scenario. Again, this is not described by the deterministic approximation Eq. (27b). However, in contrast to the balanced growth scenario, the higher level of selection is later fixed due to the stop in growth dynamics. Parameters are given by $s = 0.05$, $p = 10$, and $N_0 = 4$.

exhibits a strictly monotonous decrease in the cooperator fraction, with the difference that now the asymptotic value is arrested at some finite value. These differences are also reflected in the stochastic dynamics, where the asymmetric amplification mechanism is acting (cf. Fig. 4). In the initial phase of the dynamics, this mechanism affects the time evolution of the cooperator fraction in the same way as for balanced growth, namely it leads to an initial increase of cooperation. Differences in birth and death rates Eqs. (13) and (26) are negligible for small population size. The arrest of the dynamics only becomes effective at later times where an increase in population size implies a significantly declining birth rate. As a consequence even the stochastic dynamics becomes arrested such that the initial rise in the cooperator fraction may become manifested as a permanent increase. This will be the case if the dynamics becomes arrested during the

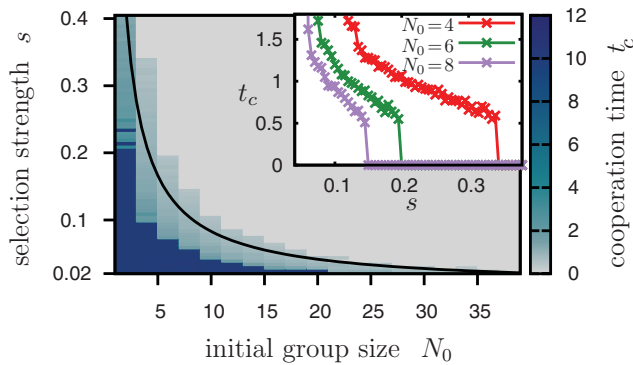


FIG. 5. (Color online) The transient increase of cooperation for the dormancy scenario. The cooperation time t_c depending on the initial population size N_0 and the strength of selection s . The condition for a transient increase of cooperation to occur is still given by Eq. (24) (black line). In addition, due to the stop in growth dynamics, there is an additional regime, where the increase becomes permanent [dark gray (dark blue) area]. The permanent increase is also shown in the inset, where the cooperation time is shown for varying strength of selection. If, for a given initial population size, selection is sufficiently slow compared to fixation of the growth dynamics, the increase of cooperation becomes permanent. Parameters are given by $p = 10, x_0 = 0.5$.

time window where the asymmetric amplification mechanism acts; see red line in Fig. 4(b).

In summary, there are now three scenarios for the dynamics (cf. Fig. 5). In addition to the immediate decline and transient increase there is now also a *permanent increase* in the cooperator fraction. The analytical expression separating the regimes of transient increase and immediate decline still holds Eq. (25) because it is due to the same mechanism as before. We did not manage to derive an explicit expression for the transition line to permanently increase. However, as the existence of a permanent increase in the cooperator fraction depends on the asymmetric amplification mechanism, the regime of permanent increase is bounded by a hyperbolic line beneath the one given by Eq. (24). The latter is a necessary but not a sufficient condition for the permanent increase to occur.

IV. CONCLUSION

In this article, we have given a synthesis of evolutionary and population dynamics. This is based on the understanding that birth and death events are the driving forces underlying changes in the size as well as the composition of a population [10]. Both processes are inherently stochastic and inevitably lead to demographic fluctuations whose magnitude depends on the population size. The ensuing stochastic formulation thereby naturally accounts for the coupling between internal evolutionary dynamics and population dynamics. The evolutionary outcome of the dynamics is determined by the interplay between selection pressure and random drift caused by demographic fluctuations. Since our approach allows one to study evolutionary dynamics with varying population size we can explore ecological situations where the relative impact of deterministic and stochastic evolutionary forces

change with time. Thereby demographic fluctuations may lead to a dynamics which is qualitatively different from the corresponding deterministic dynamics: Beyond creating a broad distribution in size and composition, the coupling can strongly distort the distribution and thus strongly influence average values. For the public good scenario, discussed in this paper, this corresponds to an asymmetric amplification mechanism which yields a transient increase in the level of cooperation.

In the absence of a coupling between internal evolution and population dynamics, the impact of population size on the internal evolutionary dynamics reduces to a modulation in the strength of demographic fluctuations. If, in addition, the deterministic population dynamics exhibits a strongly attractive fixed point at a finite population size, our model maps to a standard description of evolutionary dynamics (i.e., the Moran process).

The general observations made for the coupled stochastic dynamics are exemplified by the dilemma of cooperation in growing populations. Here, fluctuations in combination with growth lead to a transient increase of cooperation. The origin of this increase is the asymmetric amplification of fluctuations. As the presence of cooperators increases the growth rates, fluctuations toward those are enhanced. Therefore growth dynamics cannot be ignored but can be an essential part in evolution. Furthermore, the details of the growth dynamics can be crucial in determining the evolutionary outcome. As we have considered for the dilemma of cooperation and two extremes of microbial growth dynamics, cooperation can either increase only transiently or the higher level can even fixate due to dormancy. Our analytical derived transition line provides the same sufficient condition for the transient increase in both scenarios. Furthermore, the same line is also a necessary condition for the permanent increase for the dormancy scenario. In actual populations, both scenarios are present with a fraction of 20%–80% dormant bacteria [93]. While the transient increase does not depend on this fraction, the permanent increase is smaller than for purely dormant bacteria. The discussed scenarios for the increase of cooperation, rely on demographic fluctuations which are especially pronounced during population bottlenecks. Such bottlenecks may be caused by seasonal changes of the environment, migration into new habitats, and range expansion (e.g., [46,95–99]). In addition, if the permanent increase is not present, repeated bottlenecks provoking regular occurring growth phases can favor cooperative behavior by stabilizing a former transient increase. This becomes especially important in the context of biofilms where population structure and involved restructuring mechanisms can drastically change evolutionary outcome [66,71,72].

ACKNOWLEDGMENTS

We thank Jan-Timm Kuhr for discussion. Financial support from the Deutsche Forschungsgemeinschaft through the SFB TR12 “Symmetries and Universalities in Mesoscopic Systems” and the Nano Initiative Munich (NIM) is gratefully acknowledged.

- [1] B. Charlesworth, *Ecology* **52**, 469 (1971).
- [2] J. Roughgarden, *Ecology* **52**, 453 (1971).
- [3] J. Roughgarden, *Theory of Population Genetics and Evolutionary Ecology: An Introduction* (Macmillan, New York, 1979).
- [4] L. Ginzburg, *Theory of Natural Selection and Population Growth*, Series in Evolutionary Biology (Benjamin Cummings, San Francisco, 1983).
- [5] L. D. Mueller, *Am. Nat.* **132**, 786 (1988).
- [6] B. Charlesworth, *Evolution in Age-Structured Populations* (Cambridge University Press, Cambridge, 1994).
- [7] R. Cressman and G. Vickers, *J. Theor. Biol.* **184**, 359 (1997).
- [8] C. Hauert, M. Holmes, and M. Doebeli, *Proc. R. Soc. London B* **273**, 2565 (2006).
- [9] C. Hauert, J. Y. Wakano, and M. Doebeli, *Theor. Popul. Biol.* **73**, 257 (2008).
- [10] A. Melbinger, J. Cremer, and E. Frey, *Phys. Rev. Lett.* **105**, 178101 (2010).
- [11] J. Maynard Smith, *Evolution and the Theory of Games* (Cambridge University Press, Cambridge, 1982).
- [12] J. Hofbauer and K. Sigmund, *Evolutionary Games and Population Dynamics* (Cambridge University Press, Cambridge, 1998).
- [13] M. A. Nowak, *Evolutionary Dynamics: Exploring the Equations of Life* (Belknap Press, Cambridge, 2006).
- [14] G. Szabó and G. Fáth, *Phys. Rep.* **446**, 97 (2007).
- [15] R. Axelrod and W. Hamilton, *Science* **211**, 1390 (1981).
- [16] E. Szathmari and L. Demeter, *J. Theor. Biol.* **128**, 463 (1987).
- [17] M. A. Nowak and R. M. May, *Nature (London)* **359**, 826 (1992).
- [18] M. A. Nowak, S. Bonhoeffer, and R. M. May, *Proc. Natl. Acad. Sci. USA* **91**, 4877 (1994).
- [19] G. Szabó and C. Hauert, *Phys. Rev. Lett.* **89**, 118101 (2002).
- [20] C. Hauert and M. Doebeli, *Nature (London)* **428**, 643 (2004).
- [21] H. Ohtsuki, C. Hauert, E. Lieberman, and M. A. Nowak, *Nature (London)* **441**, 502 (2006).
- [22] J. M. Pacheco, A. Traulsen, and M. A. Nowak, *Phys. Rev. Lett.* **97**, 258103 (2006).
- [23] F. C. Santos, J. M. Pacheco, and T. Lenaerts, *Proc. Natl. Acad. Sci. USA* **103**, 3490 (2006).
- [24] C. P. Roca, J. A. Cuesta, and A. Sanchez, *Phys. Rev. E* **80**, 046106 (2009).
- [25] C. P. Roca, J. A. Cuesta, and A. Sanchez, *Phys. Life. Rev.* **6**, 208 (2009).
- [26] T. Reichenbach, M. Mobilia, and E. Frey, *Phys. Rev. E* **74**, 051907 (2006).
- [27] T. Reichenbach, M. Mobilia, and E. Frey, *Nature (London)* **448**, 1046 (2007).
- [28] T. Antal and I. Scheuring, *Bull. Math. Biol.* **68**, 1923 (2006).
- [29] J. Cremer, T. Reichenbach, and E. Frey, *Eur. Phys. J. B* **63**, 373 (2008).
- [30] M. Peltomäki and M. Alava, *Phys. Rev. E* **78**, 031906 (2008).
- [31] T. Reichenbach, M. Mobilia, and E. Frey, *J. Theor. Biol.* **254**, 368 (2008).
- [32] B. Andrae, J. Cremer, T. Reichenbach, and E. Frey, *Phys. Rev. Lett.* **104**, 218102 (2010).
- [33] J. C. Claussen and A. Traulsen, *Phys. Rev. Lett.* **100**, 058104 (2008).
- [34] A. Traulsen and M. A. Nowak, *Proc. Natl. Acad. Sci. USA* **103**, 10952 (2006).
- [35] C. E. Tarnita, T. Antal, H. Ohtsuki, and M. A. Nowak, *Proc. Natl. Acad. Sci. USA* **106**, 8601 (2009).
- [36] C. P. Roca, J. A. Cuesta, and A. Sanchez, *Phys. Rev. Lett.* **97**, 158701 (2006).
- [37] P. M. Altrock and A. Traulsen, *Phys. Rev. E* **80**, 011909 (2009).
- [38] C. S. Gokhale and A. Traulsen, *Proc. Natl. Acad. Sci. USA* **107**, 5500 (2010).
- [39] L. Worden and S. A. Levin, *J. Theor. Biol.* **245**, 411 (2007).
- [40] M. A. Nowak, A. Sasaki, C. Taylor, and D. Fudenberg, *Nature (London)* **428**, 646 (2004).
- [41] R. A. Blythe and A. J. McKane, *J. Stat. Mech.* (2007) P07018.
- [42] T. Galla, *Phys. Rev. Lett.* **103**, 198702 (2009).
- [43] A. Traulsen, J. C. Claussen, and C. Hauert, *Phys. Rev. Lett.* **95**, 238701 (2005).
- [44] A. Traulsen, M. A. Nowak, and J. M. Pacheco, *Phys. Rev. E* **74**, 011909 (2006).
- [45] J. Cremer, T. Reichenbach, and E. Frey, *New J. Phys.* **11**, 093029 (2009).
- [46] J. Murray, *Mathematical Biology*, 1+2 (Springer, New York, 2002).
- [47] A. Hastings, *Population Biology: Concepts and Models* (Springer Verlag, New York, 1997).
- [48] M. Kot, *Mathematical Ecology* (Cambridge University Press, Cambridge, 2001).
- [49] P. F. Verhulst, *Corresp. Math. Phys.* **10**, 113 (1838).
- [50] J. Monod, *Annu. Rev. Microbiol.* **3**, 371 (1949).
- [51] G. J. Velicer, *Trends Microbiol.* **11**, 330 (2003).
- [52] L. Hall-Stoodley, J. W. Costerton, and P. Stoodley, *Nat. Rev. Micro.* **2**, 95 (2004).
- [53] R. E. Lenski, M. R. Rose, S. C. Simpson, and S. C. Tadler, *Am. Nat.* **138**, 1315 (1991).
- [54] S. F. Elena and R. E. Lenski, *Nat. Rev. Gen.* **4**, 457 (2003).
- [55] S. A. West, A. S. Griffin, A. Gardner, and S. P. Diggle, *Nat. Rev. Microbiol.* **4**, 597 (2006).
- [56] A. Buckling, R. C. Maclean, M. A. Brockhurst, and N. Colegrave, *Nature (London)* **457**, 824 (2009).
- [57] M. E. Hibbing, C. Fuqua, M. R. Parsek, and S. B. Peterson, *Nat. Rev. Microbiol.* **8**, 15 (2010).
- [58] E. Frey, *Physica A* **389**, 4265 (2010).
- [59] J. B. Xavier, *Molecular Systems Biology* **7**, 483 (2011).
- [60] J. A. Damore and J. Gore, *J. Theor. Biol.* (in press).
- [61] D. Greig and M. Travisano, *Proc. R. Soc. London B* **271**, S25 (2004).
- [62] J. Gore, H. Youk, and A. van Oudenaarden, *Nature (London)* **459**, 253 (2009).
- [63] R. C. MacLean, A. Fuentes-Hernandez, D. Greig, L. D. Hurst, and I. Gudelj, *PLoS Biol.* **8**, e1000486 (2010).
- [64] J. Strassmann, Y. Zhu, and D. Queller, *Nature (London)* **408**, 965 (2000).
- [65] G. J. Velicer and M. Vos, *Annu. Rev. Microbiol.* **63**, 599 (2009).
- [66] P. B. Rainey and K. Rainey, *Nature (London)* **425**, 72 (2004).
- [67] C. D. Nadell, J. B. Xavier, and K. R. Foster, *FEMS Microbiol. Rev.* **33**, 206 (2009).
- [68] S. P. Diggle, A. S. Griffin, G. S. Campbell, and S. A. West, *Nature (London)* **450**, 411 (2007).
- [69] A. Buckling, F. Harrison, M. Vos, M. A. Brockhurst, A. Gardner, S. A. West, and A. Griffin, *FEMS Microbiol. Ecol.* **62**, 135 (2007).
- [70] R. Kümmerli, A. Gardner, S. West, and A. S. Griffin, *Evolution* **63**, 939 (2009).
- [71] J. S. Chuang, O. Rivoire, and S. Leibler, *Science* **323**, 272 (2009).

- [72] J. S. Chuang, O. Rivoire, and S. Leibler, *Molec. Syst. Biol.* **6**, 398 (2010).
- [73] C. W. Gardiner, *Handbook of Stochastic Methods* (Springer, New York, 2007).
- [74] N. Van Kampen, *Stochastic Processes in Physics and Chemistry*, 2nd ed., North-Holland Personal Library (North Holland, Amsterdam, 2001).
- [75] T. Yoshida, L. E. Jones, S. P. Ellner, G. F. Fussmann, and N. G. Hairston, *Nature (London)* **424**, 303 (2003).
- [76] N. G. Hairston, S. P. Ellner, M. A. Geber, T. Yoshida, and J. A. Fox, *Ecol. Lett.* **8**, 1114 (2005).
- [77] I. Saccheri and I. Hanski, *Trends Ecol. & Evol.* **21**, 341 (2006).
- [78] S. P. Carroll, A. P. Hendry, D. N. Reznick, and C. W. Fox, *Functional Ecology* **21**, 387 (2007).
- [79] P. A. Moran, *The Statistical Processes of Evolutionary Theory* (Clarendon Press Oxford, Oxford, 1964).
- [80] W. J. Ewens, *Mathematical Population Genetics*, 2nd ed. (Springer, New York, 2004).
- [81] A. Traulsen, J. C. Claussen, and C. Hauert, *Phys. Rev. E* **74**, 011901 (2006).
- [82] M. Kimura, *The Neutral Theory of Molecular Evolution* (Cambridge University Press, Cambridge, 1983).
- [83] P. M. Altrock and A. Traulsen, *New J. Phys.* **11**, 013012 (2009).
- [84] P. Stoodley, K. Sauer, D. G. Davies, and J. W. Costerton, *Annu. Rev. Microbiol.* **56**, 187 (2002).
- [85] S. E. Jones and J. T. Lennon, *Proc. Natl. Acad. Sci. USA* **107**, 5881 (2010).
- [86] J. T. Lennon and S. E. Jones, *Nat. Rev. Micro.* **9**, 119 (2011).
- [87] K. Lewis, *Nat. Rev. Micro.* **5**, 48 (2007).
- [88] N. Q. Balaban, J. Merrin, R. Chait, L. Kowalik, and S. Leibler, *Science* **305**, 1622 (2004).
- [89] E. Kussell, R. Kishony, N. Q. Balaban, and S. Leibler, *Genetics* **169**, 1807 (2005).
- [90] I. G. de Jong, P. Haccou, and O. P. Kuipers, *BioEssays* **33**, 215 (2011).
- [91] C. E. Cáceres and A. J. Tessier, *Ecology* **84**, 1189 (2003).
- [92] J. S. Webb, L. S. Thompson, S. James, T. Charlton, T. Tolker-Nielsen, B. Koch, M. Givskov, and S. Kjelleberg, *J. Bacteriol.* **185**, 4585 (2003).
- [93] J. J. Cole, *Ecosystems* **2**, 215 (1999).
- [94] D. Gillespie, *J. Comput. Phys.* **22**, 403 (1976).
- [95] O. Hallatschek, P. Hersen, S. Ramanathan, and D. R. Nelson, *Proc. Nat. Acad. Sci. USA* **104**, 19926 (2007).
- [96] C. D. Nadell, K. R. Foster, and J. B. Xavier, *PLoS Comput. Biol.* **6**, e1000716 (2010).
- [97] O. Hallatschek, *PLoS Comput. Biol.* **7**, e1002005 (2011).
- [98] J.-T. Kuhr, M. Leisner, and E. Frey, *New J. Phys.* **13**, 113013 (2011).
- [99] J. Cremer, A. Melbinger, and E. Frey (unpublished).

3 The Dilemma of Cooperation in Structured Populations

The previous chapter was concerned with the coupling of evolutionary and population dynamics and how such a coupling in combination with demographic fluctuations can result in a transient increase of cooperation. Taking this as a starting point, the idea that repeated population bottlenecks may lead to a permanent rather than a transient increase, seems natural. Therefore, we now study the dilemma of cooperation in rearranging group-structured populations. Before elaborating on the consequences of these reoccurring population bottlenecks, we give an overview on the dilemma of cooperation. Then, we introduce the framework of multilevel selection. Furthermore, we discuss group and kin selection, two closely related theories explaining cooperative behavior. Finally, we introduce a model accounting for reoccurring population bottlenecks and show that it is capable of explaining both, the evolution and maintenance of cooperation.

3.1 The Dilemma of Cooperation

Cooperative behavior is ubiquitous in nature. From rudimentary species, such as bacteria, to insects and mammals, individuals help one-another, apparently disregarding the evolutionary disadvantages that such assistance entails. In terms of Darwinian selection, these costs are tantamount to a smaller fitness, which ultimately would lead to the extinction of the cooperating species without any further influences. Essentially, this is the dilemma of cooperation: Cooperators die out, even though it was optimal if the whole population would cooperate. How nonetheless cooperation can be maintained and even has evolved in the first place, is a puzzling question in evolutionary biology [120]. Also Darwin was aware of this problem and stated¹ in “Origin of the Species” [14]:

I (...) will confine myself to one special difficulty, which at first appeared to me insuperable, and actually fatal to my whole theory.

By considering selection in more complex settings such as structured populations or individuals with advanced abilities like memory and recognition, the dilemma can in principle be solved. Before discussing these possible solutions in more detail, let us first present some examples for cooperation in the realm of nature elucidating the variety and omnipresence of such social behavior, see Fig. 3.1. In human behavior, cooperation and the ensuing dilemma can be found on almost every scale and in diverse fields ranging from politics to economics or

¹The citation actually refers to eusociality, which is an especially pronounced form of cooperation discussed in the following.



Figure 3.1: Three examples for cooperative behaviors in the realm of nature. Monkeys raise the alarm to warn their conspecifics. The picture was taken by Angelika Bentin who kindly provided it [121]. Worker bees support their queen which is reproducing solely (eusociality). The picture was taken by Dr. Silke Meyer-Arndt who kindly provided it [122]. In bacterial biofilms, some bacteria produce public goods and provide it to all other members of the colony. The picture is taken from [123].

sociology. This starts with interactions of individuals in small entities like families, *e.g.* doing the household, through to whole states, *e.g.* the reduction of CO₂ emissions. Humans are endowed with a broad range of mechanisms ensuring cooperation [124]. Due to our ability to recognize and remember other individuals, we can distinguish cooperators from cheaters and thereby prevent an interaction with them, warn others, or even punish them [125].

Other examples for cooperative behavior in mammals are the alarm calls of birds and monkeys [126]. By raising these alarms, they warn their fellows whose risk to fall to prey is thereby reduced. But as they increase their own chances for being caught by a predator at the same time, the dilemma arises. One of the most extreme examples for cooperation can be found in eusocial populations [127]. This eusocial behavior mainly emerges in insect populations, *e.g.* bees and ants, but also the naked mole rat, a mammal living in eastern africa, shows eusociality. In these species only a few individuals reproduce, *e.g.* the queen bee. All others, the so-called workers, dedicate themselves to raise the queen's offspring.

But also for less complex species, remarkable forms of cooperation are present. For example, the slime mold *Dictyostelium discoideum* forms multicellular spores if nutrient supply is low [128]. These spores consist of a stalk and an outer membrane built of individuals which do not survive but protect the inner ones. Similar sporulation is also present in myxobacteria colonies [129]. This is only one example for the astonishing forms of cooperation featured by bacterial populations. A more detailed overview is presented in the following section.

3.1.1 Social Bacteria

Bacteria are the most widespread life forms on our planet. These, only at first glance, simple organisms exhibit tremendous diversity, specification and adaptedness to various environmental conditions. Bacteria show various phenotypes [130] depending on the environmental

conditions. For instance, during prolonged starvation *Bacillus subtilis* differentiates into phenotypic distinct cell types to realize different survival strategies like the uptake of foreign RNA (competence) [131, 132, 133]. Even more surprising, bacteria also act socially: They cooperate by the production of a public good [134, 135], divide labor [136] and use quorum sensing for the organization of a whole population [137]. A prominent example for a cooperating microbe is the proteobacterium *Pseudomonas aeruginosa* [135]. Iron, which is usually bound in large cluster, is essential for the metabolism of these bacteria. Therefore, some individuals, the so-called producers, provide siderophores, which are iron scavenging proteins, and release them as a public good into the environment. Because of their large binding affinity to iron, these proteins can solve single iron molecules and build siderophore-iron complexes. The freely diffusing complexes can be equally taken up by cooperators and non-contributing free-riders. The dilemma arises due to the metabolic costs associated with the production of the public good: Producers replicate slower than free-riders and thereby have a fitness disadvantage. There exist several other examples for public goods, *e.g.* sticky polymers connecting a microbial colony and causing its ability to swim as observed in *Pseudomonas fluorescens* [134] or invertases hydrolyzing disaccharides into monosaccharides in the budding yeast *Saccharomyces cerevisiae* [138, 139, 140].

Bacteria often live in complex biofilms heightening the importance of social behavior and conflicts. [141, 130, 142]. In such biofilms, bacteria compete for resources or support each other by cooperation and division of labor [143, 144, 145]. Thus, a biofilm, as a complex entity built up of many independent subunits, is a model system for understanding the evolution of multicellularity [144]. Much research concerning the social behavior of bacteria is done in simplified model systems offering the possibility to gain understanding under well-defined conditions [146]. Experiments have been performed in artificial environments ranging from nano-landscapes on a chip [147, 148] to simple rearranging group-structures [135, 149, 82]. The latter approach is especially useful for studying the influence of reoccurring population bottlenecks. For instance, these bottlenecks can account for species showing a life cycle. In a broader interpretation group structure is also a null model for dispersal of bacteria into new habitats where an initially small founder colony grows and becomes a large subpopulation [141, 130]. Such synthetic biology experiments, which help to clarify the mechanisms promoting cooperation in simple setups, may also lead to a broader understanding of social behavior in complex biological environments.

3.1.2 *Dicrocoelium Dentriticum* - the Small Liver Fluke

The small liver fluke *Dicrocoelium dentriticum* is another remarkable example for cooperative behavior in nature. It is a parasite affecting cattle and sheep and has an astonishing life cycle where cooperation plays an essential role. The life cycle consists of three consecutive steps [150], see Fig 3.2:

1. An adult *D. dentriticum* lives in the liver of its primary hosts which are cows and sheep usually. Here, it reproduces sexually. The thereby generated eggs are excreted afterwards.
2. Then the eggs are incorporated by snails, the first intermediate hosts. There, they develop to *larvae* which the snail excretes in slime balls.

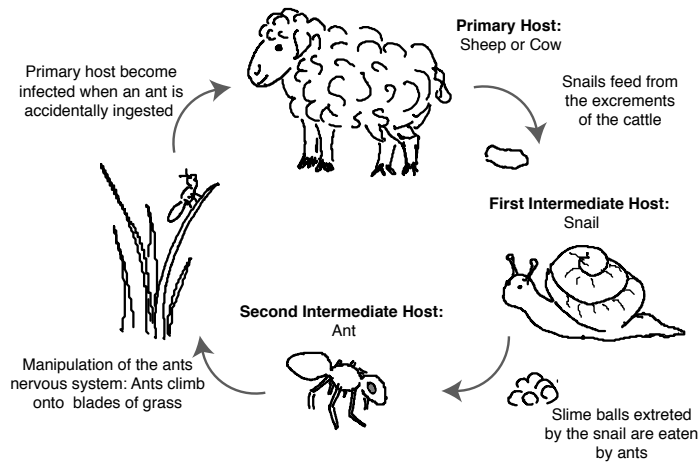


Figure 3.2: Life cycle of *D. dentriticum*. For a more detailed description see text.

3. The slime balls are eaten by ants, the second intermediate hosts, where they continue their development with asexual reproduction and become *cercariae*. The next step in their development is truly astonishing. Most of the cercariae stay in the gut of the ant, while a single one (or a few, this point is not clear in literature) sacrifices itself for the sake of the whole colony. It enters the ganglion, the nervous system of the ant, and manipulates the host's behavior in the following way: Each night an infected ant climbs onto a blade of grass where its chances of being eaten by cows or sheep are increased. At days, sun would kill the ant including the parasite. This is avoided as the ant leaves the blade of grass and fulfills its standard daily routine till the next night comes. Finally, the ant is eaten and the cycle restarts. The cycle as described above is well accepted in literature, but still many details are not known. This especially concerns the last step of the cycle and its interpretation as stated above.

In this life cycle the most extreme form of cooperation emerges: One individual sacrifices itself in order to render the survival of a whole subpopulation possible. An infiltration by cheaters would be fatal, as the fraction of cooperators would decrease until no cooperators are left and the whole population would go extinct.

The solution of the dilemma is the existence of subpopulations [151]. Groups containing no or just a few cooperative liver fluke larvae have a smaller probability to continue their live cycle. Therefore, as illustrated in Fig. 3.3, two antagonistic effects influence the time evolution of the fraction of cooperators: On the one hand its fraction is decreased due to the death of one cooperator manipulation the ganglion. On the other hand groups with no cooperators die out and the probability distribution is shifted to more cooperative groups.

By evaluating this idea mathematically, a condition for the maintenance of cooperation can be stated. For simplicity let us consider only one intermediate host which takes up N_0 liver fluke eggs according to a probability distribution $P(N_C)$, where N_C is the number of cooperators. In the worst case scenario for cooperators, this is a binomial distribution, *i.e.* there is no positive assortment mechanism favoring larger conglomerations of cooperators. In the host, the eggs become larvae and start reproduction such that the total number and the number

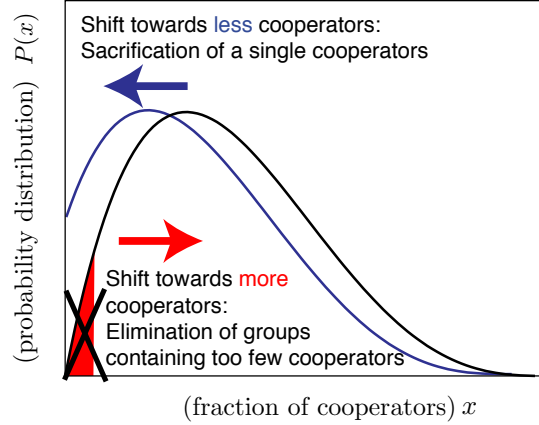


Figure 3.3: The influences of the life cycle of *D. dentriticum* on the probability distribution. Due to the selection disadvantage of cooperators, it is shifted to less cooperators during each life cycle. In contrast, the extinction of subpopulations with a low level of cooperators causes a shift to the right.

of cooperators increase to N' and N'_C , respectively. During this phase, also the probability distribution changes to $P'(N'_C)$. In fact, it is smoothened and broadened due to reproduction events, but its mean is still given by $x_0 = \langle N_C/N \rangle_{t=0}$, because both types of individuals reproduce at the same rate. To calculate the total change in the probability distribution and thereby its mean, two facts have to be considered. First, the mean is shifted to the left due to the death of a cooperator in each ant,

$$\langle N'_C \rangle \propto \sum_{N'_C} P'(N'_C)(N'_C - 1) = x_0 N' - (1 - P'(0)) = x_0 N' - 1 + P(0), \quad (3.1)$$

where the conditions $\sum_{N'_C} P'(N'_C)N'_C = x_0 N'$, $\sum_{N'_C} P'(N'_C) = 1$, and the fact that the probability for non-cooperative subpopulations does not change over time, $P'(0) = P(0)$, are employed. To account for the positive shift in the probability distribution caused by the extinction of non-cooperative subpopulations, the probability distribution has to be normalized again. Therefore, it has to be divided by the probability that a subpopulation continues the life cycle, *i.e.* the probability that initially at least one cooperator is present in the group, $1 - P(0)$. The resultant fraction of cooperators is given by,

$$x' = \underbrace{\frac{x_0}{1 - P(0)}}_{\text{Group Advantage of Cooperators}} - \underbrace{\frac{1}{N'}}_{\text{Select. Disadv. of Cooperators}}. \quad (3.2)$$

Note that a second intermediate host would additionally broaden the distribution and increase the probability $P(0)$. Therefore, the advantage of cooperators would be even larger than in Eq. (3.2). For the particular example discussed above, this approach might be extended by a certain probability that also subpopulations without any cooperators survive. In addition, the fact, that not every cooperator accomplishes manipulating the ant can be considered by a success probability $P_s(N'_C)$. If the per capita manipulation success of cooperators, s ,

was independent of the number of cooperators in the host, it would be given by $P_s(N'_C) = s^{N'_C}$. However, all these extensions do not alter the qualitative results and for a quantitative discussions the experimental data is still lacking.

3.2 Possible Solutions Solving the Dilemma

Cooperative behavior is a central thread in evolutionary theory. The solutions to the ensuing dilemma are as diverse as the observed forms of cooperation [152, 153]. In general, they can be subdivided into two classes: reciprocity and structure.

The first one, reciprocity basically relies on the assumption that individuals possess advanced abilities like memory and recognition. Due to these skills they may remember their interaction partner's strategy and adjust their own behavior accordingly. Depending on how this adjustment is achieved one can distinguish direct and indirect reciprocity, depending on whether the reward for cooperation is given by the same interaction partner or by someone else in the population [153, 154, 155]. Another related idea is punishment penalizing defecting individuals [125, 156, 157].

But cooperative behavior can also be maintained without such sophisticated abilities. Instead structure organizing individuals into subpopulations, in which members interact with each other more likely, increases the survival chances of cooperators [158, 159]. For example interactions on lattices [160, 161, 162, 163], networks [164, 165, 166] or set-structured populations [167, 168] can favor cooperation. Note that in literature sometimes the effect of spatial structure, especially networks, is also called reciprocity [154], since networks can 'memorize' previous interactions by relinking. In this thesis, we focus on interaction in groups [169, 170, 171, 172, 173, 174, 175, 140] which can be embedded in the framework of multilevel selection [21, 176] as explained in the following.

3.2.1 Multilevel Selection

Examining the example of *D. dentriticum*, we have already learned that in principle the disadvantage of cooperators can be overcome by advantages on a higher level². This idea is generalized in the framework of multilevel selection [21]. As illustrated in Fig. 3.4, on the lower level 1 different phenotypes interact in subpopulations under the pressure of selection. Thereby, the composition of a subpopulation can be changed. On a higher level 2 these subpopulations compete against each other analogously to level 1. Hence, the composition of such a subpopulation corresponds to its phenotype which determines the fitness. Analogously, even more levels can be introduced each of them consisting of entities whose phenotypes depend on the dynamics on the levels below. Therefore, disadvantages arising on one level must not necessarily lead to the extinction of the corresponding species, but can be balanced by advantages on other levels. For *D. dentriticum* this advantage of a subpopulation (higher level) is caused by better chances for infecting a host. In bacteria, the growth rate or viability

²For the small liver fluke, the advantage on the higher level arises as subpopulations consisting of only a few individuals have a reduced probability to infect their primary host.

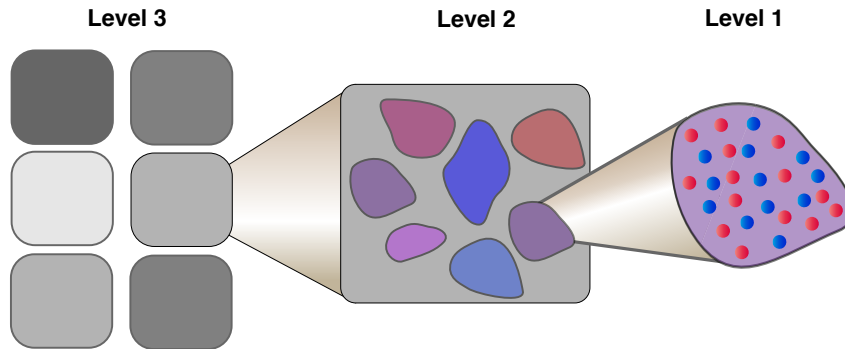


Figure 3.4: Illustration of selection acting on three different levels.

of a subpopulation containing more cooperators can be increased leading to an advantage on the level of these subpopulations.

In recent years, the theory of multilevel selection has become of considerable interest concerning the question of multicellularity, which again is an example for the dilemma of cooperation [177][56]: How can single cells build highly organized entities like human beings [178]? A single cell, which is not contributing but only reproducing as fast as possible would lead to a failure of the whole organism³. Analogous problems arise on various scales, *e.g.* on the gene, chromosome and organelle level, leading to the view that selection takes places on different levels to sustain such high forms of organization. How and under which conditions, these major transitions, *e.g.* from unicellular to multicellular life, can emerge is a tackling question [55, 179].

3.2.2 Hamilton's Rule

As we have seen above, the disadvantage of cooperative behavior can in principle be overcome by advantages on higher levels of selection. Hamilton's rule is a simple inequality comparing the benefits arising from cooperation with its total costs [79, 180],

$$\mathcal{R}\mathcal{B} > \mathcal{C} \quad (3.3)$$

where \mathcal{R} is the relatedness, which is a measure for the amount of the benefit \mathcal{B} directly supporting cooperators, and \mathcal{C} are the costs. A common misunderstanding concerns the interpretation of \mathcal{R} , \mathcal{B} and \mathcal{C} . These quantities are some complex functions assessing the relatedness, benefit and costs. They are not necessarily their direct measurable values, *e.g.* the energy which is needed for providing the benefit. Therefore, a short derivation of Hamilton's rule is provided to clarify the meaning of \mathcal{R} , \mathcal{B} and \mathcal{C} .

Hamilton's rule can be derived employing the Price equation, Eq. (2.5), on two levels: the inter- and intra-group level. On the lower intra-group level individuals compete against each other while on the upper inter-group level whole subpopulations are subject to selection. In

³This exactly happens when a mutation towards a cancer cell emerges

Level	Ind.	Abu.	Average	Small Entity	Large Entity	Gr. F.
Inter	α	H_α	$\langle X_\alpha \rangle = \sum_\alpha X_\alpha H_\alpha$	Group Z_α	Set of groups $\langle Z_\alpha \rangle$	W_α
Intra	i	$h_{i,\alpha}$	$\langle x_{i,\alpha} \rangle_\alpha = \sum_i x_{i,\alpha} h_{i,\alpha}$	Individual $z_{i,\alpha}$	Group $\langle z_{i,\alpha} \rangle_\alpha = Z_\alpha$	$w_{i,\alpha}$

Table 3.1: Comparison of the different quantities and averages on the inter and intra group level. From left to right, the summation index, the abundance, the average, the smaller and the larger entity and the growth factors are shown

the following we employ the Price equation on both levels. Hence, all quantities introduced in Sec. 2.3.1 now come into play on the intra- and inter-group level. Let us start with the lower level describing the internal evolution of a subpopulation (group). Each individual therein is classified by its trait $z_{i,\alpha} \in \{0, 1\}$ where 0 corresponds to a free-rider and 1 to a cooperator. The index i specifies the individual and α its group. The factor $h_{i,\alpha}$ corresponds to a trait's abundance. Summing them up leads to the average trait of a group $Z_\alpha = \langle z_{i,\alpha} \rangle_\alpha = \sum_i z_{i,\alpha} h_{i,\alpha}$. The reproduction success of an individual in a time interval Δt is given by the growth factor $w_{i,\alpha}$. Now let us consider the upper level where a group corresponds to an individual on the lower level. Thus, each group has a trait Z_α with the abundance H_α and again the average value in the whole ensemble, now consisting of groups, can be taken, $\langle Z_\alpha \rangle = \sum_\alpha Z_\alpha H_\alpha$. The group growth factor is given by W_α . Note, that there are two kinds of averages, the one within a group summing over all individuals, $\langle x_{i,\alpha} \rangle_\alpha$, and the inter group average summing over all groups, $\langle X_\alpha \rangle$. In Table. 3.1 the corresponding terms on both levels are summarized.

Mathematically an increase in the global level of cooperators corresponds to $\langle \Delta Z_\alpha \rangle > 0$. This condition can be evaluated employing the Price equation on the inter-group level,

$$\langle \Delta Z_\alpha \rangle \langle W_\alpha \rangle = \text{Cov}[Z_\alpha W_\alpha] + \langle \Delta Z_\alpha W_\alpha \rangle > 0. \quad (3.4)$$

The trait of a group, $Z_\alpha = \langle z_{i,\alpha} \rangle_\alpha$ depends on the group composition which is described by the Price equation on the intra-group level,

$$\Delta \langle z_{i,\alpha} \rangle_\alpha \langle w_{i,\alpha} \rangle_\alpha = \text{Cov}[z_i w_i]_\alpha. \quad (3.5)$$

In this equation, the term $\langle \Delta z_{i,\alpha} w_{i,\alpha} \rangle_\alpha$ is not present as mutations towards different phenotypes are excluded and $\Delta z_{i,\alpha} = 0$ holds. By multiplying this expression with H_α and summing over all groups, α , it transforms to,

$$\begin{aligned} \sum_\alpha H_\alpha \Delta \bar{z}_\alpha \bar{w}_\alpha &= \sum_\alpha H_\alpha \text{Cov}[z_i w_i]_\alpha \\ \langle \Delta Z_\alpha W_\alpha \rangle &= \langle \text{Cov}[z_i w_i]_\alpha \rangle. \end{aligned} \quad (3.6)$$

Combining Eqs. (3.4) and (3.6) leads to the following condition for the regime of stable cooperation,

$$\text{Cov}[Z_\alpha, W_\alpha] + \langle \text{Cov}[z_i w_i]_\alpha \rangle > 0. \quad (3.7)$$

Now, the identity $\text{Cov}[A_\alpha B_\alpha]_\alpha = K(A_\alpha, B_\alpha) \text{Var}[A_\alpha]$ (and accordingly on the intra-group level $\text{Cov}[a_{i,\alpha} b_{i,\alpha}]_\alpha = k_\alpha(a_{i,\alpha}, b_{i,\alpha}) \text{Var}[a_{i,\alpha}]_\alpha$) following from linear regression can be used to further simplify the inequality,

$$K(Z_\alpha, W_\alpha) \text{Var}[Z_\alpha] + \langle k_\alpha(z_{i,\alpha}, w_{i,\alpha}) \text{Var}[z_{i,\alpha}]_\alpha \rangle > 0. \quad (3.8)$$

The factor $k_\alpha(z_{i,\alpha}, w_{i,\alpha})$ corresponds to the disadvantage of cooperators within each group. If this disadvantage does not depend on the group α , which is for example the case for public good producing bacteria whose metabolic disadvantage is independent of the group composition, Eq. (3.8) can be further simplified:

$$\frac{\text{Var}[Z_\alpha]}{\langle \text{Var}[z_{i,\alpha}]_\alpha \rangle} K(Z_\alpha, W_\alpha) > -k_\alpha(z_{i,\alpha}, w_{i,\alpha}). \quad (3.9)$$

This expression is exactly Hamilton's rule and the relatedness, benefit and cost can now be identified: $\mathcal{R} = \frac{\text{Var}[Z_\alpha]}{\langle \text{Var}[z_{i,\alpha}]_\alpha \rangle}$, $\mathcal{B} = K(Z_\alpha, W_\alpha)$ and $\mathcal{C} = -k_\alpha(z_{i,\alpha}, w_{i,\alpha})$. Importantly these quantities are not constants but non-linear functions. Therefore, the often used simplified understanding of cost, benefit and relatedness leads to enormous misinterpretations concerning the reasons of cooperation. For example, as shown in Ref. [82], increasing the positive effect of a public good on the population does not necessarily raise the benefit, \mathcal{B} . Furthermore, the variance terms in \mathcal{R} are only fully understood when their origins are clarified. Importantly, the relatedness relies on the assumption of population structure. This fact is often not explained when the rule is stated. This becomes especially obvious when considering only one group. Then, there is no variance in the group's trait $\text{Var}[Z_\alpha] = 0$, which leads to $\mathcal{R} = 0$. Therefore, cooperation cannot be maintained, as $0 \cdot \mathcal{B} > \mathcal{C}$ never holds. Thus, population structure is essential to explain cooperation with Hamilton's rule. Furthermore, even though Hamilton's rule provides a condition for cooperative behavior, it does not include the microscopic processes underlying the dynamics. To gain further understanding for the mechanisms favoring cooperation, the full dynamics has to be analyzed carefully.

3.2.3 Group and Kin Selection

Group and kin selection are two closely related theories, which were subject to a long-standing debate. Even though both can in principle be attributed to the framework of multilevel selection and are closely related mathematically, their distinct interpretations have caused a broad gap between some of their proponents. In the following, both theories and the ensuing debate are explained.

Group Selection

The main issue of group selection, which was first brought up by Darwin [74] is based on the same idea as multilevel selection [101, 99]: There exists selection on a higher group level which may alter the evolutionary outcome. One historical problem concerning group selection is that in first approaches selection on the lower level was neglected [181]. This point entailed many concerns in the usefulness of group selection [182] even though intra-group evolution was considered later on. One of the first approaches accounting also for selection on the individual level was the haystack model introduced by Maynard Smith [183, 184, 185] which exemplarily describes the evolution of mice in different haystacks. But he and others doubted that group selection could be a general tool to explain cooperative behavior due to the restrictive conditions, such as strictly separated groups or a well-defined regrouping step, which were assumed [186]. Nowadays many extensions of the idea of group selection including

a weaker definition of the term group have been proposed successfully explaining cooperative behavior, *e.g.* [187, 151, 188, 184, 189, 170, 171, 174, 190, 21]. But still much criticism is formulated, especially from the field of kin selection.

Kin Selection

Kin selection focusses on relatedness of individuals and Hamilton's rule to explain cooperative behavior [100, 191, 192, 193]. This idea has been successfully employed in many examples [180, 194, 195, 81]. Haldane, who was one of the founders of population genetics, described this idea with a wink [196]:

You can jump into the river and risk your life to either save two brothers or eight cousins.

In literature often the following too simplified explanation is given. Helping relatives is beneficial as one's own genetic material is spread also by these relatives. Even though not entirely wrong, this statement may lead to misunderstandings: First, it implies that cooperating individuals help other ones on purpose. In general, especially without abilities like memory or recognition, this does not hold. Also, Haldane was aware of this problem when stating [196]:

But on the two occasions when I have pulled possibly drowning people out of the water (at an infinitesimal risk to myself) I had no time to make such calculations.

Furthermore there is some ambiguity concerning the term relatedness. As learned from Hamilton's rule the relatedness, \mathcal{R} , relies on the variance in the composition of subpopulations concerning cooperative traits. As this matter of fact is often ignored, we want to point out two considerations directly following from the definition of the term relatedness in Hamilton's rule: First, a high relatedness in other genes than the ones causing cooperative behavior, does not provoke the maintenance of cooperation. Second, not necessarily consanguinity, but similarity in the cooperative trait, which must not necessarily be passed by the same genes, is required. Another important side note concerns structure which is a necessary requirements for $\mathcal{R} > 0$ as already pointed out in Sec 3.2.2. Thus, also kin selection fits in the framework of multilevel selection [197].

The Debate

Taken together, both group and kin selection provide theoretical frameworks to describe the evolution and maintenance of cooperative behavior. While the theory of group selection focusses on structure to explain cooperation, kin selection concentrates on relatedness as the reason for cooperative behavior. But actually relatedness as well as structure are necessary for both theories which therefore strongly resemble each other: On the one hand, groups can only favor cooperation if some of them have a higher level of cooperators and thereby a selection advantage compared to other groups. In terms of kin selection this differences in the group composition correspond to the term relatedness. On the other hand, the relatedness, as we have learned from Hamilton's rule, is not an absolute value but depends on the variance in the composition of all groups. Thereby also structure is essential for this quantity.

Furthermore, both theories need a mechanism ensuring a high variance in the composition of the populations. This variance declines over time as populations fixate. Hence, to maintain a variance which is large enough to favor cooperative behavior a dynamic restructuring mechanism can be important. Following the considerations above, both theories are more or less equivalent [198, 199]. But still, there is a heavy debate going on between some proponents of both theories, *e.g.* [153, 200, 201] or [202, 195]. Another similar controversy arises concerning inclusive fitness theory, *e.g.* [203, 204, 205, 206, 207, 208, 209], which is closely related to kin selection [176]. In inclusive fitness theory [191] the conservative fitness term is extended by an additional term, reflecting indirect benefits as they can arise due to advantages of relatedness or structure. The heavy debate is even more peculiar when considering the open question arising in both theories [210]: Why can a high relatedness be maintained? Are there additional assortment mechanisms provoking variance in the group structure? What are the microscopic reasons leading to an inclusive fitness? What are the dynamic processes underlying both theories? How can cooperative behavior have emerged in the first place? These and many other questions are still not satisfactorily answered.

3.3 On the Role of Dynamics and Fluctuations

As already mentioned, there are a plenty of open questions concerning the evolution of cooperation. In this thesis, we especially focus on the influence of fluctuations and dynamics. In evolutionary processes these demographic fluctuations scale as \sqrt{N} . Structure, leading to small groups of interacting individuals, thereby increases the strength of fluctuations. This is not only a theoretical consideration. Many real populations undergo life cycles including phases of small population sizes, *e.g.* parasites infecting a host as *D. dendriticum*. Also for bacterial populations or biofilms, where microbes permanently undergo phases of biofilm initiation, maturation, maintenance, and dispersal, the idea of life cycles is widely accepted [211, 212, 213, 214, 215]. Furthermore, population bottlenecks can also be induced by environmental catastrophes or seasonal changes. In addition, populations may also explore new habitats. Usually only few individuals form such a founder colony, which again is an example for a bottleneck in the population size. All in all, demographic fluctuations, which are especially enhanced during phases of small populations sizes, are not negligible. These fluctuations can have a considerable impact on the dynamics and thereby explain cooperative behavior [216, 217, 218]. Furthermore, the restructuring mechanisms, which as mentioned above are essential to maintain a high variance in the composition of subpopulations, are often associated with fluctuations since the population size is often small after such a restructuring event.

Aside from demographic fluctuations, also dynamics are crucial for evolution. While the Price equation compares only two time snapshots, dynamic approaches also account for each time step in between. Only by considering this full dynamic behavior, the evolutionary outcome depending on the parameters can be fully understood, as exemplified in the following section. Therefore, individual based modeling including both, dynamics and fluctuations, is essential. This can for example be achieved by the approaches considered in the previous chapter. In this context, models accounting for both, population and evolutionary dynamics, are also important [114, 115, 116, 117]. Employing those, the evolutionary advantages and disadvantages on all levels of selection can be fully understood.

3.4 Papers and Manuscripts

3.4.1 Growth dynamics and the evolution of cooperation in microbial populations

In the article “Growth dynamics and the evolution of cooperation in microbial populations”, *Scientific Reports*, **2**, 281 (2012), by Jonas Cremer, Anna Melbinger and Erwin Frey, we analyze the evolution of cooperation in group-structured populations. In our model, groups are randomly formed and then evolve according to the model introduced in Sec. 2.4 [118]. We thereby account for both, stochastic and dynamic effects, which both are crucial as our analysis shows. After a certain time T , groups are merged and the cycle restarts. By thoroughly analyzing the stochastic dynamics two distinct fluctuation driven mechanisms promoting cooperation can be found. The group-growth mechanisms, which relies on asymmetric amplification of fluctuations, can cause a transient increase of cooperation in a single regrouping step. If the merging time T lies in the time interval of the transient increase, stable coexistence between cooperators and defectors can be reached in the long run. Intriguingly this also enables the evolution of cooperation, as a single mutation towards a cooperator can spread in the population. The second effect, the group-fixation mechanism, relies on a larger group size of cooperative groups. If the number of purely cooperating groups is high enough, the fraction of cooperators does not decline. Under permanent regrouping, this makes cooperation an evolutionary stable strategy above a certain threshold value, *i.e.* cooperation is stable against invasion by cheaters.

3.4.2 Conclusion and Outlook

In our model we investigated the influence of group structure on the evolution of cooperative behavior. We especially focussed on the role of demographic fluctuations and the dynamic intra-group evolution. As it turned out, both play a crucial role. Demographic fluctuations result in two distinct mechanisms promoting cooperation. For small regrouping times the group-growth mechanism acts, while the group-fixation mechanism is only present for large regrouping times. In this context it would be interesting to study how varying regrouping times alter the evolutionary outcome. Distinct sequences of short and long times could lead to different evolutionary outcomes, *e.g.* a single mutant could overtake the whole population.

In addition, it would be very interesting to confirm our predictions experimentally. By varying the regrouping time the influence of the group-growth and group-fixation mechanism can be adjusted. We plan to perform such experiments in collaboration with Prof. Kerstin Jung and Prof. Heinrich Jung from the chair of microbiology at Ludwig-Maximilians University. They designed a cooperating *Pseudomonas putida* mutant producing the siderophore pyoverdine. First results from their measurements are promising and we are looking forward to upcoming results.

Furthermore, the influence of mutations has to be studied. These mutations may result in a changed phenotype and thereby disturb the system. Also migration of individuals has a similar effect. The robustness of our results against these perturbations is of large relevance and a pending research project.

In our model, we incorporated the benefit of cooperation as growth advantage, which was motivated by bacteria like *P. aeruginosa* [135]. But there exist also other examples for beneficial behavior supporting a population. For instance, some biofilms are only able to swim on a liquid if enough cooperators are present (*P. fluorescens* [134]). Studying how these other advantages influence the evolutionary outcome would be very interesting. As our model highlights details of the dynamics matter. Hence it is not sufficient to identify two antagonistic effects, but it is also essential to uncover the underlying mechanisms. Only then the emergence and maintenance of cooperative behavior can be understood.



Growth dynamics and the evolution of cooperation in microbial populations

Jonas Cremer, Anna Melbinger & Erwin Frey

Arnold Sommerfeld Center for Theoretical Physics (ASC) and Center for NanoScience (CeNS), Department of Physics, Ludwig-Maximilians-Universität München, Theresienstrasse 37, D-80333 München, Germany.

SUBJECT AREAS:

THEORY

STATISTICAL PHYSICS,
THERMODYNAMICS AND
NONLINEAR DYNAMICS

ECOLOGY

COMPUTATIONAL BIOLOGY

Received

28 October 2011

Accepted

3 February 2012

Published

21 February 2012

Correspondence and
requests for materials
should be addressed to
E.F. (frey@lmu.de)

Microbes providing public goods are widespread in nature despite running the risk of being exploited by free-riders. However, the precise ecological factors supporting cooperation are still puzzling. Following recent experiments, we consider the role of population growth and the repetitive fragmentation of populations into new colonies mimicking simple microbial life-cycles. Individual-based modeling reveals that demographic fluctuations, which lead to a large variance in the composition of colonies, promote cooperation. Biased by population dynamics these fluctuations result in two qualitatively distinct regimes of robust cooperation under repetitive fragmentation into groups. First, if the level of cooperation exceeds a threshold, cooperators will take over the whole population. Second, cooperators can also emerge from a single mutant leading to a robust coexistence between cooperators and free-riders. We find frequency and size of population bottlenecks, and growth dynamics to be the major ecological factors determining the regimes and thereby the evolutionary pathway towards cooperation.

One pivotal question in evolutionary biology is the emergence of cooperative traits and their sustainment in the presence of free-riders^{1–6}. By providing a public good, cooperative behavior of every single individual would be optimal for the entire population. However, non-contributing free-riders may take evolutionary advantage by saving the costs for providing the benefit and hence jeopardize the survival of the whole population. In evolutionary theory kin selection^{1,7–9}, multi-level selection^{10–13}, and reciprocity¹⁴ have been found to provide conceptual frameworks to resolve the dilemma^{4–6}. For higher developed organisms, stable cooperation is generally traced back to specific mechanisms like repeated interaction^{2,14}, punishment^{15,16}, and kin discrimination^{1,6,17,18}. But how can cooperation emerge in the first place and be maintained without abilities like memory or recognition? Answering this question is especially important within the expanding field of biofilm formation^{19–24}. There, a successfully cooperating collective of microbes runs the risk to be undermined by non-producing strains saving the metabolically costly supply of biofilm formation^{18,20,23,24}. Sophisticated social behavior cannot be presumed to explain the high level of cooperation observed in nature and experiments^{18–20,24–31}. Instead, different forms of limited dispersal, such as spatial arrangements, or fragmentation into groups are essential to resolve the dilemma of cooperation among such microbial organisms^{1,32,33}. Indeed, in nature microbes typically live in colonies and biofilms. Remarkable, although details strongly differ from species to species, most microbial populations follow a life-cycle of colony initiation, maturation, maintenance and dispersal leading to new initiation, see e.g.^{24,34–37}. Well-studied examples include *Pseudomonas aeruginosa*³⁸, *Escherichia coli*³⁹, *Bacillus subtilis*⁴⁰ and *Myxococcus xanthus*⁴¹. Even though such a life-cycle is often complexly regulated e.g. by environmental impacts and including collective behavior of colonies, populations bottlenecks alternating with growth phases are essential components of most microbial life-cycles. Employing simplified setups, recent experiments address the role of population bottlenecks and growth by studying structured microbial populations of cooperators and free-riders^{25,26,28,29,31}. In these setups small founder colonies differing in composition were cultivated in separate habitats. For example, Chuang et al.²⁹ used 96-well plates as structured environment with a dilution of synthetically designed *E. coli* strains where the cooperative strain is producer of a public good provoking antibiotic resistance. A microbial life-cycle was generated in the lab by regularly mixing all colonies after a certain time and inoculating new cultures. Under these conditions, an increase in the overall level of cooperation was observed even though free-riders have a growth advantage within every colony. However, the precise conditions under which cooperation is favored are subtle^{8,9,11,13,31,33,42–49}. A possible theoretical explanation for the observed increase in cooperation is the antagonism between two levels of selection, as widely discussed in the literature¹². Here, these levels, *intra-* and *inter-group* evolution, arise as population dynamics alternates between independent evolution in subpopulations (groups) and global competition in a merged well-mixed population. Due to the dilemma of cooperation, free-riders are always better off than cooperators within each



group (intra-group evolution). In contrast, on the inter-group level, groups with a higher fraction of cooperators are favored over groups with a lower one.

In this article, we study the interplay between the dynamics at the intra- and inter-group evolution and how it may provoke the maintenance or even the emergence of cooperation. We propose a generic individual-based model which includes three essential elements: a growth disadvantage of cooperators within each group, an advantage of groups incorporating more cooperative individuals, and regularly occurring regrouping events; cf. Fig. 1. Well-known from the theories of kin^{1,7,9,49} and multi-level selection^{12,29,49,50}, cooperation can increase in principle: While, within a group i , the fraction of cooperators, ξ_i , decreases, groups also change their size, v_i , such that the fraction of cooperators in the total population, given by the weighted average, $x = \sum_i v_i \xi_i / \sum_i v_i$, may still increase. Such an increase is an example of Simpson's paradox²⁹. To occur, a decreasing fraction of cooperators, ξ_i , within groups must be compensated by changing weights, v_i/N , in the total population of size $N = \sum_i v_i$, i.e. by a sufficiently high positive correlation between a group's size and its fraction of cooperators⁵⁰. Here we want to go beyond stating this mathematical fact and reveal the ecological factors underlying these correlations. To this end the full stochastic dynamics at the intra- and inter-group level will be analyzed. A key element will be the intricate coupling between the dynamics of the composition and the dynamics of the overall size of a group. This applies in particular to microbial populations where the reproduction rate of microbes strongly depends on environmental conditions and thereby also on the composition of the population⁵¹. Therefore, a proper theoretical formulation has to account for a dynamics in the group size^{52,53} rather than assuming it to be constant as in most classical approaches^{54–56}. Such a dynamic formulation will allow us to investigate ecological mechanisms for the evolution and maintenance of cooperation.

Motivated by microbial life-cycles^{24,34–37} and the aforementioned experiments^{25,26,28,29,31}, we consider a population of cooperators and free-riders and its evolution in a repetitive cycle consisting of three consecutive steps³³, cf. Fig. 1. In the *group formation step*, the total

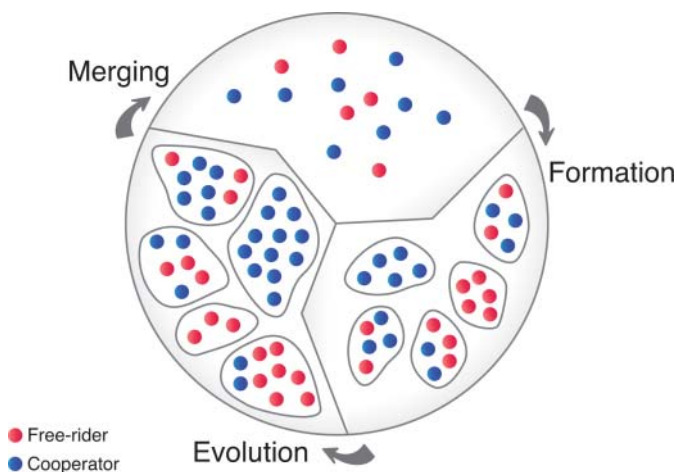


Figure 1 | Repetitive cycle of population dynamics. The time evolution of a population composed of cooperators (blue) and free-riders (red) consists of three cyclically recurring steps. *Group formation step*: we consider a well-mixed population which is divided into M separate groups ($i = 1, \dots, M$) by an unbiased stochastic process such that the initial group size and the fraction of cooperation vary statistically with mean values n_0 and x_0 , respectively. *Group evolution step*: groups grow and evolve separately and independently; while the fraction of cooperators decrease within each group, cooperative groups grow faster and can reach a higher carrying capacity. *Group merging step*: after a regrouping time, T , all groups are merged together again. With the ensuing new composition of the total population, the cycle starts anew.

population with a fraction of cooperators, x_0 , is divided into a set of M groups by an unbiased stochastic process such that the group size and the fraction of cooperation vary statistically with mean values n_0 and x_0 , respectively. Subsequently, the groups evolve independently (*group evolution step*). In each group, both the fraction of cooperators and the group size vary dynamically and change over time. Independent of the specific details, the groups' internal dynamics has the following characteristic features: First, because of the costs for providing the benefit, cooperators have a selection disadvantage, s , compared to cheaters in the same group. In particular, cooperators reproduce slower than cheaters and hence the fraction of cooperators decreases within each group (intra-group evolution). Second, considering the benefit of cooperation, groups with more cooperators grow faster and can reach a higher maximum size (carrying capacity) than groups of mainly cheaters (inter-group evolution)^{52,53}. The benefit of cooperators is implemented by the growth rate of an individual proportional to $(1 + p\xi_i(t))$, where $\xi_i(t)$ is the fraction of cooperators in the group the individual belongs to. Resource-limited logistic growth is considered by a death term depending on the group size. For specificity we assume growth conditions comparable to those observed by Chuang et al.²⁹. Details are given in the materials and method section and the supplementary information. After evolving separately for a certain time $t = T$, all groups are merged (*group merging*), and the cycle restarts by forming new groups according to the current fraction of cooperators, x , in the whole population. It is the interplay of these three steps, characterized by the initial group size, n_0 , the selection strength, s , and the regrouping time, T , which determines the long-term evolution of the population.

Results

Fig. 2A shows the time evolution of the overall fraction of cooperators during a group evolution step. We find three distinct scenarios: decrease (red), transient increase (green), and permanent increase of cooperation (blue). Their origin can be ascribed to two ecological mechanisms: more cooperative groups grow faster (*group-growth mechanism*) and purely cooperative groups can reach a larger carrying capacity (*group-fixation mechanism*).

A permanent increase of cooperation can be explained on the basis of the *group-fixation* mechanism: for asymptotically long times the intra-group evolution reaches a stationary state, where each group consist solely of either cooperators or free-riders. Which state is favored depends on the interplay between selection pressure and stochastic effects. Because cheaters have a relative fitness advantage, they tend to outcompete cooperators in groups with a mixed initial composition. However, there are two stochastic effects leading to purely cooperative groups. First, the stochastic process of group formation results in a distribution of group compositions also containing a fraction of groups which consist of cooperators only. Second, random drift^{57,58}, which is most pronounced during a population bottleneck where group sizes are small, can cause a group to become fixed in a state with cooperators only. Due to the benefit of cooperators for the whole group, these purely cooperative groups reach a much higher carrying capacity than those left without any cooperator. Hence, although inferior in terms of number of groups, purely cooperative groups through their large group size contribute with a large statistical weight to the total composition of the population, and thereby ensure maintenance or even increase of the level of cooperation for long times, cf. Fig. 2A blue curve.

In order for the *group-fixation* mechanism to become effective the evolutionary dynamics has to act for time scales longer than the selection time, $t_s = 1/s$, which measures the time scale on which selection acts. For smaller times, a temporary increase in cooperation level is observed provided the initial group size is small enough, cf. Fig. 2A. The initial rise is caused by the *group-growth mechanism* during the growth phase of colonies, see Fig. 2C. Given a distribution of initial group compositions, it asymmetrically amplifies the size of

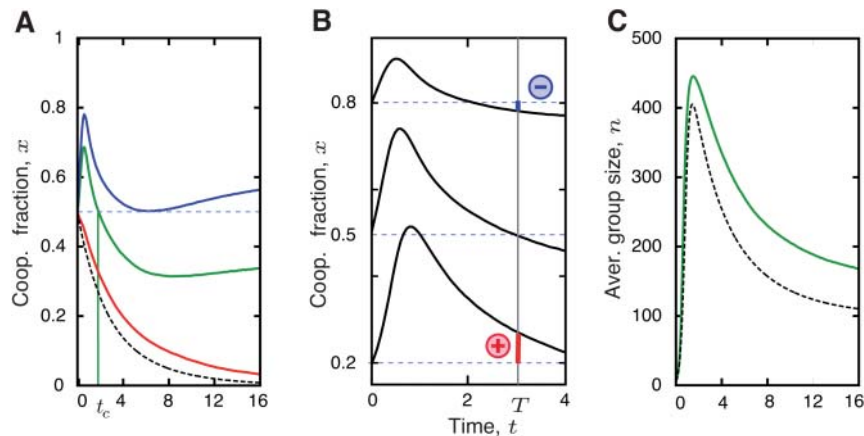


Figure 2 | Evolution while individuals are arranged in groups (group-evolution step). (A) Population average of cooperators fraction, x , as a function of time t . Depending on the average initial group size, n_0 , three different scenarios arise: *decrease of cooperation* (red line, $n_0 = 30$), *transient increase of cooperation* (green line, $n_0 = 6$, increase until cooperation time t_c) and *permanently enhanced cooperation* (blue line, $n_0 = 4$). These three scenarios arise from the interplay of two mechanisms. While the *group-growth mechanism*, due to faster growth of more cooperative groups, can cause a maximum in the fraction of cooperators for short times, the *group-fixation mechanism*, due to a larger maximum size of purely cooperative groups, assures cooperation for large times. Both mechanisms become less efficient with increasing initial group sizes and are not effective in the deterministic limit (dashed black line, solution of Eq. (S7) for $N_0 = 6$) as they rely on fluctuations. (B) The strength of the group-growth mechanism decreases with an increasing initial fraction of cooperators. This is illustrated by comparing the time evolution for three different initial fractions of cooperators and a fixed initial group size $n_0 = 5$. After a fixed time, here $t = 3.03$, the fraction of cooperators is larger than the initial one for $x_0 = 0.2$, equal to it for $x_0 = 0.5$, and eventually becomes smaller than the initial value, as shown for $x_0 = 0.8$. (C) Change of the average group size, $n = \sum_i n_i / M$. At the beginning the groups grow exponentially, while they later saturate to their maximum group size. As this maximum size depends on the fraction of cooperators, the average group size declines with the loss in the level of cooperation ($n_0 = 6$, green line). The deterministic solution for the same set of parameters which does not account for fluctuations (dashed black line, solution of Eq. (S7)) describes this behavior qualitatively. $s = 0.1$, $p = 10$.

those groups which contain more cooperators. This effect becomes stronger with a broader distribution, or, equivalently, a smaller initial group size n_0 . Eventually the initial rise has to decline since, due to the internal selection advantage of free-riders, the fraction of cooperators is always decreasing within each mixed group. As a consequence, the overall benefit of cooperators through faster growth of more cooperative groups is only transient. After a certain time, the cooperation time, t_c , the fraction of cooperators, $x(t)$, falls again below its initial value, x_0 , unless the group-fixation mechanism is strong enough to ensure a permanent increase. Finally, if group-internal selection is too strong compared with the growth advantage of cooperative groups, the level of cooperation cannot increase even transiently, cf. Fig. 2A, red curve.

Combining all three steps of the cycle we now ask for the evolutionary outcome after many iterations, k , of the cycle. For very small bottlenecks, $n_0 \leq 3$, both the groupfixation and the group-growth mechanism result in a purely cooperative population and cannot be distinguished. This is shown in Fig. 3A for parameters corresponding to the experiments by Chuang et al.²⁹; the experimental results and the results of our stochastic model are in excellent agreement. For larger bottlenecks, $n_0 = 5$, and depending on the relative magnitude of the *regrouping time* T , we find two fundamentally distinct scenarios, see Fig. 3B. For large regrouping times, $T \gg t_s$, there is a threshold value, x_0^* , for the initial cooperators fraction, x_0 , above which cooperators take over the whole population and below which they go extinct. In contrast, for regrouping times smaller than the selection time, $T \leq t_s$, independent of the initial value, x_0 , the population reaches a stationary state where cooperators are in stable coexistence with free-riders. As explained next, these two scenarios are closely tied to the group-growth and group-fixation mechanisms; for an illustration see the supplementary videos. The threshold value for maintenance of cooperation at large regrouping times is a consequence of group-fixation and the larger carrying capacity of purely cooperative groups. Since for $T \gg t_s$, the intra-group dynamics has reached a stationary state, fixation leaves the population with groups

consisting of either cooperators or defectors only. The probability of fixation in the respective state and hence the fraction of purely cooperative groups after completing one cycle strongly depends on the initial cooperators fraction. Now, if the initial cooperators fraction becomes too low, the number of cooperative groups will be too rare such that even their larger maximum group size is no longer sufficient for them to gain significant weight in the total population, and the overall cooperators fraction in the population will decline. Thus there must be a critical value for the cooperators fraction, x_0^* , below which, upon iterating the cycle the fraction of cooperators will decline more and more, see Fig. 3B (red line). In contrast, above the critical value purely cooperating groups are becoming more frequent upon regrouping, and therefore cooperators will eventually take over the population completely, cf. Fig. 3B (blue line).

When groups are merged during the phase of transient increase of cooperation, $T \leq t_s$, the stationary level of cooperation does not depend on the initial one. This behavior is due to the dependence of the change of the cooperators fraction during one cycle, Δx , on the initial fraction, x_0 as discussed in the following; see also Fig. 2B. As we have already eluded to in the discussion of the group-growth mechanism, stochasticity during group formation and during the initial neutral phase of the group evolution dynamics results in a broad distribution of group compositions. The evolutionary dynamics is acting on this distribution in an antagonistic fashion. While, due to the higher growth rate of more cooperative groups, the distribution develops a positive skew leading to an increase in the average overall cooperation, the group-internal selection pressure is counteracting this effect by reducing the cooperators fraction within each group. The relative strength of the former effect is largest for small initial cooperators fraction since this allows the largest positive skew to develop. Hence, for a given regrouping time, if the change in overall cooperators fraction Δx is positive for small x_0 it must become negative for sufficiently large x_0 , as illustrated in Fig. 2B. For a more detailed mathematical discussion of these effects we refer to the supplementary information. As a consequence, in populations with

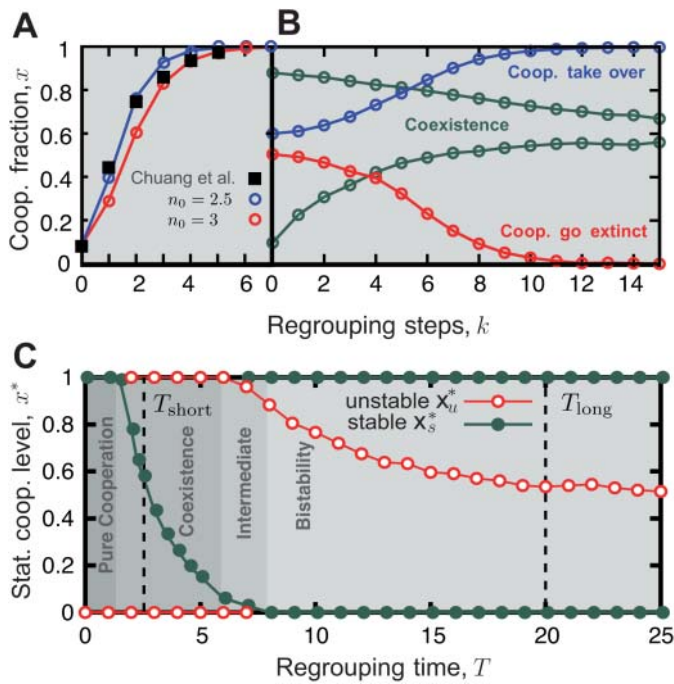


Figure 3 | Evolution of the overall cooperator fraction under repeated regrouping. After many iterations, k , of the evolutionary cycle, a stationary level of cooperation is reached. (A) For small population bottlenecks, $n_0 \leq 3$, group-growth and group-fixation mechanisms are effective and lead to purely cooperative populations. Growth parameters, bottleneck size and the regrouping time are chosen according to the experiments by Chuang et al.²⁹, see supplementary information. Without any fitting parameters, our simulation results (colored lines) are in good agreement with the experimental data (black points). (B) For larger bottlenecks, $n_0 = 5$, and depending on the relative efficiency of the group-growth and group-fixation mechanism, two qualitatively different regimes can be distinguished. While the group-growth mechanism leads to stable coexistence of cooperators and free-riders (green lines), the group-fixation mechanism can lead to a pure state of either only cheaters (red line) or only cooperators (blue line). The relative impact of these mechanisms depends strongly on the regrouping time T . For short regrouping times ($T_{\text{short}} = 2.5 < t_s$, green lines), the group-growth mechanism is effective, while for sufficiently long regrouping times ($T_{\text{long}} = 20 > t_s$, blue and red lines) the group-fixation mechanism acts more strongly. (C) With parameters equal to (B), the detailed interplay of the group-growth and group-fixation mechanisms is summarized in a bifurcation diagram showing the stationary levels of cooperation as a function of the regrouping time T . Depending on the relative efficiency of both mechanism, four different regimes arise: pure cooperation, coexistence, intermediate, and bistability. The times T_{short} and T_{long} correspond to the green and red/blue lines shown in (B). Parameters are $x_0 = 0.086$, $T = 3.1$, $s = 0.05$ and $p = 6.6$ in (A); see also supplementary information. In (B), $x_0 = \{0.1 \text{ (green)}, 0.9 \text{ (green)}\}$ and $x_0 = \{0.5 \text{ (red)}, 0.6 \text{ (blue)}\}$ for $T_{\text{short}} = 2.5$ and $T_{\text{long}} = 20$, respectively. $s = 0.1$ and $p = 10$ in (B/C).

a small initial fraction of defectors, the defectors increase in frequency. At the same time, when the initial fraction of cooperators is low, they also increase in number, finally leading to stable coexistence of cooperators and defectors at some fraction x_s^* . This stationary fraction of cooperators is independent of the starting fraction and solely determined by the parameters of the evolutionary dynamics.

The interplay of both the group-growth and group-fixation mechanism leads, depending on the regrouping time, to different scenarios for the levels of cooperation. These are summarized in the bifurcation diagram Fig. 3C, where the stable and unstable fixed points of the regrouping dynamics, x_s^* and x_u^* , are shown as functions of the

regrouping time. The scenarios can be classified according to their stability behavior under regrouping as follows: For large regrouping times, $T \gg t_s$, the group-fixation mechanism leads to *bistable* behavior. With decreasing T , the fixation mechanism loses ground while the group-growth mechanism becomes more prominent. There is an *intermediate* scenario: the dynamics is bistable with full cooperation as well as coexistence as stable fixed points. For even smaller times, only the group-growth mechanism remains effective and the rare strategy here always outperforms the common one such that each strategy can invade but not overtake the other: *coexistence*. Finally, for $T \ll t_s$, cooperators always take over the population, effectively leading to *purely cooperative populations*.

Discussion

In this article, we have studied the influence of population dynamics and fluctuations on the evolution and maintenance of cooperation. We specifically account for alternating population bottlenecks and phases of microbial growth. Thereby, our model serves as a null-model for cooperation in rearranging populations^{25,26,28,29,31}, e.g. during microbial and parasitic life-cycles^{24,41,59–61}, and bacterial biofilm formation^{24,34–37}. The final outcome of the dynamics depends on the interplay between the time evolution of size and composition of each subpopulation. While a growth advantage of more cooperative groups favors cooperators, it is counteracted by the evolutionary advantage of free-riders within each subpopulation. We have investigated the stochastic population dynamics and the ensuing correlations between these two opposing factors. Depending on whether groups are merged while they are still exponentially growing or already in the stationary phase, two qualitatively different mechanisms are favored, the group-growth and the group-fixation mechanism. Importantly, our analysis identifies demographic noise as one of the main determinants for both mechanisms. First, demographic noise during population bottlenecks creates a broad distribution in the relative abundance of cooperators and free-riders within the set of subpopulations. The growth advantage of more cooperative subpopulations implies an asymmetric amplification of fluctuations and possibly yields to an increase of cooperation in the whole population (group-growth mechanism). Our analysis shows that this can enable a single cooperative mutant to spread in the population which then, mediated by the dynamics, reaches a stationary state with coexisting cooperators and free-riders. Second, if the founder populations contain only very few individuals, demographic fluctuations strongly enhance the fixation probability of each subpopulation which then consists of cooperators or free-riders only. Purely cooperative groups can reach a much higher carrying capacity. However, only if the relative weight of purely cooperative groups is large enough, this effect leads to an increase in the level of cooperation in the whole population (group-fixation mechanism). From our theoretical analysis of the population dynamics we conclude this to be the case only if the initial fraction of cooperators is above some threshold value.

As shown by comparison with experiments by Chuang et al.²⁹ the proposed model is able to describe microbial dynamics quantitatively. Moreover, our model makes predictions how the evolutionary outcome varies depending on population dynamics and bottlenecks, and how the discussed mechanisms can provoke cooperation. These predictions can be tested experimentally by new experiments similar to those of Chuang et al. and others^{25,26,28,29,31}. For example, by varying easily accessible parameters like the bottleneck size n_0 or the regrouping time T , the relative influence of both mechanisms can be tuned. Then the resulting level of cooperation and the ensuing bifurcation diagrams can be quantitatively compared with our theoretical predictions.

As we assume the worst case scenario for cooperators, e.g. randomly formed groups and no additional assortment, our findings are robust: The discussed pathways towards cooperation based on a growth-advantage of more cooperative groups and restructuring



are expected to stay effective when accounting also for other biological factors like positive assortment, spatial arrangements of groups, mutation, or migration¹.

Shown by our analysis, a regular life-cycle favors cooperation. Besides better nutrient exploitation, this advantage for cooperation might be one reason for the evolution of more complex, controlled life-cycles including collective motion of microbes, local lysis, and sporulation^{24,34–37}.

Methods

We used a stochastic, individual-based model where each individual is either a cooperators or a free-rider. In the group formation step groups are formed at random. The initial group size, $v_{0,i}$ is Poisson distributed (with mean n_0). Given this size, the fraction of cooperators $\xi_{0,i}$ follows by a binomial distributed number of cooperators. During the evolution step, each individual is subject to random birth and death events. The dynamics is given by a time-continuous Markov process where the change of the probability, $\partial_t P(v_i, \xi_i; t)$, is given by a master equation. In detail, the basal per capita birth rate of each individual depends linearly on the group level of cooperation ξ_i , while the per capita death rate increases linearly with the group size v_i the individual belong to. In addition, free-riding individuals have a higher birth-rate where the strength of selection s measures the advantage of free-riding individuals. Full details are given in the supplementary information. The time scale is such that a small population of only free-riders initially grows exponentially with the average size $v_{i,0} \exp t$. To investigate the dynamics and both evolutionary mechanisms we performed extensive computer simulations by employing the Gillespie algorithm⁶². Group size is $M = 5 \cdot 10^3$ in Fig. 2, and $M = 5 \cdot 10^4$ in Fig. 3.

- Hamilton, W. D. The genetical evolution of social behaviour. I+II. *J. Theor. Biol.* **7**, 1–52 (1964).
- Axelrod, R. & Hamilton, W. The evolution of cooperation. *Science* **211**, 1390–1396 (1981).
- Maynard-Smith, J. & Szathmari, E. *The Major Transitions in Evolution* (Oxford University Press, Oxford, 1995).
- Frank, S. A. *Foundations of Social Evolution* (Princeton University Press, 1998).
- Nowak, M. A. Five rules for the evolution of cooperation. *Science* **314**, 1560–1563 (2006).
- West, S. A. & Gardner, A. Altruism, spite, and greenbeards. *Science* **327**, 1341–1344 (2010).
- Michod, R. E. The theory of kin selection. *Ann. Rev. Ecol. Syst.* **13**, 23–55 (1982).
- Foster, K. R., Wenseleers, T. & Ratnieks, F. L. W. Kin selection is the key to altruism. *Trends Ecol. Evol.* **21**, 57–60 (2006).
- West, S. A., Griffin, A. S. & Gardner, A. Evolutionary explanations for cooperation. *Curr. Biol.* **24**, 661–672 (2007).
- Hamilton, W. *Biosocial Anthropology*, chap. Innate social aptitudes of man: an approach from evolutionary genetics, 129–151 (Wiley, 1975).
- Wilson, D. S. Theory of group selection. *Proc. Natl. Acad. Sci. USA* **72**, 143–146 (1975).
- Okasha, S. *Evolution and the Levels of Selection* (Oxford University Press, Oxford, 2006).
- Nowak, M. A., Tarnita, C. E. & Wilson, E. O. The evolution of eusociality. *Nature* **466**, 1057–1065 (2010).
- Trivers, R. L. The evolution of reciprocal altruism. *Quart. Rev. Biol.* **46**, 35–57 (1971).
- Yamagishi, T. The provision of a sanctioning system as a public good. *J. Pers. Soc. Psychol.* **51**, 110–116 (1986).
- Fehr, E. & Fischbacher, U. The nature of human altruism. *Nature* **425**, 785–791 (2003).
- Queller, D., Ponte, E., Bozzaro, S. & Strassmann, J. E. Single-gene greenbeard effects in the social amoeba *dictyostelium discoideum*. *Science* **299**, 105–106 (2003).
- West, S. A., Griffin, A. S., Gardner, A. & Diggle, S. P. Social evolution theory for microorganisms. *Nat. Rev. Microbiol.* **4**, 597–607 (2006).
- Rainey, P. B. & Rainey, K. Evolution of cooperation and conflict in experimental bacterial populations. *Nature* **425**, 72–74 (2003).
- Velicer, G. J. Social strife in the microbial world. *Trends Microbiol.* **11**, 330–337 (2003).
- Keller, L. & Surette, M. G. Communication in bacteria: an ecological and evolutionary perspective. *Nat. Rev. Microbiol.* **4**, 249–258 (2006).
- Stewart, P. S. & Franklin, M. J. Physiological heterogeneity in biofilms. *Nat. Rev. Microbiol.* **6**, 199–210 (2008).
- Nadell, C. D., Xavier, J. B. & Foster, K. R. The sociobiology of biofilms. *FEMS Microbiol. Rev.* **33**, 206–224 (2009).
- Xavier, J. B. Social interaction in synthetic and natural microbial communities. *Molecular Systems Biology* **7**, 1–11 (2011).
- Griffin, A. S., West, S. A. & Buckling, A. Cooperation and competition in pathogenic bacteria. *Nature* **430**, 1024–1027 (2004).
- Buckling, A. *et al.* Siderophore-mediated cooperation and virulence in *Pseudomonas aeruginosa*. *FEMS Microbiol. Ecol.* **62**, 135–141 (2007).
- Ackermann, M. *et al.* Self-destructive cooperation mediated by phenotypic noise. *Nature* **454**, 987–990 (2008).
- Kümmerli, R., Gardner, A., West, S. & Griffin, A. S. Limited dispersal, budding dispersal, and cooperation: an experimental study. *Evolution* **63**, 939–949 (2009).
- Chuang, J. S., Rivoire, O. & Leibler, S. Simpson's paradox in a synthetic microbial system. *Science* **323**, 272–275 (2009).
- Gore, J., Youk, H. & van Oudenaarden, A. Snowdrift game dynamics and facultative cheating in yeast. *Nature* **459**, 253–256 (2009).
- Chuang, J. S., Rivoire, O. & Leibler, S. Cooperation and Hamilton's rule in a simple synthetic microbial system. *Molec. Syst. Biol.* **6**, 398 (2010).
- Nowak, M. A. & May, R. M. Evolutionary games and spatial chaos. *Nature* **359**, 826–829 (1992).
- Maynard Smith, J. Group selection and kin selection. *Nature* **201**, 1145–1147 (1964).
- Costerton, J. W. *et al.* Bacterial biofilms in nature and disease. *Annual Review Of Microbiology* **41**, 435–464 (1987).
- O'Toole, G., Kaplan, H. & Kolter, R. Biofilm formation as microbial development. *Annual Review Of Microbiology* **54**, 49–79 (2000).
- Hall-Stoodley, L., Costerton, J. W. & Stoodley, P. Bacterial biofilms: From the natural environment to infectious diseases. *Nat. Rev. Micro.* **2**, 95–108 (2004).
- McDougald, D., Rice, S. A., Barraud, N., Steinberg, P. D. & Kjelleberg, S. Should we stay or should we go: mechanisms and ecological consequences for biofilm dispersal. *Nature reviews Microbiology* **10**, 39–50 (2011).
- Sauer, K., Camper, A., Ehrlich, G., Costerton, J. & Davies, D. *Pseudomonas aeruginosa* displays multiple phenotypes during development as a biofilm. *Journal Of Bacteriology* **184**, 1140–1154 (2002).
- Beloin, C., Roux, A. & Ghigo, J. M. *Escherichia coli* biofilms. *Current topics in microbiology and immunology* **322**, 249–289 (2008).
- Lemon, K. P., Earl, A. M., Vlamakis, H. C., Aguilar, C. & Kolter, R. Biofilm development with an emphasis on *Bacillus subtilis*. *Current topics in microbiology and immunology* **322**, 1–16 (2008).
- Velicer, G. J. & Vos, M. Sociobiology of the myxobacteria. *Annu. Rev. Microbiol.* **63**, 599–623 (2009).
- Szathmari, E. & Demeter, L. Group selection of early replicators and the origin of life. *J. Theor. Biol.* **128**, 463–486 (1987).
- Motro, U. Co-operation and defection: Playing the field and the ESS. *Journal of Theoretical Biology* **151**, 145–154 (1991).
- Szathmari, E. Co-operation and defection: Playing the field in virus dynamics. *Journal of Theoretical Biology* **165**, 341–356 (1993).
- Pfeiffer, T., Schuster, S. & Bonhoeffer, S. Cooperation and competition in the evolution of ATP-producing pathways. *Science* **292**, 504–507 (2001).
- Killingback, T., Bieri, J. & Flatt, T. Evolution in group-structured populations can resolve the tragedy of the commons. *Proc. R. Soc. B* **273**, 1477–1481 (2006).
- Traulsen, A. & Nowak, M. A. Evolution of cooperation by multilevel selection. *Proc. Natl. Acad. Sci. USA* **103**, 10952–10955 (2006).
- Wilson, D. S. & Wilson, E. O. Rethinking the theoretical foundation of sociobiology. *Quart. Rev. Soc. Biol.* **82**, 327–348 (2007).
- Traulsen, A. Mathematics of kin- and group-selection: Formally equivalent? *Evolution* **64**, 316–323 (2009).
- Price, G. R. Selection and covariance. *Nature* **227**, 520–521 (1970).
- Monod, J. The growth of bacterial cultures. *Annu. Rev. Microbiol.* **3**, 371–394 (1949).
- Melbinger, A., Cremer, J. & Frey, E. Evolutionary game theory in growing populations. *Phys. Rev. Lett.* **105**, 178101 (2010).
- Cremer, J., Melbinger, A. & Frey, E. Evolutionary and population dynamics: A coupled approach. *Phys. Rev. E* **84**, 051921 (2011).
- Moran, P. A. *The Statistical Processes of Evolutionary Theory* (Clarendon Press Oxford, Oxford, 1964).
- Fisher, R. A. *The Genetical Theory of Natural Selection* (Oxford University Press, Oxford, 1930).
- Wright, S. Evolution in mendelian populations. *Genetics* **16**, 97–159 (1931).
- Kimura, M. *The Neutral Theory of Molecular Evolution* (Cambridge University Press, Cambridge, 1983).
- Cremer, J., Reichenbach, T. & Frey, E. The edge of neutral evolution in social dilemmas. *New J. Phys.* **11**, 093029 (2009).
- Strassmann, J., Zhu, Y. & Queller, D. Altruism and social cheating in the social amoeba *dictyostelium discoideum*. *Nature* **408**, 965–967 (2000).
- Wilson, D. How nepotistic is the brain worm? *Behavioral Ecology and Sociobiology* **2**, 421–425 (1977).
- Dronamraju, K. R. & Arese, P. *Malaria: Genetic and Evolutionary Aspects* (Springer, 2006).
- Gillespie, D. A general method for numerically simulating the stochastic time evolution of coupled chemical reactions. *Journal of Computational Physics* **22**, 403–434 (1976).

Acknowledgments

We thank Jan-Timm Kuhr and Matthias Lechner for helpful discussions. We thank Katherina Rasp for designing Fig. 1. Financial support by the Deutsche Forschungsgemeinschaft through the SFB TR12 “Symmetries and Universalities in Mesoscopic Systems” is gratefully acknowledged.



Author contributions

J.C., A.M., and E.F. designed the research. J.C., and A.M. performed the stochastic simulations and analyzed the data. J.C., A.M., and E.F. wrote the manuscript.

Additional information

Supplementary information accompanies this paper at <http://www.nature.com/scientificreports>

Competing financial interests: The authors declare no competing financial interests.

License: This work is licensed under a Creative Commons Attribution-NonCommercial-ShareAlike 3.0 Unported License. To view a copy of this license, visit <http://creativecommons.org/licenses/by-nc-sa/3.0/>

How to cite this article: Cremer, J., Melbinger, A. & Frey, E. Growth dynamics and the evolution of cooperation in microbial populations. *Sci. Rep.* 2, 281; DOI:10.1038/srep00281 (2012).

Supplementary Information

Population dynamics and the evolution of cooperation in group-structured populations

Jonas Cremer,¹ Anna Melbinger,¹ Erwin Frey^{1*}

¹ Arnold Sommerfeld Center for Theoretical Physics (ASC) and Center for NanoScience (CENS),
Department of Physics, Ludwig-Maximilians-Universität München,
Theresienstrasse 37, D-80333 München, Germany

*To whom correspondence should be addressed; E-mail: frey@lmu.de.

In this supplementary text, we give a more detailed discussion of our model and the group-growth mechanism. Furthermore we show comparisons of our analysis with experiments by Chuang et al. [1].

1 The Model

Here, we give details on the consecutive steps of the "life-cycle" of the meta-population. We first specify the group formation step before considering the dynamics within groups (group evolution step).

1.1 The Group Formation Step

Starting with an initial fraction of cooperators x_0 in the population, M groups are formed. Both, group size and group composition, are randomly distributed. Each group $i \in [1, M]$ initially consists of $\nu_{0,i}$ individuals. If the population from which the groups are formed

is much larger than Mn_0 , $\nu_{0,i}$ follows a Poisson distribution¹,

$$P(\nu_{0,i}) = \frac{n_0^{\nu_{0,i}}}{\nu_{0,i}!} \exp(-n_0), \quad (\text{S1})$$

with mean n_0 . Further, the initial composition of each group is also formed randomly. The probability for $\zeta_{0,i}$ cooperators in a group i is assumed to be given by a Binomial distribution

$$P(\zeta_{0,i}) = \binom{\nu_{0,i}}{\zeta_{0,i}} x_0^{\zeta_{0,i}} (1-x_0)^{\nu_{0,i}-\zeta_{0,i}} \quad (\text{S2})$$

with mean $x_0\nu_{0,i}$. The initial fraction of cooperators $\xi_{0,i}$ within each group is thereby given by $\xi_{0,i} = \frac{\zeta_{0,i}}{\nu_{0,i}}$.

By this we assume the groups to be formed at random without any bias. This corresponds to a worst case scenario for cooperators which gain no additional advantage due to positive assortment. Note, that the same initial distribution of group compositions is reached if one assumes both, the initial number of cooperators (C) and free-riders (F), to be Poisson distributed with mean values λ_C and λ_F , respectively. The mean values are related by $n_0 = \lambda_C + \lambda_F$ and $x_0 = \lambda_C/(\lambda_C + \lambda_F)$.

1.2 The Group Evolution Step

After the groups were formed randomly, they grow and evolve separately. In the following, we consider the dynamics within one specific group i in detail. As emphasized in the main text, we include two essential requirements experiments on microbial systems have in common. First, in each group cooperators (C) grow slower than free-riders (F). Second, groups with a higher fraction of cooperators grow faster and are bounded by a higher maximum group size (carrying capacity) than groups with a lower one. To account for these facts, the growth rates have to consist of a group related and a trait/type specific

¹This holds for typical conditions of small population bottlenecks as observed in bacterial life-cycles.

part [2, 3]. We, therefore, denote the per capita growth rate of an individual of type $S \in \{C, F\}$ within group i as

$$G_S(\xi_i) = g(\xi_i) \frac{f_S(\xi_i)}{\langle f \rangle}, \quad (\text{S3})$$

where $g(\xi_i)$ is the group related, $f_S(\xi_i)$, $S \in \{C, F\}$ is the species related part, and $\langle f \rangle = \xi_i f_C(\xi_i) + (1 - \xi_i) f_F(\xi_i)$ is the average fitness. The normalization of the fitness, $f_S(\xi_i)/\langle f \rangle$, is a convenient choice to disentangle the influence of global and relative parts more easily. Further, the group related part, $g(\xi_i)$, which accounts for the growth advantage of more cooperative groups, is assumed to increase linearly with ξ_i . For specificity, we use experimental conditions similar to those presented in reference [1, 4]. In these experiments, a purely cooperating population growth to an about ten times higher population size than a purely defecting one. In our model, the maximum population size scales with g and therefore we set

$$g(\xi_i) = r(1 + p\xi_i). \quad (\text{S4})$$

Here r determines the overall time scale for growth and defines our units of time, i.e. it is set to one unless specified otherwise. In the main text we have used $p = 10$ for specificity; see also section 3 where we compare with the experimental data by Chuang et al. [1].

Note, however, that the qualitative findings, especially both evolutionary mechanisms, do not depend on the exact form of $g(\xi_i)$ but only on the fact that $g(\xi_i)$ is monotonically increasing with the fraction of cooperators. The trait specific part, $f_S(\xi_i)$, includes the different growth rates of cooperators and free-riders within group i . We here employ the standard formulation of evolutionary game theory and assume it to be given by the payoff matrix of a Prisoner's dilemma game [5, 6]. The trait specific parts are given by

$$\begin{aligned} f_C(\xi_i) &= 1 + s[b\xi_i - c], \\ f_F(\xi_i) &= 1 + sb\xi_i, \end{aligned} \quad (\text{S5})$$

and the fitness advantage of free-riders $\Delta f = f_F(x) - f_C(x) = -sc$ is frequency independent. For specificity, we set $b = 3$ and $c = 1$. Thereby, the selection strength s is the only free parameter controlling the fitness difference, Δf , which corresponds to the advantage of free-riders within each group. In the experiments [1, 4], the selection strength was of the order $s \sim 0.05$. In our manuscript, we set $s = 0.1$ as an upper approximation of this value.

To model growth bounded by restricted resources we further introduce per capita death rates which increase linearly with the number of individuals in a group,

$$D_S(\nu_i) = \frac{\nu_i}{K}. \quad (\text{S6})$$

These are independent of the specific type S and lead to logistic-like growth within each group. K sets the scale of the maximum group size [7]. In detail, for purely defecting groups the carrying capacity is K while it is $(1+10)K$ for purely cooperating ones. For the discussed results, only the ratio of group sizes and not their absolute values are important. Hence, for numerical convenience, we set K to a constant value, $K = 100$.

The full stochastic dynamics follows a master equation which can be derived by the per capita growth and death rates, Eqs. (S3) and (S6). This master equation gives the temporal evolution of $P(\xi_i; \nu_i; t)$, the probability for group i to consist of ν_i individuals with a fraction of ξ_i cooperators at time t . We use the Gillespie algorithm to perform stochastic simulations [8].

While fluctuations strongly affect the dynamics, it is still instructive to look at the deterministic description where fluctuations during the group-evolution step are neglected. This deterministic dynamics within each group, i , is then given by rate equations for the

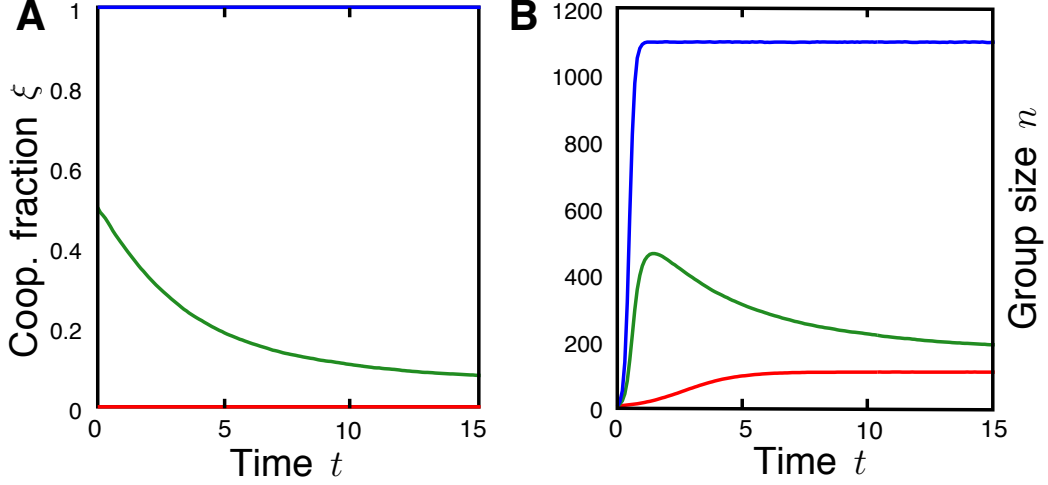


Figure S1: Dynamics in single groups. **A** Evolution of cooperation. For a mixed group (green), the fraction of cooperators declines due to the fitness advantage of free-riders while it stays constant for purely cooperating (blue) or defecting (red) groups. **B** Logistic like growth of the group size. For pure groups, the group-related advantage of more cooperative groups is most visible. Purely cooperating groups (blue) grow faster and reach a larger maximum carrying capacity than groups of only free-riders (red). A mixed group (green) grows faster than a group of only free-riders at the beginning. However also in the initially mixed group only free-riders can remain in the long run, and the carrying capacities of both groups become the same. The simulation average over different realizations of only one group. Parameters are $n_0 = 6$ and $s = 0.1$, ξ_0 is equal to 0 (red), 0.5 (green), and 1 (blue).

fraction of cooperators ξ_i and the total group size ν_i :

$$\begin{aligned}
 \partial_t \xi_i &= -s(1 + 10\xi_i)\xi_i(1 - \xi_i), \\
 \partial_t \nu_i &= (1 + 10\xi_i - \nu_i/K)\nu_i.
 \end{aligned}
 \tag{S7}$$

Thus, in a deterministic manner, intra-group evolution is described by a replicator-like dynamics while the size of each group follows logistic growth (with a ξ_i dependent growth rate and carrying capacity). We illustrate this dynamics in Fig. SS1 for three different initial conditions.

Table S1: Per capita growth rates of cooperators and free-riders in two groups

	group 1	group 2
fraction of cooperators ξ_i	3/4	1/4
per capita growth rate cooperators, $g(\xi_i)f_C(\xi_i)/\langle f \rangle$	8.31	3.33
per capita growth rate free-riders, $g(\xi_i)f_F(\xi_i)/\langle f \rangle$	9.05	3.58

Two groups, $i = 1$ and $i = 2$ in comparison. While the per capita growth rates of cooperators are smaller than the per capita growth rates of free-riders within every group, the per capita growth rate of cooperators in the more cooperative group 1 strongly exceeds the per capita growth rate of free-riders in the less cooperative group 2 due to the group related fitness $g(\xi_i)$. The strength of selection is given by $s = 0.1$.

2 The Group-Growth Mechanism

As stated in the main text, the group-growth mechanism relies on the faster growth of more cooperative groups. Even though cooperators reproduce slower compared to free-riders in the same group, the positive effect on group-growth can outbalance this disadvantage. For an illustration, see the specific example given in Table S1.

Here, we quantify the growth advantage of more cooperative groups. For this, we consider only short times $t \ll 1/s$. Then, and in the limit of weak selection, $s \ll 1$, the deterministic time evolution, given by Eqs. (S7), is

$$\begin{aligned}\xi_i &= \xi_{0,i} \\ \nu_i &= \nu_{0,i} \exp [g(\xi_{0,i})t].\end{aligned}$$

The overall fraction of cooperators can be calculated by averaging over all possible initial group compositions,

$$x(t) = \frac{\sum_i P(\xi_{0,i}; \nu_{0,i}) \xi_i \nu_i}{\sum_i P(\xi_{0,i}; \nu_{0,i}) \nu_i}.$$

By differentiating with respect to time t , we find the following expression

$$\frac{d}{dt}x = \text{Cov}(x, g(x)). \tag{S8}$$

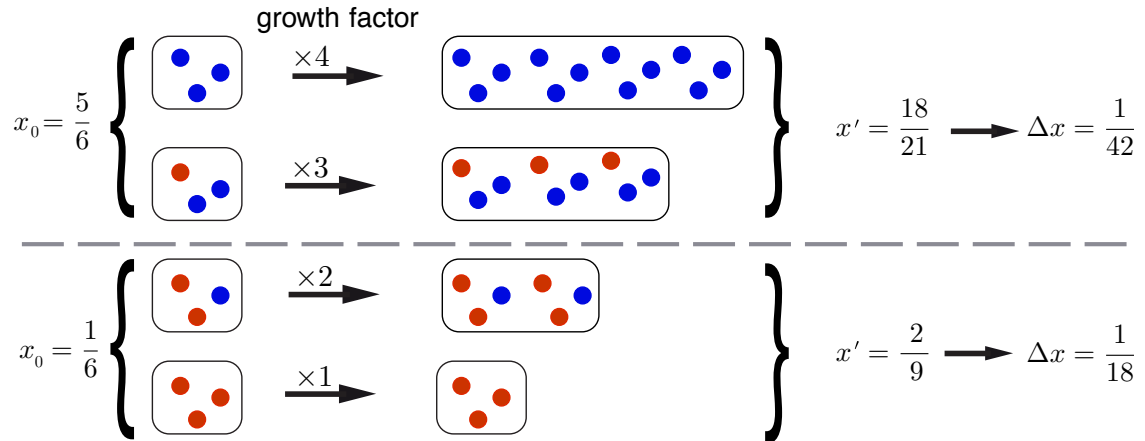


Figure S2: How the group-growth mechanism depends on the fraction of cooperators. Two sets of two groups are compared, one with a low fraction of cooperators (bottom) and one with a high one (top). Both groups evolve for a certain time, here with $g \propto 1 + 3x$ and no selection advantage for free-riders, $s = 0$. As can be readily seen, the change in the fraction of cooperators is larger for groups with a smaller initial fraction of cooperators.

This corresponds to a Price equation on the group level [9, 10], here stating that an increase in the fraction of cooperators is possible in principle if there is a positive correlation between x and the group related growth $g(x)$. However, for longer times $t > 1/s$ the selection advantage of free-riders counteracts the group-growth mechanism such that it can only act transiently.

As shown in the main text, the strength of the group-growth mechanism depends strongly on the initial fraction of cooperators. This is illustrated in Fig. SS2.

3 Comparison with experiments on synthetic microbial system by Chuang, Rivoire and Leibler

We have compared our theoretical analysis with recent experiments by Chuang et al. [1] on a synthetic microbial model system. They have studied regrouping populations with initial population size n_0 in the range between 2 and 3, an initial cooperator fraction

of $x_0 = 0.086$, and a regrouping time $T = 12 - 13$ h. Other model parameters were estimated as follows. The inherent fitness advantage of free-riders relative to cooperators was observed to be in the range between 1.04 and 1.05. In our model this translates to

$$f_C = 1, \quad (\text{S9})$$

$$f_D = 1.05, \quad (\text{S10})$$

where in contrast to equation (S3) we did not normalize the species related part, i.e. $\langle f \rangle \equiv 1$. The growth curves for different compositions of the population (see Fig.S3 in [1]) give access to the overall growth rate and its frequency dependence. From Fig.S3 in [1] we estimate:

$$r = 6.8 \times 10^{-4} \text{ min}^{-1}, \quad (\text{S11})$$

$$p = 6.6. \quad (\text{S12})$$

Employing these parameters in our model we have simulated the regrouping dynamics and find good agreement with the experimental results, cf. Fig. S3a. Since the population dynamics is still within the exponential growth phase at the regrouping time, we interpret the observed increase of cooperation as a group-growth mechanism. However, because of the particular set of experimental parameters, the resulting stationary cooperator fraction is very close to one which makes it difficult to observe coexistence between cooperators and free-riders. We can now use our theoretical model to explore the effects of an increase in the regrouping time. Changing the regrouping time from $T = 12.5$ h to $T = 375$ h we find that the time evolution of the cooperator fraction remains qualitatively similar, despite the fact that now cooperation increases because of the group-fixation mechanism, cf. Fig. S3b. Thus even by changing the regrouping time these small values of n_0 do not allow to distinguish between the two mechanisms. However, as discussed in the main text,

larger values of n_0 (in the range of 4–6) give a clear signature of each of the mechanisms upon varying the regrouping time.

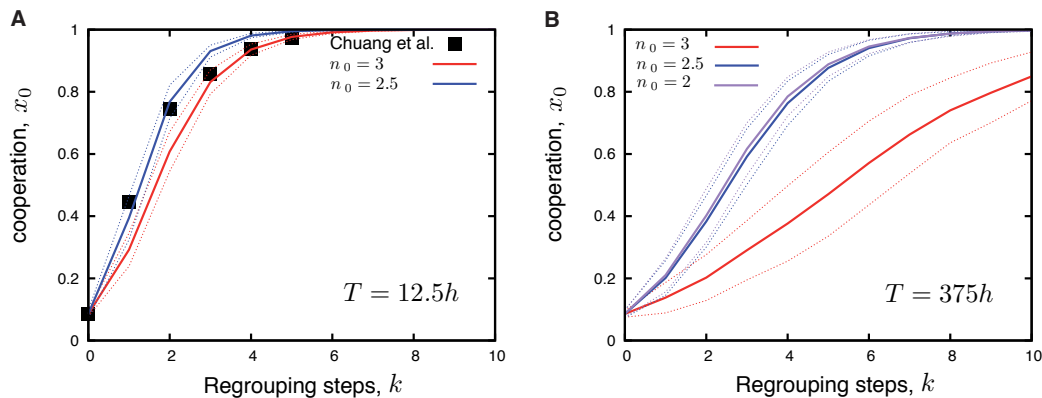


Figure S3: Increase in the level of cooperation for conditions resembling those examined by Chuang et al. [1]. **A** Short regrouping time, $T = 12.5h$. The measurements by Chuang et al. (black points) in comparison with the predictions of our model. Solid lines denote the expected level of cooperation. The dashed lines show the corresponding mean plus/minus the standard deviation. **B**, Large regrouping time $T = 375h$. For similar conditions, but a longer regrouping time, the outcome is qualitatively the same and only cooperators prevail. For both parts of the figure parameters are $x_0 = 0.086$, $r = 6.8 \times 10^{-4} \text{ min}^{-1}$, $f_C = 1$, $f_D = 1.05$, $p = 6.6$. In **A**, $K = 1.5 \times 10^6$. In **B**, $K = 1.5 \times 10^5$.

4 Captions of supporting videos

The two supplementary videos illustrate the group-growth and the group-fixation mechanism:

1. Video S1: Evolution of cooperation, caused by the group-growth mechanism
2. Video S2: Reaching purely cooperative behavior, caused by the group-fixation mechanism.

In detail, both videos show the probability distribution for groups of size N containing a fraction of cooperators, x and how it changes with time during the group evolution

step. The green dot indicates the mean fraction of cooperators. For several regrouping steps the evolutionary outcome depends strongly on the relative impact of the growth and fixation mechanisms. Here, this is exemplary shown for regrouping times $T = 2.5$, [video 1, group-growth mechanism dominates] and $T = 20$ [video 2, group-fixation mechanism dominates]. Parameters are given by $n_0 = 5$, $s = 0.1$, and $M = 5000$ for both videos.

4.1 Video S1

Small regrouping times (group-growth mechanism, see text): A single cooperating mutant can spread in the population. Starting from a very low initial fraction of cooperators, the level of cooperation increases during every regrouping step until a stable level of cooperation is reached. This behavior is caused by the faster growth of more cooperative groups as illustrated in the video by the strong correlation between the level of cooperation within a group and its speed of growth.

4.2 Video S2

Large regrouping times (group-fixation mechanism, see text): Above a certain threshold value in the level of cooperation, cooperators can overtake the entire population since purely cooperative groups are present and can play out their advantage in reaching a higher maximum group size even though all initially mixed groups are taken over by cheaters only.

Part II

Molecular Motors and their Interaction with Microtubules

4 Transport on Microtubules

The second part of this thesis focusses on motor proteins interacting with microtubules (MTs) which are filamentous constituents of the cytoskeleton [1]. In this chapter, the basis to understand MT-motor interactions, like transport processes and length-regulation, is provided. First, the cytoskeleton and its constituents, with a special focus on microtubules, are introduced. Then, we discuss motor proteins which play a central role in transport processes as well as in the length-regulation of microtubules. The latter is addressed in more detail in Chapter 5. Subsequently, we provide a brief overview on the theoretical models describing the movement of such molecular motors along microtubules. Finally, a specific example is discussed. Therein, motor proteins on two parallel microtubule filaments obstruct each other due to large cargos bound to them. Thereby the transport properties of the system are strongly altered compared to a non-obstruction scenario.

4.1 Cytoskeleton

The cell is not merely an accumulation of proteins, organelles and other building blocks bounded by the cell membrane. Rather it is a highly structured entity including various compartments, functional areas and interconnections of these [1]. The cytoskeleton is the scaffolding stabilizing and organizing the cell. For long times, it was generally acknowledged that only eukaryotes have such stabilizing structures, but recent studies also uncovered cytoskeletal filaments in prokaryotes [219] and evidence for them in archaea [220]. The cytoskeleton is highly dynamic and adapted to diverse requirements which go far beyond a simple provision of mechanical support: It has to deal with stress and hence be elastic. At the same time rigidity is required to stabilize the cell structure. Moreover, dynamic rearrangements of the cytoskeleton which happen during each cell cycle have to be feasible. The cytoskeleton meets all these ostensibly contradicting challenges and thereby facilitates many cellular processes which are essential for the metabolism. Just to mention a few, cytoskeletal filaments play a central role in intracellular transport processes [26], cell division [1], neuronal morphogenesis [221] and cell locomotion [222].

The purpose of these structures is versatile and so is their design. In principle, three distinct classes of fibrous proteins forming the cytoskeleton can be distinguished: microfilaments, intermediate filaments and microtubules.

Microfilaments

Microfilaments, as their name indicates, are the smallest cytoskeletal filaments with a diameter of approximately 6 nm . They consist of filamentous actin (F-actin) and exist across species

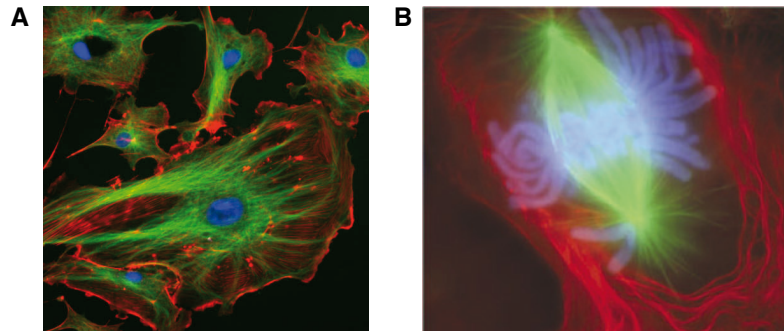


Figure 4.1: **A** Microscopic picture of endothelial cells. The nucleus is labelled in blue, the microtubules in green and the actin network in red. **B** Mitotic spindle formed of microtubules (green) during cell division. The mitotic spindle attaches to chromatids and pulls them apart. The pictures are taken from [223] and [224].

in slightly modified forms [1]. Each filament is built of two intertwined actin α -helices and is polar, *i.e.* it has a distinguished direction. This polarity and the elasticity (the persistence length is given by $l_p \approx 15\mu m$) play a crucial role for the functionality of microfilaments. Actin is the most dynamic constituent of the cytoskeleton. Organized in bundles or in networks which are stabilized by cross-linkers, actin filaments fulfill several tasks: elastic stabilization of cells, muscle contraction, cell motility and transport due to molecular motors walking along them [225].

Intermediate Filaments

Intermediate filaments, as keratin or vimentin, usually have a diameter of 10 nm and are often highly elastic. Due to their high rigidity and flexibility they are perfectly suited to cope with mechanical stress. Intermediate filaments are present at the nucleus and at the cell membrane where they are among others important for cell-cell junctions. Many diseases, as muscular dystrophy, are caused by disfunction of intermediate filaments which then lose their flexibility [226].

Microtubules

With a diameter of 25 nm and a length up to 25 μm , microtubules (MTs) are the largest cytoskeletal filaments. They are hollow tubes, mostly consisting of 13 protofilaments, which in turn are built of $\alpha\beta$ -tubulin heterodimers, cf. Fig. 4.2. In contrast to micro- and intermediate filaments, MTs are rigid and not elastic ($l_p = 6mm$). As actin, they are polar and have a minus and a plus end. Tubulin, which diffuses in the cytosol, can attach at both sides, but its attachment rate at the plus end is much higher than at the minus end [227]. Hence, MTs grow mainly at the plus end and thereby explore cellular space. Due to their dynamic length [228], they are important for processes as cell division. For instance, recent studies in fission yeast studied the role of MTs for the nucleus positioning [229]: Fission yeast is a rod-shaped cell. In the interphase the nucleus has to be positioned in the middle of the cell

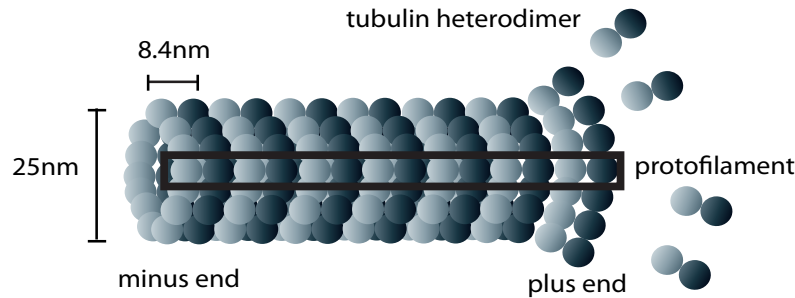


Figure 4.2: Illustration of a microtubule. It consists of 13 protofilaments which form a hollow tube with a diameter of 25 nm. The protofilaments are composed of α - and β -tubulin heterodimers.

to facilitate correct cell division. Even though the details are not fully resolved yet, MTs play a central role in this process. Growing from the nucleus towards the cell periphery, where they push against the cell walls, MTs are able to locate the cell center. Also in a later stage of cell division MTs play a crucial role. During mitosis, they form the mitotic spindle (see Fig. 4.1) most likely organized by centrosomes located at opposing cell poles [230, 6]. After the nucleus has dissolved, MTs attach to the chromatids via kinetochores and push them apart such that one set of chromosomes is finally located at each cell pole. Therefore, dynamic length changes are essential for a proper separation of chromosomes. Concerning this length-regulation much insights were gained in recent years: MTs display stochastic changes between growth and shrinkage states, called dynamic instability [231, 232]. The reason for this behavior seems to be the molecular structure of the protofilaments [233]. $\alpha\beta$ -tubulin can either bind GTP or GDP and thereby form GTP- and GDP-bound heterodimers, respectively. The latter have a curved structure and therefore organization of 13 filaments into a microtubule causes internal stress. This is balanced by a cap at the MT tip consisting of straight GTP-bound tubulin. Within the MT the tubulin dimers hydrolyze to GDP-bound tubulin which does not have the ability to stabilize the MT. As long as hydrolysis does not emerge at the tip, the cap is able to compensate for the mechanical stress in the MT. If also the tip is hydrolyzed, the 13 filaments are not longer held together and large parts of the MT dissolve due to the intrinsic curvature of the filaments: a so-called catastrophe happens. Afterwards, MTs recover as tubulin dimers constantly attach at the tip. This ensuing growth phase is called rescue. Recent studies suggest that these rescue dynamics also rely on the presence of GTP heterodimers in the interior of the MT, *i.e.* the MT depolymerizes till the tip reaches an inner GTP-bound area [234]. Also theoretical work was done to explain dynamic instability [235, 236, 237, 238]. Besides this intrinsic length-dynamics, MTs change their length due to interactions with molecular motors or in response to force [239]. Thereby, length can be regulated, see Chapter 5. Furthermore, MTs play a crucial role for the movement of prokaryotic cells. In combination with the molecular motor dynein which produces forces, MTs actuate the flagella and thereby the cells. Another example for the functionality of MTs is the transport of large cellular building blocks through the cell, for which diffusion through the crowded cytosol is slow. Instead, molecular motors “walk” along MTs having attached cargos, like organelles or other macromolecules.

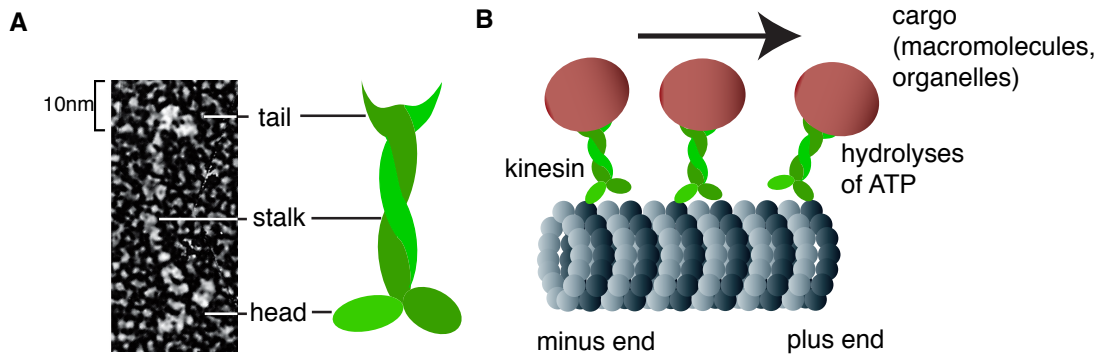


Figure 4.3: Illustration of the structure and functionality of kinesin. **A** Microscopic and schematic picture of kinesin. John Heuser kindly provided the freeze-etch electron micrograph on the left. **B** Kinesins walking along the MT transport cargos bounded to their tail.

4.2 Molecular Motors

Microtubules obtain a large part of their functionality in combination with associated proteins. These proteins do not only transport cargos along the filament, but also exert forces or interact with the filaments and thereby trigger polymerization and depolymerization [240]. The most prominent examples of these proteins are dynein and kinesin. Kinesin consists of a head domain, a stalk and a tail where cargos can bind, see Fig. 4.3A. Molecular motors literally walk along single filaments of an MT [241, 242] gaining energy from the hydrolysis of ATP [243], cf. Fig. 4.3B. For kinesins and myosins¹, this hydrolysis leads to conformational changes in the protein which in turn cause a power stroke [244]. While dyneins walk from the plus to the minus end along the protofilament axis and hence transport cargos from the cell periphery to the nucleus, kinesins move vice versa [241]. Each of their steps covers the distance of a tubulin dimer (8.4 nm) [245]. Though the exact molecular mechanisms for this movement are not fully resolved, for kinesins the most promising hypothesis is the hand-over-hand mechanism [246, 247]. It suggests that both heads (corresponding to the feet of the motor) move alternately. Most kinesins walk processively [248], *i.e.* they do not detach from the MT for large run-lengths [249]. Taken together, molecular motors can walk unidirectionally on polar MTs, have the ability to bind large cargos, and can be regulated [243]. Thereby, they are optimal machineries to perform intracellular transport processes [250].

Besides transporting cellular building blocks, molecular motors accomplish also other important tasks. A prominent example are MT polymerases and depolymerases [240, 251]. Due to the stabilizing GTP cap at the tip, length-dynamics can consequently be regulated at the plus end. This makes motors walking towards the tip perfect candidates to govern length-dynamics. Besides these walking motors, there exist also other forms of so called plus-end tracking proteins (+TIPs) which have specific binding rates to the tip or which are associated with other +TIPs [227]. For example the depolymerizing kinesin MCAK diffuses unbiased on the MT until it reaches the tip [252, 31]. Motors from the kinesin-8 or kinesin-13 (also known as Kin I or M-type kinesin) protein families, play a crucial role in length-regulation [253, 254].

¹Myosin is a molecular motor interacting with actin and plays a crucial role for muscle contraction.

Kinesin-13 motors are in the focus of research and best characterized. *In vivo* studies highlight their essential role for spindle formation and nucleus positioning [255]. That supports the idea that a proper length-regulation is necessary for these processes. To gain further understanding of the molecular mechanisms underlying this length-regulation of MTs, several *in vitro* experiments were performed where the interaction of just a few motor types with the MT was studied [256, 32, 257, 34], cf. Chapter 5. However, the exact mechanisms of length-regulation and the reasons for the use of molecular motors are not fully resolved yet. From an evolutionary point of view, it seems to be obvious that a complex regulatory mechanism employing motors has a certain functionality for cells, *e.g.* length-dependent regulation: Molecular motors need plenty of ATP, the cellular energy unit, for their movement along filaments. For the depolymerization of a single tubulin dimer, not only the energy for the depletion but also for the motor running towards the tip has to be provided. If the sole purpose was to shorten the MT, also diffusive proteins could be employed which do not need energy for reaching the tip. Instead motors are used. The advantage seems to be the possibility of length-regulation which arises due to crowding effects as discussed in Chapter 5.

4.3 Driven Exclusion Processes

Molecular transport along MTs can be described by driven exclusion processes. This class of models accounts for directional transport including crowding effects due to an on-site interaction, *i.e.* each site is occupied by at most one particle. In the following we review the most important models in the context of this thesis.

4.3.1 Totally Asymmetric Simple Exclusion Process

The **T**otally **A**symmetric **S**imple **E**xclusion **P**rocess (TASEP) is a paradigm of non-equilibrium statistical physics [258, 259, 260, 261]. It was originally proposed by MacDonald to describe the translation of mRNA [262]: To build proteins, ribosomes ‘read’ the genetic code and translate it into a chain of amino acids. In doing so, they walk uni-directionally along a mRNA strand and mutually obstruct each other. Nowadays, the TASEP also serves as a simplistic model describing the movement of molecular motors along MTs. This description especially accounts for crowding effects and the ensuing traffic jams. Actually these crowding effects can strongly influence the transport properties of a system [263, 264, 265, 266].

As shown in Fig. 4.4², the TASEP consists of a one-dimensional lattice with L sites. The particle configuration is described by a set of discrete occupation numbers, $n_i \in \{0, 1\}$ with $i = \{1, 2, \dots, L\}$. On the lattice, particles can move uni-directionally to the right provided that the next site is empty. Their hopping rate ν can be set to one, corresponding to a rescaling of time. At the boundaries particles enter and leave the system at rates α and β , respectively. Despite the simple considerations leading to the TASEP, it shows a comparably rich phenomenology including some characteristic properties of systems far away from equilibrium. This fact is one of the reasons for the outstanding position of TASEP in non-equilibrium statistical physics which is comparable to the Ising model’s importance for equilibrium statistical

²In this figure the more general TASEP/LK model is shown which reduces to the TASEP for $\omega_a = \omega_d = 0$.

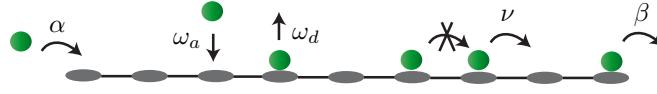


Figure 4.4: Illustration of the TASEP with Langmuir kinetics (TASEP/LK). Particles enter at the left-hand side of the system at rate α and leave at the right-hand side at rate β . On the lattice, they move uni-directionally to the right provided that the next site is empty. Their hopping rate $\nu = 1$ sets the time scale of the system. Particles from the surrounding can attach at empty lattice sites at rate ω_a . Analogously particles can detach from the lattice at rate ω_d . Setting the rate ω_a and ω_d to zero, the model reduces to the standard TASEP.

mechanics. This view is encouraged by the fact that it can be solved analytically by employing recursion relations [267], the matrix product ansatz [268, 269] or the Bethe ansatz [269, 270]. Remarkably, also a simple mean-field approach (or hydrodynamic limit), where correlations between neighboring sites are neglected, $\langle n_{i-1}n_i \rangle = \langle n_{i-1} \rangle \langle n_i \rangle$, leads to the exact current-density relation³. The resulting current, J , depends solely on the particle density in bulk. As the density is constant except for boundary effects, $\langle n_i \rangle = \rho(x) = \rho$, the current is given by,

$$J = \rho(1 - \rho), \quad (4.1)$$

where the factor $1 - \rho$ accounts for exclusion as it is the probability that the next site is unoccupied.

The phase behavior sensitively depends on the boundary conditions. Those play such an important role as the system is driven far away from equilibrium: Due to transport, boundary effects are directly fed into the system [258]. Therefore, also in one dimension, several phases and phase transitions emerge [271]. In contrast, in equilibrium physics such one-dimensional phase transitions only arise under very restrictive conditions, *e.g.* zero temperature, long-range interactions or infinite interaction energy [272, 273, 258]. Besides derivations from the full analytic solutions or the *extremal current principle* [271, 274, 275], the phase behavior can also be understood intuitively as follows: For $\alpha < \beta$ and $\alpha < 0.5$, the left boundary is the bottleneck of the system, *i.e.* less particles can enter the system than leave it. Therefore, the entering current determines the system and equating $J_{\text{IN}} = \alpha(1 - \rho)$, with the bulk current, Eq. (4.1), leads to the bulk density $\rho = \alpha$ in the so-called low density phase. Analogously, the bulk density follows if the bottleneck is at the right, $\beta < \alpha$ and $\beta < 0.5$. Employing the exiting current $J_{\text{EX}} = \beta\rho$, the bulk density $\rho = 1 - \beta$ in the high density phase can be derived. If neither the entering nor the exiting current are bottlenecks, $\alpha, \beta > 0.5$, the transport behavior of the system sets the density to a value where the current is maximized (maximal current phase). This is the case for $\rho = 0.5$, since the number of particles and the number of holes, onto which particles can hop, is optimized for half filled systems. A summary of the ensuing phase behavior depending on α and β is shown in Fig. 4.5.

³Due to particle exclusion, it is not obvious that these correlations cancel out.

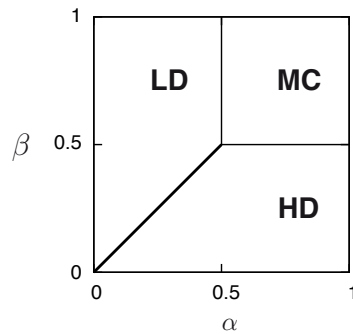


Figure 4.5: Phase diagram of the TASEP. For small entering rates $\alpha < 0.5$ and $\alpha < \beta$ the system is determined by the entering current and a low density is realized in the system (LD). In contrast, for $\beta < 0.5$ and $\beta < \alpha$ crowding effects cause the high density phase (HD). If both boundary rates are large $\alpha, \beta > 0.5$, the maximal current phase (MC) arises.

4.3.2 TASEP/LK

In contrast to the considerations above, molecular motors do not only enter the MT at its first site and leave at its last site. Instead, motor proteins freely diffuse in the cytosol and are able to attach anywhere at the MT. This is illustrated in Fig. 4.6 where an MT consisting of 13 filaments surrounded by motors diffusing in the cytosol is depicted. For a more realistic description, the TASEP/LK model was proposed [276, 277]. Here, the standard TASEP model is extended with Langmuir kinetics, *i.e.* attachment and detachment rates, ω_a and ω_d , at each site of the lattice, see Fig. 4.4. Thus, the particle density is not constant anymore but explicitly depends on the spatial position: Particles accumulate over the lattice and are lost due to detachment kinetics. Employing the hydrodynamic and continuum limit, the following

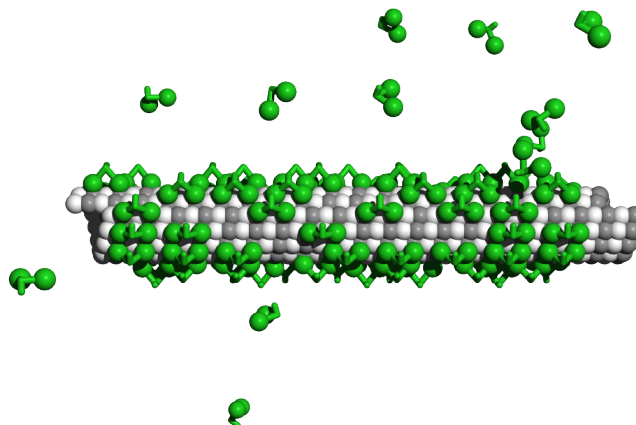


Figure 4.6: Illustration of the role of collective phenomena on an MT. Motors diffusing in the cytosol can attach anywhere at the MT. Also interactions between motors on neighboring protofilaments are possible. A. Vilfan kindly provided the figure.

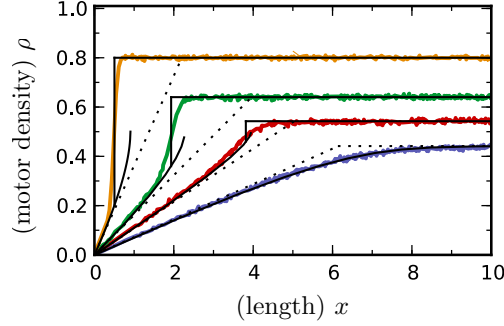


Figure 4.7: Typical density profiles for the TASEP/LK model with $\alpha = 0$ and $\beta = \frac{\omega_d}{\omega_a + \omega_d}$. At the left motors accumulate and thereby cause an approximately linear increase in the density until the Langmuir density is reached. Colored lines are simulation result, while solid and dotted black lines correspond to the full and approximative analytic solutions of Eq. (4.2), respectively.

differential equation for the particle density depending on the lattice position can be obtained,

$$\partial_t \rho(x) = [2\rho(x) - 1] \partial_x \rho(x) + \omega_a - (\omega_a + \omega_d)\rho(x). \quad (4.2)$$

The density profiles can be calculated analytically employing Lambert W functions [276, 277]. As the phenomenology of the model is rich, we restrict our discussion of the density profiles to a specific set of parameters⁴. We set the right boundary to $\beta = \frac{\omega_d}{\omega_a + \omega_d}$ as then its influence is not visible in bulk. As particle-hole symmetry holds, effects similar to the ones arising at the left boundary are possible in more general situations. Further, we set $\alpha = 0$. This specific value of the boundary is especially relevant for transport along MTs, *i.e.* the first site is not populated at a higher rate than the bulk. In Fig. 4.7 typical ensuing steady state density profiles are shown. Starting from the left, particles accumulate at the lattice with an approximately linear density profile with slope ω_a . In this approximation the density profile at the minus end is given by $\rho^-(x) = \omega_a x$. At the right hand side of the system, the density reaches the constant Langmuir density. This density can be calculated from Eq. (4.2) employing $\partial_x \rho(x) = 0$ and is given by $\rho_{\text{La}} = \frac{\omega_a}{\omega_a + \omega_d}$. Only for $\rho_{\text{La}} \leq 0.5$, the linear profile can match the Langmuir density continuously and the position of the domain wall, ℓ^- , is determined by the condition, $\rho^-(\ell^-) = \rho_{\text{La}}$. In contrast, for $\rho_{\text{La}} > 0.5$, the transition to the Langmuir density is discontinuous and can be calculated assuming current conservation, $\rho^-(\ell^-) = 1 - \rho_{\text{La}}$. Current conservation holds for $\omega_a \ll 1$ and $\omega_d \ll 1$. Taken together, in linear approximation the transition from the regime, where particles accumulate, to the regime, where the Langmuir density is reached, happens at [278],

$$\ell^- = \begin{cases} \frac{1}{\omega_d(K+1)} & \text{for } K < 1, \\ \frac{1}{c\omega_a(K+1)} & \text{for } K > 1. \end{cases} \quad (4.3)$$

Here, $K = \omega_a/\omega_d$ is the binding constant characterizing the interplay of attachment and detachment.

⁴For a detailed description of the density profiles and phases see [277].

4.3.3 Extensions of these Models

In biological scenarios, various other effects come into play. In order to find more realistic descriptions for biological transport processes, many interesting extensions of the TASEP have been studied. For example, the fact that motors are not just particles but enzymes following complex biochemical cycles [279, 280] was included. Further, compartmentalization and the interaction of diffusive and directed transport areas [281, 282] or complex binding properties of the motors [283] were investigated. In addition, the influence of defects on the molecular track [284, 285, 286] and spatially extended particles [287] were studied.

Since motors do not only move on single protofilaments of the MT, multilane models are also of large relevance [288, 289, 290, 291, 292, 293, 294, 295, 296, 297, 298, 299]. Therefore, many models accounting for two or more coupled lanes have been investigated. Particles can change lanes [288, 289, 290] or obstruct each others movement [292, 294, 296, 297]. The latter arises due to attractive or repulsive forces and steric exclusion as motors sometimes carry large cargos. Taken together, the coupling between lanes can be either caused by lane switching events or an interaction between particles on different lanes. For both scenarios much progress has been achieved and interesting phenomena, like non-trivial density profiles [288, 289], spontaneous symmetry breaking [294, 296, 297] and domain walls [288, 289, 293] have been discovered.

4.4 Papers and Manuscripts

4.4.1 Two Lanes with Particle Exclusion and Obstruction

In the article “Driven transport on two lanes with particle exclusion and obstruction”, Phys. Rev. E **83**, 031923 (2011), we employing a two lane model to study how the movement of motors is influenced by an obstruction of neighboring particles. As it turned out, this obstruction, *e.g.* stemming from large cargos attached to motors, has a strong impact on the transport dynamics. We neglected lane changes since they seem to play a minor role [300].

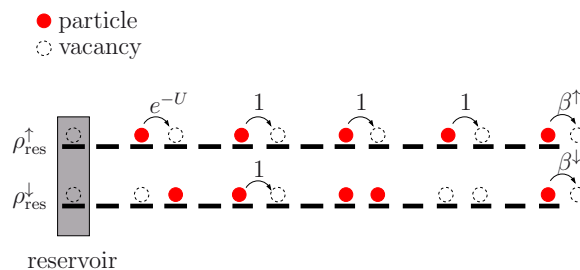


Figure 4.8: Illustration of the two-channel model including obstruction between neighboring particles on different lanes. The hopping rates are set to 1 if the next site is empty, except for the scenario when particles obstruct each other. Then, the hopping rate is reduced to e^{-U} . At the left boundary particles enter from reservoirs $\rho_{\text{res}}^{\uparrow\downarrow}$ while they leave the system at rates $\beta^{\uparrow\downarrow}$ on the right.

Several phases emerge which cannot be found in single lane models. These phases can be divided into two classes: boundary and bulk induced phases. The transport properties of the latter are robust against small changes of the rates at the boundaries. Hence, they might be relevant if a constant particle current is needed, *e.g.* a constant supply by a certain macromolecule transported by motors. In contrast, boundary induced phases are tunable by the entering and exiting rates and thereby offer the possibility to regulate the particle currents.

4.4.2 Conclusion and Outlook

Transport on MTs is an important task which is often accomplished by molecular motors. In particular, the transport of large macromolecules which otherwise would diffuse slowly, is essential. Here, we focussed on the influence of a mutual obstruction between particles moving on two different filaments on the same MT. It would be interesting to extend this two lane approach to more lanes. Especially, the realistic situation of 13 filaments which form a hollow tube could be considered to estimate the effects of such an obstruction for the movement of motors along MTs.

Much progress has been achieved in applying driven diffusive systems to biological transport phenomena. However, still many questions are unsolved, especially, when thinking about the simultaneous influence of several extensions of the TASEP. For instance, it would be important to study the influence of lane changes on the two lane model presented above. In principle, these lane changes can lead to position dependent density profiles. It would be interesting, how the ensuing phase behavior alters compared to the scenario presented here. In addition, particles in the cytosol can be taken into account explicitly by also allowing motors to attach to and detach from the lattice.

Driven transport on parallel lanes with particle exclusion and obstructionAnna Melbinger,¹ Tobias Reichenbach,² Thomas Franosch,^{1,3} and Erwin Frey¹¹*Arnold Sommerfeld Center for Theoretical Physics (ASC) and Center for NanoScience (CeNS), Department of Physics, Ludwig-Maximilians-Universität München, Theresienstraße 37, D-80333 München, Germany*²*Laboratory of Sensory Neuroscience, The Rockefeller University, 1230 York Avenue, New York, New York 10065, USA*³*Institut für Theoretische Physik, Friedrich-Alexander-Universität Erlangen-Nürnberg, Staudtstraße 7, D-91058 Erlangen, Germany*

(Received 20 February 2010; revised manuscript received 2 February 2011; published 31 March 2011)

We investigate a driven two-channel system where particles on different lanes mutually obstruct each other's motion, extending an earlier model by Popkov and Peschel [*Phys. Rev. E* **64**, 026126 (2001)]. This obstruction may occur in biological contexts due to steric hinderance where motor proteins carry cargos by “walking” on microtubules. Similarly, the model serves as a description for classical spin transport where charged particles with internal states move unidirectionally on a lattice. Three regimes of qualitatively different behavior are identified, depending on the strength of coupling between the lanes. For small and large coupling strengths the model can be mapped to a one-channel problem, whereas a rich phase behavior emerges for intermediate ones. We derive an approximate but quantitatively accurate theoretical description in terms of a one-site cluster approximation, and obtain insight into the phase behavior through the current-density relations combined with an extremal-current principle. Our results are confirmed by stochastic simulations.

DOI: [10.1103/PhysRevE.83.031923](https://doi.org/10.1103/PhysRevE.83.031923)

PACS number(s): 87.10.Mn, 05.70.Ln, 05.40.–a

I. INTRODUCTION

Driven diffusive systems are of importance in various fields of physics and biology [1,2], since they serve as simplistic models for biological transport phenomena [3–6], traffic flow [7–10], fast ionic conductors [11], as well as quasiclassical spin transport [12]. Furthermore, they provide valuable insights into nonequilibrium statistical mechanics. As an example, and in contrast to equilibrium systems, their bulk behavior is sensitive to the boundaries [13]. Boundary induced phase transitions in one dimension may emerge resulting in complex phase behavior.

The most prominent example of driven lattice gases, the totally asymmetric exclusion process (TASEP), was originally proposed as a simple model for the motion of multiple ribosomes along a mRNA strand during protein translation [14]. In this model, particles move unidirectionally along a one-dimensional lattice, provided the next site is empty. Exact solutions, e.g., by employing the Bethe ansatz [15] or a matrix product ansatz [16], are feasible, yet much insight can readily be obtained from simple mean-field considerations [2].

Intracellular transport constitutes another fascinating biological application [17] of driven systems. Here, molecular motors such as kinesin or dynein, driven by the hydrolysis of adenosine triphosphate (ATP), move unidirectionally along microtubules [3]. Macromolecules or other cellular constituents, which often are too large to diffuse fast enough through the crowded cytosol, are carried by motor proteins, and are then actively transported to the location where they are needed. Recent theoretical studies motivated by these processes have investigated the influence of attachment and detachment of the motors to the microtubules [18–22], extended particles [23], the influence of defects on the track [24–26], and the competition between different motor species [27,28]. Further attention has been paid to transport along several coupled channels where particles move in parallel. This coupling can be either achieved by allowing lane-switching events [12,29–37] or by a possible influence of a particle in

one channel on the motion in the other channel [7,38]. Here we consider the latter case and investigate how mutual obstruction of motor proteins on neighboring lanes, for example, stemming from large cargos attached to them, affects the transport properties of the system.

Driven diffusive systems may also serve as a description for spin transport with possible applications in the field of spintronics. For instance, such spin currents flow in a chain of quantum dots where electrons are driven by an external voltage in a way that only the lowest energy levels can be occupied [39]. Hence not more than one electron of each internal state is permitted per site and electrons located in the immediate vicinity repel each other due to Coulomb interaction. A model taking Pauli's exclusion principle into account while ignoring phase coherence has been investigated recently [12,30,31], yet Coulomb blockade has been neglected. In the present paper we focus on the influence of a mutual obstruction mimicking, for example, Coulomb interaction. To identify its effect on the collective transport properties in the clearest way, we disregard spin-flip events which can cause intriguing behavior on their own [12,30,31].

A simple lattice model that incorporates mutual obstruction on two lanes has been investigated by Popkov and Peschel [7]. The steric hindrance there is manifested in the hopping rates that explicitly depend on the configuration on the opposing lane. As a consequence of this coupling of the lanes, a variety of peculiar phases arises which has been neatly rationalized in terms of a cluster approximation. Particularly, symmetry breaking, which arises even though the boundary conditions are symmetric, is observed and analyzed.

In this paper we extend the model of Ref. [7] by considering asymmetric boundary conditions and rates instead of reservoirs at the right boundary. We introduce the model in Sec. II, both in the two-lane and in the spin-transport picture. In Sec. III we describe the stochastic simulations and provide first insights in how particle obstruction affects the behavior. Namely, we identify three regimes of qualitatively different behavior. In

Sec. IV, we analytically compute the current-density relations within a one-site cluster approximation. Section V presents a discussion on how the current-density relation, obtained via an extremal-current principle, allows us to identify the system's different phases and to analytically predict the phase diagram. We summarize our main findings in Sec. VI and provide a brief conclusion.

II. MODEL

We examine a driven diffusive system which serves as a minimal model for the transport on two parallel lanes, which are coupled by a repulsive short-range interaction. The same model describes classical driven spin transport with Coulomb blockade. In the following we specify the dynamics in detail, presenting both the two-lane and the spin-transport representation.

A. Two-channel representation

Consider particle transport along two parallel channels, each of them containing N discrete lattice sites; see Fig. 1. Each site may contain at most one particle (on-site exclusion), such that the occupation number of site i on the upper (lower) channel, n_i^\uparrow (n_i^\downarrow), can only take values 0 or 1, corresponding to a vacant or an occupied site, respectively.

Particles enter from two entangled reservoirs located at the left-hand side of the system. At each time step, the reservoir is in one of the four possible states: (i) double occupation with probability κ^* , (ii) only the upper reservoir is occupied with probability $\rho_{\text{res}}^\uparrow - \kappa^*$, (iii) only the lower reservoir is occupied with probability $\rho_{\text{res}}^\downarrow - \kappa^*$, and (iv) both reservoir sites are empty with probability $1 - \rho_{\text{res}}^\uparrow - \rho_{\text{res}}^\downarrow + \kappa^*$. Thus $\rho_{\text{res}}^\uparrow$ and $\rho_{\text{res}}^\downarrow$ are the average densities on the upper and lower reservoir, respectively, and κ^* corresponds to the double-occupation density in the reservoir.

In bulk, particles move unidirectionally to the right. Due to obstruction, the hopping rate thereby depends on the particle configuration at the other lane. A particle attempting to proceed by one site is obstructed if a particle resides on the subsequent site of the other channel. However, this obstruction is relevant only when the particle does not experience obstruction in its current position, meaning when its current neighboring site on

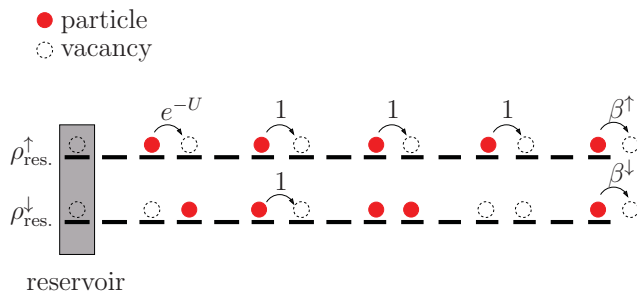


FIG. 1. (Color online) Illustration of the two-lane representation. Particles enter from two reservoirs at the left boundary with densities $\rho_{\text{res}}^\uparrow, \rho_{\text{res}}^\downarrow$. In bulk, hopping rates depend on the particle configuration of the, respective, other lane. At the right boundary particles leave at rates $\beta^\uparrow, \beta^\downarrow$.

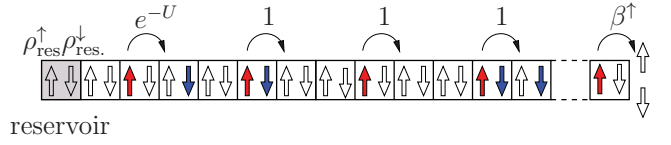


FIG. 2. (Color online) Illustration of an exclusion model with two internal states, adopting the language of spin transport. Particles in state \uparrow (\downarrow) enter the system at the left boundary from a reservoir with density $\rho_{\text{res}}^\uparrow$ ($\rho_{\text{res}}^\downarrow$) and leave at the right boundary with rate β^\uparrow (β^\downarrow). In bulk, particles hop to the right, always respecting Pauli's exclusion principle. If an unpaired particle moves to a site which is already occupied by a particle of the other spin state the hopping rate is decreased to e^{-U} ; otherwise, the hopping rate is set to 1.

the other channel is empty. We model this effect by reducing the hopping rate to a value e^{-U} ($U > 0$) in this case, while the rate is unity for all other configurations. In the biological context of molecular motors walking along microtubuli, the reduced hopping rate corresponds to the spatial obstruction stemming from large cargos attached to motor proteins.

Last, the rules of the model are completed by specifying how particles leave the system after traversing the bulk. Here, we consider that particles at the right boundary leave with the exiting rates $\beta^\uparrow, \beta^\downarrow$ in contrast to [7] (see Fig. 1).

B. Spin-transport representation

The model can be readily interpreted in the context of spin transport where it serves as a description for classical spin currents (see Fig. 2). The analogy to the two-channel picture is the following: A particle situated at the upper (lower) lane maps to a particle with spin up (spin down). At the left boundary particles enter from a spin reservoir with densities $\rho_{\text{res}}^\uparrow, \rho_{\text{res}}^\downarrow$. Having traversed the lattice, they leave the system at the right boundary with exiting rates $\beta^\uparrow, \beta^\downarrow$. In bulk, the particles move to the right always respecting Pauli's exclusion principle, i.e., only one particle per internal state is permitted per site. According to the two-lane representation, the hopping rates depend on the particle configuration of the system. A short-range repulsive interaction reduces the hopping rate for an unpaired particle onto a site which is already occupied by a particle of the other spin state to e^{-U} , as compared to 1 for the other configurations. The parameter $U > 0$ may be viewed as an effective interaction potential, originating from a repulsive Coulomb interaction, where particles on the same site (though different spin states) gain potential energy. In this context, one can also consider an increased hopping rate away from a double occupation, yet, one can show that this does not change our results qualitatively [40]. For clarity, we employ only the two-channel representation in the following.

A model similar to the one introduced above was recently proposed in [7]. However, only symmetric situations were considered with entrance/exit reservoirs that were equal in both lanes. As a further difference to our model the authors did model the exiting processes through reservoirs at the right side instead of exiting rates. Because we explicitly investigate the asymmetric case, with entrance and exit properties that differ for the two lanes, and because of our usage of exit rates we find a multitude of interesting phenomena, summarized in Sec. VI. The asymmetry between the two lanes requires

a two-dimensional generalization of the extremal-current principle. The derivation of this two-dimensional extremal-current principle constitutes a key result of our work; we show how it successfully describes much of the system's behavior.

III. CLASSIFICATION OF THE SYSTEM'S SENSITIVITY ON THE POTENTIAL

The steady-state bulk densities $\rho_i^\uparrow = \langle n_i^\uparrow \rangle, \rho_i^\downarrow = \langle n_i^\downarrow \rangle$, where $\langle \cdot \rangle$ indicates a coarse-grained time average, constitute key observables. Because of particle conservation, their temporal evolution can be obtained from the particle flux j_{i-1} onto site i and the one away from it, j_i :

$$\begin{aligned} \partial_t \rho_i^\uparrow &= j_{i-1}^\uparrow - j_i^\uparrow, \\ \partial_t \rho_i^\downarrow &= j_{i-1}^\downarrow - j_i^\downarrow. \end{aligned} \quad (1)$$

The currents, $j_i^\uparrow, j_i^\downarrow$, contain correlations between neighboring sites on the lattice. To find an analytic description, these correlations have to be accounted for by a suitable closure relation, e.g., by a mean-field approximation or a one-site cluster approximation.

Stochastic simulations provide another route to gain insight into the system's behavior. In this section we first detail the simulation algorithm, and then describe three classes of behavior that emerge for different interaction strength.

A. Stochastic simulations

We have determined the system's stationary state via stochastic simulations with random sequential updating, using the dynamic rules introduced in the previous section and employing the Gillespie algorithm [41,42]. We have performed time averages over about 10^5 time intervals, each containing $10 \times L$ time steps and the lattice size is set to $L = 1000$. At the left boundary, the reservoir dynamics is specified in terms of the three parameters, $\rho_{\text{res}}^\uparrow, \rho_{\text{res}}^\downarrow$, and κ^* . Here, we restrict the discussions to the case of *relaxed* reservoirs, where the correlations in the reservoirs reflect the ones in bulk, which is particularly illuminating and amenable to a theoretical description. Then, the double occupation density can be determined from the average densities, $\rho_{\text{res}}^\uparrow, \rho_{\text{res}}^\downarrow$ according to Eq. (A4) derived in the Appendix. In general, and apart from boundary effects such as boundary layers, we found constant density profiles in the system. To determine the corresponding value of the average density in bulk for constant density profiles, we only considered the $0.2 \times L$ sites in the center of both channels. Our simulations confirm to a large extent the analytic approximations which are to be discussed in the following sections.

B. Dependence on the interaction strength U

In the case of vanishing coupling, i.e., $U = 0$, the system simply corresponds to two uncoupled TASEPs. In the presence of obstruction, and thereby coupling between both channels, this picture changes drastically upon increasing the effective interaction strength. Our stochastic simulations show three regimes of qualitatively different behavior, which are illus-

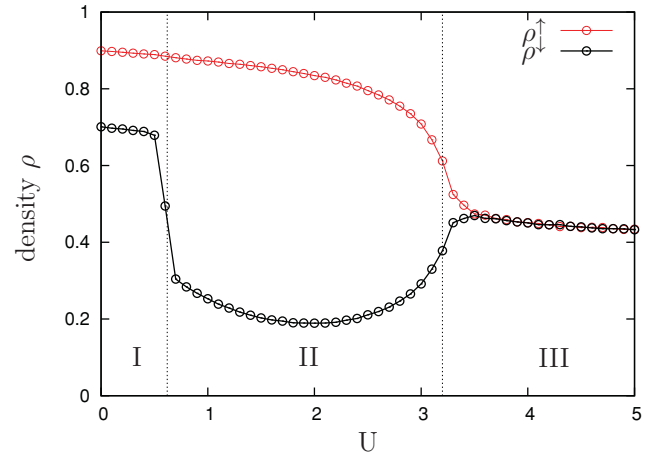


FIG. 3. (Color online) Average bulk densities obtained by stochastic simulations on the upper (red, gray) and lower lane (black) for varying potential strength U . The parameters are $\rho_{\text{res}}^\uparrow = \rho_{\text{res}}^\downarrow = 0.5$, $\beta^\uparrow = 0.1$, and $\beta^\downarrow = 0.3$. Three regimes of qualitatively different behavior emerge. In the first one (I) the system qualitatively behaves like two uncoupled systems. In regime II, the density in the lower channel strongly decreases, while the density in the upper channel is still large. This nontrivial behavior is discussed in detail in Secs. IV and V. In regime III, for strong coupling, the system behaves like a one-channel TASEP.

trated in Fig. 3. In the following, we discuss these regimes, and provide a mapping on TASEP for two of them.

1. Weak coupling

In the first regime (I), for small coupling strength U , the system almost behaves like two uncoupled lanes, except for the fact that the densities are slightly reduced. This regime can be well described by a simple mean-field approximation, where correlations between different lattice sites, $i \neq j$, are neglected, $\langle n_i^{\uparrow(\downarrow)} n_j^{\uparrow(\downarrow)} \rangle \approx \langle n_i^{\uparrow(\downarrow)} \rangle \langle n_j^{\uparrow(\downarrow)} \rangle$, or by a one-site cluster approximation which is to be discussed in detail in the following section. In this regime the phase behavior qualitatively corresponds to the one already known from TASEP. On a quantitative level, differences arise as the phase transition lines are shifted compared to the uncoupled case.

2. Intermediate coupling

In regime II, the one of intermediate coupling strength, an intriguing phase behavior emerges. For instance, for the set of parameters shown in Fig. 3, the density in the upper channel remains rather undisturbed by the obstruction, while the one in the lower channel drops to a comparatively small value. The nontrivial behavior in regime II is caused by the influence of the potential on the transport properties in bulk as well as on the boundaries. Especially, the exiting current is strongly influenced by the interaction potential resulting in smaller densities at the right boundary than expected for uncoupled systems. We rationalize this behavior in the following section. Because the system operates far from equilibrium, this change in the boundary conditions has a strong impact on the system.

Second, the transport properties in bulk also react sensitively to the coupling. As discussed in detail in the following

section, this causes changes in the currents' dependences on the bulk densities for potentials larger than a critical strength $U_C = \ln 4 \approx 1.4$.

Furthermore, other intriguing phenomena, such as domain walls between a low and a high density phase, are found. Also, there exist phases where the system depends sensitively on both boundaries, namely, the total current of the system is fixed by the right boundary while the exact value of the densities in bulk depends on the left boundary.

3. Strong coupling

A further increase in U leads to strong obstruction between the lanes with new qualitative behavior. In this regime of strong coupling (III) double occupancy of a site almost never occurs due to the vanishing hopping rate e^{-U} that would yield this configuration. Therefore the transport properties of two coupled channels is similar to a single-channel TASEP. This mapping cannot always be performed if the boundaries are reservoirs. It then only holds for the special case of small reservoir densities. Otherwise correlations between the upper and the lower reservoir are large. They are transported in the bulk and there destroy the effective one-lane behavior. Especially, the behavior shown in Fig. 3 would drastically change, if the exiting rates $\beta^\uparrow = 0.1$ and $\beta^\downarrow = 0.3$ would be replaced by the corresponding right reservoirs, namely the description holding for regime II would then apply and the bulk densities would not show the one-channel behavior.

Introducing the total density, $\tau_i = \langle n_i^\uparrow + n_i^\downarrow \rangle$, and performing the limit $e^{-U} \rightarrow 0$, which yields $\langle n_i^\uparrow n_i^\downarrow \rangle = 0$, in the expression for the currents [Eq. (A1)], one can identify the following mean-field current-density relation, already familiar from TASEP:

$$J = \tau(1 - \tau). \quad (2)$$

Due to the large potential in this regime, particles on different lanes are not able to "overtake" each other. Hence the ratio of the densities in both channels is fixed to the value given by the reservoir densities at the left boundary,

$$\frac{\rho^\uparrow}{\rho^\downarrow} = \frac{\rho_{\text{res}}^\uparrow}{\rho_{\text{res}}^\downarrow}. \quad (3)$$

In Fig. 3 we have used equal reservoir densities for the upper and the lower lane, and as a consequence the bulk densities of both lanes are equal.

The exact phase behavior can be determined by relating the boundary conditions of the two-lane system to the corresponding boundary conditions of the effective one-lane TASEP, for which the exact phase diagram is known. For reservoir densities $\rho_{\text{res}}^\uparrow, \rho_{\text{res}}^\downarrow < 0.5$, the effective entering rate is obtained by simply adding both reservoir densities:

$$\alpha_{\text{eff}} = \rho_{\text{res}}^\uparrow + \rho_{\text{res}}^\downarrow. \quad (4)$$

The effective exiting rate displays a more complex dependence on the boundary processes because the individual exiting rates influence the exiting current on both channels. To find a good estimate of the effective exiting rate, we consider the average time a particle spends on the last lattice site before it leaves the channel. This time is the inverse of the corresponding exiting rate. The weight of both waiting times is given by the

ratio of particles in the upper and lower lane. Hence a fraction $\rho_{\text{res}}^\uparrow / (\rho_{\text{res}}^\uparrow + \rho_{\text{res}}^\downarrow)$ of all particles spend $1/\beta^\uparrow$ time units on the last lattice site, and a fraction $\rho_{\text{res}}^\downarrow / (\rho_{\text{res}}^\uparrow + \rho_{\text{res}}^\downarrow)$ of the particles $1/\beta^\downarrow$ time units. The average time is the sum of both times weighted with their frequency,

$$\frac{\rho_{\text{res}}^\uparrow}{\rho_{\text{res}}^\uparrow + \rho_{\text{res}}^\downarrow} \frac{1}{\beta^\uparrow} + \frac{\rho_{\text{res}}^\downarrow}{\rho_{\text{res}}^\uparrow + \rho_{\text{res}}^\downarrow} \frac{1}{\beta^\downarrow},$$

yielding the effective exiting rate,

$$\beta_{\text{eff}} = \frac{(\rho_{\text{res}}^\uparrow + \rho_{\text{res}}^\downarrow)\beta^\uparrow\beta^\downarrow}{\rho_{\text{res}}^\uparrow\beta^\downarrow + \rho_{\text{res}}^\downarrow\beta^\uparrow}. \quad (5)$$

For reservoir densities $\rho_{\text{res}}^\uparrow, \rho_{\text{res}}^\downarrow > 0.5$, the double occupation density at the reservoir does not vanish and is transported into the system. Hence the system can exhibit total densities larger than one if its bulk behavior is determined by the left boundary. In this case, the description we introduce below for the regime of intermediate coupling applies.

IV. CURRENT-DENSITY RELATION

The interaction between neighboring particles directly affects the transport properties of the system. The current's dependence on the bulk densities is very sensitive on the coupling. Above a certain value the current-density relation changes qualitatively resulting in a rich phase behavior as we show in the following section.

A. One-site cluster approximation

With increasing coupling strength U , the occupation numbers of the same site on different lanes become more and more correlated and a simple mean-field approximation fails. However, by employing a one-site cluster approximation we obtain a valuable expression for the currents depending on the bulk densities as demonstrated in [7]. To account for correlations between the same site on different lanes, we introduce, besides the single particle densities $\rho_i^\uparrow = \langle n_i^\uparrow \rangle, \rho_i^\downarrow = \langle n_i^\downarrow \rangle$, the double occupation density on site i , $\kappa_i := \langle n_i^\uparrow n_i^\downarrow \rangle$ as an additional variable [43].

Then, the probabilities for the other three particle configurations on site i , unoccupied or occupied by one particle either on the upper or the lower lane, can be expressed in terms of $\rho_i^\uparrow, \rho_i^\downarrow$, and κ_i . We neglect all other correlations and employ the standard decoupling approximation scheme there.

Assuming spatially homogeneous density profiles, the currents on the upper and the lower lane can be expressed in terms of $\rho^\uparrow, \rho^\downarrow$, and κ . The details of the calculations are presented in the Appendix. We obtain

$$\begin{aligned} j^\uparrow &= \rho^\uparrow(1 - \rho^\uparrow) + \mu, \\ j^\downarrow &= \rho^\downarrow(1 - \rho^\downarrow) + \mu, \end{aligned} \quad (6)$$

where $\rho^{\uparrow(\downarrow)}(1 - \rho^{\uparrow(\downarrow)})$ is the particle current known from TASEP and $\mu = \kappa - \rho^\uparrow\rho^\downarrow$ is the correlation correction reducing the current compared to the case without any coupling. Here, the double occupation density κ is the positive solution of the quadratic equation,

$$0 = (1 - e^{-U})\kappa^2 + [1 - (1 - e^{-U})\rho]\kappa - e^{-U}\rho^\uparrow\rho^\downarrow, \quad (7)$$

where $\rho = \rho^\uparrow + \rho^\downarrow$ is the total density. We will employ these results in the following section within the framework of an extremal-current principle to investigate the phase behavior as a function of the coupling strength.

In agreement with the considerations in the previous section, the double occupation density vanishes in the limit $U \rightarrow \infty$, while it simplifies to $\kappa = \rho^\uparrow \rho^\downarrow$ for $U \rightarrow 0$. The latter limit connects the one-site cluster approximation to the simple mean-field approximation, which is accurate for small potentials.

B. Dependence of the currents on the potential U

The current displays a sensitive dependence on the strength of interaction, U . For small interaction strength, the currents on each lane are almost independent of the density on the other lane. Indeed, these currents are approximately parabolic with respect to the density in the respective lane; see Fig. 4(a). The maximal current on the upper channel j_{\max}^\uparrow occurs for $\rho^\uparrow = 1/2, \rho^\downarrow = 0$, and $\rho^\uparrow = 1/2, \rho^\downarrow = 1$ since the obstruction does not affect the transport on the upper lane for these densities. With an increase in the potential U , the particle flux decreases, in particular, for densities around $\rho^\uparrow = \rho^\downarrow = 1/2$, as shown in Fig. 4(b).

This behavior is also reflected in the total current as shown in Figs. 4(c) and 4(d). For small potentials, the total current

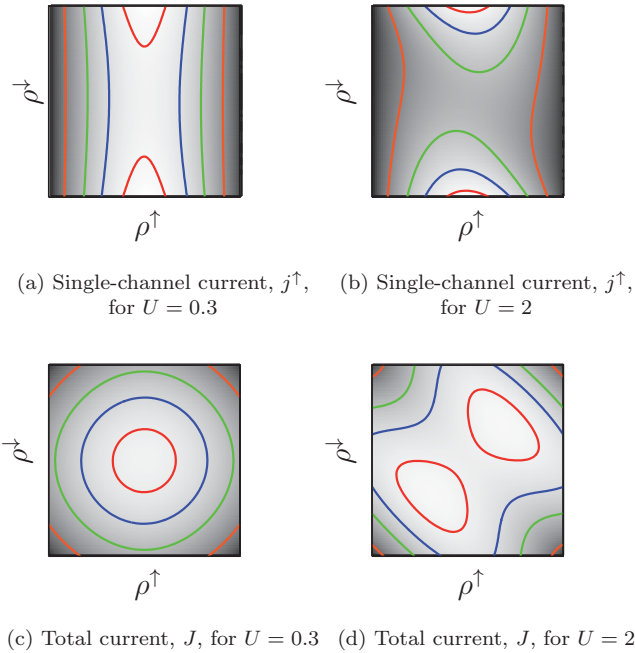


FIG. 4. (Color online) Contour plots for the individual (top) and the total current (bottom), depending on the bulk densities, for $U = 0.3$ (left) and $U = 2$ (right) using Eq. (6). In gray scale, black corresponds to vanishing current, and white to the respective maximal currents $j_{\max}^\uparrow, J_{\max}$. The colored (gray) contour lines indicate currents of value $0.95 \cdot j_{\max}^\uparrow$ and $0.95 \cdot J_{\max}$ (red), $0.8 \cdot j_{\max}^\uparrow$ and $0.8 \cdot J_{\max}$ (blue), $0.5 \cdot j_{\max}^\uparrow$ and $0.5 \cdot J_{\max}$ (green), $0.3 \cdot j_{\max}^\uparrow$ and $0.3 \cdot J_{\max}$ (orange) from inside to outside. Increasing the obstruction strength, the single maximum splits into two, separated by a saddle. The transition happens at a critical value of the interaction, $U_C = \ln 4 \approx 1.4$.

in bulk displays a single maximum located at $\rho^\uparrow = \rho^\downarrow = 1/2$; see Fig. 4(c). In this regime the potential only affects the value of the maximum but not its position, i.e., it does not change the topology of the phase diagrams. Beyond a critical value of the potential, $U_C = \ln 4 \approx 1.4$, the total current displays a qualitatively different behavior, as has been described in Ref. [7]. At the critical value, two maxima separated by a saddle evolve in the current-density relation for the total current; see Fig. 4(d). The location of these maxima is evaluated in the Appendix. Upon further increasing U , the maxima move apart. In the limit of large potentials two elongated maxima evolve and the saddle becomes a valley located at $\rho^\uparrow = 1 - \rho^\downarrow$. The bimodal structure leads to a richer phase diagram than in the weak coupling regime, $U < \ln 4$. Similar extrema in the currents were found previously for one-channel systems, e.g., when next-nearest-neighbor interactions are taken into account [44].

C. Influence of the potential U on the right boundary

At the right boundary ($i = L$) exiting rates control the currents out of the system:

$$\begin{aligned} j_{\text{EX}}^\uparrow &= \beta^\uparrow \rho_L^\uparrow, \\ j_{\text{EX}}^\downarrow &= \beta^\downarrow \rho_L^\downarrow. \end{aligned} \quad (8)$$

These currents are either determining the system or are virtual currents which are important for predicting the phase behavior in the system as explained in the following section. If these exiting currents also set the bulk currents, i.e., if $j^\uparrow = j_{\text{EX}}^\uparrow$ and $j^\downarrow = j_{\text{EX}}^\downarrow$, we can compute the bulk densities (which then equal the densities at the right boundary) depending on the exiting rates via Eq. (8). The densities at the right boundary also play a key role for determining the phase diagrams, as we will see below. For a small coupling strength, we find $\rho^{\uparrow(\downarrow)} \approx 1 - \beta^{\downarrow(\uparrow)}$, as familiar from TASEP. The transport properties change rapidly when repulsion between particles increases. In particular, for potentials larger than U_C the double-maxima structure of the bulk current comes into play and causes a discontinuous dependence of the bulk density on the exiting rates. Such a jump in the densities is exemplified in Fig. 5 for the case of equal exiting rates.

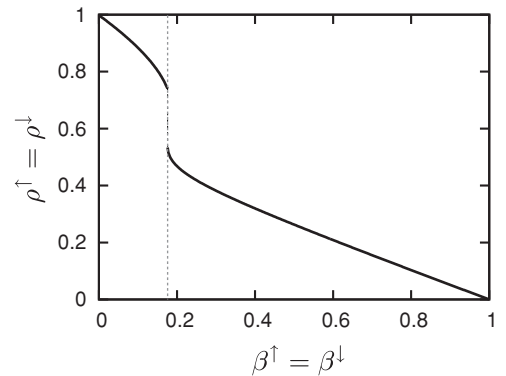


FIG. 5. The dependence of the bulk densities, $\rho^\uparrow = \rho^\downarrow$, on equal exiting rates $\beta^\uparrow = \beta^\downarrow$ for systems determined by the right boundary. It is obtained by evaluating Eq. (8). The interaction strength $U = 3.0$ is above the critical value U_C .

V. PHASE BEHAVIOR

The system's phases depend on the boundary conditions as well as on the strength of internal obstruction. In the following, we employ the extremal-current principle to evaluate the analytic expressions for the currents obtained in the previous section to get insight into the phase behavior. We then discuss these phases and point out some special features arising from the coupling.

A. Extremal-current principle

The extremal-current principle (ECP) often governs the phase behavior of driven diffusive systems [13,44,45]. So far the ECP has only been established for one-dimensional systems. Here we describe a two-dimensional generalization and show that it successfully describes the phase behavior of our two-lane model. We start with a short description of the standard one-dimensional ECP, and then extend it to two coupled lanes.

The ECP for transport on a single lane can be formulated by considering two characteristic velocities. The first is the collective velocity, $v_c = \partial j / \partial \rho$, which reveals information of the stability of a given bulk density ρ against perturbations: only densities with $v_c = 0$ (as well as those determined by the boundaries) are stable. The second quantity is the shock velocity $v_s = [j(\rho_1) - j(\rho_2)] / (\rho_1 - \rho_2)$ that gives the direction in which a domain wall between two densities, ρ_1 and ρ_2 , travels. In this way, v_s determines which of both densities, ρ_1 or ρ_2 , dominates. To find the system's bulk density, it therefore suffices to first identify the stable densities, using the collective velocity, and then, by pairwise comparison via the shock velocity, single out the bulk density. These considerations are summarized by the extremal-current principle:

$$\begin{aligned} j &= \max_{\rho \in [\rho_+, \rho_-]} j(\rho) \quad \text{for } \rho_+ > \rho_-, \\ j &= \min_{\rho \in [\rho_+, \rho_-]} j(\rho) \quad \text{for } \rho_+ < \rho_-, \end{aligned} \quad (9)$$

where ρ_+ is the density at the left boundary, and ρ_- is the density at the right boundary. Hence the system is either determined by the entering or exiting current or by an extremal current corresponding to a density in between the boundary densities.

On two coupled lanes, the currents in bulk are generically influenced by both lanes. We therefore have to consider the dependence of the currents on both ρ^\uparrow and ρ^\downarrow . As in the one-dimensional case, either the maximal or the minimal (total) current (see Fig. 6, blue and green area) determines the transport in the system, and the velocities v_c and v_s govern which of both scenarios is realized. However, in order to decide which of both cases applies it is no longer sufficient to compare the densities at the boundaries. Because of many potentially conflicting cases a rigorous derivation of the ECP provides a considerable challenge. We have, however, observed that the following intuitive version of the ECP describes our model's phase behavior in the full parameter space.

In the one-dimensional ECP an extremal current belonging to a density in the interval determines the system. In the two-dimensional scenario the interval is replaced by a rectangle

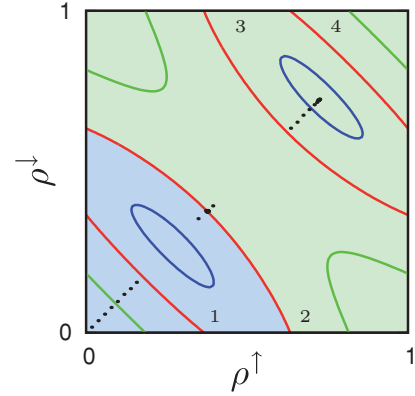


FIG. 6. (Color online) Contour plot of the total current, depending on the bulk densities. The bulk densities emerging for special values of equal reservoir densities ($\rho_{\text{res}}^\uparrow = \rho_{\text{res}}^\downarrow$), namely continuously increasing from 0 to 1, are displayed as black dots. The other parameters are $\beta^\uparrow = \beta^\downarrow = 0.3$ and $U = 3.0$. The red contour line corresponds to the total exiting current as emerges if the right boundary determines the bulk densities. It marks the transition from the minimal (blue area, lower left corner) to the maximal (green area, upper right corner) current principle and two phase transitions. In the lower left corner the system is in the IN/IN phase, crossing the red contour line it enters the EX/EX phase. Upon further increase in the reservoir densities the IN/IN phase is reached again in the upper right corner, before the MC/MC phase arises where the densities are limited by the bulk properties.

bounded by the boundary densities, $(\rho_L^\uparrow, \rho_L^\downarrow)$ and $(\rho_{\text{res}}^\uparrow, \rho_{\text{res}}^\downarrow)$. Depending on the boundary conditions either the minimal or the maximal current gives the bulk currents. The currents, which have to be considered are the entering and the exiting current or a mixture of both, i.e., one lane is determined by the left while the other one is determined by the right boundary. The exiting current can be calculated by equating Eqs. (6) and (8) with Eq. (7). For the specific example $U = 3, \beta^\uparrow = \beta^\downarrow = 0.3$, the corresponding contour line of the current-density relation consists of several disjoint lines; see Fig. 6 where the red line has four parts which are denoted as 1, 2, 3, and 4. Then, the part that includes the point $(\rho_L^\uparrow, \rho_L^\downarrow)$ marks the boundary where the maximal or minimal current is selected. In the example discussed here this boundary is given by line 2 in Fig. 6. The extrema to be considered for the ECP are located at the boundary of the rectangle given by $(\rho_L^\uparrow, \rho_L^\downarrow)$ $(\rho_{\text{res}}^\uparrow, \rho_{\text{res}}^\downarrow)$, or at the extremum on the rectangle. This extremum can be inside the rectangle or also at its boundary.

To illustrate the extremal-current principle we consider a path where the reservoir densities are gradually increased along the diagonal $\rho_{\text{res}}^\uparrow = \rho_{\text{res}}^\downarrow$ for fixed exiting rates and interaction strength. Even though we choose this path as an example, our results hold for arbitrary boundary conditions as exemplified in the following. Figure 7 displays the bulk densities and the phase transitions that occur. For small reservoir densities the minimal current is selected, which is given by the left reservoirs there. Upon crossing the current contour line (1) for the first time, the left reservoir current is larger than the exiting current, and transport is determined by the exiting rates. Crossing the contour line that includes

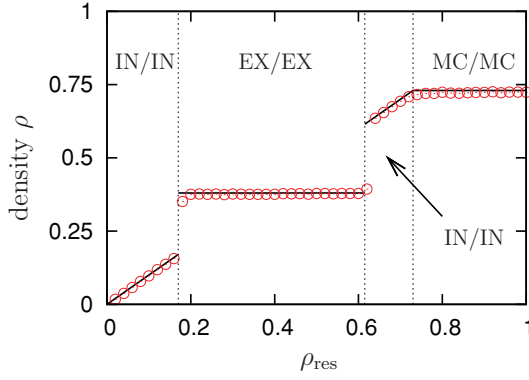


FIG. 7. (Color online) Average bulk densities for increasing reservoir densities $\rho_{\text{res}} = \rho_{\text{res}}^{\uparrow} = \rho_{\text{res}}^{\downarrow}$. The parameters are set to $\beta^{\uparrow} = \beta^{\downarrow} = 0.3$ and $U = 3$; the situation corresponds to Fig. 6. The phases introduced here are discussed in Sec. VB. Red (gray) circles denote simulation results; black lines correspond to analytical predictions from the ECP.

the point $(\rho_L^{\uparrow}, \rho_L^{\downarrow})$ (line 2), does not give rise to a phase transition, since now the maximum current determines the bulk current. In this domain the exiting current is larger than the left reservoir current. The next phase transition happens when the current at the left boundary exceeds the exiting current. Again, the phase transition occurs at a segment of the red contour line (line 3). Upon a further increase, the second maximum of the current-density relation is reached, and the maximal-current phase is entered. For reservoir densities larger than $(\rho_I^{\uparrow}, \rho_I^{\downarrow})$, i.e., for the maximum bulk current, see Eq. (A6) in the Appendix, a maximum current is attained.

B. Phases

As discussed above the system either adopts its minimal or maximal current, depending on the boundary conditions. These extremal currents can be either given by one boundary or by an extremum of the current-density relation itself. Hence we can distinguish two classes of phases in the system, boundary- and bulk-induced phases. The first one is highly sensitive to small changes in the boundary conditions, while in the latter one the densities are determined by the bulk properties and do not depend on the entering and exiting parameters.

1. Boundary-induced phases

The boundary-induced phases depend either on the entering or exiting processes, and we consequently differentiate between IN and EX phases. In our model, we employ particle reservoirs at the left boundary, but exiting rates at the right one. As a consequence the left and the right boundary influence the bulk densities in qualitatively different ways. Indeed, in the case where both lanes are determined by the left boundary (IN/IN phase), the bulk densities are given by the reservoir densities, $\rho^{\uparrow} = \rho_{\text{res}}^{\uparrow}, \rho^{\downarrow} = \rho_{\text{res}}^{\downarrow}$. In contrast, if a system is in the EX/EX phase, only the total current is fixed to the value given by the right boundary, whereas the bulk densities also depend on the reservoir densities at the left boundary, for $\rho_{\text{res}}^{\uparrow} \leq \rho_{\text{res}}^{\downarrow}$ holds $\rho^{\uparrow} \leq \rho^{\downarrow}$. Further mixed phases (IN/EX or EX/IN) may

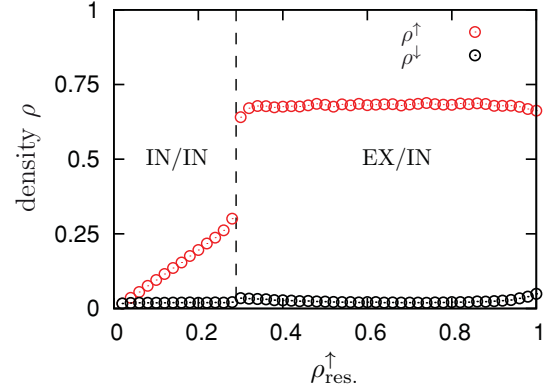


FIG. 8. (Color online) Average bulk densities for different upper reservoir densities $\rho_{\text{res}}^{\uparrow}$. Parameters are $\rho_{\text{res}}^{\downarrow} = 0.02$, $\beta^{\uparrow} = \beta^{\downarrow} = 0.3$, $U = 3.0$. If both reservoir densities are small, the system is in the IN/IN phase where both bulk densities are given by the reservoirs. This changes for larger $\rho_{\text{res}}^{\uparrow}$. While the lower lane is still determined by the left boundary, the upper lane is governed by the right boundary (EX/IN phase).

become relevant where the current on one lane is determined by the left boundary and the current on the other is fixed by the exiting current.

The IN/IN and the EX/IN phase are exemplified in Fig. 8 where we show the average bulk densities depending on the upper reservoir density $\rho_{\text{res}}^{\uparrow}$. Parameters are chosen such that a transition from the IN/IN to the EX/IN phase emerges at a certain value of $\rho_{\text{res}}^{\uparrow}$. Only in the IN/IN phase do the bulk densities vary when changing the upper reservoir density $\rho_{\text{res}}^{\uparrow}$; in the EX/IN phase they are almost undisturbed by changes in $\rho_{\text{res}}^{\uparrow}$.

2. Bulk-induced phases

In the bulk-determined phases, the current is given by an extremum of the current-density relation. Here we restrict the discussion to the case where a maximum occurs (MC phase), yet one can find parameter regions where a saddle fixes the phase behavior [40].

In the maximum-current phase a localized domain wall can emerge, separating a high-density regime at the left and a low-density regime at the right; see Fig. 9. This scenario, previously found in Ref. [13], occurs if both maxima $(\rho_I^{\uparrow}, \rho_I^{\downarrow})$ and $(\rho_{II}^{\uparrow}, \rho_{II}^{\downarrow})$, Eq. (A6) in the Appendix, are accessible. Each domain along the lane then corresponds to one of the maximal currents. In particular, the current is continuous at the domain wall. In Fig. 9, the reservoir density at the left boundary is larger than the density corresponding to the second maximum, while the density at the right boundary is smaller than the density corresponding to the first maximum. Hence in the vicinity of each boundary the density which is closer to the respective boundary density arises. Depending on the exact values of the boundary densities, the domain wall is located between the left hand side and the middle of the system. Increasing the reservoir densities the domain wall moves further to the right. In Fig. 7, the MC/MC phase is shown for symmetric boundary conditions. The black line denotes the analytically obtained density corresponding to the second maximum of the

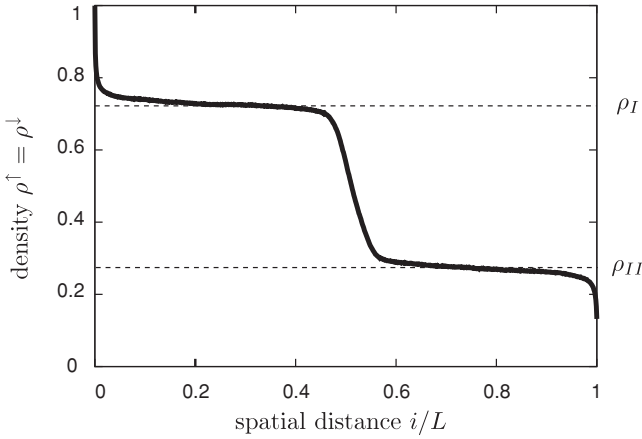


FIG. 9. Density profile of a state exhibiting maximal current. The parameters are $\rho_{\text{res}}^{\uparrow} = \rho_{\text{res}}^{\downarrow} = 1$, $\beta^{\uparrow} = \beta^{\downarrow} = 1$, $U = 3.0$, and $L = 1000$. The current remains spatially constant while the density shows a high value at the left and a low value at the right. Both densities correspond to maxima in the current-density relation, ρ_I, ρ_{II} . An unusual localized domain wall forms between them; see text.

current density relation. It is in excellent agreement with the simulation results.

C. Phase diagrams

Employing the extremal-current principle, the phase diagrams can be characterized completely also for unequal boundary densities. As described above, there exist several phases which are either determined by the boundaries or by the bulk transport properties of the system. According to the ECP the phase transition lines are given by equating the entering and exiting currents or by the structure of the current-density relation. The bulk current dominates if the maximum on the rectangle bounded by the corners $(\rho_{\text{res}}^{\uparrow}, \rho_{\text{res}}^{\downarrow}), (\rho_L^{\uparrow}, \rho_L^{\downarrow})$ is not given by either of these points. It is clear that a transition from a left-reservoir or right-exiting-currents dominated phase to a maximum-current phase can emerge only if the extremum traverses the boundary of the rectangle considered. Further transitions to an IN/EX and EX/IN phase are identified using again the extremal-current principle employing contour lines corresponding to the total current in the mixed phases.

In Fig. 10 we exemplify a phase diagram depending on unequal reservoir densities. The exiting rates are fixed to $\beta^{\uparrow} = \beta^{\downarrow} = 0.3$ and the potential is set to $U = 3$, a value where the current-density relation shows two maxima. The parameters are identical to the ones of Figs. 6 and 7. In Fig. 10, the stochastic simulations (red dots) are in good agreement with the analytic calculations (black lines). Because the latter ones were obtained employing the ECP also for unequal reservoir densities, the strength and generality of the ECP can be confirmed. Due to the symmetry between both lanes, the phase diagram is symmetric along its diagonal, $\rho_{\text{res}}^{\uparrow} = \rho_{\text{res}}^{\downarrow}$.

In the lower left corner, where both reservoir densities are small, both channels are determined by the entering current (IN/IN phase). Increasing only one reservoir density, the minimal current is no longer given by the entering current on the respective lane. Hence the system reaches the EX/IN

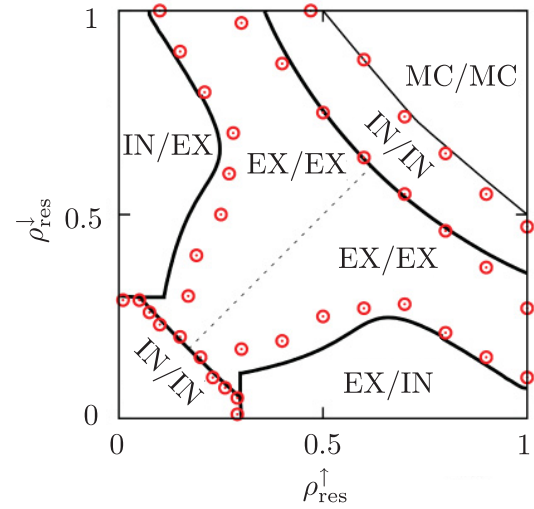


FIG. 10. (Color online) A generic phase diagram with the reservoir densities as control parameters. The exiting rates are fixed to $\beta^{\uparrow} = \beta^{\downarrow} = 0.3$ and the interaction strength is set to $U = 3.0$. The red (gray) dots denote simulation results of the transition lines, while the black lines are calculated employing the ECP. Besides the combinations of phases which are determined by entering or exiting currents, phases which do not exist for $U < \ln 4$ are also present. Namely, a second IN/IN phase, which exhibits a high density, and the MC/MC, where the maximal current determines the bulk densities, occur.

phase (IN/EX phase). The phase-transition lines between the IN/IN and IN/EX phase, as well as the ones between the IN/EX and the EX/EX phase, are given by contour lines of the current on an individual lane, Eq. (6). In the middle of the phase diagram, both channels are determined by the exiting currents. As mentioned above, only the total current is fixed in this phase, in contrast to the bulk densities which also depend on the reservoir densities at the left boundary. The dotted line marks the region where the bulk densities on both channels are equal. On this line the bulk densities can be calculated employing Eq. (8). For a further increase in the reservoir densities, the IN/IN phase arises again where the bulk currents as well as the bulk densities are given by the left boundary. This phase would not arise if we had chosen entering rates, rather than particle reservoirs, at the left boundary, because boundary densities larger than $1/2$ would then not emerge. In our case, such large densities cause currents larger than the entering current. These dominate the system according to the extremal-current principle. For even larger reservoir densities the crest of the current-density relation, which marks the phase transition from the IN/IN to the MC/MC phase, is reached, and the bulk densities remain constant at the values where the second maximum is located.

VI. SUMMARY AND CONCLUSION

In this paper we have examined a driven two-channel model where the motion of particles along both channels is coupled via a repulsive short-range interaction. The latter causes intriguing phenomena and phases. Varying the strength of particle obstruction, three regimes of qualitatively different

behavior evolve. First, for small coupling the system approximately acts as two uncoupled lanes, i.e., the phases and phase diagram qualitatively correspond to the ones already known from TASEP. These results can be confirmed by employing a simple mean-field approach or a one-site cluster approximation. Second, for moderate interaction strength the transport properties of the system are strongly influenced by the obstruction between neighboring particles. This regime emerges around a critical interaction strength, $U_C = \ln 4$ [7], where a single maximum of the current-density relation splits into two, separated by a saddle. Third, when the obstruction is large, the two coupled lanes effectively behave as a single one. In this case, we have identified a mapping from the parameters governing entering and exiting processes in our system to effective rates for a single-lane TASEP. This mapping then allows us to carry over known results from TASEP, such as its phase diagram. Hence for different strengths of the obstruction a variety of peculiar phases surface which can be accessed by manipulating the system at the boundary only. The boundary-sensitive phases respond gradually upon tuning the left reservoir or the exiting rates, whereas the maximal-current phase is robust against such changes.

In contrast to previous work [7], we explicitly investigated the two-channel system with a broken lane symmetry. We thereby followed the proposition in [7] that the ECP might be generic for multichannel system. As a key result we indeed derive a suitable generalization of the ECP to two dimensions. We thereby approve that not the densities but the currents govern the transitions between the minimal and the maximal current principle, a distinction that cannot be made within one-dimensional or symmetric situations. The accuracy with which the system's phase behavior can be predicted with our two-dimensional ECP is astonishing and suggests it for further applications. In further contrast to [7] we specifically investigated the dependence on the potential U . For small potentials the system's behavior is not sensitive on whether reservoir or rates are chosen at the boundaries. However, for intermediate and large potentials, reservoirs or rates at the boundaries make a difference. For example, the system does not behave like a one-channel system for large potentials if reservoirs are chosen instead of rates at the right boundary, as has been done in [7]. Because we employ exiting rates at the right boundary, we observe interesting effects such as a strong impact of the potential U on the exiting current (Fig. 5), and two transitions instead of one in the bulk densities upon increasing U (Fig 3).

It would be interesting to consider also lane changes (respectively, spin flips) of the particles as they proceed along the channel. Such events are expected in realistic applications such as intracellular transport, highway traffic on multiple lanes, or hopping transport of electrons through a chain of quantum dots. The correlations induced by frequent lane changes [32,46], ignoring mutual obstruction, are accurately described by a one-site cluster approximation similar to the one we employed. Yet, for rare lane changes a simple mean-field approximation suffices to describe the arising localized domain walls [12]. The combination of obstruction, lane switching, and possibly also defects constitutes a promising route to discover novel and unexpected collective phenomena in driven transport.

In conclusion, we have shown that the ECP can be generalized to higher dimensions to serve as an appropriate tool for the investigation of driven multichannel systems. We therefore think that extremal-current principle is a promising starting point to achieve a deeper understanding of complex transport phenomena.

ACKNOWLEDGMENTS

This project was supported by the collaborative research center SFB TR12 ("Symmetries and Universalities in Mesoscopic Systems") and the German Excellence Initiative via the program "Nanosystems Initiative Munich (NIM)." T.R. acknowledges funding by the Elite-Netzwerk Bayern.

APPENDIX: CURRENT-DENSITY RELATION

In this Appendix, we derive an analytic description for the current-density relation within a one-site cluster approximation. The individual currents onto a site i can be obtained by evaluating the particle fluxes onto this site,

$$j_i^\uparrow = \langle e^{-U} (n_{i-1}^\uparrow - n_{i-1}^\uparrow n_{i-1}^\downarrow) (n_i^\uparrow - n_i^\uparrow n_i^\downarrow) \rangle + \langle (n_{i-1}^\uparrow - n_{i-1}^\uparrow n_{i-1}^\downarrow) (1 - n_i^\uparrow - n_i^\downarrow + n_i^\uparrow n_i^\downarrow) \rangle + \langle n_{i-1}^\uparrow n_{i-1}^\downarrow (1 - n_i^\uparrow) \rangle, \quad (\text{A1})$$

and similarly for j_i^\downarrow . This expression is evaluated employing the one-site cluster approximation discussed in Sec. IV A. The essence of the approach consists of considering all four possible states of the two opposing sites, whereas all correlations between neighboring sites are factorized. Thus a complete description is achieved in terms the mean double-occupation density $\kappa_i = \langle n_i^\uparrow n_i^\downarrow \rangle$ besides the average densities $\rho_i^\uparrow = \langle n_i^\uparrow \rangle$ and $\rho_i^\downarrow = \langle n_i^\downarrow \rangle$. Then the closure relation for the currents is derived,

$$j_i^\uparrow = e^{-U} (\rho_{i-1}^\uparrow - \kappa_{i-1}) (\rho_i^\uparrow - \kappa_i) + (\rho_{i-1}^\uparrow - \kappa_{i-1}) (1 - \rho_i^\uparrow - \rho_i^\downarrow + \kappa_i) + \kappa_{i-1} (1 - \rho_i^\uparrow). \quad (\text{A2})$$

Similar to Eq. (A1), the time evolution for the double-occupation density κ_i involves averages of products of occupation variables n_i . Within the same truncation of the hierarchy, one finds

$$\partial_t \kappa_i = e^{-U} (\rho_{i-1}^\uparrow - \kappa_{i-1}) (\rho_i^\downarrow - \kappa_i) + e^{-U} (\rho_{i-1}^\downarrow - \kappa_{i-1}) (\rho_i^\uparrow - \kappa_i) + \kappa_{i-1} (\rho_i^\uparrow + \rho_i^\downarrow - 2\kappa_i) - \kappa_i (2 - \rho_{i+1}^\uparrow - \rho_{i+1}^\downarrow). \quad (\text{A3})$$

In the steady state and for spatially homogeneous density profiles, the double occupation density κ obeys a quadratic equation with solution

$$\kappa = \frac{\lambda \rho - 1 + \sqrt{(\lambda \rho - 1)^2 + 4\lambda(1 - \lambda)\rho^\uparrow \rho^\downarrow}}{2\lambda}. \quad (\text{A4})$$

Here, $\lambda = 1 - e^{-U}$ corresponds to the inverse dwell time in the obstructed case and $\rho = \rho^\uparrow + \rho^\downarrow$ to the total density. Combining this result with the closure relation for the current,

Eq. (A2), the closed expression for the current-density relation follows,

$$\begin{aligned} j^\uparrow &= \rho^\uparrow(1 - \rho^\uparrow - \rho^\downarrow) + \kappa, \\ j^\downarrow &= \rho^\downarrow(1 - \rho^\uparrow - \rho^\downarrow) + \kappa. \end{aligned} \quad (\text{A5})$$

The total current $J = j^\uparrow + j^\downarrow$ displays a single maximum for small interactions U located at $\rho^\uparrow = \rho^\downarrow = 1/2$. This

maximum is replaced a saddle for strong coupling and two maxima of equal height appear on the diagonal. These new maxima are located at

$$\rho_{I,II}^\uparrow = \rho_{I,II}^\downarrow = \frac{1}{2} \pm \frac{\sqrt{1 - 5e^{-U} + 4e^{-2U}}}{4(1 - e^{-U})}. \quad (\text{A6})$$

These solutions are only real for potentials larger than the critical value, $U_C = \ln 4$.

-
- [1] B. Schmittmann and R. Zia, in *Phase Transitions and Critical Phenomena*, edited by C. Domb and J. Lebowitz (Academic Press, London, 1995), Vol. 17, pp. 1–120.
- [2] G. Schütz, in *Phase Transitions and Critical Phenomena* (Ref. [1]), Vol. 19, pp. 1–251.
- [3] N. Hirokawa, *Science* **279**, 519 (1998).
- [4] T. Chou and D. Lohse, *Phys. Rev. Lett.* **82**, 3552 (1999).
- [5] J. Howard, *Mechanics of Motor Proteins and the Cytoskeleton* (Sinauer, Sunderland, MA, 2001).
- [6] H. Hinsch, R. Kouyos, and E. Frey, in *Traffic and Granular Flow '05*, edited by A. Schadschneider, T. Pöschel, R. Kühne, M. Schreckenberg, and D. E. Wolf (Springer, New York, 2006), pp. 205–202.
- [7] V. Popkov and I. Peschel, *Phys. Rev. E* **64**, 026126 (2001).
- [8] D. Helbing, *Rev. Mod. Phys.* **73**, 1067 (2001).
- [9] D. Chowdhury, L. Santen, and A. Schadschneider, *Phys. Rep.* **329**, 199 (2000).
- [10] B. Schmittmann, J. Krometsch, and R. K. P. Zia, *Europhys. Lett.* **70**, 299 (2005).
- [11] S. Katz, J. L. Lebowitz, and H. Spohn, *Phys. Rev. B* **28**, 1655 (1983).
- [12] T. Reichenbach, T. Franosch, and E. Frey, *Phys. Rev. Lett.* **97**, 050603 (2006).
- [13] J. Krug, *Phys. Rev. Lett.* **67**, 1882 (1991).
- [14] C. MacDonald, J. Gibbs, and A. Pipkin, *Biopolymers* **6**, 1 (1968).
- [15] B. Derrida and J. L. Lebowitz, *Phys. Rev. Lett.* **80**, 209 (1998).
- [16] B. Derrida, M. Evans, V. Hakim, and V. Pasquier, *J. Phys. A* **26**, 1493 (1993).
- [17] A. Vilfan, E. Frey, F. Schwabl, M. Thormählen, Y. Song, and E. Mandelkow, *J. Mol. Biol.* **312**, 1011 (2001).
- [18] A. Parmeggiani, T. Franosch, and E. Frey, *Phys. Rev. Lett.* **90**, 086601 (2003).
- [19] S. Klumpp and R. Lipowsky, *J. Stat. Phys.* **113**, 233 (2003).
- [20] K. Nishinari, Y. Okada, A. Schadschneider, and D. Chowdhury, *Phys. Rev. Lett.* **95**, 118101 (2005).
- [21] P. Greulich, A. Garai, K. Nishinari, A. Schadschneider, and D. Chowdhury, *Phys. Rev. E* **75**, 041905 (2007).
- [22] A. Parmeggiani, T. Franosch, and E. Frey, *Phys. Rev. E* **70**, 046101 (2004).
- [23] P. Pierobon, E. Frey, and T. Franosch, *Phys. Rev. E* **74**, 031920 (2006).
- [24] G. Tripathy and M. Barma, *Phys. Rev. Lett.* **78**, 3039 (1997).
- [25] P. Pierobon, M. Mabilia, R. Kouyos, and E. Frey, *Phys. Rev. E* **74**, 031906 (2006).
- [26] P. Greulich and A. Schadschneider, *J. Stat. Mech.* (2008) P04009.
- [27] C. Kural, H. Kim, S. Syed, G. Goshima, V. I. Gelfand, and P. R. Selvin, *Science* **308**, 1469 (2005).
- [28] M. J. I. Müller, S. Klumpp, and R. Lipowsky, *Proc. Natl. Acad. Sci. USA* **105**, 4609 (2008).
- [29] W. Knospe, L. Santen, A. Schadschneider, and M. Schreckenberg, *J. Phys. A* **35**, 3369 (2002).
- [30] T. Reichenbach, E. Frey, and T. Franosch, *New J. Phys.* **9**, 159 (2007).
- [31] T. Reichenbach, T. Franosch, and E. Frey, *Eur. Phys. J. E* **27**, 47 (2008).
- [32] E. Pronina and A. B. Kolomeisky, *J. Phys. A* **37**, 9907 (2004).
- [33] R. Jiang, M.-B. Hu, Y.-H. Wu, and Q.-S. Wu, *Phys. Rev. E* **77**, 041128 (2008).
- [34] T. Mitsudo and H. Hayakawa, *J. Phys. A* **38**, 3087 (2005).
- [35] R. Juhasz, *Phys. Rev. E* **76**, 021117 (2007).
- [36] D. Chowdhury, A. Garai, and J.-S. Wang, *Phys. Rev. E* **77**, 050902 (2008).
- [37] K. Tsekouras and A. B. Kolomeisky, *J. Phys. A* **41**, 465001 (2008).
- [38] E. Pronina and A. B. Kolomeisky, *J. Phys. A* **40**, 2275 (2007).
- [39] R. Hanson, L. Kouwenhoven, J. Petta, S. Tarucha, and L. Vandersypen, *Rev. Mod. Phys.* **79**, 1217 (2007).
- [40] A. Melbinger, Diploma thesis, Ludwig-Maximilians-Universität München, 2007.
- [41] D. T. Gillespie, *J. Comput. Phys.* **22**, 403 (1976).
- [42] D. T. Gillespie, *J. Phys. Chem.* **81**, 2340 (1977).
- [43] D. ben-Avraham and J. Köhler, *Phys. Rev. A* **45**, 8358 (1992).
- [44] V. Popkov and G. M. Schütz, *Europhys. Lett.* **48**, 257 (1999).
- [45] J. S. Hager, J. Krug, V. Popkov, and G. M. Schütz, *Phys. Rev. E* **63**, 056110 (2001).
- [46] E. Pronina and A. B. Kolomeisky, *Physica A* **372**, 12 (2006).

5 Length-Dependent Regulation

In the previous chapter, the basic biological and physical properties of molecular motors interacting with MTs were summarized. In this chapter, we focus on these motors acting as depolymerases or polymerases. Their influence on the MT length plays a key role for cell division. In the following, we concentrate on two specific proteins, the depolymerase Kip3p and the polymerase XMAP215. We briefly summarize recent experimental findings concerning their interactions with MTs. Then, we introduce a model combining molecular traffic on MTs with the length-dynamics arising from polymerases and depolymerases. We validate this model by comparing it to experimental results which were obtained without polymerization. Finally, we discuss the interplay between depolymerization and polymerization dynamics [301]. We there especially focus on the scenarios where a well-regulated length is achieved.

5.1 Experimental Findings

In vivo experiments show that the presence of certain proteins interacting with MTs is crucial for cell division and affects nucleus positioning as well as the mitotic spindle [27, 302, 28, 29, 30]. A common explanation is, that this originates from proteins facilitating length-regulation of MTs through which cell division is supported. Up to the present, a multitude of these proteins were discovered, for an overview see [240]. Their importance is also confirmed by computer simulations, which show that length-regulation is crucial to optimize nucleus positioning during interphase [303]. In order to gain a deeper molecular understanding for the underlying mechanisms, *in vitro* experiments were performed [31, 32, 33, 34]. In these experiments, only a few selected proteins and their interactions with the MT and among each other were investigated. In addition, also theoretical models were employed to describe dynamic length changes caused by directed or diffusing depolymerases [304, 305, 306].

XMAP215 - A Polymerizing Protein

Concerning polymerizing activity, the microtubule associated protein XMAP215 is a well-studied example [307, 27, 256, 308, 33]. *In vivo* and *in vitro* experiments display that this protein enhances growth of MTs. An up to tenfold enhancement of the growth speed was observed *in vitro*. However, the exact mechanism causing polymerization is still not resolved. Recent studies indicate that XMAP215 surfs on the MT tip where it processively polymerizes the MT, while older studies argue that it acts as a template and thereby adds several tubulin

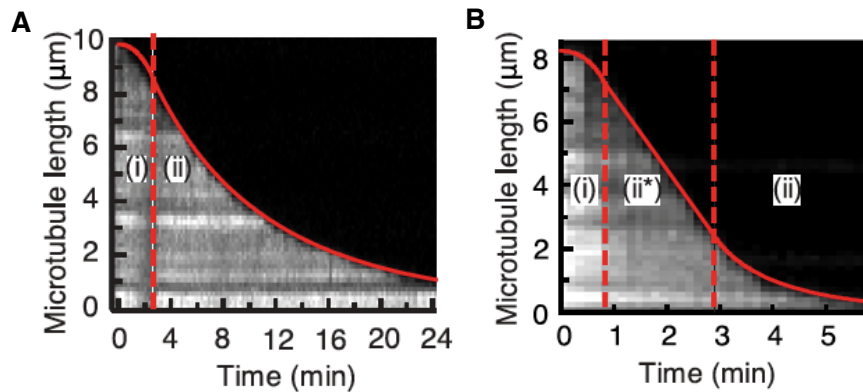


Figure 5.1: Experimental kymographs of the MT length versus time as measured by Varga *et al.* [34]. Depending on the length three different regimes can be distinguished: (i) initial accumulation, (ii) exponentially decreasing MT length, and (ii*) constant depolymerization speed.

dimers at the same time [309]. In other polymerizing proteins also treadmilling¹ was found to be the mechanism, *i.e.* particles attach at the tip where they facilitate polymerization and detach afterwards [310, 257]. In contrast to other TIP+ proteins, XMAP215 is not a motor but diffuses on the MT as well as in the cytosol to reach the tip.

Kip3p - A Depolymerizing Motor

Several experiments observing the interplay of depolymerases with MTs showed, that the depolymerization speed is length-dependent, *i.e.* longer MTs depolymerize faster than shorter ones [32, 29, 30, 34]. Understanding this length-dependent speed might be an essential step for uncovering the mechanisms behind length-regulation. In experiments of Varga *et al.* [32, 34], kinesin-8 from budding yeast, Kip3p, was investigated. This motor and its homologs show depolymerizing activity [311, 28, 312]. To purify the findings from effects of dynamic instability, the MTs were stabilized to inhibit catastrophes. Fluorescently labeled motors were employed to study the motor density governing length-dependent depolymerization. In Fig. 5.1, typical kymographs, *i.e.* the MT length versus time, are shown. In general, shorter MTs depolymerize slower than longer ones, but depending on the parameters the depolymerization behavior can also be described in more detail: For small motor concentrations in the surrounding, the MT length decays exponentially (ii) after a short initialization time (i), see Fig. 5.1A. For larger concentrations an additional regime comes into play, where the MT has a constant depolymerization speed (ii*), cf. Fig. 5.1B. But also for these concentrations, the MT length decays exponentially below a certain length (ii). Taken together, the experiments revealed that, depending on the MT length and the motor concentration, which triggers the motor density on the MT, the depolymerization speed alters. In addition, also other quantitative measurements were performed to further clarify the role of depolymerizing motors. For

¹The term treadmilling is ambiguous. It is also and more frequently used to describe the following movement mechanism of filaments. Their constituents detach at one side of the filament and attach at the opposite side.

example, the question whether depolymerization happens processively was addressed. In this context, processive means that motors stay at the plus end after depolymerizing a tubulin dimer. Experiments measuring the stoichiometry [34] indicate the non-processive scenario. In addition, quantities as the end-residence time of motors at the last site and the particle flux were measured. The main findings of these measurements in Ref. [34] are:

- The end-residence time of Kip3p at the tip of the MT depends on its concentration in the surrounding media. This finding indicates that depolymerization happens cooperatively, *i.e.* more than one motor is needed to cause a depolymerization event. For non-cooperative depolymerization, the end-residence time would not depend on the motor concentration.
- The end-residence time is the inverse of the macroscopic depolymerization speed.
- The macroscopic depolymerization speed is directly proportional to the particle flux towards the tip.

5.2 Depolymerization

To gain further understanding of the experimentally observed depolymerization dynamics, we employ a stochastic model. As shown in Fig. 5.2, we extend the TASEP/LK model, discussed in the previous chapter, with a dynamic right boundary. The model consists of a lattice of

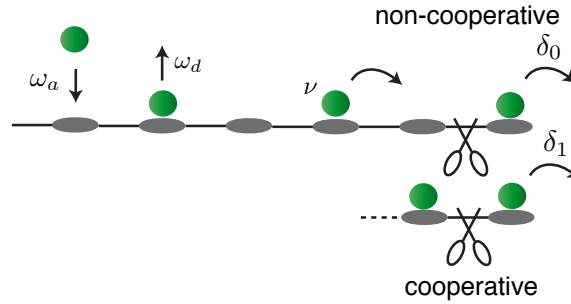


Figure 5.2: Illustration of the model including depolymerization and crowding effects. Particles attach and detach at rates $\omega_a = c\tilde{\omega}_a$ and ω_d , respectively. In bulk, they move unidirectionally to the right provided the next site is empty. At the right boundary particles leave the lattice coincidentally removing the last lattice site (indicated by scissors). This can either happen non-cooperatively (only one particle is involved) or cooperatively (two particles are needed) at rates δ_0 and δ_1 , respectively.

size L with occupied or empty sites, $n_i \in \{0, 1\}$. On the lattice particles can move to the right provided the next site is empty. Again we set the hopping rate to $\nu = 1$. This corresponds to a rescaling of time with the basic time unit $\tau = 1/\nu$. In addition, motors (particles) attach at rate $\omega_a = c\tilde{\omega}_a$ and detach at rate ω_d . The factor c in the attachment rate corresponds to the proportionality of this rate to the motor concentration in the surrounding. As binding to and unbinding from the MT happen on larger time scales than hopping events [32], we consider the biological relevant scenario of weak kinetics, $\omega_a \ll 1$ and $\omega_d \ll 1$, in the following. In contrast to standard TASEP-like models, the length of the lattice, L , is not fixed, but

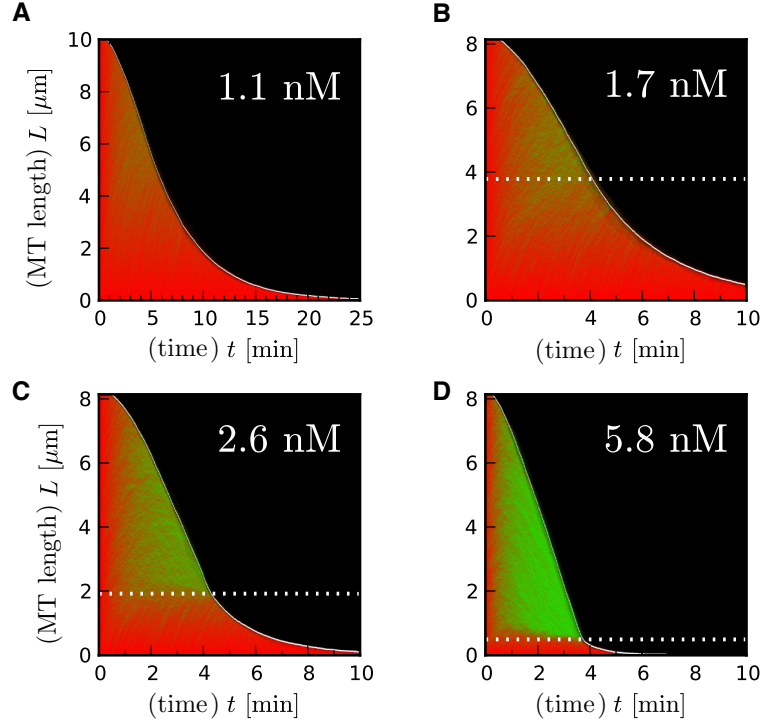


Figure 5.3: Kymographs from our stochastic simulations corresponding to the ones measured in experiments for the motor concentrations: $c = 1.1, 1.7, 2.6$ and 5.8 nM (**A, B, C, D**) and fixed depolymerization rates $\delta_0 = \nu$ and $\delta_1 = 0$. The other parameters are extracted from Ref. [34] and are given by $\tau = \nu^{-1} = 0.16$ s, $\omega_a \approx 5.3 \times 10^{-4} \text{ nM}^{-1} \text{ site}^{-1} \tau^{-1}$ and $\omega_d \approx 7.6 \times 10^{-4} \text{ site}^{-1} \tau^{-1}$. Individual trajectories of molecular motors are shown in green, MTs in red. For low concentrations, $c < 1.4$ nM, depolymerization slows down gradually [34]. At higher concentrations, $c > 1.4$ nM, there is a rather abrupt change in depolymerization speed, from linear to exponential. This change is correlated with a steep decrease in the motor density (DW), indicated as white dashed lines.

shrinks in the presence of motors. In the non-cooperative scenario, a single motor is sufficient to depolymerize a tubulin dimer at rate δ_0 . In contrast, for cooperative depolymerization, a tubulin dimer is only removed at rate δ_1 after another particle has arrived at the second to last site. The total depolymerization rate is therefore given by,

$$\Delta = \delta_0 n_L + \delta_1 n_{L-1} n_L. \quad (5.1)$$

Consequently, the macroscopic depolymerization speed depends on both depolymerization rates, δ_0 and δ_1 , and the particle configuration at the tip,

$$\partial_t L = V_{\text{depol}} = -(\delta_0 \rho_+ + \delta_1 \kappa_+). \quad (5.2)$$

Here $\rho_+ := \langle n_L \rangle$ is the probability that the last site is occupied, and $\kappa_+ := \langle n_{L-1} n_L \rangle$ denotes the probability that both the last and second to last site are populated.

As stated in the previous chapter, the density in the TASEP/LK model increases approximately linearly at the left-hand side of the system before it saturates to the value ρ_{L_a} at

ℓ^- , see Fig. 4.7. This gives rise to the observed length-dependency: For small MT length, the density increases linearly triggering the depolymerization speed. Therefore, shortening of the MT reduces the motor density at the tip and slows down the depolymerization speed. Calculating this in detail leads exactly to the observed exponential shortening. In contrast, if the MT is longer than ℓ^- initially, the Langmuir density is present at the tip. Shortening does not result in a change of this density as long as ℓ^- is not reached. In this regime, the depolymerization speed is constant. For a more detailed discussion see the paper at the end of this chapter. Importantly, depolymerization dynamics are strongly influenced by microscopic traffic jams arising at the tip. As other models excluded crowding or studied parameter regimes where it is unimportant, they could not observe these crowding phenomena which lead to length-dependent depolymerization dynamics [304, 305].

The length-dependent polymerization speed is also reflected in the kymographs of our model which were obtained via stochastic simulations, see Fig. 5.3. Note, that all parameters of the model were directly extracted from measurements and no fitting parameter is involved. The different concentrations result in different Langmuir densities and different slopes at the initial accumulation phase. The parameters used in Fig. 5.3A and 5.3B correspond to the experimental data shown in Fig. 5.1. Both, the time scales as well as the existence of a length-dependent and a constant speed regime agree nicely with our results. In Fig. 5.3C and 5.3D even higher motor concentrations are shown where the difference between both regimes is more pronounced.

The manuscript in Sec. 5.4 provides a more detailed description of our findings regarding length-dependent depolymerization, the effect of cooperativity and bottlenecks causing microscopic traffic jams.

5.3 Depolymerization and Polymerization

Despite the fact that molecular motors depolymerize MTs, also polymerization is present, see Sec. 4.1. Single tubulin dimers diffusing in the cytosol attach to the MT plus end and thus increase its length. This polymerization can also be catalyzed by molecular motors, like XMAP215, which diffuse along the MT. The antagonism between polymerization and length-dependent depolymerization can in principle lead to a well-defined MT length [301].

According to the previous section, we model such MTs with a one dimensional lattice, see Fig. 5.4. We extend the model accounting for shrinkage by polymerization happening at rate γ . We study two possible scenarios for this growth process at the right boundary corresponding to the MT tip. First, in the *exclusive* scenario, polymerization events only take place if the tip is not occupied by a depolymerizing motor. This accounts for depolymerizing motors which hinder polymerization, *e.g.* because they slightly buckle the filaments at the plus end or shield the tip. Second, we consider the *non-exclusive* scenario where polymerization may also happen when the last site is occupied, see Fig. 5.4. In recent studies, the effect of polymerization dynamics triggered by motor proteins was investigated without taking depolymerization into account; these models apply to hyphal growth in fungi [313, 314].

One of our aims is to uncover the macroscopic consequences of the microscopic differences between exclusive and non-exclusive depolymerization. We thereby want to suggest new

experiments which help to clarify whether polymerization happens exclusively, non-exclusively or as a mixture of both. Further, as mentioned above, the ability of length-regulation is crucial for the biological functioning of processes like cell division. We want to answer how this length-regulation works and why it is such robust. Therefore, we first discuss both, the exclusive and the non-exclusive scenario, separately focussing on the mechanisms triggering the MT length. Finally, both scenarios are compared.

5.3.1 The Exclusive Scenario

The dynamics of the MT length is determined by the particle density at the plus end, ρ_+ , which triggers depolymerization and polymerization,

$$\partial_t L = -\delta\rho_+ + \gamma(1 - \rho_+). \quad (5.3)$$

The critical density, ρ_+^c , which separates the regimes of MT growth and shrinkage, follows from $\partial_t L = 0$,

$$\rho_+^c = \frac{\gamma}{\gamma + \delta}. \quad (5.4)$$

For $\rho_+ < \rho_+^c$ the MT grows, while it shrinks for $\rho_+ > \rho_+^c$.

Consequently, the tip density has to be calculated to determine whether the MT is in a growth or shrinkage state. It strongly depends on the right hand side boundary, *i.e.* the rates δ and γ , and the incoming particle flux $J_{IN} = \rho(x)(1 - \rho(x))$. To simplify our calculations, we neglect the spatially non-trivial density profiles arising in the TASEP/LK for the moment. Instead, we study a simplified model where the Langmuir density, ρ_{La} , is adjusted at the left hand side of the system². This enables us to predict the depolymerization behavior depending on a fixed bulk density. In Sec. 5.3.3, the results obtained in the simplified model are extended to the full model where particles accumulate at the left boundary (antenna profile) and then reach the density ρ_{La} .

The analysis of the tip density is performed in a comoving frame: The frame of observation moves with the MT tip such that a polymerization event corresponds to the movement of

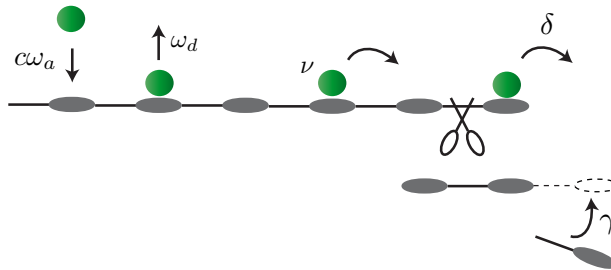


Figure 5.4: Illustration of the model including depolymerization and exclusive polymerization. The model shown in Fig. 5.2 is extended by exclusive polymerization, *i.e.* tubulin dimers can attach at rate γ if the tip is free from motors.

²For the TASEP/LK model introduced in the previous chapter, this corresponds to $\alpha = \rho_{La}$.

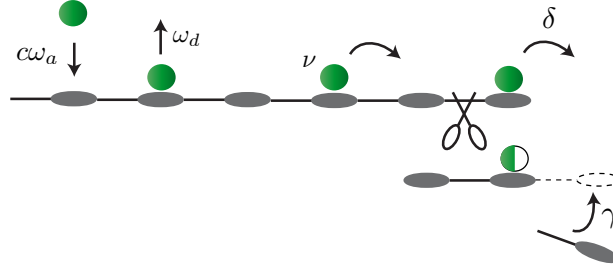


Figure 5.5: Illustration of the model including depolymerization and non-exclusive polymerization. In contrast to the exclusive model shown in Fig. 5.4, tubulin dimers attach at rate γ independently of the tip occupancy.

all particles to left, while depolymerization causes all particles to hop to the right, for an illustration see Fig. 5.6. This simplifies our calculations as the tip triggering the dynamics is static in this frame. The time evolution of the tip density is then given by,

$$\partial_t \rho_+ = \underbrace{\rho_B(1 - \rho_B)}_{\text{particle current}} - \underbrace{\gamma(1 - \rho_+)\rho_B}_{\text{frame shift, left}} + \underbrace{\delta\rho_+\rho_B}_{\text{frame shift, right}} - \underbrace{\delta\rho_+}_{\text{ex. current}}. \quad (5.5)$$

The first term corresponds to particles hopping to the right if the next site is empty, the particle current. The second and third term arise due to frame shifts caused by polymerization and depolymerization events, respectively. The last term is the exiting current for particles leaving the system at the right boundary. The bulk density, ρ_B , is either given by the left boundary ρ_{La} for $\rho_{La} < \rho_{\max}$ or ρ_{\max} , the density causing the maximal current. This can be understood intuitively: If the number of particles entering the system exceeds its transport capacity, a jam at the left boundary arises. This leads to a reduction in the number of entering particles till exactly ρ_{\max} is reached. For simplicity, we only consider bulk densities smaller than the maximal density in the following. A more detailed discussion of the consequences of the maximal current is presented for the non-exclusive scenario, Sec. 5.3.2. However, the maximal current can be also derived in the exclusive scenario. But as the calculations are involved and it turns out that ρ_{\max} does not influence the outcome in the relevant parameter regime, we skip them at this point.

Eq. (5.5) has a fixed point which is given by,

$$\rho_+^* = \frac{\rho_B(1 - \rho_B) - \gamma\rho_B}{\delta(1 - \rho_B) - \gamma\rho_B}. \quad (5.6)$$

Importantly, this fixed point can be stable or unstable. Furthermore, it may lie outside the physical parameter range, $\rho_+^* \in [0, 1]$. For an illustration see Fig. 5.7. In the following, we analyze the stability in particular for the physically relevant parameter regimes.

Assuming small perturbations around the fixed point, $\rho_+^* + \epsilon$ in Eq. (5.5), the stability can be evaluated. The following critical line separates a stable and an unstable area in the phase space,

$$\tilde{\gamma} = \frac{1 - \rho_B}{\rho_B} \delta. \quad (5.7)$$

For $\gamma < \tilde{\gamma}$ the fixed point is stable, while it is unstable for $\gamma > \tilde{\gamma}$. In the unstable regime, the

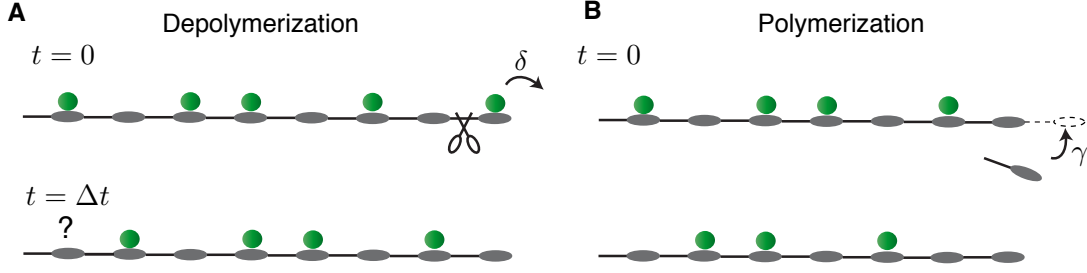


Figure 5.6: Illustration of the comoving frame. A depolymerization event corresponds to the instantaneous movement of all particles to the right while polymerization causes movement to the left.

system can show bistability. Then, the tip density at a later time strongly depends on the initial condition ρ_0 . Neglecting fluctuations trivially yields, $\rho_+ = 0$ for $\rho_0 < \rho_+^*$ and $\rho_+ = 1$ for $\rho_0 > \rho_+^*$, see Fig. 5.7C. Only in regimes where the unstable fixed point does not lie in the physical parameter range, $\rho_+^* < 0$ or $\rho_+^* > 1$, the tip density does not depend on the initial condition, cf. Fig. 5.7D. The reason for this behavior is that the drift does not change sign in the physical parameter range, *i.e.* $\partial_t \rho_+ < 0$ for $\rho_+^* > 1$ and $\partial_t \rho_+ > 0$ for $\rho_+^* < 0$. For all other values of the unstable fixed point, fluctuations play a crucial role. They can push the tip density from one side to the other side of the fixed point and thereby cause a change in the tip density from 0 to 1 and vice versa. This change in the tip density is equivalent to phases of persistent growth ($\rho_+ = 0$) and shrinkage ($\rho_+ = 1$). Therefore, the regime of an unstable fixed point seems to be inappropriate for length-regulation.

In contrast, if the fixed point is stable, tip density fluctuations play a less pronounced role as they decay at a fast time scale $1/\nu$. The resulting tip density is again bounded, $\rho_+ \in [0, 1]$, and reads,

$$\rho_+ = \begin{cases} 0 & \text{for } \rho_{La} > 1 - \gamma, \\ 1 & \text{for } \rho_{La} > \delta, \\ \rho_+^* & \text{else.} \end{cases} \quad (5.8)$$

Note that due to the condition for a stable fixed point, $\gamma < \frac{1-\rho_B}{\rho_B} \delta$, the first ($\gamma > 1 - \rho_B$) and the second condition ($\rho_B > \delta$) can never be fulfilled simultaneously. In Fig. 5.8, stochastic simulations of the tip density for different sets of parameters are shown and compared to the analytic results. Both agree extremely well. For small depolymerization rates, the tip density is always one because the tip acts as a bottleneck hindering particles to leave the system. Above the value $\rho_B = \rho_{La}$, the tip density decreases according to Eq. (5.6).

Using this validated description of the tip density, we can now quantify the regimes of polymerization and depolymerization. In the unstable regime, the outcome sensitively depends on initial conditions and fluctuations. A regulatory mechanism is not feasible. In contrast, a well regulated tip density triggers the length-dynamics in the stable regime. Equating Eqs. (5.4) and (5.8) yields the transition line from the regime of depolymerization to the regime of

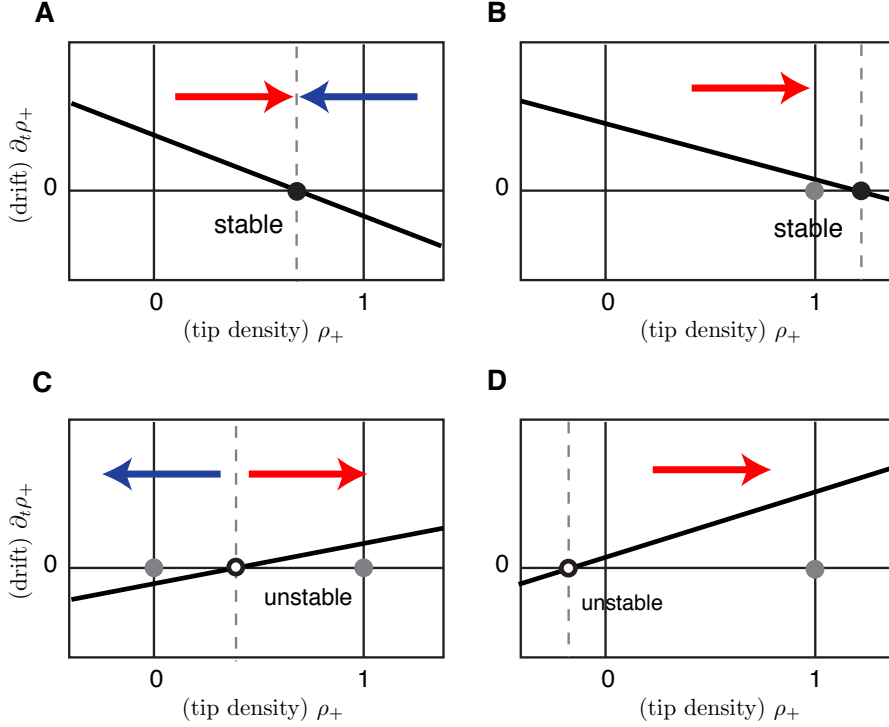


Figure 5.7: Illustration of the stability of the fixed point. In **A** and **B** the fixed point is stable, while it is unstable in **C** and **D**. The positive and negative drift causing the stability is illustrated with red and blue arrows, respectively. In **B** and **C**, the fixed point lies outside the realistic parameter range. Analyzing the drift, leads to the grey fixed points which then determine the system.

unbounded growth for a stable fixed point, $\gamma < \frac{1-\rho_B}{\rho_B} \delta$. The phase boundary is given by,

$$\frac{1}{\gamma} = \frac{1}{\rho_B(1-\rho_B)} - \frac{1}{\delta}. \quad (5.9)$$

In Fig. 5.9, this analytic solution is compared with simulation results. The drift of the MT tip, *i.e.* the speed of the tip, is shown for different sets of parameters. In the gray area, where the drift is negative, MTs mainly depolymerize and shrink, while they grow to infinity in the colored area. At first sight, the shape of the phase boundary might seem to be counterintuitive, because the regime where MTs depolymerize is more pronounced for small depolymerization rates, *i.e.* the MT shrinks even for comparably large polymerization rates. The reason for that behavior is a bottleneck at the tip: Small depolymerization rates, δ , lead to long end-residence times of the motors at the tip, $\tau_{\text{res}} = 1/\delta$. During this time interval, motors from bulk can accumulate at the tip, where a traffic jam emerges. Although depolymerization happens slowly, the tip is always occupied suppressing polymerization completely. This changes in the non-exclusive scenario as discussed in the following.

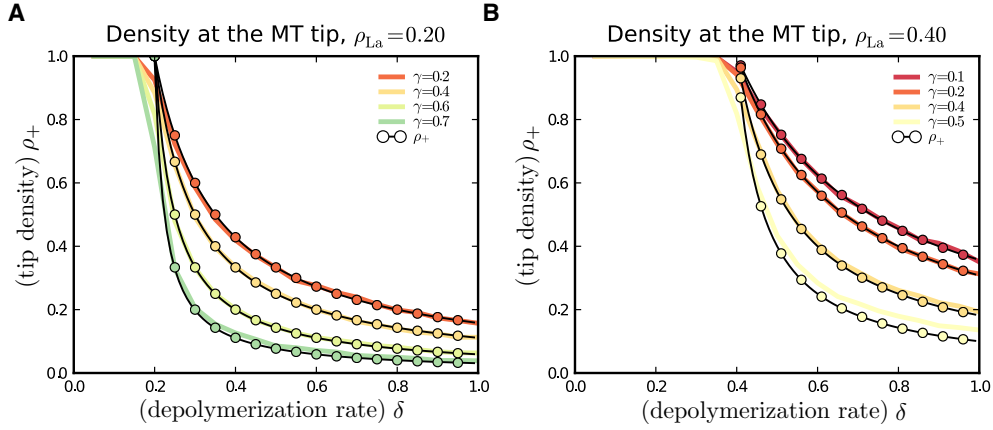


Figure 5.8: Tip density ρ_+ versus the depolymerization rate δ for different parameters. Solid lines indicate simulation results, while the analytic calculations are shown as bullets. For small depolymerization rates and a thereby strong bottleneck at the right-hand side of the system, the tip density always takes its maximal values, while it steadily decreases with increasing δ for $\delta > \rho_{La}$.

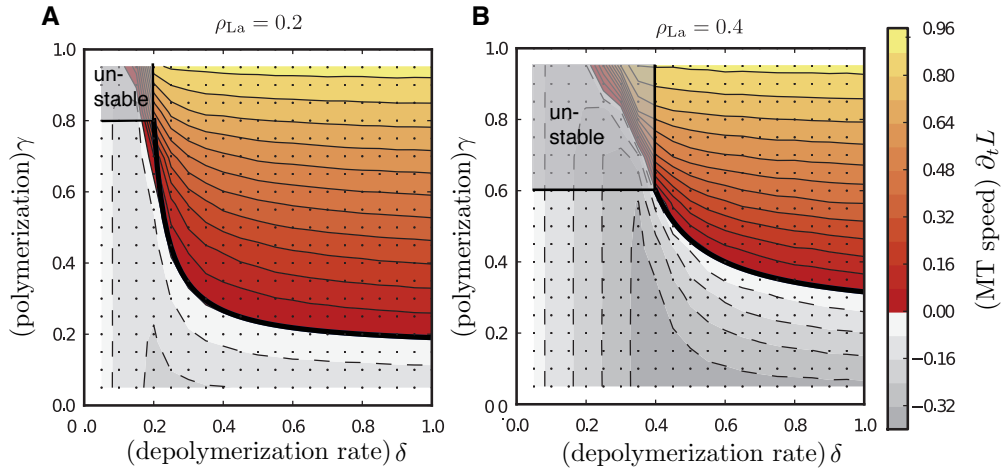


Figure 5.9: Netto drift of the MT tip for different sets of parameters. In the grey shaded area the drift is negative and the MT depolymerizes, while it is positive in the colored area. The black lines are the analytic solutions, see Eq. (5.9), and describe the phase boundary very well. In the upper left corner the fixed point is unstable and the analytic solution fails due the sensitiveness of the outcome γ on the initial conditions and fluctuations.

5.3.2 The Non-Exclusive Scenario

The phase behavior of the non-exclusive scenario can be derived in analogy to the exclusive scenario. The differential equation for the lattice length now reads,

$$\partial_t L = -\delta\rho_+ + \gamma. \quad (5.10)$$

In contrast to Eq. (5.3), polymerization does not depend on the occupation of the last lattice site resulting in the term γ instead of $\gamma\rho_+$. The critical density is now given by,

$$\rho_+^c = \frac{\gamma}{\delta}. \quad (5.11)$$

To decide, whether the system is in the depolymerizing or polymerizing regime, the tip density has to be calculated. In contrast to the exclusive scenario, some more involved arguments are necessary here. Let us first consider the differential equation for the tip density, which analogously to Eq. (5.5) reads,

$$\partial_t \rho_+ = \rho_B(1 - \rho_B) - \gamma\rho_B - \delta\rho_+(1 - \rho_B). \quad (5.12)$$

As already seen in the exclusive scenario, the tip density ρ_+ depends on the bulk density ρ_B . Importantly, this bulk density is determined by the phase of the system. If the system is in the IN phase (corresponding to the LD phase in standard TASEP) $\rho_B = \rho_{La}$ holds, while $\rho_B = \rho_{max}$ in the MC phase. Furthermore, the system can also be determined by the right boundary (EX or HD phase), again leading to different bulk and tip densities. Note, that for the standard TASEP, different phases do not entail differing boundary conditions. In contrast, here each phase shows different bulk densities ρ_B and tip densities ρ_+ . To determine whether the entering, the exiting or the maximal current regulate the system, we employ the *extremal current principle* (ECP) relying on two velocities) [271, 274, 275]: The *collective velocity* $v_{coll}(\rho) = \partial_\rho J$ determines the direction in which a local density perturbation spreads. Thereby, one is able to determine whether a certain bulk density is stable against perturbations, i.e. for a density ρ stable at the left (right) boundary $v_{coll}(\rho) > 0$ ($v_{coll}(\rho) < 0$) has to hold. The boundary conditions result in densities at the plus and the minus-end, respectively, whose stabilities can now be tested employing v_{coll} . If these densities are stable against small perturbations, we call them ρ^{left} and ρ^{right} as they are given by the system's left and right boundary, respectively. If either one or both of these boundary densities are not stable, perturbations change these densities and ρ^{left} and ρ^{right} are given by the first stable density which is determined by $v_{coll}(\rho) = 0$. The *shock velocity* $v_{shock}(\rho^{left}, \rho^{right}) = (J(\rho^{left}) - J(\rho^{right})) / (\rho^{left} - \rho^{right})$ determines the direction in which a virtual domain wall between the densities at the left and the right, ρ^{left} and ρ^{right} , moves and thereby which of these densities is realized in bulk. In more detail, for $v_{shock} > 0$ the left density, ρ^{left} , dictates the bulk density, while for $v_{shock} < 0$ the right density, ρ^{right} , is realized. In the model discussed, particles are transported to the right and therefore jams spread from right to left. Hence, the virtual domain wall arises at the right boundary and the tip densities ρ_+^{left} and ρ_+^{right} determine v_{shock}

Let us first consider the density at the left boundary which is given by $\rho^{left} = \min[\rho_{La}, \rho_{max}]$. The reason for this cut-off is as follows. Above ρ_{max} the bulk density is not robust against

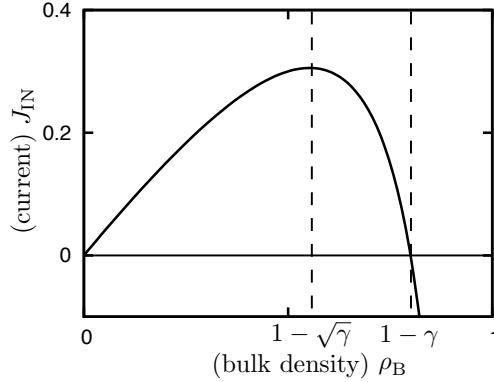


Figure 5.10: Current-density relation for a system determined by the entering current. The current is positive for $\rho_B \in [0, 1 - \gamma]$ and its maximum is located at $1 - \sqrt{\gamma}$.

perturbations as $v_{\text{coll}} = \partial_\rho J(\rho)|_{\rho_{\text{La}}} < 0$ holds. Thereby the bulk density decreases to the value where the current is maximal. The exact value of ρ_{max} and all other relevant densities are derived in the following. Let us first consider the IN phase: The bulk density is determined by the left boundary, $\rho_B = \rho_{\text{La}}$. The tip density, $\rho_{+, \text{IN}}$, can be calculated evaluating Eq. (5.12),

$$\rho_{+, \text{IN}} = \frac{\rho_{\text{La}}(1 - \rho_{\text{La}}) - \gamma \rho_{\text{La}}}{\delta(1 - \rho_{\text{La}})}. \quad (5.13)$$

We can use this identity to find the density, at which the entering current is maximal. Therefore, we need the particle current in the comoving frame which is given by,

$$J(\rho_B, \rho_+) = \rho_B(1 - \rho_B) - \gamma \rho_B + \delta \rho_+ \rho_B. \quad (5.14)$$

Plugging in the tip density, Eq. (5.13), leads to the following current-density relation,

$$J = \frac{\rho_B(1 - \rho_B - \gamma)}{1 - \rho_B}. \quad (5.15)$$

Fig. 5.10 shows the current depending on the bulk density. It is fairly surprising that the current is only positive for densities smaller $1 - \gamma$. But in the regime, where regulation is feasible, $\rho_B \leq 1 - \gamma$ always holds as we show in the following. Well-known from other driven diffusive systems [260], the maximum of the current-density relation determines the transport behavior in broad parameter regimes. If the entering density exceeds ρ_{max} , *i.e.* for Langmuir densities $\rho_{\text{La}} > 1 - \sqrt{\gamma}$, Eq. (5.13) directly transforms to,

$$\rho_{+, \text{MC}} = \frac{(1 - \sqrt{\gamma})^2}{\delta}, \quad (5.16)$$

the tip density in the MC phase. In this regime, the tip density does not depend on the density at the left boundary.

The third possibility for the tip density comes into play when the right boundary and the exiting current, J_{EX} , determine the system. Consequently, the bulk density equals the tip density, $\rho_B = \rho_+$, and Eq. (5.12) simplifies to,

$$\partial_t \rho_+ = \rho_+(1 - \rho_+) - \gamma \rho_+ - \delta \rho_+(1 - \rho_+). \quad (5.17)$$

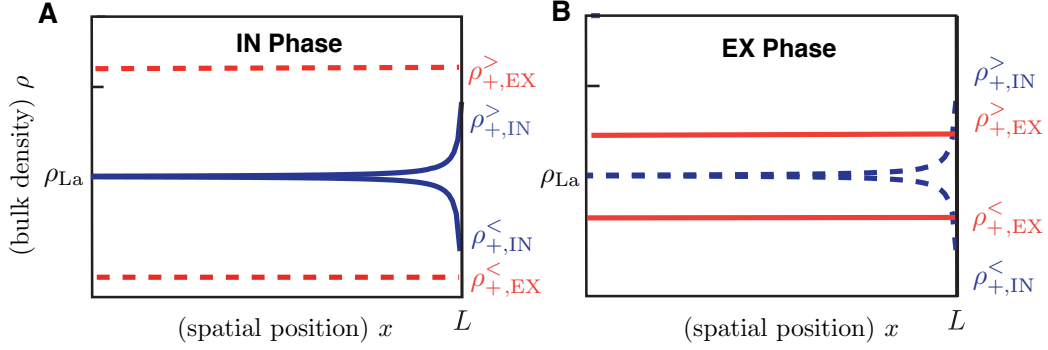


Figure 5.11: Illustration of the right boundary determining the phase behavior for Langmuir densities, ρ_{La} , smaller than the maximal current density $1 - \gamma$. Density profiles corresponding to the IN phase are shown in blue while the ones corresponding to the EX phase are red. The tip densities can either both be smaller or larger than the Langmuir density, $\rho_{+,IN}^<$, $\rho_{+,EX}^<$ and $\rho_{+,IN}^>$, $\rho_{+,EX}^>$ respectively. Both scenarios are depicted here. If this system is determined by the entering current as in this illustration, the tip density, which would arise in the EX phase, $\rho_{+,EX}$, serves as a virtual bottleneck. Therefore the tip density corresponding to the maximal exiting current is chosen. In other words, the IN phase arises for $\rho_{+,IN}^< > \rho_{+,EX}^<$ or $\rho_{+,IN}^> < \rho_{+,EX}^>$ (A), while the EX phase emerges for $\rho_{+,IN}^< < \rho_{+,EX}^<$ or $\rho_{+,IN}^> > \rho_{+,EX}^>$ (B).

In the steady state, the tip density is given by,

$$\rho_{+,EX} = 1 - \frac{\gamma}{1 - \delta}. \quad (5.18)$$

To decide which phase is realized in bulk, a slightly modified form of the *extremal current principle* (ECP) can be used [271, 274, 275]. In principle one can determine the phase behavior of the system employing the shock velocity v_{shock} as introduced above. In the following we provide a more intuitive explanation which is equivalent to the ECP. For simplicity, let us assume $\rho_{La} < \rho_{\text{max}}$, *i.e.* the maximal current never determines the transport in bulk. Thus, we focus on the IN and EX phase and the corresponding phase transition. The regime $\rho_{La} > \rho_{\text{max}}$ and the phase transition from MC to EX phase can be analyzed analogously simply by replacing ρ_{La} by ρ_{max} . For $\rho_{La} < \rho_{\text{max}}$, there are two possible scenarios for the bulk densities as sketched in Fig. 5.11: In the IN phase (blue line), the density at the left boundary is given by ρ_{La} and the tip density has a distinct value, $\rho_{+,IN}$, which lies either above or below ρ_{La} . In contrast, in the EX phase (red line), both the bulk and the tip density are given by the same value $\rho_{+,EX}$. Before turning to the question which phase is realized depending on the parameters, we first show that either both possible tip densities lie above ρ_{La} (indicated by a '>' superscript), $\rho_{+,IN}^>$ and $\rho_{+,EX}^>$, or below ρ_{La} (indicated by a '<' superscript), $\rho_{+,IN}^<$ and $\rho_{+,EX}^<$. Upon employing Eq. (5.13), $\rho_{La} \geq \rho_{+,IN}$ can be expressed as,

$$\rho_{La} \geq \frac{\rho_{-}(1 - \rho_{-} - \gamma)}{\delta(1 - \rho_{-})}. \quad (5.19)$$

Rearranging yields,

$$\rho_{La} \geq 1 - \frac{\gamma}{1 - \delta} = \rho_{+,EX}. \quad (5.20)$$

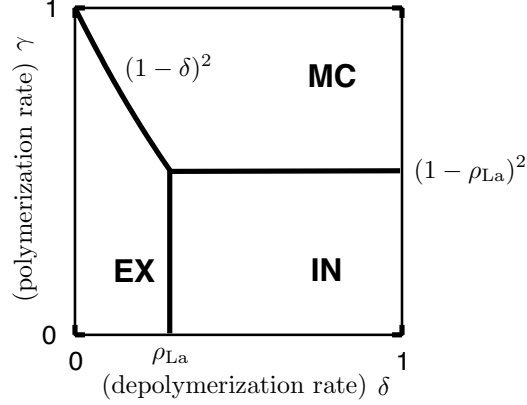


Figure 5.12: Phase diagram depending on the depolymerization and polymerization rates. The phase boundaries are given by $\gamma = (1 - \delta)^2$, $\gamma = (1 - \rho_{La})^2$ and $\delta = \rho_{La}$.

With these results at hand we can now decide which phase is realized in the system. To this end we need to compare the current from the left boundary [Eq. (5.14)], $J^{\text{left}} = J(\rho_{La}, \rho_{+,IN})$ and the current from the right [$J^{\text{right}} = J(\rho_{+,EX}, \rho_{+,EX})$]. If $\rho_{+,IN}^< > \rho_{+,EX}^< >$ or $\rho_{+,IN}^> < \rho_{+,EX}^>$ holds, the particle current from the left is always smaller than the one from the right. Therefore, no traffic jams arise at the right boundary. Hence the density profile resulting from the left boundary is not disturbed and the IN phase is present, see Fig. 5.11A. In contrast, for $\rho_{+,IN}^< < \rho_{+,EX}^< >$ or $\rho_{+,IN}^> > \rho_{+,EX}^>$, the tip density determined by the exiting current, $\rho_{+,EX}$, acts as a bottleneck and a traffic jam arises at the tip. As this traffic jam becomes macroscopic, *i.e.* it spreads back into the system it results in a bulk density given by the tip density $\rho_{+,EX}$; the system is in the EX phase, (Fig 5.11B). Analogously, one can analyze the phase transition between the MC- and EX-phase for Langmuir densities larger than ρ_{max}

The phase behavior derived by these jamming arguments can also be interpreted in terms of the ECP: The boundary which determines the system is the one corresponding to the larger exiting current. Taken together, the phase behavior is the following:

- IN phase: The bulk density is given by the Langmuir density ρ_{La} . According to the considerations above, this phase emerges if the conditions $(\rho_{La} < 1 - \sqrt{\gamma}) \wedge (\delta > \rho_{La})$ are fulfilled.
- EX phase: The bulk density is given by the tip density, $\rho_{+,EX}$, determined by the right boundary if $[(\rho_{La} < 1 - \sqrt{\gamma}) \wedge (\delta < \rho_{La})] \vee [(\rho_{La} > 0.5) \wedge (\delta < 1 - \sqrt{\gamma})]$ holds.
- MC phase: The bulk density is given by ρ_{max} for $(\rho_{La} > 1 - \sqrt{\gamma}) \wedge (\delta > 1 - \sqrt{\gamma})$.

The resulting phase diagram depending on the depolymerization and polymerization rates is shown in Fig. 5.12. Depending on the left boundary, ρ_{La} , the transition lines shift. In particular, the IN phase becomes smaller for larger Langmuir densities.

To complete our calculations, we have to combine the conditions for the different phases with the corresponding tip densities, Eqs. (5.13),(5.16) and (5.18),

$$\rho_+ = \begin{cases} \rho_{+,IN} & \text{for } (\rho_{La} < 1 - \sqrt{\gamma}) \wedge (\delta > \rho_{La}), \\ \rho_{+,EX} & \text{for } [(\rho_{La} < 1 - \sqrt{\gamma}) \wedge (\delta < \rho_{La})] \vee [(\rho_{La} > 0.5) \wedge (\delta < 1 - \sqrt{\gamma})] \\ \rho_{+,MC} & \text{for } (\rho_{La} > 1 - \sqrt{\gamma}) \wedge (\delta > 1 - \sqrt{\gamma}). \end{cases} \quad (5.21)$$

In Fig. 5.13, these analytic results for the tip density are compared with simulation data. While the latter is indicated by solid lines, black lines with different colored symbols correspond to analytic solutions in different phases: circles (IN), squares (EX) and diamonds (MC). All agree very well with the stochastic simulations and thereby also validate the phase diagram presented above. Another interesting aspect is that the tip density never exceeds $1 - \gamma$, the root of the current-density relation. This can also be understood intuitively. Consider a full occupied bulk, resulting in an occupied tip. For vanishing depolymerization rates, the tip density only changes if polymerization events happen. Therefore the tip density is 1 with probability $1 - \gamma$ and 0 with probability γ . Accordingly, the mean is given by $1 - \gamma$.

Now the boundary between a steadily depolymerizing and polymerizing regime can be calculated by equating ρ_+ with the critical density. Then, for the different phases also three different but continuously matching boundaries follow,

$$\gamma_c = \begin{cases} \rho_{La}(1 - \rho_{La}) & \text{for } (\rho_{La} < 1 - \sqrt{\gamma}) \wedge (\delta > \rho_{La}), \\ \delta(1 - \delta) & \text{for } [(\rho_{La} < 1 - \sqrt{\gamma}) \wedge (\delta < \rho_{La})] \vee [(\rho_{La} > 0.5) \wedge (\delta < 1 - \sqrt{\gamma})], \\ \frac{1}{4} & \text{for } (\rho_{La} > 1 - \sqrt{\gamma}) \wedge (\delta > 1 - \sqrt{\gamma}). \end{cases} \quad (5.22)$$

In Fig. 5.14, the analytic phase boundary is compared to simulation results. A sharp line separates the regime of unbounded growth (colored) from the depolymerizing regime (gray). In contrast to the exclusive scenario, small depolymerization rates do not favor shrinkage, since they do not block polymerization events. In this regime, the phase boundary is approximately linear indicating the antagonism between polymerization and depolymerization. For larger values of δ , the phase boundary is independent of the depolymerization rate. This is surprising as the microscopic model does not seem to have features independent of δ . Actually, the influences of the depolymerization rate on the tip density and the critical density exactly cancel out.

5.3.3 Length-Regulation

In contrast to the simplified model system discussed so far, the full model has space-dependent density profiles. As shown in Fig. 4.7, starting at the zero on the left-hand side of the lattice, the density increases until it has reached the Langmuir density. Instead of the constant Langmuir density, now this bulk density feeds the tip density. The polymerizing regime is not affected by this spatial density profiles. This can be understood intuitively: If the Langmuir density (the highest bulk density), which causes the fastest depolymerization speed, is not sufficient to overcome the growth due to polymerization, the full density profile which, depending on the spatial position, is even smaller can never lead to shrinking MTs. In contrast, for sets of parameters in the depolymerizing regime of the simplified model, $\gamma < \gamma_c$, the MT shortens until the tip is in the antenna profile. There, the bulk density decreases

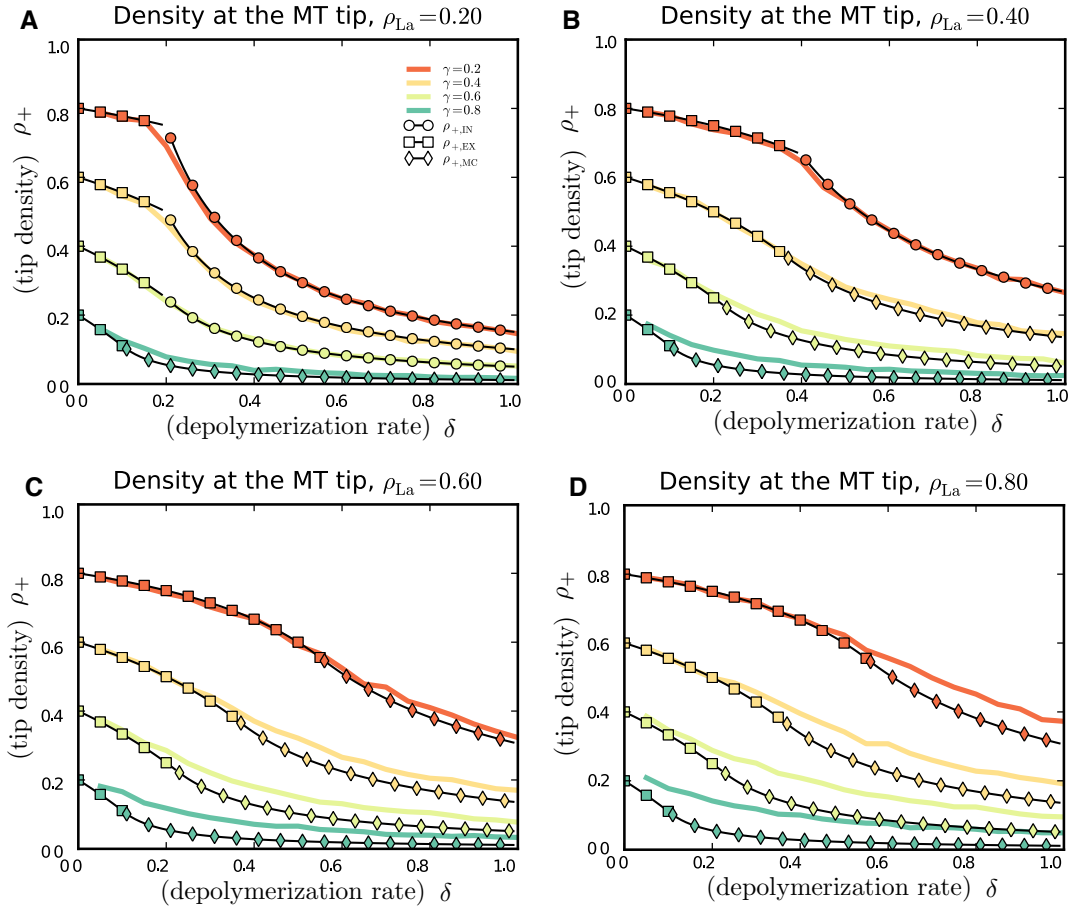


Figure 5.13: Tip density, ρ_+ , versus the depolymerization rate δ for different parameters. Solid lines indicate simulation results while the analytic calculations are shown as bullets, squares and diamonds for the IN, EX and MC phase, respectively. Starting from its maximal value $1 - \gamma$ at $\delta = 0$, the tip densities decrease with increasing δ .

with every depolymerization event until a stable fixed point is reached. The resulting MT length can be calculated for both the exclusive and the non-exclusive scenario. Furthermore, regulation to a length equal to the domain wall position, ℓ^- , is also feasible for $\rho_{La} > 0.5$. This happens, if the Langmuir density is large enough to cause depolymerization and the highest antenna density, $1 - \rho_{La}$, results in polymerization. In this scenario the variance of the MT length is very small, because small length fluctuations lead to drastic changes in the density and thereby to a large reset force. To calculate the fixed point, the density profiles have to be equated with the regulation density, at which the boundary between the polymerizing and the depolymerizing regime is reached, $\rho_{r,n}$ and $\rho_{r,ne}$ for the exclusive and non-exclusive scenario, respectively. These regulation densities can be obtained by solving Eqs. (5.6) and (5.13) for the density, ρ_{La} . The density profiles can be obtained by solving Eq. (4.2) as shown in detail in Ref. [277]. Here, only a short summary of all relations which are utilized is presented. The rescaled density reads,

$$\sigma(x) = \frac{K+1}{K-1} [2\rho(x) - 1] - 1, \quad (5.23)$$

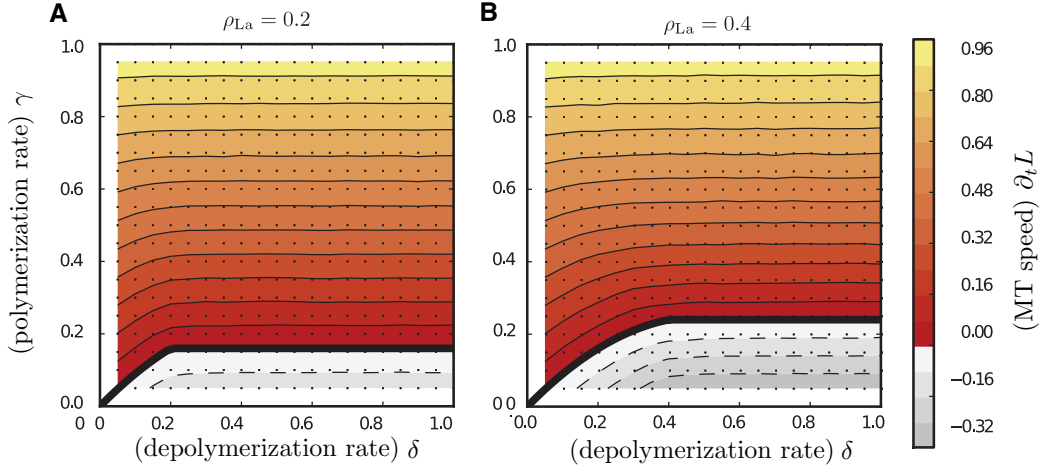


Figure 5.14: Tip speed of the MT tip for different sets of parameters. In the gray shaded area the drift is negative and the MT depolymerizes, while it is positive in the colored regime. The black lines are the analytic solutions, see Eq. 5.22 and describe the phase boundary very well.

and solves Eq. (4.2) at the left boundary under the following condition,

$$|\sigma(x)|e^{\sigma(x)} = \frac{2K}{1-K} \exp \left[\omega_d \frac{(K+1)^2}{K-1} x + \frac{2K}{1-K} \right]. \quad (5.24)$$

In combination with Eqs. (5.6) or (5.13), the resulting length of the MT can be derived. With $\rho_{r,e} = \frac{1}{2} \left(1 - \sqrt{1 - \frac{4\gamma\delta}{\gamma+\delta}} \right)$ and $\rho_{r,ne} = \frac{1}{2} \left(1 - \sqrt{1 - 4\gamma} \right)$ for the exclusive and non-exclusive scenario, respectively, it reads,

$$x^* = \frac{2\rho_r}{(K+1)\omega_d} + \frac{K-1}{(K+1)^2\omega_d} \ln \left[\frac{(K+1)(1-2\rho_r) + K-1}{2K} \right]. \quad (5.25)$$

In Fig. 5.15, these analytic results (black) are compared with simulation data (colored). We only show parameter regimes where regulation is possible, *i.e.* the gray areas in Figs. 5.9 and 5.14. In the exclusive scenario, the achieved mean length depends on both, the depolymerization and the polymerization rates. In contrast, the position of the fixed point does not depend on the depolymerization rate in the non-exclusive scenario. The reason is the same one already causing the boundary of polymerizing and depolymerizing regime to be independent of δ (in the EX or MC phase), see Fig. 5.14: The effect of the depolymerization rate cancels out.

5.3.4 Comparison of the Exclusive and Non-Exclusive Scenario

In real biological settings both, the exclusive and the non-exclusive scenario, seem to be plausible. Therefore, a comparison between both might lead to experiments which are able to clarify the microscopic details underlying length-regulation. Suitable observables have to be measurable and controllable. We choose the speed of the MT tip, $\partial_t L$, depending on

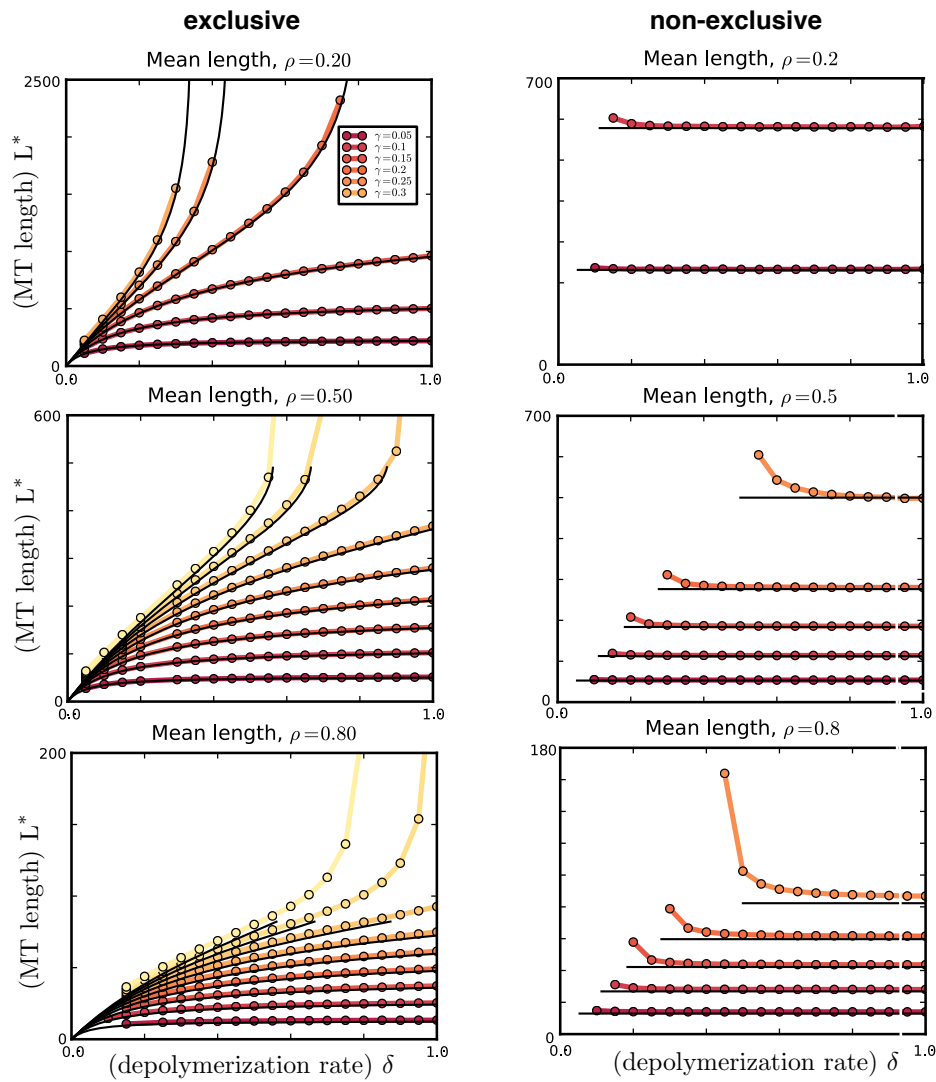


Figure 5.15: Length of the MT depending on δ and γ for the exclusive (left) and non-exclusive scenario (right). The simulation results match nicely the analytic calculation (black lines). Interestingly, the MT length does only depend on the depolymerization rate δ in the exclusive scenario.

the Langmuir density, ρ_{La} , and the polymerization rate, δ . The tip speed is a macroscopic quantity allowing for measurements which are comparably easy to perform while both the polymerization rate and the Langmuir density can be regulated. The latter depends on the motor and the salt concentration³ in the surrounding. The polymerization rate γ can be modified by different tubulin concentrations or by adding polymerizing proteins. In Fig. 5.16, the tip speed for different sets of parameters for the exclusive (left) and non-exclusive (right) scenario is shown for the simplified model disregarding spatial density profiles. In the full model, the gray area corresponds to MT with a well-defined length, while the filaments grow to infinity in the colored regime.

Even though the instability of the tip density reduces the adjustability in the exclusive scenario, the depolymerizing regime where regulation can be achieved is more extended. In contrast in the non-exclusive scenario, the gray area is much smaller and also less sensitive on a change in the depolymerization rate δ . Especially, in the EX phase, the bulk density does not influence the tip density anymore. Thereby, the exclusive scenario seems to be more suitable for length-regulatory mechanisms, while the non-exclusive scenario can robustly trigger polymerization and depolymerization. This is especially interesting when considering that both scenarios are possible in real biological systems. For example, the production of certain proteins could lead to a change from the exclusive to the non-exclusive scenario and vice versa.

5.3.5 Discussion

Taken together, we characterized the interplay between depolymerases shortening the MT and polymerization lengthening it. We therefore investigated two models. Both include motor induced depolymerization and two distinct forms of polymerization: In the exclusive scenario, MTs only grow if the tip is unoccupied by depolymerizing motors. In contrast, the model with non-exclusive polymerization allows MTs to grow independently of the tip occupation. In the simplest scenario, the polymerization rate reflects the intrinsic attachment rate of tubulin dimers at the tip. For this kind of polymerization in principle both, the exclusive and non-exclusive scenario, are conceivable. Our analysis also holds, if γ is increased by TIP+ proteins, which either have a high binding affinity to the MT plus end or diffuse along the MT. Experiments with XMAP215 suggest, that its diffusion rate is much larger than the speed of depolymerases. Then, in a first approximation, polymerases fill up the sites which are not occupied by depolymerases and thereby increase the polymerization rate if the last site is unoccupied. This interpretation leads to the exclusive-scenario. One interesting extension of the model would be to account for polymerizing motors explicitly. Furthermore, polymerization may also happen cooperatively. How this changes the length-dynamics is also an interesting question for future research.

In both models, the tip density triggers the growth dynamics of the MT, *i.e.* there exists a critical tip density above which the MT grows persistently. Below, length-regulation is in principle possible. For the exclusive scenario, the regulated regime, where a certain fixed length adjusts, is broader than for the non-exclusive scenario. We quantified the regimes of unbounded growth and depolymerization for both polymerization types. Thereby we hope to

³By changing the salt concentration the run-length can be tuned [315]

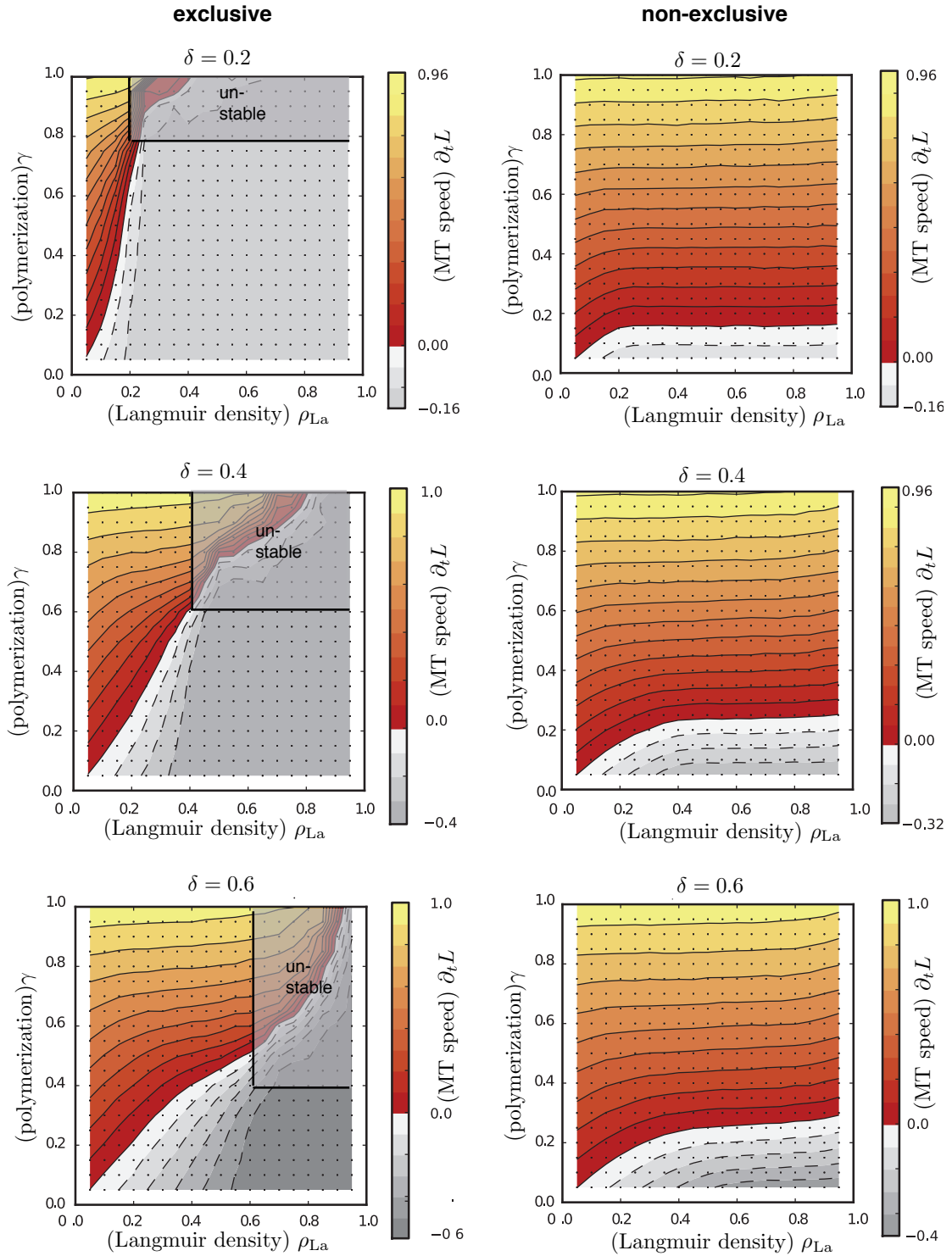


Figure 5.16: Comparison of the exclusive (left) and non-exclusive scenario (right). Plots of the tip speed depending on ρ_{La} and γ are shown for different depolymerization rates, δ . For the exclusive scenario, the grey area where length-regulation is possible is larger than for the non-exclusive scenario.

make a contribution helping to decide which scenario describes MT dynamics more accurately. Depending on the growth rate, which is tunable by changing the tubulin concentration, and the Langmuir density, which depends on the motor and salt concentration, we compared both scenarios. While in the exclusive scenario the regime of length-regulation is relatively broad, the non-exclusive scenario allows for robust unbounded growth or shrinkage.

5.4 Papers and Manuscripts

5.4.1 Crowding of Molecular Motors Determines Microtubule Depolymerization

In the paper “Crowding of molecular motors determines microtubule depolymerization”, *Biophys. J.* **101**, 2190 (2011), by Louis Reese, Anna Melbinger and Erwin Frey, we investigated the interaction of depolymerizing motors with MTs. We employed the model introduced in Sec. 5.2. Besides the good agreement with the experiments already discussed, we investigated the influence of cooperative depolymerization, *i.e.* the MT only degrades if both the last and the second to last site are occupied. Intriguingly, cooperativity does not influence the depolymerization speed. Only the end-residence time of motors at the tip is changed. This quantity is thereby well-suited to further investigate experimentally the role of cooperativity. In addition, we studied the dependence of the depolymerization speed on the bulk density and the microscopic depolymerization rate. Here, bottleneck effects play a crucial role [284, 285]. Due to such bottlenecks at the tip, microscopic traffic jams arise altering the depolymerization dynamics. We found, that two qualitatively different scenarios can be distinguished. In the *rate-limited regime* only the microscopic depolymerization rate δ gives the depolymerization speed. In contrast, in the *density-limited regime* the speed solely depends on the bulk density which in turn depends on the position on the MT. Thereby, the experimentally found length-dependent depolymerization speed can only be observed in the latter regime.

5.4.2 Conclusion and Outlook

We were able to validate our model by comparing it to experimental result. Thereby, it seems to be a promising starting point for various other investigations concerning the length-dynamics of MTs. As already discussed above, one possibility is to include also polymerization dynamics. Furthermore, one can account for correlations in the attachment and detachment rates to make our model more realistic. If a motor has detached from the MT the probability that it attaches in close vicinity of its former position is increased. This extension might cause an even better quantitative agreement of our results with experimental data. But also depolymerization itself has to be studied further. For example, until now the model describes the behavior of artificially stabilized MTs which do not exhibit dynamic instability. How these stochastic length changes are influenced by depolymerases is relevant to understand MT regulation in living cells. Especially, if these polymerases allow to trigger the stochastic growth and shrinkage would be interesting. Concerning experiments, our model also is a starting point for new measurements. In combination with theoretical considerations these experiments might be able to elucidate the microscopic rates and mechanisms governing depolymerization and, thereby, length-regulation.

Crowding of Molecular Motors Determines Microtubule Depolymerization

Louis Reese, Anna Melbinger, and Erwin Frey*

Arnold Sommerfeld Center for Theoretical Physics and Center for NanoScience, Department of Physics, Ludwig-Maximilians-Universität München, Munich, Germany

ABSTRACT The assembly and disassembly dynamics of microtubules (MTs) is tightly controlled by MT-associated proteins. Here, we investigate how plus-end-directed depolymerases of the kinesin-8 family regulate MT depolymerization dynamics. Using an individual-based model, we reproduce experimental findings. Moreover, crowding is identified as the key regulatory mechanism of depolymerization dynamics. Our analysis reveals two qualitatively distinct regimes. For motor densities above a particular threshold, a macroscopic traffic jam emerges at the plus-end and the MT dynamics become independent of the motor concentration. Below this threshold, microscopic traffic jams at the tip arise that cancel out the effect of the depolymerization kinetics such that the depolymerization speed is solely determined by the motor density. Because this density changes over the MT length, length-dependent regulation is possible. Remarkably, motor cooperativity affects only the end-residence time of depolymerases and not the depolymerization speed.

INTRODUCTION

Microtubules (MTs) are cytoskeletal filaments that serve a central role in intracellular organization (1,2) and several cellular processes, including mitosis (3,4), cytokinesis (5), and intracellular transport (6). They can cope with these diverse tasks because they are highly dynamic structures that continually assemble and disassemble through the addition and removal of tubulin heterodimers at their ends. GTP hydrolysis is the energy source that drives switching between persistent states of growth and shrinkage, in a stochastic process termed dynamic instability (7–10). Each cellular process uses a specific set of MT-associated proteins (MAPs) to tightly regulate the rates of growth and shrinkage as well as the rate of transition between these states (11–13).

Depolymerases from the kinesin-8 and kinesin-13 protein families (e.g., Kip3p and MCAK, respectively) are important regulators of MT dynamics. They are thought to promote switching of MTs from growth to shrinkage (catastrophes) (12). Whereas MCAK lacks directed motility and diffuses along MTs (14), Kip3p is a highly processive plus-end-directed motor (15,16). Proteins from the kinesin-8 family are important for regulating MT dynamics in diverse organisms. Kif18A is a key component in chromosome positioning in mammalian cells (17–19), where it regulates plus-end dynamics. Its orthologs, the plus-end-directed motors Kip3p in budding yeast (16) and Klp5/6 in fission yeast (20–22), show depolymerizing activity. A notable feature shared by these MT plus-end depolymerases is that they depolymerize longer MTs more rapidly than they do shorter ones (15,17,21,23). A similar length-dependent regulation of MT assembly by kinesin-5 motors was observed in *in vivo* studies of chromosome congression in

budding yeast (24). The key experimental observations from *in vitro* studies of Kip3p (23) are that 1), the end-residence time of Kip3p at the tip depends on the bulk concentration of Kip3p and correlates inversely with the macroscopic depolymerization speed; and 2), the macroscopic depolymerization rate is directly proportional to the flux of Kip3p toward the MT plus-end.

It is thought that length-dependent depolymerization kinetics serves several purposes (2). For example, positioning of the nucleus at the cell center during interphase is achieved by growing MTs that push against the cell poles while remaining attached to the nucleus. A higher rate of catastrophes for longer MTs implies that shorter MTs have an increased contact time with the cell poles. Computer simulations show that this leads to a higher efficiency of nuclear positioning during interphase (25).

There is convincing experimental evidence that molecular traffic along MTs strongly affects the MT depolymerization dynamics. However, *in vitro* experiments cannot yet fully explore the underlying traffic dynamics. Theoretical investigations using individual-based models can be instrumental in furthering a mechanistic understanding of this process. Fortunately, such models can be constructed on the basis of substantial quantitative data available from *in vitro* experiments (15,23) characterizing the binding kinetics and the motor activity of plus-end-directed motors. Therefore, we sought to identify the molecular mechanisms underlying the observed correlation between depolymerization dynamics and molecular traffic along MTs.

In this study, we constructed an individual-based model for the coupled dynamics of MT depolymerization and molecular traffic of plus-end-directed motors. This model quantitatively reproduces previous experimental results (15,23). Moreover, we make precise quantitative predictions for the density profiles of molecular motors on the MT and

Submitted April 28, 2011, and accepted for publication September 2, 2011.

*Correspondence: frey@lmu.de

Editor: R. Dean Astumian.

© 2011 by the Biophysical Society
0006-3495/11/11/2190/11 \$2.00

doi: 10.1016/j.bpj.2011.09.009

demonstrate that molecular crowding and ensuing traffic jams regulate the depolymerization dynamics. We find two qualitatively distinct regimes of depolymerization dynamics: At low bulk concentrations of depolymerases, the depolymerization speed of MTs is density-limited and is a function of the bulk concentration and average motor speed alone. There is a sharp threshold in bulk depolymerase concentration above which macroscopic traffic jams emerge and the depolymerization speed is simply given by the microscopic depolymerization rate. Of note, none of these features are affected by the degree of cooperativity in the depolymerization kinetics. In contrast, the end-residence time of a depolymerase (i.e., the typical time it spends at the plus-end) is strongly correlated with cooperativity. We outline how these predictions from our theoretical analysis can be tested experimentally.

RESULTS

Model definition

We use an individual-based model, as illustrated in Fig. 1, to describe the dynamics of plus-end-directed depolymerases. Motor proteins, present at a constant bulk concentration c , are assumed to randomly bind to and unbind from the MT lattice with rates ω_a and ω_d , respectively. Bound motors are described as Poisson steppers (A more detailed biochemical model for motors on MTs has to await further experimental analysis. One of the different possible schemes has recently been studied by Klumpp et al. (26).) that processively walk along individual protofilaments toward the plus-end at an average speed u (27). These motors hinder each other sterically because individual binding sites $i = 1, \dots, L$ on each protofilament can be either empty ($n_i = 0$) or occupied by a single motor ($n_i = 1$). Because switching between protofilaments is rare (27), transport along each of the protofilaments can be taken as independent, and the model becomes effectively one-dimensional (28) (Fig. 1 B). Models of this type were recently discussed as minimal models for intracellular transport (29–32). In its given formulation, where the cytosol is considered as a homogeneous and constant reservoir of motors, it is equivalent to the driven lattice gas model known as the totally asymmetric simple exclusion process with Langmuir kinetics (TASEP/LK) (29). A central finding from this model is that the interplay between on-off (Langmuir) kinetics and directed transport along protofilaments can result in “traffic jams” in which the density profile of motors along a protofilament shows a sharp increase from a low-density to a crowded high-density regime (29,31). Crowding effects such as these (33,34) are important for a molecular understanding of MT dynamics. Previous theoretical studies on this topic largely disregarded crowding effects or considered parameter regimes in which they are unimportant (35–37). Depolymerization, including crowd-

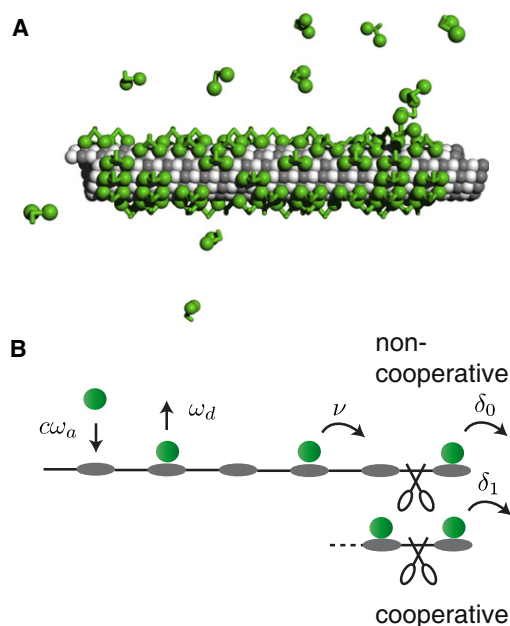


FIGURE 1 Illustration of MT and motor dynamics. Molecular motors present at concentration c randomly attach to unoccupied tubulin dimers along the MT lattice with rate ω_a . While bound, they processively move toward the plus-end at rate ν , and unbind with rate ω_d . Because motors do not switch lanes (protofilaments), the MT lattice (A) becomes effectively one-dimensional (B). Each lattice site n_i (with $i = 1, \dots, L$ numbering the sites) may be empty ($n_i = 0$) or occupied by a single motor ($n_i = 1$). At the plus-end, the motors act as depolymerases (indicated by scissors) either alone with rate δ_0 or cooperatively with rate δ_1 .

ing effects, has also been investigated for diffusive depolymerases such as MCAK (38).

At the plus-end of the systems, we consider depolymerization dynamics that arise due to the interaction of molecular motors with the MT tip. Motivated by recent experiments (23), we assume nonprocessive depolymerization, i.e., a molecular motor dissociates from the lattice after triggering depolymerization. Because the molecular mechanisms are not yet fully resolved, we study two scenarios of depolymerization (see Fig. 1 B). In the noncooperative scenario, the dissociation rate depends only on whether the last site is empty or occupied by a motor. If the last site is occupied, $n_L = 1$, the MT depolymerizes at rate δ_0 . However, recent single-molecule studies indicate that Kip3p may act cooperatively (23), which we consider as our second scenario. After arriving at the plus-end, the motor is observed to pause and depolymerize a tubulin dimer only after a second Kip3p has arrived behind it. In this scenario, a tubulin dimer is depolymerized with rate δ_1 if both the last and the second-to-last sites are occupied, $n_{L-1} = n_L = 1$. Therefore, the total depolymerization rate can be written as:

$$\Delta = \delta_0 n_L + \delta_1 n_{L-1} n_L. \quad (1)$$

For stabilized MTs, the spontaneous depolymerization rate is small (23) and thus is not considered here. The relative

magnitude of the noncooperative rate δ_0 and the cooperative rate δ_1 determines the degree of cooperativity of the depolymerization kinetics. In an average over many realizations of the stochastic process (ensemble average), the depolymerization speed V_{depol} depends on the occupation of the last two binding sites by depolymerases (Fig. 1 B):

$$V_{\text{depol}} = (\delta_0 \rho_+ + \delta_1 \kappa_+) a, \quad (2)$$

where a is the lattice spacing. Here $\rho_+ := \langle n_L \rangle$ is the probability that the last site is occupied (i.e., the expected motor density at the plus-end), and $\kappa_+ := \langle n_{L-1} n_L \rangle$ denotes the probability that both the last and second-to-last sites are occupied. We analyzed this model via stochastic simulations and analytic calculations (for further details, see the [Supporting Material](#)).

Validation of the model and its parameters

The model parameters are, as far as they are available, fixed by experimental data. The motor speed, u , the motor run length, ℓ , and motor association rate, ω_a , were measured previously (23):

$$\begin{aligned} u &= 3.2 \mu\text{m min}^{-1}, \\ \omega_a &= 24 \text{ nM}^{-1} \text{ min}^{-1} \mu\text{m}^{-1}, \\ \ell &\approx 11 \mu\text{m}. \end{aligned}$$

Using an MT lattice spacing of $a = 8.4 \text{ nm}$, we derive the corresponding parameters in our model as follows: The motor speed v corresponds to 6.35 lattice sites per second, i.e., a hopping rate of $v = u/a = 6.35 \text{ s}^{-1}$. The inverse hopping rate $\tau := v^{-1} = 0.16 \text{ s}$ and the size a of a tubulin dimer serve as our basic timescale and length scale, respectively. Then, the measured association rate corresponds to a rate $\omega_a \approx 5.3 \times 10^{-4} \text{ nM}^{-1} \text{ site}^{-1} \tau^{-1}$. The dissociation rate, $\omega_d = u/\ell$, is derived as the ratio of the mean motor speed, v , and the mean motor run length, ℓ . The latter equals 1310 lattice sites. Thus, the dissociation rate is expressed as $\omega_d \approx 7.6 \times 10^{-4} \text{ site}^{-1} \tau^{-1}$. In contrast to the transport behavior on the MT, the parameters concerning the depolymerization rates, $\delta_{0/1}$, cannot be directly extracted from experiments. However, there is evidence for a depolymerization rate as high as the motor speed, u (15,23). As a starting point for the following discussion, we tentatively take $\delta_0 = v$.

Using the above set of parameters, we now phenomenologically compare the results from numerical simulations of our model with observations from experiments. Specifically, we consider kymographs of the MT, which show how the MT length and the motor density on the MT evolve over time. For the simulation data shown in Fig. 2, we consider an MT consisting of 14 independent protofilaments and investigate the dynamics for the noncoopera-

tive scenario and a range of motor concentrations, $c = 1.2, 1.8, 2.6 \text{ nM}$ (Fig. 2, A–C). Surprisingly, as shown later, neither the cooperativity of the motors nor a decrease in the depolymerization rates led to different shapes of kymographs (see also Fig. S1).

We find an initial time period in which, starting from an empty MT lattice, the motors first fill up the lattice (39,40). This is followed by a time window in which the motor density exhibits a quasi-stationary profile, i.e., the density at a certain distance from the minus-end does not change except for boundary effects induced by the plus-end. The corresponding density profiles are illustrated in Fig. 2 E and discussed in more detail in the following section. In this quasi-stationary regime, the depolymerization dynamics shows qualitatively different behavior depending on the concentration of free motor molecules: At a low concentration, $c < 1.4 \text{ nM}$, and thus a low density of motors on the MT, depolymerization slows down gradually in the course of time (Fig. 2 A). When the motor concentration increases to larger values, $c > 1.4 \text{ nM}$, an intermediate regime emerges in which the depolymerization speed stays roughly constant (Fig. 2, B and C). Remarkably, we find that during this regime, the depolymerization speed is directly proportional to the motor density, $V_{\text{depol}}(L) = \rho_-(L) u$ (Fig. 2 D). At a third stage in the depolymerization process, there is a rather abrupt change in the depolymerization speed right where the density profile also shows a steep drop (Fig. 2, C–E). After we have elaborated more on the theoretical model, we will discuss why there is such a tight correlation between the depolymerization dynamics and the density profile.

All of these qualitative features of MT dynamics are identical to those found experimentally (15,23), and suggest that the density profile and, in particular, traffic jams formed on the MT lattice are the main determinants of the depolymerization dynamics. Moreover, the timescales of the dynamics agree quantitatively well with experimental results for the same motor concentrations (15,23). This validates our theoretical model because up to the depolymerization rate δ , all of the model parameters were derived from experimental data (23).

Density profiles at the minus-end (bulk density)

The above observations strongly point toward a tight correlation between the depolymerization speed and the motor density profile at the minus-end, $\rho_-(x)$, which we henceforth call the bulk (motor) density. The quasi-stationary bulk density profiles shown in Fig. 2 E were obtained by assuming very long lattices; effects caused by the plus-end are not visible in the vicinity of the minus-end. A more detailed discussion of these simulations can be found in the [Supporting Material](#). Because this bulk density will play an important role in the following analysis, we summarize its features here as obtained from analytical calculations detailed in the [Supporting Material](#).

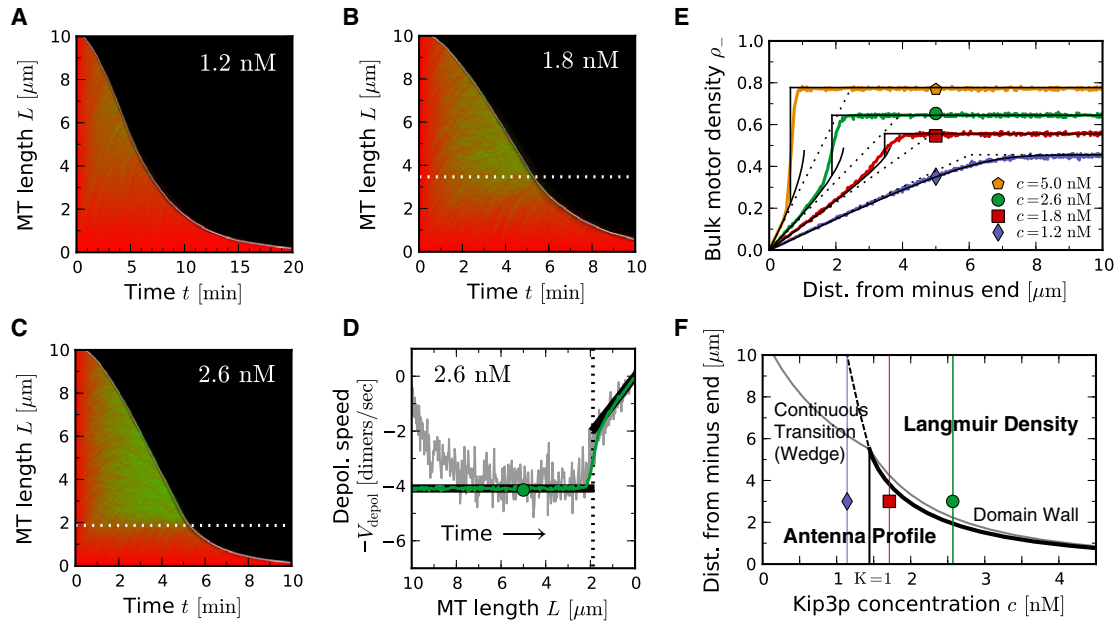


FIGURE 2 Validation of the theoretical model. (A–C) Time-space plots of stochastic simulations for a range of motor concentrations and depolymerization rate $\delta_0 = 6.35$ sites s^{-1} . The density of molecular motors is shown as the bright area (green), and the MT is shown as the dim area (red; for details, see Supporting Material). For low concentrations, $c < 1.4$ nM, depolymerization slows down gradually (23). At higher concentrations, $c > 1.4$ nM, there is a rather abrupt change in MT shortening. This change is correlated with a steep decrease in the motor density (DW), indicated as dotted lines. (D) The depolymerization speed, V_{depol} , as a function of the length of the shrinking MT $L(t)$, extracted from the simulation data shown in the kymograph (gray). The position of the DW (dotted), and the predicted depolymerization speed, $V_{\text{depol}} = u\rho(L)$ (see also Eq. 10), using the linear approximation for the motor density profile (black) and the density profile extracted from stochastic simulations (green), coincide very well with the observed depolymerization speed; $u = 6.35$ sites s^{-1} is the walking speed of the motors. (E) Density profiles at the minus-end from stochastic simulations (lines with symbols), exact solutions (solid), and linearized theory (dotted) are shown. (F) As a function of the motor concentration, c , and the distance from the minus-end, there are distinct types of density profiles. At motor concentration lower than $c = 1.4$ nM (thin black), the density of motors along the MT is low and the profile is smooth. The Langmuir density is reached continuously after a certain MT length (dashed, numerical). At high concentrations, $c > 1.4$ nM, there are two regions along the MT separated by an intervening DW (black, exact; see Supporting Material): an approximately linear antenna profile and a flat profile (Langmuir density). Linear approximations for the continuous and discontinuous transitions (Eq. 4) are shown as well (gray). Thin lines refer to the density profiles shown in E.

At the minus-end, the density profiles show an initial linear increase. This is an “antenna effect” (15), as illustrated in Fig. 3 A. Motors that attach in proximity to the MT minus-end immediately move toward the plus-end, thereby generating an approximately linearly increasing accumulation of motors. The slope is given by K/ℓ , where $K = c\omega_a/\omega_d$ denotes the binding constant. At sufficiently large distances from the minus-end, the density profile becomes flat and dominated by Langmuir kinetics with the ensuing Langmuir density:

$$\rho_{\text{La}} = \frac{K}{1+K} = \frac{c\omega_a}{c\omega_a + \omega_d}. \quad (3)$$

The full density profile is obtained by concatenating the antenna profile and the flat Langmuir profile such that the motor current is continuous along the MT. We find two qualitatively distinct scenarios (Fig. 2 E). For low concentrations of molecular motors, c , the antenna profile matches the asymptotic Langmuir density continuously, resulting in a wedge-like profile. In contrast, above a certain threshold value for the concentration, determined by the

binding constant $K_c^- = 1$, the two profiles can no longer be matched continuously and the density profile displays a sharp discontinuity, also termed a “domain wall” (DW) (29). In other words, if the Langmuir density rises above a critical value of $\rho_{\text{La}}^c = 0.5$, a crowding-induced traffic jam will result (41) (Fig. 3 A). The density profiles obtained from the analytic calculations and the stochastic simulations agree nicely, as illustrated in Fig. 2 E. In particular, the theoretical analysis gives an explicit expression for the width of the antenna-like profile:

$$\ell^- \approx \ell \begin{cases} \frac{1}{1+K} & \text{for } K < 1, \\ \frac{1}{K(1+K)} & \text{for } K > 1. \end{cases} \quad (4)$$

This result reduces to the average run length of molecular motors, $\ell = u/\omega_d$, in the limit of a very low binding constant, $K \ll 1$, where crowding effects can be neglected (37). However, with increasing K , the regime with an antenna-like profile becomes significantly shorter than ℓ (Fig. 2 F).

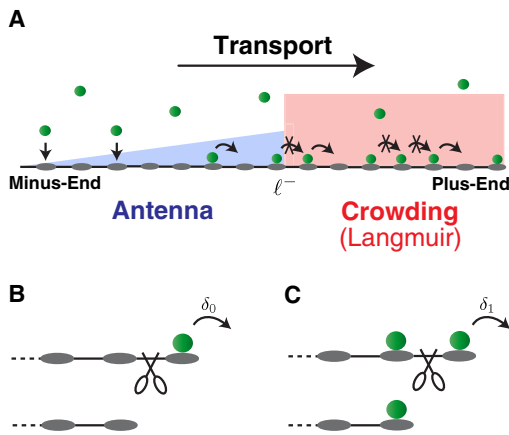


FIGURE 3 Illustration of the antenna and crowding regimes, and cooperativity. (A) Starting from an empty MT, motors start to accumulate on the MT lattice by attachment and subsequent transport to the plus-end. The combined effect of Langmuir kinetics and steric exclusion between the motors leads to two sharply separated regimes. Starting from the minus-end, the motor density increases linearly (antenna profile). At a certain critical length ℓ^- , a macroscopic traffic jam arises because particles hinder each other and crowding dominates the MT density. (B and C) Illustration of noncooperative (B, nc) and fully cooperative (C, fc) depolymerization kinetics. With regard to the depolymerization speed, both models are effectively equal (see main text).

Depolymerization dynamics is independent of cooperativity

We now address how the cooperativity of the depolymerization kinetics affects the macroscopic depolymerization speed. There are two limiting cases: noncooperative depolymerization (nc) with $(\delta_0, \delta_1) = (\delta, 0)$, and fully cooperative depolymerization (fc) with $(\delta_0, \delta_1) = (0, \delta)$ (for an illustration, see Fig. 3, B and C). Remarkably, we find from our stochastic simulations, shown in Fig. 4, that there is no difference in depolymerization speed for these two limiting cases. Even when the depolymerization dynamics contains cooperative as well as noncooperative terms, we do not find any significant differences in the depolymerization speed (Fig. 4 B).

This observation from our stochastic simulations can be explained by the following molecular mechanism: Consider a model with fully cooperative depolymerization kinetics. Then, after the first motor has arrived at the plus-end, the terminal site of the MT will remain occupied from that time on. Depolymerization only occurs if another motor arrives at the second-to-last site. In other words, while the last site remains occupied, the second-to-last site triggers the depolymerization. Hence, as far as the depolymerization speed is concerned, the fully cooperative model is identical to a noncooperative model with the same molecular rate δ . In the noncooperative model, the terminal tubulin dimer is removed at rate δ once a molecular motor has arrived at the last site (Fig. 3 B). In the fully cooperative model, the terminal tubulin dimer is removed once a molecular motor

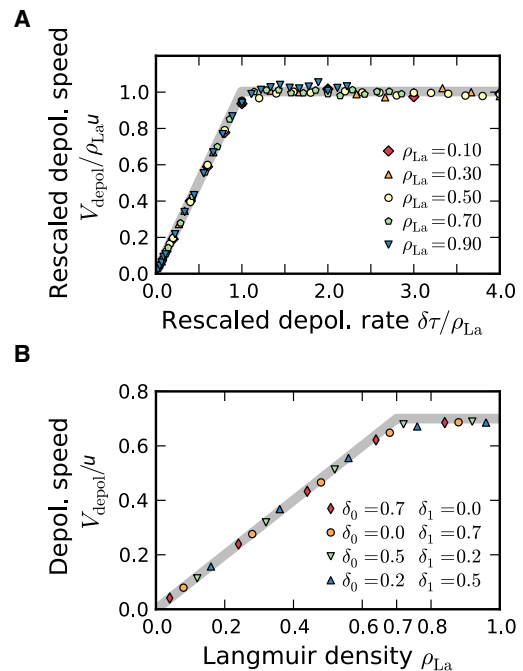


FIGURE 4 Scaling plot for the depolymerization speed V_{depol} . (A) Upon rescaling, both the macroscopic depolymerization speed, V_{depol} , and the microscopic depolymerization rate, δ , with the Langmuir density, ρ_{La} , all data collapse onto one universal scaling function \mathcal{V} (solid gray). A sharp transition at $\delta\tau = \rho_{\text{La}}^*$ distinguishes the rate-limited regime from the density-limited regime. (B) Comparison of cooperative and noncooperative depolymerization, with the macroscopic depolymerization speed V_{depol} as a function of Langmuir density ρ_{La} . For $\delta := \delta_0 + \delta_1 = 0.7\nu$ different degrees of cooperativity are displayed as indicated in the graph.

has arrived at the second-to-last site next to a permanently occupied last site (Fig. 3 C).

Depolymerization dynamics is strongly affected by crowding

To gain further insights in the correlation between the depolymerization speed and the density of motors on the MT, we performed stochastic simulations focusing on the MT plus-end by regarding the dynamics in a comoving frame. Instead of simulating the full-length MT with an antenna profile and a subsequent flat Langmuir density, we considered a reduced model in which the density at the left end is set equal to the Langmuir density ρ_{La} . For long MTs, the Langmuir density is always reached, so that the reduced system is fully equivalent to the original model. Our simulations show two clearly distinct regimes of depolymerization dynamics (Fig. 4): For small, microscopic depolymerization rates, $\delta\tau < \rho_{\text{La}}$, the polymerization speed is rate-limited: $V_{\text{depol}} = a\delta$. In contrast, for rates $\delta\tau > \rho_{\text{La}}$, the depolymerization speed is density-limited, and the Langmuir density is the limiting factor: $V_{\text{depol}} = \rho_{\text{La}}u$. The boundary between the two regimes is remarkably sharp and given by

$$\rho_{La}^* = \delta\tau. \quad (5)$$

This implies that the depolymerization speed can switch between being density-limited and rate-limited by changing the concentration c or the values of the biochemical rates of depolymerases binding to and unbinding from the MT lattice. Overall, the depolymerization speed obeys a scaling law

$$V_{\text{depol}} = \rho_{La} u \mathcal{V}\left(\frac{\delta\tau}{\rho_{La}}\right) = \begin{cases} a\delta & \text{for } \delta\tau \leq \rho_{La} \\ \rho_{La} u & \text{for } \delta\tau > \rho_{La} \end{cases}, \quad (6)$$

where $\mathcal{V}(x)$ is a universal scaling function with the simple form $\mathcal{V}(x) = x$ for $x < 1$ and $\mathcal{V}(x) = 1$ for $x > 1$. Experimentally, this implies that one should find data collapse when using such a scaling plot (Fig. 4 A).

To gain a molecular understanding of these remarkable features of the depolymerization speed, one needs to have a closer look at the density profile of the molecular motors at the MT tip. If the depolymerization rate is small, $\delta < \nu$, motors leave the tip more slowly than they arrive. Therefore, the MT tip acts as a bottleneck for molecular transport that disturbs the density profiles either locally or macroscopically. A weak bottleneck induces a local perturbation (“spike”) (33). These spikes are sharp changes of the density profile with a typical extension that scales with the size of a heterodimer. However, if the strength of a bottleneck exceeds a threshold value, the spike extends to a macroscopic perturbation (“traffic jam”) (33). Fig. 5 A illustrates how, for a given Langmuir density, $\rho_{La} = 2/3$, the effect on the density profile changes from a spike (blue) to an extended traffic jam (red and green) when the depolymerization rate is δ .

Let us now analyze the conditions and consequences of such bottlenecks in more detail. Suppose we are in a parameter regime where the plus-end disturbs the density profile only locally, i.e., on the scale of a heterodimer. Then, we may take the bulk density to be equal to the Langmuir density, ρ_{La} , up to the last site (the plus-end) where it jumps to some higher or lower value ρ_+ . The particle loss current at the plus-end due to MT depolymerization is then given by

$$J_{\text{depol}} = (1 - \rho_{La})\rho_+\delta. \quad (7)$$

The factor $1 - \rho_{La}$ arises because the particle number decreases only if a particle depolymerizes the MT and the second-to-last site, $L - 1$, is unoccupied. Otherwise, the depolymerization dynamics and the associated frame shift of the MT lattice do not change the occupation of the last site. This particle loss has to be balanced by the incoming particle flux,

$$J_{La} = \rho_{La}(1 - \rho_{La})\nu. \quad (8)$$

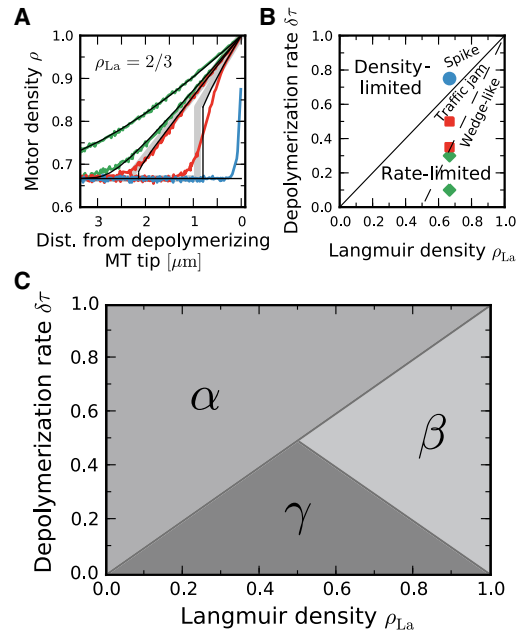


FIGURE 5 Density profiles at the plus-end, corresponding phase diagram, and depolymerization scenarios. (A) Density profiles at the MT plus-end in the comoving frame for $c = 2.9$ nM, and $\delta = 0.1, 0.3$ (left), 0.35, 0.5 (middle), and 0.8ν (right). The simulation results and analytical solutions (black; see Supporting Material) agree nicely. (B) Depending on the value of δ and the density of motors, ρ_{La} , there are three different classes of density profiles at the plus-end: wedge-like (diamonds), traffic jams with a DW (square), and spikes (circles). The transition between profiles with an extended traffic jam and a localized spike (solid line) also marks a qualitative change in the depolymerization speed. Whereas the depolymerization speed is density-limited in the spike regime, it is rate-limited in the DW and wedge regime. Symbols correspond to parameters as displayed in panel A. (C) Depending on the value of δ and the density of motors, ρ_{La} , there are three different regimes of depolymerization dynamics. In regime α , depolymerization is density-limited for arbitrary MT length. In contrast, depolymerization is rate-limited for long MTs and density-limited for short MTs in regimes β and γ . For details, see the main text.

Equating these particle fluxes (Eqs. 7 and 8) implies the following condition for the motor density at the plus-end:

$$\rho_+ = \begin{cases} \frac{\rho_{La}}{\delta\tau} & \text{for } \rho_{La} \leq \delta\tau \\ 1 & \text{for } \rho_{La} > \delta\tau \end{cases}, \quad (9)$$

where the fact that the motor density is bounded $\rho_+ \leq 1$ is already accounted for. The particle density on the last site, in turn, determines the depolymerization speed. For $\rho_{La} < \delta\tau$, one obtains according to Eqs. 2 and 9:

$$V_{\text{depol}} = \rho_+\delta a = \rho_{La} u. \quad (10)$$

Remarkably, here the effect of the depolymerization kinetics (δ) cancels out such that the macroscopic depolymerization speed is independent of the molecular details of depolymerization kinetics and is solely determined by the Langmuir density, i.e., the motor density in the bulk,

$\rho_-(x)$, and not at the tip of the MT. This result crucially depends on the presence of a microscopic spike. It explains the hitherto puzzling experimental result that the depolymerization speed is directly proportional to the bulk motor current along the MT (23) (Fig. S2).

Because the density is bounded, $\rho_+ \leq 1$, density profiles with a spike are only possible if the densities are not too large, $\rho_{La} < \delta\tau$. This is the case for the blue curve in Fig. 5 A. For densities exceeding the critical density, $\rho_{La}^* = \delta\tau$, the bottleneck-induced perturbation in the density profile can no longer remain a local spike, but has to become macroscopic in extent (33) (see *green and red curves* in Fig. 5 A and the Supporting Material).

One finds that over an extended region, the binding sites at the plus-end then remain permanently occupied such that $\rho_+ = 1$. This immediately implies that the depolymerization speed becomes density-independent and proportional to the microscopic depolymerization rate:

$$V_{\text{depol}} = a\delta. \quad (11)$$

There is a tight correlation between the shape of the density profiles and the macroscopic depolymerization speed. The analytic results explain the molecular mechanism behind the numerically observed scaling law (Eq. 6), with a sharp transition from density-regulated to rate-limited depolymerization dynamics at a critical value of $\rho_{La}^* = \delta\tau$ (cf. the classification of density profiles and depolymerization regimes shown in Fig. 5 B).

Actually, the above calculations can be generalized to the regime in which the motor density exhibits an antenna-like linear profile, i.e., for MT length shorter than ℓ^- . As detailed in the Supporting Material, we find that the depolymerization speed is rate-limited, $V_{\text{depol}} = a\delta$, if MTs are shorter than ℓ^- but still longer than a second threshold length:

$$\ell_d := \frac{\delta a}{c\omega_a} = \frac{\ell \delta\tau}{K}. \quad (12)$$

In contrast, for $\ell_d > \ell^-$, the depolymerization speed in the antenna regime is always length-dependent and strictly follows the shape of the antenna profile, $\rho_-(x)$:

$$V_{\text{depol}} = \rho_-(L)u. \quad (13)$$

Using Eq. 4, the condition $\ell_d > \ell^-$ on the threshold lengths is equivalent to $\delta\tau > \rho_{La}$ for $K < 1$, and to $\delta\tau > 1 - \rho_{La}$ for $K > 1$.

Combining all of the above results, we find three mechanisms that govern the depolymerization dynamics, as illustrated in Fig. 5 C:

α . For $\delta\tau > \rho_{La}$, the depolymerization speed is always density-regulated and given by $V_{\text{depol}}(L) = \rho_-(L)u$, where L is the time-dependent length of the MT. In this parameter regime, the depolymerization speed is a direct map of the bulk motor density profile on the

MT, $\rho_-(x)$, a feature that can be exploited experimentally to measure the profile.

- β . For $\rho_{La} > \delta\tau > 1 - \rho_{La}$, the depolymerization speed is rate-limited for MTs longer than ℓ^- , and becomes density-limited as soon as the MT length falls below ℓ^- , where the density profile is antenna-like. This implies that there is a discontinuous jump in the depolymerization speed right at $L = \ell^-$.
- γ . Finally, for all other values of $\delta\tau$, the depolymerization speed of the MT remains rate-limited for lengths larger than a threshold length ℓ_d . At ℓ_d , which is smaller than ℓ^- in this parameter regime, there is again a discontinuous jump to a density-limited depolymerization dynamics.

If the depolymerization rate is larger or equal to the hopping rate of molecular motors, $\delta\tau \geq 1$, then $\delta\tau > \rho_{La}$ is always obeyed simply because $\rho_{La} \leq 1$. In this regime, all of the molecular details of the depolymerization kinetics are irrelevant. Neither the cooperativity nor the actual value of the depolymerization rate matters in terms of the depolymerization speed; instead, only the bulk density regulates the speed. Note that this was the case for the data shown in Fig. 2, where we tentatively made the parameter choice $\delta\tau = 1$. If the motors are faster than the depolymerization process, $\delta\tau < 1$, we have to distinguish between the parameter regimes (α , β , and γ , Fig. 5 C). Here the value of the depolymerization rate matters if the bulk density exceeds a certain threshold concentration, $\rho_{La} > \delta\tau$, and the MTs are long enough. Finally, the depolymerization speed always becomes density-dependent and hence length-dependent if the MT length is short enough; the corresponding threshold length is $\ell_{\text{reg}} = \min[\ell^-, \ell_d]$.

The end-residence time strongly depends on cooperativity

In contrast to the depolymerization speed, the mean end-residence time τ_{res} is strongly affected by the degree of cooperativity. Fig. 6 displays τ_{res} as obtained from our stochastic simulations for noncooperative and fully cooperative depolymerization kinetics. Our simulations show that the end-residence time for the fully cooperative model is identical to the average lifetime of a terminal tubulin dimer $\tau_{\text{res}}^{\text{fc}} = \tau_d := a/V_{\text{depol}}$ (Fig. 6 A). Even for the noncooperative model, $\tau_{\text{res}}^{\text{nc}}$ equals τ_d for large residence times and deviates from it only at small values. The relatively sharp transition to a constant lifetime of the terminal tubulin dimer occurs right at $\tau_{\text{res}}^{\text{nc}} = \tau/\rho_{La}$, i.e., the end-residence time equals the waiting time for a molecular motor to arrive at the MT tip. For $\tau_{\text{res}}^{\text{nc}} < \tau/\rho_{La}$, the lifetime of the terminal tubulin dimer is identical to the arrival time (Fig. 6, A and B). Once the arrival time becomes shorter than the inverse depolymerization rate, the end-residence time levels off at $\tau_{\text{res}}^{\text{nc}} = 1/\delta$. These results show that the dependence of the end-residence time on density can be used to quantify the

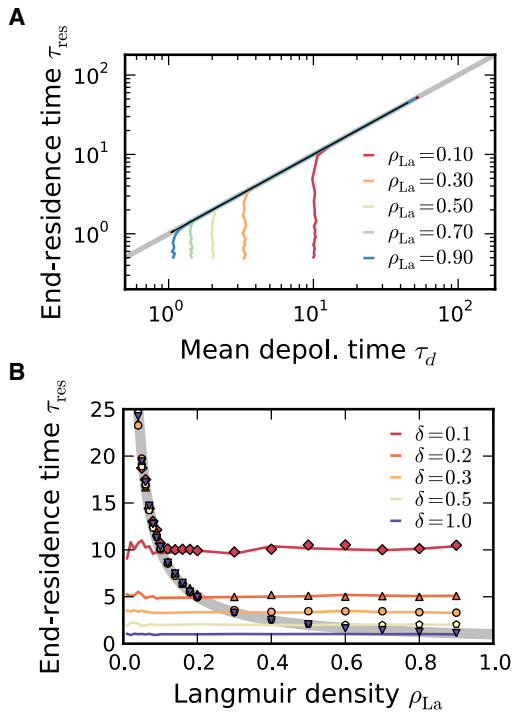


FIGURE 6 Motor end-residence times τ_{res} for cooperative and noncooperative depolymerization. (A) Mean end-residence time τ_{res} plotted against the mean depolymerization time τ_d . Data were recorded for a range of depolymerization rates $\delta = 0.02 \dots 2\nu$. Noncooperative (shaded) and cooperative (black) dynamics are shown for different densities. (B) Mean end-residence time τ_{res} as a function of the Langmuir density ρ_{La} for various depolymerization rates (in units of ν). For noncooperative depolymerization, τ_{res} is given by $1/\delta$ (shaded lines). For the fully cooperative scenario (symbols), τ_{res} depends on whether the system is in the density-limited ($\delta\tau > \rho_{\text{La}}$) or in the rate-limited ($\delta\tau < \rho_{\text{La}}$) regime. While, for $\delta\tau > \rho_{\text{La}}$, the end-residence time is given by $\tau_{\text{res}} = \tau/\rho_{\text{La}}$ (solid gray line), for $\delta\tau < \rho_{\text{La}}$, it is density-independent and determined by the microscopic depolymerization rate $\tau_{\text{res}} = 1/\delta$ (see also Eq. 16).

degree of cooperativity. This would require experiments with motor densities on the MT larger than those studied up to now (15,23).

The observation that the depolymerization speed is independent of the degree of cooperativity seems to be at odds with the experimental finding that the end-residence time, τ_{res} , of Kip3p depends on the total Kip3p concentration and is inversely proportional to the macroscopic depolymerization speed (23). Actually, however, there is no contradiction and the findings are readily explained within our theoretical model: For a noncooperative model, $\tau_{\text{res}}^{\text{nc}}$ is simply given by the depolymerization rate, because after they arrive, the particles stay at the tip until they depolymerize the MT:

$$\tau_{\text{res}}^{\text{nc}} = \frac{1}{\delta}. \quad (14)$$

For a fully cooperative model, $\tau_{\text{res}}^{\text{fc}}$ depends not only on δ but also on the rate at which the second-to-last site

becomes populated. Say the probability for the second-to-last site to be occupied is ρ_+ . Then, $\tau_{\text{res}}^{\text{fc}}$ is given by a sum of two contributions arising from the cases in which the second-to-last site is empty or occupied, respectively:

$$\tau_{\text{res}}^{\text{fc}} = (1 - \rho_+) \left(\frac{\tau}{\rho_{\text{La}}} + \frac{1}{\delta} \right) + \rho_+ \frac{1}{\delta}. \quad (15)$$

If the second-to-last site is empty (which is the case with probability $1 - \rho_+$) τ_{res} is the sum of arrival time τ/ρ_{La} and depolymerization time $1/\delta$. Otherwise, the end-residence time τ_{res} simply equals $1/\delta$.

As shown in the previous section, two distinct scenarios arise: For small bulk densities such that $\rho_{\text{La}} < \delta\tau$, the density profile at the plus-end exhibits a microscopic spike with $\rho_+ = \rho_{\text{La}}/\delta\tau$. For large densities, $\rho_{\text{La}} > \delta\tau$, a macroscopic traffic jam emerges such that $\rho_+ = 1$. This result obtained for the motor density at the MT tip (Eq. 9) may now be used to calculate $\tau_{\text{res}}^{\text{fc}}$ using Eq. 15:

$$\tau_{\text{res}}^{\text{fc}} = \begin{cases} \frac{1}{\delta} & \text{for } \rho_{\text{La}} > \delta\tau, \\ \frac{\tau}{\rho_{\text{La}}} & \text{else.} \end{cases} \quad (16)$$

This agrees well with the results from stochastic simulations displayed in Fig. 6. A comparison with Eq. 6 shows that the end-residence time equals the typical depolymerization time, i.e., the expected lifetime of a terminal tubulin dimer, $\tau_{\text{res}}^{\text{fc}} = \tau_d$. This is in agreement with experimental findings regarding the unbinding rate of motors at the plus-end (23) and strongly supports the conclusion that depolymerization of MTs by Kip3p is fully cooperative. Varga et al. (23) measured the end-residence time of motors on double stabilized MTs, i.e., where depolymerization is switched off. They observed that the end-residence time is inversely correlated with the concentration of Kip3p, and fit their data with an exponential using a cutoff. This is in accordance with our results shown in Fig. 6 B. However, because depolymerization has been switched off in the experiment, the rate δ , corresponding to the cutoff, now has to be interpreted as an unbinding-rate of motors at the plus-end. It would be highly interesting to design experiments in which the depolymerization kinetics remains switched on, because this would allow one to measure the magnitude of the microscopic depolymerization rate δ .

DISCUSSION

In this work, we analyzed the effect of crowding and cooperativity on the depolymerization dynamics of MTs. To that end, we constructed an individual-based model for the coupled dynamics of plus-end-directed motor traffic and MT depolymerization kinetics. The model is based on well-established molecular properties of motors from the

kinesin-8 family, i.e., the motors move on single protofilaments with high processivity at an average speed u , and exchange of motors between the bulk and the MT follows Langmuir kinetics. All parameters of the model, including the average walking speed, run length, and attachment rate, were directly extracted from available *in vitro* data (23). We validated our model by reproducing the onset of length-dependent depolymerization as studied recently (15,23). Without using any additional fitting parameter, we found the same regimes of density profiles and ensuing depolymerization dynamics as in the experiments, i.e., a linear antenna-profile with a length-dependent depolymerization speed and a flat profile with a constant depolymerization speed. Moreover, we identified a threshold density of motors above which a crowding-induced traffic jam emerges at the minus-end. The predicted shape and extent of these traffic jams should be amenable to experiments that raise the depolymerase concentration c or change its rates of binding to and unbinding from the MT.

The interplay between motor traffic and depolymerization kinetics at the MT plus-end leads to strong correlations between the depolymerization dynamics and density profiles of depolymerases. The plus-end acts as a bottleneck, and crowding effects cause traffic jams. We find two qualitatively distinct regimes: Motor densities below a critical threshold value, $\rho_{La}^* = \delta\tau$, always show a local spike-like perturbation at the plus-end, the extent of which is the size of a heterodimer. Above this threshold density, macroscopic traffic jams may emerge. These distinct density profiles at the plus-end affect the depolymerization speed and the end-residence time in qualitatively different ways. A quantitative analysis of the model using stochastic simulations as well as analytical calculations led to the following main results:

The end-residence time of a depolymerase strongly depends on the degree of cooperativity. Whereas for noncooperative depolymerization kinetics the end-residence time is given by the microscopic depolymerization rate δ , it is density-dependent in the fully cooperative case: Increasing the Langmuir density above the threshold value $\rho_{La}^* = \delta\tau$, the end-residence time changes from being inversely proportional to the density ρ_{La} to a constant value δ^{-1} . These results suggest an interesting way to determine the cooperativity of depolymerization kinetics and measure the value of the depolymerization rate δ . Although when the concentration c is increased, the end-residence time should be independent of concentration for noncooperative kinetics, it should strongly depend on concentration in the cooperative case. Experimental evidence points toward the latter (23).

In contrast, the depolymerization speed does not depend on the degree of cooperativity of the depolymerization kinetics. Noncooperative and fully cooperative versions of the model give identical results. As a function of depolymerase concentration and the MT length, the depolymerization

dynamics exhibits two qualitatively distinct regimes: The depolymerization speed is either density-limited and determined by the bulk density of molecular motors, $\rho_-(x)$, or rate-limited and dictated by the value of the microscopic depolymerization rate, δ . Both regimes emerge due to crowding of molecular motors at the plus-end, which acts as a bottleneck for molecular traffic.

Density-limited regimes are correlated with microscopic traffic jams (“spikes”) at the plus-end: The density profile self-organizes into a shape that cancels out all the effects of the depolymerization kinetics such that the depolymerization speed is solely determined by the bulk motor density, $\rho_-(x)$, and the average motor speed, u . Note that only in this regime length-dependent regulation is possible, because the density changes over the MT length. As emphasized above, if the depolymerization rate δ is larger than the hopping rate of the molecular motors, $\delta > \nu$, this remains the only regime of depolymerization dynamics. Then, the depolymerization speed is limited by the velocity of the plus-end directed motors, which is in accordance with recent experimental findings for Kip3p (23). In a parameter regime where motors depolymerize more slowly than they walk, $\delta < \nu$, there is a second rate-limited regime above the threshold density ρ_{La}^* and for MTs longer than some threshold length l_{reg} where $V_{depol} = a\delta$. In this regime, the plus-end acts as a strong bottleneck for molecular traffic. This causes a macroscopic traffic jam such that the motor density steeply rises to full occupation of all lattice sites at the plus-end of the MT. The cellular system sacrifices its ability to regulate the speed of depolymerization and only regains it once the MT length falls below l_{reg} , where the depolymerization speed again becomes density-regulated. From an evolutionary perspective, one might speculate that the system has evolved toward $\delta = \nu$, because this would allow regulation of the depolymerization dynamics over the broadest possible range.

Beyond these observations, other predictions of our stochastic model can be put to the test in experiments. By varying the motor concentration, two interesting observations could be made: First, the phase diagram for the density profiles at the minus-end could be scrutinized experimentally. Second, the predictions on the density-profiles at the plus-end and their predicted strong correlations to the macroscopic depolymerization dynamics might be accessible to single-molecule studies. Manipulation of the molecular properties of the motor (e.g., the run length, attachment rate (42), average speed, and depolymerization rate) would change the intrinsic biochemical rates of the system and could potentially lead to new parameter regimes. In addition, our results regarding the length and concentration dependence of the depolymerization process might be relevant *in vivo*, e.g., for mitotic chromosome alignment (18). In our theoretical studies, we explored the full parameter range, and therefore clear predictions are available for comparison.

We believe that in a more general context, our theoretical work provides new conceptual insights into the role of collective and cooperative effects in MT assembly and disassembly dynamics. Future research could focus on the antagonism between polymerases and depolymerases (12,43,44), spontaneous MT dynamics mediated by GTP hydrolysis, the abundance of molecular motors in a cell, or more-detailed modeling of molecular motors (26). This may finally lead to a molecular understanding of the regulatory mechanisms of cellular processes in which MT dynamics plays a central role.

SUPPORTING MATERIAL

Additional details, 37 equations, one table, two figures, and references are available at [http://www.biophysj.org/biophysj/supplemental/S0006-3495\(11\)01063-0](http://www.biophysj.org/biophysj/supplemental/S0006-3495(11)01063-0).

The authors thank Cécile Leduc for discussions; Varga et al. (23) for kindly providing their data; Ulrich Gerland, Günther Woehlke, and Jonas Cremer for critical readings of the original manuscript; Anton Winkler for helpful suggestions on the revised manuscript; and Andrej Vilfan for drawing Fig. 1 A.

This work was supported by the Deutsche Forschungsgemeinschaft in the framework of the SFB 863 and the German Excellence Initiative via the program “Nanosystems Initiative Munich”.

REFERENCES

- Hayles, J., and P. Nurse. 2001. A journey into space. *Nat. Rev. Mol. Cell Biol.* 2:647–656.
- Tolić-Nørrelykke, I. M. 2010. Force and length regulation in the microtubule cytoskeleton: lessons from fission yeast. *Curr. Opin. Cell Biol.* 22:21–28.
- Sharp, D. J., G. C. Rogers, and J. M. Scholey. 2000. Microtubule motors in mitosis. *Nature.* 407:41–47.
- Karsenti, E., and I. Vernos. 2001. The mitotic spindle: a self-made machine. *Science.* 294:543–547.
- Eggert, U. S., T. J. Mitchison, and C. M. Field. 2006. Animal cytokinesis: from parts list to mechanisms. *Annu. Rev. Biochem.* 75:543–566.
- Hirokawa, N., Y. Noda, ..., S. Niwa. 2009. Kinesin superfamily motor proteins and intracellular transport. *Nat. Rev. Mol. Cell Biol.* 10:682–696.
- Mitchison, T., and M. Kirschner. 1984. Dynamic instability of microtubule growth. *Nature.* 312:237–242.
- Dogterom, M., and S. Leibler. 1993. Physical aspects of the growth and regulation of microtubule structures. *Phys. Rev. Lett.* 70:1347–1350.
- Desai, A., and T. J. Mitchison. 1997. Microtubule polymerization dynamics. *Annu. Rev. Cell Dev. Biol.* 13:83–117.
- Howard, J., and A. A. Hyman. 2003. Dynamics and mechanics of the microtubule plus end. *Nature.* 422:753–758.
- Wordeman, L. 2005. Microtubule-depolymerizing kinesins. *Curr. Opin. Cell Biol.* 17:82–88.
- Howard, J., and A. A. Hyman. 2007. Microtubule polymerases and depolymerases. *Curr. Opin. Cell Biol.* 19:31–35.
- Howard, J., and A. A. Hyman. 2009. Growth, fluctuation and switching at microtubule plus ends. *Nat. Rev. Mol. Cell Biol.* 10:569–574.
- Helenius, J., G. Brouhard, ..., J. Howard. 2006. The depolymerizing kinesin MCAK uses lattice diffusion to rapidly target microtubule ends. *Nature.* 441:115–119.
- Varga, V., J. Helenius, ..., J. Howard. 2006. Yeast kinesin-8 depolymerizes microtubules in a length-dependent manner. *Nat. Cell Biol.* 8:957–962.
- Gupta, Jr., M. L., P. Carvalho, ..., D. Pellman. 2006. Plus end-specific depolymerase activity of Kip3, a kinesin-8 protein, explains its role in positioning the yeast mitotic spindle. *Nat. Cell Biol.* 8:913–923.
- Mayr, M. I., S. Hümmer, ..., T. U. Mayer. 2007. The human kinesin Kif18A is a motile microtubule depolymerase essential for chromosome congression. *Curr. Biol.* 17:488–498.
- Stumpff, J., G. von Dassow, ..., L. Wordeman. 2008. The kinesin-8 motor Kif18A suppresses kinetochore movements to control mitotic chromosome alignment. *Dev. Cell.* 14:252–262.
- Du, Y., C. A. English, and R. Ohi. 2010. The kinesin-8 Kif18A dampens microtubule plus-end dynamics. *Curr. Biol.* 20:374–380.
- Unsworth, A., H. Masuda, ..., T. Toda. 2008. Fission yeast kinesin-8 Klp5 and Klp6 are interdependent for mitotic nuclear retention and required for proper microtubule dynamics. *Mol. Biol. Cell.* 19:5104–5115.
- Tischer, C., D. Brunner, and M. Dogterom. 2009. Force- and kinesin-8 dependent effects in the spatial regulation of fission yeast microtubule dynamics. *Mol. Syst. Biol.* 5:250.
- Grissom, P. M., T. Fiedler, ..., J. R. McIntosh. 2009. Kinesin-8 from fission yeast: a heterodimeric, plus-end-directed motor that can couple microtubule depolymerization to cargo movement. *Mol. Biol. Cell.* 20:963–972.
- Varga, V., C. Leduc, ..., J. Howard. 2009. Kinesin-8 motors act cooperatively to mediate length-dependent microtubule depolymerization. *Cell.* 138:1174–1183.
- Gardner, M. K., D. C. Bouck, ..., D. J. Odde. 2008. Chromosome congression by kinesin-5 motor-mediated disassembly of longer kinetochore microtubules. *Cell.* 135:894–906.
- Foethke, D., T. Makushok, ..., F. Nédélec. 2009. Force- and length-dependent catastrophe activities explain interphase microtubule organization in fission yeast. *Mol. Syst. Biol.* 5:241.
- Klumpp, S., Y. Chai, and R. Lipowsky. 2008. Effects of the chemomechanical stepping cycle on the traffic of molecular motors. *Phys. Rev. E.* 78:041909.
- Howard, J. 1996. The movement of kinesin along microtubules. *Annu. Rev. Physiol.* 58:703–729.
- Ray, S., E. Meyhöfer, ..., J. Howard. 1993. Kinesin follows the microtubule’s protofilament axis. *J. Cell Biol.* 121:1083–1093.
- Parmeggiani, A., T. Franosch, and E. Frey. 2003. Phase coexistence in driven one-dimensional transport. *Phys. Rev. Lett.* 90:086601.
- Parmeggiani, A., T. Franosch, and E. Frey. 2004. Totally asymmetric simple exclusion process with Langmuir kinetics. *Phys. Rev. E.* 70:046101.
- Lipowsky, R., S. Klumpp, and T. M. Nieuwenhuizen. 2001. Random walks of cytoskeletal motors in open and closed compartments. *Phys. Rev. Lett.* 87:108101.
- Klumpp, S., and R. Lipowsky. 2003. Traffic of molecular motors through tube-like compartments. *J. Stat. Phys.* 113:233–268.
- Pierobon, P., M. Mabilia, ..., E. Frey. 2006. Bottleneck-induced transitions in a minimal model for intracellular transport. *Phys. Rev. E.* 74:031906.
- Telley, I. A., P. Bieling, and T. Surrey. 2009. Obstacles on the microtubule reduce the processivity of kinesin-1 in a minimal in vitro system and in cell extract. *Biophys. J.* 96:3341–3353.
- Govindan, B. S., M. Gopalakrishnan, and D. Chowdhury. 2008. Length control of microtubules by depolymerizing motor proteins. *Europhys. Lett.* 83:40006.
- Brun, L., B. Rupp, ..., F. Nédélec. 2009. A theory of microtubule catastrophes and their regulation. *Proc. Natl. Acad. Sci. USA.* 106:21173–21178.

37. Hough, L. E., A. Schwabe, ..., M. D. Betterton. 2009. Microtubule depolymerization by the kinesin-8 motor Kip3p: a mathematical model. *Biophys. J.* 96:3050–3064.
38. Klein, G. A., K. Kruse, ..., F. Jülicher. 2005. Filament depolymerization by motor molecules. *Phys. Rev. Lett.* 94:108102.
39. Vilfan, A., E. Frey, ..., E. Mandelkow. 2001. Dynamics and cooperativity of microtubule decoration by the motor protein kinesin. *J. Mol. Biol.* 312:1011–1026.
40. Frey, E., and A. Vilfan. 2002. Anomalous relaxation kinetics of biological lattice-ligand binding models. *Chem. Phys.* 284:287–310.
41. Frey, E., A. Parmeggiani, and T. Franosch. 2004. Collective phenomena in intracellular processes. *Genome Inform.* 15:46–55.
42. Cooper, J. R., M. Wagenbach, ..., L. Wordeman. 2010. Catalysis of the microtubule on-rate is the major parameter regulating the depolymerase activity of MCAK. *Nat. Struct. Mol. Biol.* 17:77–82.
43. Kinoshita, K., I. Arnal, ..., A. A. Hyman. 2001. Reconstitution of physiological microtubule dynamics using purified components. *Science.* 294:1340–1343.
44. Brouhard, G. J., J. H. Stear, ..., A. A. Hyman. 2008. XMAP215 is a processive microtubule polymerase. *Cell.* 132:79–88.

Supporting Material to “Crowding of molecular motors determines microtubule depolymerization”

Louis Reese* Anna Melbinger[†]
Erwin Frey[‡]

Arnold Sommerfeld Center for Theoretical Physics and
Center for NanoScience, Department of Physics,
Ludwig-Maximilians-Universität München,
Theresienstraße 37, D-80333 Munich, Germany

In this Supporting Material, details concerning the mathematical formulation and the stochastic simulations are given. In particular, the density profiles and the domain wall positions at the minus- and the plus-end are derived analytically. Further, some additional results are provided: (i) We show that the shapes of MT depolymerization curves (kymographs) are to a large extent independent of the choice of the depolymerization rate δ ; see Fig. S1. (ii) Analytical and numerical results from our theory are compared to experimental data on the relation between depolymerization speed and motor current (1); see Fig. S2.

Mathematical formulation

In this article, we employ a lattice gas model. Its state is described by a set of occupation numbers $n_i \in \{0, 1\}$ where $i = 1, \dots, L$ denotes the lattice sites. In contrast to the notation in the main text, we here choose units of length and time such that the hopping rate from site to site and the lattice constant are both set to one. For an analytical description of the steady state density profiles of the molecular motors along the MT we consider the ensemble-averaged densities and currents:

$$\rho_i := \langle n_i \rangle, \tag{S1}$$

$$J_i := \langle n_i(1 - n_{i+1}) \rangle. \tag{S2}$$

Note that the current J_i accounts for particle exclusion: a particle at site i moves to site $i + 1$ at rate $\nu = 1$ only if site $i + 1$ is unoccupied. The steady state results from a local

*Email: louis.reese@physik.lmu.de

[†]Email: anna.melbinger@physik.lmu.de

[‡]Corresponding author. Email: frey@lmu.de

balance between the transport current (2),

$$J_i^T := \langle n_{i-1}(1 - n_i) \rangle - \langle n_i(1 - n_{i+1}) \rangle, \quad (\text{S3})$$

the particle exchange with the bulk,

$$J_i^{La} := c\omega_a \langle 1 - n_i \rangle - \omega_d \langle n_i \rangle, \quad (\text{S4})$$

and the depolymerization current, which sets the boundary condition at the plus-end. We now perform a mean-field approximation, where all spatial correlations are neglected, and a continuum limit keeping only the leading order terms (3). Then, the transport current simplifies to,

$$J^T(x) = (2\rho(x) - 1)\partial_x \rho(x), \quad (\text{S5})$$

i.e. the transport current is proportional to the density gradient like a diffusion current in Fick's law but modified with a density-dependent prefactor which reflects site-exclusion between motors. The Langmuir current is given by

$$J^{La}(x) = c\omega_a(1 - \rho(x)) - \omega_d\rho(x). \quad (\text{S6})$$

Density profiles at the minus-end

Within the above introduced framework the motor density profiles on the MT can be calculated analytically. In particular, the domain wall position, can be derived exactly as well as upon employing a linear approximation for the density profile close to the minus-end. For simplicity, we first consider the latter, especially because its results approximate the exact solution rather well over a broad range of parameters.

Linear approximation

In the immediate vicinity of the minus-end ($x = 0$) the density is small such that the full equation for the current balance, $J^T + J^{La} = 0$,

$$(2\rho(x) - 1)\partial_x \rho(x) + c\omega_a(1 - \rho(x)) - \omega_d\rho(x) = 0, \quad (\text{S7})$$

reduces to $\partial_x \rho = c\omega_a$, which is solved by a linear (antenna) profile:

$$\rho_-(x) \approx c\omega_a x. \quad (\text{S8})$$

At sufficiently large distances from the minus-end the density profile becomes flat. Therefore, J^T vanishes and the system is dominated by the Langmuir kinetics, $J^{La} = 0$. Then, an asymptotic solution of Eq. S7 is given by the Langmuir density

$$\rho_{La} = \frac{K}{1 + K} = \frac{c\omega_a}{c\omega_a + \omega_d}. \quad (\text{S9})$$

The full density profile is obtained by concatenating the antenna profile and the flat Langmuir profile such that the (local) current is continuous along the MT. There are

two qualitatively distinct scenarios. For low bulk concentrations of molecular motors, c , the antenna profile matches the asymptotic Langmuir density continuously resulting in a *wedge-like* profile; compare Fig. 2E in the main text. Approximately, the matching point, $\rho_-(d_w^-) = \rho_{La}$, is

$$\ell_w^- \approx \frac{K}{c\omega_a(K+1)}. \quad (\text{S10})$$

In contrast, above a certain threshold value for the bulk concentration, determined by $K_c^- = 1$, the two profiles can no longer be matched continuously and the density profile displays a localized discontinuity (2), also termed a “*domain wall*” (DW). Its position is determined by a local current continuity condition (2, 3), $\rho_-(d^-) = 1 - \rho_{La}$, and can again be estimated using the linear antenna profile:

$$\ell^- \approx \frac{1}{c\omega_a(K+1)}. \quad (\text{S11})$$

Taken together, Eq. (5) from the main text is obtained,

$$\ell^- = \begin{cases} \frac{1}{\omega_d(K+1)} & \text{for } K < 1, \\ \frac{1}{c\omega_a(K+1)} & \text{for } K > 1. \end{cases} \quad (\text{S12})$$

Exact solution and domain wall position

To obtain the full solution Eq. S7 has to be solved as already demonstrated in Ref. (3). Introducing a rescaled density at the minus-end $\sigma_-(x) = \frac{K+1}{K-1}(2\rho(x) - 1) - 1$ in Eq. S7 a transformed differential equation can be obtained

$$\partial_x \sigma_-(x) + \partial_x \ln |\sigma_-(x)| = \omega_d \frac{(K+1)^2}{K-1},$$

which is mathematically equivalent to Eq. S7 and can be solved analytically

$$\sigma_-(x) = W_{-1}(-Y_-(x)). \quad (\text{S13})$$

Here W_{-1} is the second real branch of the Lambert W -function (4) and $Y_-(x)$ reads (3)

$$Y_-(x) = \left| \frac{-2K}{K-1} \right| \exp \left\{ \omega_d \frac{(K+1)^2}{K-1} x - \frac{2K}{K-1} \right\}. \quad (\text{S14})$$

Herein the boundary condition $\rho_-(0) = 0$ corresponding to $\sigma_-(0) = -2K/(K-1)$ has already been accounted for. The local current condition for the domain wall, $\rho_-(d^-) = 1 - \rho_{La}$ which corresponds to $\sigma_-(d^-) = -2$ for the rescaled density, now enables us to calculate the DW position. Combining this condition with Eqs. S13 and S14 leads to

$$d^-(\omega_d, K) = \frac{2 + (K-1) \ln(1 - 1/K)}{\omega_d(K+1)^2}. \quad (\text{S15})$$

Density profiles at the plus-end

Analogously to the minus-end, we now evaluate the density profiles and ensuing DW at the plus-end. Because the tip steadily depolymerizes, the calculations have to be performed in a comoving frame which is introduced first.

Comoving frame

In the comoving frame, the above defined last lattice site L , i.e. the plus-end, is defined as the first site of the MT. This is equivalent to reverting the motor movement. Since molecular motors in the comoving frame move towards the first site of the lattice, the transport current changes sign $J_i^T = -J_i^{T;Co}$

$$J_i^{T;Co} := \langle n_{i+1}(1 - n_i) \rangle - \langle n_i(1 - n_{i-1}) \rangle, \quad (\text{S16})$$

using the mean-field approximation as introduced above this leads to

$$J^{T;Co}(x) = -(2\rho - 1)\partial_x \rho(x). \quad (\text{S17})$$

The particle adsorption/desorption current J_i^{La} is unaffected. However, there is another contribution to the current balance in the comoving frame due to depolymerization: Similar to the above definitions of the local currents, a local current which accounts for depolymerization in the comoving frame arises

$$J_i^{Co} = \delta(n_{i+1} - n_i). \quad (\text{S18})$$

Employing a mean-field approximation this expression simplifies to,

$$J^{Co}(x) = \delta\partial_x \rho(x). \quad (\text{S19})$$

This current term can be understood as follows. Due to the depolymerizing activity of a motor at the plus-end, in the comoving frame all motors on the MT simultaneously approach the plus-end. In summary, by introducing a comoving frame the mean-field equation for the density at the MT plus-end $\rho_+(x)$ is obtained. In the steady state it reads

$$(2\rho_+ - 1 - \delta)\partial_x \rho_+ + c\omega_a(1 - \rho_+) - \omega_d\rho_+ = 0. \quad (\text{S20})$$

Density profiles

The above equation is solved in close analogy to Eq. S7. In terms of a rescaled density

$$\sigma_+(x) = \frac{2\rho_+(x) - 2\frac{K}{K+1}}{2\frac{K}{K+1} - (1 + \delta)}, \quad (\text{S21})$$

the rescaled differential equation reads

$$\sigma'_+(x) + \partial_x \ln |\sigma_+(x)| = \frac{\omega_d(K+1)^2}{K-1 - (K+1)\delta}. \quad (\text{S22})$$

The exact solutions to this equation are compared to stochastic simulations in the main text (Fig. 5A).

The solutions of this equation for $\delta = 0$ are discussed in (3) and in parts above. However, in the case of depolymerization, i.e. for $\delta > 0$, two special solutions exist: Depending on the density of motors on the MT two classes of solutions for the density at the plus-end $\rho_+(x)$ can be distinguished. These are wedge-like or traffic jam density profiles; see Fig. 5A in the main text. The boundary condition for these qualitatively distinct density profiles is $\rho_+(L) = 1$. Defining

$$Y(x) = |\sigma_+(L)| \exp \left\{ \frac{\omega_d(K+1)^2}{K-1-\delta(K+1)}(x-L) + \sigma_+(L) \right\}, \quad (\text{S23})$$

the two solutions for density profiles in the main text (black lines in Fig. 5A) are

$$\rho(x) = \begin{cases} \rho_{La} + \frac{1}{2}(2\rho_{La} - (1+\delta))W_0(Y(x)) & \text{wedge-like} \\ \rho_{La} + \frac{1}{2}(2\rho_{La} - (1+\delta))W_{-1}(-Y(x)) & \text{traffic jam.} \end{cases} \quad (\text{S24})$$

W_0 and W_{-1} denote the first and the second real branch of the Lambert function. The reason for the form of these two solutions is the bottleneck (5) arising due to depolymerization (see main text). This bottleneck fixes the value of the tip density to its maximum $\rho_+(L) = 1$ for $\rho_{La} > \delta$. The transition from a traffic jam to a wedge-like density profile is thus not boundary-induced, i.e. due to a particular value of $\rho_+(L) < 1$, but may be attributed to the depolymerizing activity of motors at the plus-end. As discussed in the main text, this transition is sharp and can be quantified in terms of ρ_{La} and δ ; see Fig. 5B.

Domain wall position at the plus-end

As already shown in the main text, microscopic jams can substantially influence the depolymerization dynamics. For large bulk concentrations, this perturbation no longer remains a local spike, but affects the profile on a macroscopic scale (5). Because the perturbation is macroscopic we can again use a hydrodynamic description, now with the boundary condition $\rho_+(L) = 1$. Close to the plus-end Eq. S20 gives an approximately linear profile

$$\rho_+(x) \approx 1 - \frac{\omega_d}{1-\delta}(L-x). \quad (\text{S25})$$

The slope increases with increasing depolymerization rate δ , c.f. Fig. 5A in the main text. In close analogy with the discussion for the minus-end there are two scenarios for concatenating this linear profile with the Langmuir density. Here, for large enough Langmuir density and/or small enough depolymerization rates, we obtain a wedge-like profile with a matching point given by $\rho_+(d_w^+) = \rho_{La}$:

$$d_w^+ \approx L - \frac{1-\delta}{\omega_d(1+K)}; \quad (\text{S26})$$

compare the green curves in Fig. 5A in the main text. Upon increasing the depolymerization rate or decreasing the Langmuir density a DW emerges whose position can be determined using current conservation, $\rho_+(d_+) = 1 - \rho_{La} + \delta$:

$$d^+ \approx L - \left[\frac{K}{1+K} - \delta \right] \frac{1-\delta}{\omega_d}; \quad (\text{S27})$$

compare the red curves in Fig. 5A. The DW is most pronounced for $K < 1$. The height of the DW vanishes as K approaches the threshold value

$$K_c^+ = \frac{1+\delta}{1-\delta} \quad (\text{S28})$$

from below. Equivalently, for a given K , the critical depolymerization rate reads

$$\delta_c = \frac{K-1}{K+1} = 2\rho_{La} - 1 = \frac{c\omega_a - \omega_d}{c\omega_a + \omega_d}. \quad (\text{S29})$$

Together with the condition for spikes, $\rho_{La} < \delta$, this relation organizes the shapes of the density profiles into three classes: Microscopic jams at the tip, wedge profiles and DW profiles.

Depolymerization dynamics of the antenna profile

In the main text we have discussed how a spatially uniform density ρ_{La} affects depolymerization dynamics. Here we briefly show that our approach is also applicable to linear antenna profiles, i.e. for MTs shorter than a certain threshold length, $L < \ell_-$, cf. Eq. (S12) and main text. Just as in the main text we equate the particle loss current due to depolymerization,

$$J_{\text{depol}}(x) = [1 - \rho_-(x)] \rho_+(x) \delta, \quad (\text{S30})$$

and the particle flux towards the plus-end,

$$J_-(x) = [1 - \rho_-(x)] \rho_-(x), \quad (\text{S31})$$

and find

$$\rho_+(x) = \begin{cases} \frac{\rho_-(x)}{\delta} & \text{for } L < \frac{\delta}{c\omega_a}, \\ 1 & \text{for } L > \frac{\delta}{c\omega_a}. \end{cases} \quad (\text{S32})$$

Since, according to Eq. (2) in the main text, the density at the plus-end determines the depolymerization speed, $V_{\text{depol}} = \delta\rho_+(x)$, the position-dependence of the tip density maps to a length-dependence of the polymerization speed. For MTs shorter than ℓ_- but longer than a certain depolymerization length $\ell_d = \delta/c\omega_a$ the depolymerization speed is length-independent

$$V_{\text{depol}} = \rho_+ \delta = \delta. \quad (\text{S33})$$

Analogously to the result for constant bulk densities, this result shows that for MTs longer than the depolymerization length ℓ_d the dynamics of depolymerization of the antenna profile can not be distinguished from the dynamics as induced by a flat density profile. In contrast, at a MT length shorter than ℓ_d the depolymerization speed becomes length-dependent and follows the shape of the antenna density profile $\rho_-(x)$:

$$V_{\text{depol}}(L) = \rho_+(L)\delta = \rho_-(L). \quad (\text{S34})$$

These results generalize the rate-limited and density-limited regimes discussed in the main text to non-uniform densities. Moreover, they show that once filaments become shorter than ℓ_- , i.e. the density profile is antenna-like, there is a second spike-induced length scale ℓ_d which is the relevant length scale for the onset of length-dependent depolymerization of MTs.

Combining these results with the analogous conditions for the Langmuir plateau discussed in the main text, leads to the depolymerization regimes summarized in Fig. 5C and Table S1. Simply put, the depolymerization dynamics changes from rate-limited to density-limited when the *bulk density* falls below the threshold density δ : $\rho_-(L) \leq \delta$. For Langmuir densities below the threshold density, $\rho_{\text{La}} < \delta$, the bulk density remains below the threshold density for the whole MT length such that the depolymerization dynamics is always density-limited and given by: $V_{\text{depol}} = \rho_-(L)$. This corresponds to regime (α) in Fig. 5C. For Langmuir densities above the threshold, $\rho_{\text{La}} > \delta$, the depolymerization dynamics is rate-limited in the Langmuir plateau and given by $V_{\text{depol}} = \delta$. In the antenna-like regime of the density profile, i.e. for $L \leq \ell^-$, we have to distinguish between two cases: (i) $K > 1$ ($\rho_{\text{La}} > 0.5$) where the *bulk* density profile exhibits a domain wall, and (ii) $K < 1$ ($\rho_{\text{La}} < 0.5$) where the *bulk* density profile is wedge-like. In the latter case, the bulk-density profile changes slowly and hence remains above the threshold δ for some time even below $L = \ell^-$. Only for MTs shorter than ℓ_d , given by $\rho_-(\ell_d) = \delta$, the dynamics changes from rate- to density-limited. This corresponds to regime (γ) in Fig. 5C. In contrast, for $K > 1$ ($\rho_{\text{La}} > 0.5$), the bulk density $\rho_-(x)$ exhibits a discontinuous jump from the Langmuir density to $1 - \rho_{\text{La}}$ right at ℓ^- . If this maximum value of the antenna-like profile is less than the threshold density, $1 - \rho_{\text{La}} < \delta$, then the depolymerization dynamics discontinuously switches from rate-limited to density-limited. This defines regime (β) in Fig. 5C. Otherwise, if $1 - \rho_{\text{La}} > \delta$, we are back to regime (γ). In summary, all regimes show a constant depolymerization speed for long MTs in the Langmuir plateau. Depending on the relative magnitude of the Langmuir density and the depolymerization rate this regime is either density-limited and given by ρ_{La} or rate-limited and given by δ , cf. second column in Table S1. In all scenarios the dynamics becomes length-dependent at some scale which is, however, different. While for regimes α and β , it coincides with the beginning of the antenna-like density profile ℓ^- , it is given by ℓ_d for regime (γ) cf. third column in Table S1.

Regime	Condition	Constant V_{depol}	Critical MT length
(α)	$\rho_{\text{La}} < \delta$	$V_{\text{depol}} = \rho_{\text{La}}$	ℓ_-
(β)	$\rho_{\text{La}} > \delta > 1 - \rho_{\text{La}}$	$V_{\text{depol}} = \delta$	ℓ_-
(γ)	else	$V_{\text{depol}} = \delta$	ℓ_d

TABLE S1: Summary of the similarities and differences in the depolymerization regimes (α), (β) and (γ). While for MTs longer than a critical length (third column) the depolymerization speed is constant (second column), it becomes length-dependent below this critical length and is then given by $V_{\text{depol}} = \rho_-(L)$.

Numerical implementation

The stochastic dynamics of the individual-based model was simulated using a Gillespie algorithm (6) and employing the rates introduced above. Note that this method provides the mathematically exact stochastic dynamics. This is essential for the investigation of dynamic phenomena like length-dependent shortening.

In Fig. 2A-D, our simulations of the motor traffic started from an initial condition where the MT lattice was empty and subsequently filled up with motors triggering the depolymerization dynamics. To visualize time-dependent MT length and motor densities in one kymograph we implemented 14 protofilaments and averaged the motor intensities and MT lengths, see Fig. 2A-C. In detail, the visualization of kymographs was achieved as described in the following. From stochastic simulation data of the MT, each second the occupation numbers of motors along the MT $n_i^{(j)}$, where j indexes the 14 protofilaments of the MT, were evaluated and converted to *RGB* color values:

$$R_i = \frac{\sum_{j=1}^{14} 1 - n_i^{(j)}}{14}, \quad G_i = \frac{\sum_{j=1}^{14} n_i^{(j)}}{14}, \quad B_i = 0. \quad (\text{S35})$$

These values display the density of motors as green and the uncovered MT surface as red. Hence, if the MT is completely empty it is red, while at complete motor coverage it is green.

Steady state motor densities as shown in Figs. 2E and 5A were obtained by time-averaging over 10^4 independent realizations after an equilibration time of 2000 time steps; note that for a constant lattice size time and ensemble averages yield identical results (2). In Fig. 5A, the density profiles were recorded in the comoving frame of the MT plus-end, while density profiles in Fig. 2E were recorded in the rest frame of the MT minus-end. In Fig. 2E, the density profiles resulting from the minus end without any influences from the plus end are shown. This can be viewed as an infinitely long lattice. To simulate such a lattice, we chose the following boundary conditions. We neglected depolymerization as it arises at infinity. Further, we set the exiting rate for motors at the last site equal to $1 - \rho_{\text{La}}$. Then, the transport behavior at the tip is the same as on the lattice, if the Langmuir density is reached, $\rho(x) = \rho_{\text{La}}$.

In the second part of the article we focus on the dependence of the depolymerization speed on the motor density. To this end, simulations were performed in a comoving

frame where the density at the minus-end was fixed to the Langmuir density. This was achieved by extending the lattice one site to left with each depolymerization step and filling the thereby created site with the probability ρ_{La} . This procedure may also be interpreted as an infinite MT allowing to observe motor dynamics at the MT tip without perturbations arising from the length-dependent depolymerization regime.

We measured the mean end-residence time of individual motors at the plus-end τ_{res} and the mean lifetime of the terminal tubulin dimer τ_d . Data of these were obtained by averaging over 10^4 time steps τ , cf. Figs. 4 and 6.

How kymographs become independent of the depolymerization rate

In Fig. S1 we provide data that explicitly shows the parameter independence of MT depolymerization. This results has been generalized in the main text to all possible motor concentrations and depolymerization rates.

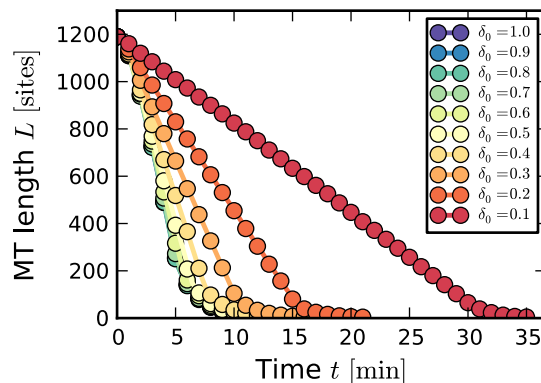


FIGURE S1: *Kymographs as they become independent of the depolymerization rate δ .* Time-space plots of depolymerizing MTs for different depolymerization rates are shown, ranging from $\delta = 0.1\nu$ (red) to 1.0ν (blue), the latter value corresponds to the motor speed of $v = 6.35 \text{ sites s}^{-1}$. For slow depolymerization rate, $\delta \lesssim 0.5$, the depolymerization speed is related to the microscopic depolymerization rate δ , whereas for rates $\delta \gtrsim 0.5$ the depolymerization speed is independent of the depolymerization rate but depends on the density of motors on the MT, as outlined in the main text.

Comparison with experiments: dependence of the depolymerization speed on the bulk flux and bulk density

Experimentally it was found that the depolymerization speed is linearly correlated with the flux of molecular motors towards the plus-end (1). We have collected data from our

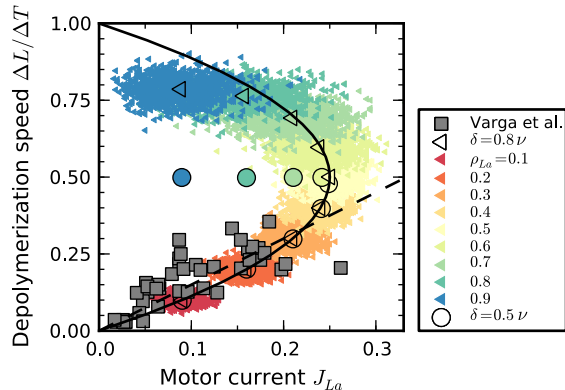


FIGURE S2: *Depolymerization speed $\Delta L/\Delta T$ as a function of the bulk motor current on the MT, J_{La} .* Data from stochastic simulations for two different depolymerization rates $\delta = 0.5\nu$ (\circ) and 0.8ν (\triangleleft) are shown, each for a set of Langmuir densities (colors) corresponding to concentrations $c = 0.16 \dots 13$ nM. To illustrate the effect of statistics, small symbols show individual measurements as obtained from 10^3 fixed time measurements $\Delta T = 500\tau$, while large symbols indicate their mean $\langle \Delta L/\Delta T \rangle$. Good agreement with experimental data (\square) measured in the low density regime is found (1). Here, the theoretical prediction given by J_{La} (solid) is hardly discernible from a linear best fit to experiments (dashed).

simulations similar to experiments. Figure S2 shows a scatter plot for the depolymerization speed as a function of the bulk flux of motors, J_{La} , for two values of the microscopic depolymerization rate δ . The noise in the ensemble of realizations has two sources. The bulk current fluctuates since the Langmuir kinetics responsible for the bulk density ρ_{La} is a stochastic process. The depolymerization speeds vary from realization to realization because the depolymerization kinetics is a Poisson-like process. Also shown in Fig. S2 are ensemble averages. These mean values, as predicted in the main text, show the following behavior. For a macroscopic depolymerization speed lower than the depolymerization rate, $\Delta L/\Delta T < \delta a$, it is density-limited and identical to the bulk density:

$$\frac{\Delta L}{\Delta T} = \rho_{La}v \quad \text{for} \quad \rho_{La} < \delta\tau. \quad (\text{S36})$$

Rewriting this relation in terms of the bulk current means that the data should fall on the parabola displayed as the solid curve in Fig. S2. For low densities, $\rho_{La} \lesssim 0.25$, where crowding effects are weak, this implies $\Delta L/\Delta T = \rho_{La}v \approx J_{La}$ as observed experimentally (1); see Fig. S2.

As the bulk density is increased two things happen. First, crowding effects become important invalidating the linear relationship between bulk current and depolymerization speed. It would be interesting to test our prediction that the depolymerization speed is linear in the bulk density by using higher motor concentrations or changed biochemical rates such that K becomes significantly larger than 1. Second, if $\rho_{La} > \delta\tau$, the

depolymerization speed becomes rate-limited:

$$\frac{\Delta L}{\Delta T} = a\delta \quad \text{for } \rho_{La} > \delta\tau. \quad (\text{S37})$$

This puts an obvious upper bound on the depolymerization speed. It cannot become larger than the microscopic rate of depolymerization at the plus-end. If the depolymerization rate is larger than the hopping rate of the molecular motors, $\delta > \nu$, the depolymerization speed is, for all possible values of the bulk density, strictly given by the bulk density.

Supporting References

- [1] Varga, V., C. Leduc, V. Bormuth, S. Diez, and J. Howard. 2009. Kinesin-8 motors act cooperatively to mediate length-dependent microtubule depolymerization. *Cell*. 138:1174–1183.
- [2] Parmeggiani, A., T. Franosch, and E. Frey. 2003. Phase coexistence in driven one-dimensional transport. *Phys. Rev. Lett.* 90:086601.
- [3] Parmeggiani, A., T. Franosch, and E. Frey. 2004. Totally asymmetric simple exclusion process with langmuir kinetics. *Phys. Rev. E.* 70:046101.
- [4] Corless, R., G. Gonnet, D. Hare, D. Jeffrey, and D. Knuth. 1996. On the lambert w function. *Adv. Comput. Math.* 5:329–359.
- [5] Pierobon, P., M. Mabilia, R. Kouyos, and E. Frey. 2006. Bottleneck-induced transitions in a minimal model for intracellular transport. *Phys. Rev. E.* 74:031906.
- [6] Gillespie, D. T. 1976. Stochastic simulations of chemical processes. *J. Comp. Phys.* 22:403–434.

Bibliography

- [1] B. Alberts, A. Johnson, J. Lewis, M. Raff, K. Roberts, and P. Walter, *Molecular Biology of the Cell*, Garland Science, 2002.
- [2] J. Watson and F. Crick, Molecular structure of nucleic acids. A structure for deoxyribose nucleic acid, *Nature* **171**, 737 (1953).
- [3] F. Crick, L. Barnett, S. Brenner, and R. Watts-Tobin, General nature of the genetic code for proteins, *Nature* **192**, 1227 (1961).
- [4] A. Eldar and M. Elowitz, Functional roles for noise in genetic circuits, *Nature* **467**, 167 (2010).
- [5] M. Samoilov, S. Plyasunov, and A. Arkin, Stochastic amplification and signaling in enzymatic futile cycles through noise-induced bistability with oscillations, *Proc. Natl. Acad. Sci. USA* **102**, 2310 (2005).
- [6] E. Karsenti and I. Vernos, Cell cycle - the mitotic spindle: A self-made machine, *Science* **294**, 543 (2001).
- [7] E. A. Nigg, Mitotic kinases as regulators of cell division and its checkpoints, *Nat. Rev. Mol. Cell Biol.* **2**, 21 (2001).
- [8] M. Ptashne and A. Gann, *Genes & Signals*, CSHL Press, 2002.
- [9] H. McAdams and A. Arkin, It's a noisy business! Genetic regulation at the nanomolar scale., *Trends Genet.* **15**, 65 (1999).
- [10] M. Elowitz, A. Levine, E. Siggia, and P. Swain, Stochastic gene expression in a single cell, *Science* **297**, 1183 (2001).
- [11] M. Kærn, T. Elston, W. Blake, and J. Collins, Stochasticity in gene expression: from theories to phenotypes, *Nat. Rev. Gen.* **6**, 451 (2005).
- [12] S. E. Luria and M. Delbrück, Mutations of bacteria from virus sensitivity to virus resistance., *Genetics* **28**, 491 (1943).
- [13] J. Lamarck, *Philosophie zoologique*, F. Savy, 1809.
- [14] C. Darwin, *Origin Of Species*, John Murray, 1859, Online Version.
- [15] H. Newcombe, Origin of bacterial variants, *Nature* **164**, 150 (1949).
- [16] P. Sniegowski, T. Gerrish, P.J. Johnson, and A. Shaver, The evolution of mutation-rates: seperating causes from consequences, *Bioessays* **22**, 1057 (2000).

-
- [17] A. Bird, Perceptions of epigenetics, *Nature* **447**, 396 (2007).
- [18] E. Schrödinger, *What is life?*, Cambridge Univ. Press, 1967.
- [19] M. Delbrück, A physicists renewed look at biology – twenty years later, *Science* **168**, 1312 (1970).
- [20] S. J. Gould, *The Structure of Evolutionary Theory*, Harvard University Press, Harvard, 2002.
- [21] S. Okasha, *Evolution and the Levels of Selection*, Oxford University Press, Oxford, 2006.
- [22] S. P. Hubbell, *The Unified Neutral Theory of Biodiversity and Biogeography*, Princeton University Press, Princeton, 2001.
- [23] M. Kimura, *The Neutral Theory of Molecular Evolution*, Cambridge University Press, Cambridge, 1983.
- [24] J. Megerle, G. Fritz, U. Gerland, J. K., and J. O. Rädler, Timing and dynamics of single cell gene expression in the arabinose utilization system, *Biophys. J.* **95**, 2103 (2008).
- [25] S. Leibler and E. Kussell, Individual histories and selection in heterogeneous populations, *Proc. Natl. Acad. Sci. USA* **107**, 18183 (2009).
- [26] J. Howard, *Mechanics of Motor Proteins and the Cytoskeleton*, Sinauer Associates, 2001.
- [27] R. Tournebize, K. Popov, A. Kinoshita, A. Ashford, S. Rybina, A. Pozniakovsky, T. U. Mayer, C. E. Walczak, E. Karsenti, and A. Hyman, Control of microtubule dynamics by the antagonistic activities of Xmap215 and Xkcm1 in xenopus egg extracts, *Nat. Cell Biol.* **2**, 13 (2000).
- [28] M. L. Gupta, P. Carvalho, D. M. Roof, and D. Pellman, Plus end-specific depolymerase activity of Kip3, a kinesin-8 protein, explains its role in positioning the yeast mitotic spindle, *Nat. Cell Biol.* **8**, 913 (2006).
- [29] M. I. Mayr, S. Hümmer, J. Bormann, T. Grüner, S. Adio, G. Woehlke, and T. U. Mayer, The human kinesin Kif18a is a motile microtubule depolymerase essential for chromosome congression, *Curr. Biol.* **17**, 488 (2007).
- [30] C. Tischer, D. Brunner, and M. Dogterom, Force- and kinesin-8-dependent effects in the spatial regulation of fission yeast microtubule dynamics, *Mol. Syst. Biol.* **5**, 250 (2009).
- [31] J. Helenius, G. Brouhard, Y. Kalaidzidis, S. Diez, and J. Howard, The depolymerizing kinesin MCAK uses lattice diffusion to rapidly target microtubule ends, *Nature* **441**, 115 (2006).
- [32] V. Varga, J. Helenius, K. Tanaka, A. A. Hyman, T. U. Tanaka, and J. Howard, Yeast kinesin-8 depolymerizes microtubules in a length-dependent manner, *Nat. Cell Biol.* **8**, 957 (2006).

- [33] G. J. Brouhard, J. H. Stear, T. L. Noetzel, J. Al-Bassam, K. Kinoshita, S. C. Harrison, J. Howard, and A. A. Hyman, XMAP215 is a processive microtubule polymerase, *Cell* **132**, 79 (2008).
- [34] V. Varga, C. Leduc, V. Bormuth, S. Diez, and J. Howard, Kinesin-8 motors act cooperatively to mediate length-dependent microtubule depolymerization, *Cell* **138**, 1174 (2009).
- [35] E. Odum and G. Barrat, *Fundamentals of Ecology*, Brooks Cole, 2005.
- [36] M. Hassel, Density dependence in single species populations, *J. Anim. Ecol.* **44**, 283 (1975).
- [37] B. Drossel, P. G. Higgs, and A. J. McKane, The influence of predator prey population dynamics on the long-term evolution of food web structure, *J. Theor. Biol.* **208**, 91 (2000).
- [38] A. J. Lotka, Undamped oscillations derived from the law of mass action, *J. Am. Chem. Soc.* **42**, 1595 (1920).
- [39] V. Volterra, Variazioni e fluttuazioni del numero d'individui in specie animali conviventi, *Mem. R. Acca. Naz. dei Lincei* **2** (1926).
- [40] D. Boucher, editor, *The biology of mutualism: ecology and evolution*, Oxford University Press, 1985.
- [41] A. Hastings, *Population biology: Concepts and Models*, Springer Verlag, 1997.
- [42] M. Kot, *Mathematical Ecology*, Cambridge University Press, 2001.
- [43] T. R. Malthus, *An Essay on the Principle of Population*, J. Johnson, 1798.
- [44] P. F. Verhulst, Notice sur la loi que la population poursuit dans son accroissement, *Corresp. Math. Phys.* **10**, 113 (1838).
- [45] A. Hastings, Transients: the key to long-term ecological understanding?, *Trends Ecol. Evol.* **19**, 39 (2004).
- [46] B. Charlesworth, *Evolution in age-structured populations*, Cambridge University Press, Cambridge, 1994.
- [47] J. Monod, The growth of bacterial cultures, *Annu. Rev. Microbiol.* **3**, 371 (1949).
- [48] K. Lewis, Persister cells, dormancy and infectious disease, *Nat. Rev. Micro.* **5**, 48 (2007).
- [49] F. J. Richards, A flexible growth function for empirical use, *J. Exp. Bot.* **10**, 290 (1959).
- [50] A. G. Cairns-Smith, *Seven Clues to the Origin of Life*, Cambridge University Press, 1985.
- [51] B. Obermayer and E. Frey, Escalation of error catastrophe for enzymatic self-replicators, *Europhys. Lett.* **88**, 48006 (2009).

- [52] B. Obermayer and E. Frey, Error thresholds for self- and cross-specific enzymatic replication, *J. Theor. Biol.* **267**, 652 (2010).
- [53] P. Baaske, F. M. Weinert, S. Duhr, K. H. Lemke, M. J. Russell, and D. Braun, Extreme accumulation of nucleotides in simulated hydrothermal pore systems, *Proc. Natl. Acad. Sci. USA* **104**, 9346 (2007).
- [54] C. B. Mast and D. Braun, Thermal trap for DNA replication, *Phys. Rev. Lett.* **104**, 188102 (2010).
- [55] J. T. Bonner, *First Signals - the evolution of multicellular development*, Princeton University Press, Princeton, 2001.
- [56] R. E. Michod, Y. Viossat, C. A. Solari, M. Hurand, and A. M. Nedelcu, Life-history evolution and the origin of multicellularity, *J. Theor. Biol.* **239**, 257 (2006).
- [57] J. L. Sachs, Resolving the first steps to multicellularity, *Trends Ecol. Evol.* **23**, 245 (2008).
- [58] C. Darwin, On the tendency of species to form varieties; and on the perpetuation of varieties and species by natural means of selection. i. Extract from an unpublished work on species, ii. Abstract of a letter from C. Darwin, esq., to Prof. Asa Gray., *J. Proc. Linn. Soc. London* **3**, 45 (1858).
- [59] A. R. Wallace, On the tendency of species to form varieties; and on the perpetuation of varieties and species by natural means of selection. iii. On the tendency of varieties to depart indefinitely from the original type., *J. Proc. Linn. Soc. London* **3**, 53 (1858).
- [60] U. Kutschera, A comparative analysis of the Darwin-Wallace papers and the development of the concept of natural selection, *Theory Biosci.* , 343 (2003).
- [61] R. C. Lewontin, The units of selection, *Annu. Rev. Ecol. Syst.* **1**, 1 (1970).
- [62] P. Godfrey-Smith, *Darwinian Populations and Natural Selection*, Oxford University Press, Oxford, 2009.
- [63] E. Haeckel, *Generelle Morphologie der Organismen*, Georg Reimer, 1866, Online version.
- [64] G. Mendel, Versuche über pflanzenhybriden, *Verhandlungen des Naturforschenden Vereines in Brünn* **4**, 3 (1866).
- [65] J. H. Gillespie, *Population Genetics*, The Johns Hopkins University Press, 2004.
- [66] J. A. J. Metz, R. M. Nisbet, and S. A. H. Geritz, How should we define 'fitness' for general ecological scenarios?, *TREE* **7**, 198 (1992).
- [67] A. Ariew and R. C. Lewontin, The confusions of fitness, *Brit. J. Phil. Sci.* **55**, 347 (2004).
- [68] J. Grinnell, The niche-relationships of the California trasher, *Auk* **39**, 373 (1922).
- [69] M. Dworkin, editor, *The Prokaryotes: Ecophysiology and biochemistry*, Springer, 2006.

- [70] D. J. Merrell, *The Adaptive Seascape*, Minnesota University Press, 1994.
- [71] V. Mustonen and M. Lässig, From fitness landscapes to seascapes: non-equilibrium dynamics of selection and adaptation, *Trends Genet.* **25**, 111 (2009).
- [72] J. Maynard Smith, *Evolution and the Theory of Games*, Cambridge University Press, Cambridge, 1982.
- [73] J. A. Fletcher, M. Zwick, M. Doebeli, and D. S. Wilson, What's wrong with inclusive fitness?, *Trends Ecol. Evol.* **21**, 597 (2006).
- [74] C. Darwin, *The Descent of Man*, John Murray, 1871.
- [75] J. Katiaho, N. LeBas, M. Puurtinen, and J. Tomkins, On the resolution of the lek paradoxon, *Trend Ecol. Evol.* **23**, 1 (2008).
- [76] J. F. C. Kingman, The coalescent, *Stoch. Proc. Appl.* **13**, 235 (1982).
- [77] M. Eigen, Selforganization of matter and the evolution of biological macromolecules, *Naturwissenschaften* **58**, 465 (1971).
- [78] M. Eigen and P. Schuster, A principle of natural self-organization, *Naturwissenschaften* **64**, 541 (1977).
- [79] G. R. Price, Selection and covariance, *Nature* **227**, 520 (1970).
- [80] W. Hamilton, Innate social aptitudes of man: an approach from evolutionary genetics, *Biosoc. Anthropol.* (1975).
- [81] S. A. Frank, The price equation, Fisher's fundamental theorem, kin selection, and causal analysis, *Evolution* **51**, 1712 (1997).
- [82] J. S. Chuang, O. Rivoire, and S. Leibler, Cooperation and Hamilton's rule in a simple synthetic microbial system, *Mol. Syst. Biol.* **6**, 398 (2010).
- [83] J. Hofbauer and K. Sigmund, *Evolutionary Games and Population Dynamics*, Cambridge University Press, 1998.
- [84] P. Taylor and L. Jonker, Evolutionary stable strategies and game dynamics, *Math. Biosci.* **40**, 145 (1978).
- [85] J. Maynard Smith and G. R. Price, The logic of animal conflict, *Nature* **246**, 15 (1973).
- [86] J. von Neumann and O. Morgenstern, *Theory of Games and Economic Behavior*, Princeton Univ. Press, 1944.
- [87] M. A. Nowak, *Evolutionary Dynamics: Exploring the Equations of Life*, Belknap Press, 2006.
- [88] J. Cremer, T. Reichenbach, and E. Frey, The edge of neutral evolution in social dilemmas, *New J. Phys.* **11**, 093029 (2009).
- [89] B. Sinervo and C. M. Lively, The rock-paper-scissors game and the evolution of alternative male strategies, *Nature* **380**, 240 (1996).

-
- [90] B. Kerr, M. A. Riley, M. W. Feldman, and B. J. M. Bohannan, Local dispersal promotes biodiversity in a real-life game of rock-paper-scissors, *Nature* **418**, 171 (2002).
- [91] B. C. Kirkup and M. A. Riley, Antibiotic-mediated antagonism leads to a bacterial game of rock-paper-scissors in vivo, *Nature* **428**, 412 (2004).
- [92] T. Reichenbach, M. Mobilia, and E. Frey, Coexistence versus extinction in the stochastic cyclic Lotka-Volterra model, *Phys. Rev. E* **74**, 051907 (2006).
- [93] T. Reichenbach, M. Mobilia, and E. Frey, Mobility promotes and jeopardizes biodiversity in rock-paper-scissors games, *Nature* **448**, 1046 (2007).
- [94] J. C. Claussen and A. Traulsen, Cyclic dominance and biodiversity in well-mixed populations, *Phys. Rev. Lett.* **100**, 058104 (2008).
- [95] T. Reichenbach, M. Mobilia, and E. Frey, Self-organization of mobile populations in cyclic competition, *J. Theor. Biol.* **254**, 368 (2008).
- [96] T. Reichenbach, *Dynamic patterns of biological systems*, PhD thesis, Ludwig Maximilians Universität München, 2008.
- [97] M. Berr, T. Reichenbach, M. Schottenloher, and E. Frey, Zero-one survival behavior of cyclically competing species, *Phys. Rev. Lett.* **102**, 048102 (2009).
- [98] B. Andrae, J. Cremer, T. Reichenbach, and E. Frey, Entropy production of cyclic population dynamics, *Phys. Rev. Lett.* **104**, 218102 (2010).
- [99] S. Wright, *Evolution and the Genetics of Populations*, University of Chicago Press, 1968.
- [100] R. A. Fisher, *The Genetical Theory of Natural Selection*, Oxford University Press, Oxford, 1930.
- [101] S. Wright, Evolution in Mendelian populations, *Genetics* **16**, 97 (1931).
- [102] W. J. Ewens, *Mathematical Population Genetics*, Springer, 2nd edition, 2004.
- [103] D. Gillespie, A general method for numerically simulating the stochastic time evolution of coupled chemical reactions, *J. Comp. Phys.* **22**, 403 (1976).
- [104] P. A. Moran, *The Statistical Processes of Evolutionary Theory*, Clarendon Press Oxford, Oxford, 1964.
- [105] A. Traulsen, J. C. Claussen, and C. Hauert, Coevolutionary dynamics: from finite to infinite populations, *Phys. Rev. Lett.* **95**, 238701 (2005).
- [106] R. A. Blythe and A. J. McKane, Stochastic models of evolution in genetics, ecology and linguistics, *J. Stat. Mech.* **2007**, P07018 (2007).
- [107] N. Van Kampen, *Stochastic Processes in Physics and Chemistry*, North Holland, 2nd edition, 2001.

- [108] H. Risken, *The Fokker-Planck Equation - Methods of Solution and Applications*, Springer-Verlag, Heidelberg, 1984.
- [109] D. Brockmann and L. Hufnagel, Front propagation in reaction-superdiffusion dynamics: Taming levy flights with fluctuations, *Phys. Rev. Lett.* **98**, 178301 (2007).
- [110] O. Hallatschek and D. R. Nelson, Life at the front of an expanding population, *Evolution* **64**, 193 (2010).
- [111] R. Hermsen and T. Hwa, Sources and sinks: A stochastic model of evolution in heterogeneous environments, *Phys. Rev. Lett.* **105**, 248104 (2010).
- [112] K. Jain and S. Krug, J. Park, Evolutionary advantage of small populations on complex fitness landscapes, *Evolution* (2011).
- [113] E. Leigh, Neutral theory: a historical perspective, *J. Evol. Biol.* **20**, 5504 (2007).
- [114] U. Dieckmann and R. Law, The dynamical theory of coevolution: a derivation from stochastic ecological processes, *J. Math. Biol.* **34**, 579 (1996).
- [115] C. Hauert, M. Holmes, and M. Doebeli, Evolutionary games and population dynamics: maintenance of cooperation in public goods games, *Proc. Roy. Soc. Lond. B.* **273**, 2565 (2006).
- [116] J. Roughgarden, Density-dependent natural selection, *Ecology* **52**, 453 (1971).
- [117] R. Cressman and G. Vickers, Spatial and density effects in evolutionary game theory, *J. Theor. Biol.* **184**, 359 (1997).
- [118] A. Melbinger, J. Cremer, and E. Frey, Evolutionary game theory in growing populations, *Phys. Rev. Lett.* **105**, 178101 (2010).
- [119] J. Cremer, A. Melbinger, and E. Frey, Evolutionary dynamics and population size: A coupled approach, in preparation .
- [120] R. Axelrod, *The Evolution of Cooperation*, Basic Books, New York, 1984.
- [121] <http://view.stern.de/de/picture/Affe-schreiend-dressierter-affe-schreiender-Affe-Gruen-221360.html>.
- [122] <http://www.imker-badschwalbach.de/index.html>.
- [123] R. M. Donlan, Biofilms: Microbial life on surfaces, *Emerg. Infect. Dis.* **8**, 881 (2002).
- [124] E. Fehr and U. Fischbacher, The nature of human altruism, *Nature* **425**, 785 (2003).
- [125] R. Boyd, H. Gintis, S. Bowles, and P. J. Richerson, The evolution of altruistic punishment, *Proc. Natl. Acad. Sci. USA* **100**, 3531 (2003).
- [126] M. Hauser, *The evolution of communication*, MIT Press, 1996.
- [127] B. Hölldobler and E. O. Wilson, *The Superorganism: The Beauty, Elegance, and Strangeness of Insect Societies*, W. W. Norton, 2009.

- [128] J. Strassmann, Y. Zhu, and D. Queller, Altruism and social cheating in the social amoeba *dictyostelium discoideum*, *Nature* **408**, 965 (2000).
- [129] G. J. Velicer and M. Vos, Sociobiology of the myxobacteria, *Annu. Rev. Microbiol.* **63**, 599 (2009).
- [130] K. Sauer, A. Camper, G. Ehrlich, J. Costerton, and D. Davies, *Pseudomonas aeruginosa* displays multiple phenotypes during development as a biofilm, *J. Bacteriol.* **184**, 1140 (2002).
- [131] S. Finkel and R. Kolter, Evolution of microbial diversity during prolonged starvation, *Proc. Natl. Acad. Sci. USA* **96**, 4023 (1999).
- [132] I. Chen and D. Dubnau, DNA uptake during bacterial transformation, *Nat. Rev. Microbiol.* **2**, 241 (2004).
- [133] M. Leisner, J.-T. Kuhr, J. O. Rädler, E. Frey, and B. Maier, Kinetics of genetic switching into the state of bacterial competence, *Biophys. J.* **96**, 1178 (2009).
- [134] P. B. Rainey and K. Rainey, Evolution of cooperation and conflict in experimental bacterial populations, *Nature* **425**, 72 (2004).
- [135] A. Buckling, F. Harrison, M. Vos, M. A. Brockhurst, A. Gardner, S. A. West, and A. Griffin, Siderophore-mediated cooperation and virulence in *pseudomonas aeruginosa*, *FEMS Microbiol. Ecol.* **62**, 135 (2007).
- [136] J. Crespi, The evolution of social behaviour in microorganisms, *Trends Ecol. Evol.* **16**, 178 (2001).
- [137] C. D. Nadell, J. B. Xavier, S. A. Levin, and K. R. Foster, The evolution of quorum sensing in bacterial biofilms, *PLoS Biol.* **6**, e14 (2008).
- [138] D. Greig and M. Travisano, The prisoner's dilemma and polymorphism in yeast suc genes, *Proc. Roy. Soc. Lond. B* **271**, S25 (2004).
- [139] J. Gore, H. Youk, and A. van Oudenaarden, Snowdrift game dynamics and facultative cheating in yeast, *Nature* **459**, 253 (2009).
- [140] R. C. MacLean, A. Fuentes-Hernandez, D. Greig, L. D. Hurst, and I. Gudelj, A mixture of 'cheats' and 'co-operators' can enable maximal group benefit, *PLoS Biol.* **8**, e1000486 (2010).
- [141] P. Stoodley, K. Sauer, D. G. Davies, and J. W. Costerton, Biofilms as complex differentiated communities, *Annu. Rev. Microbiol.* **56**, 187 (2002).
- [142] P. S. Stewart and M. J. Franklin, Physiological heterogeneity in biofilms, *Nat. Rev. Microbiol.* **6**, 199 (2008).
- [143] J. B. Xavier and K. R. Foster, Cooperation and conflict in microbial biofilms, *Proc. Natl. Acad. Sci. USA* **104**, 876 (2007).
- [144] C. D. Nadell, J. B. Xavier, and K. R. Foster, The sociobiology of biofilms, *FEMS Microbiol. Rev.* **33**, 206 (2009).

- [145] M. E. Hibbing, C. Fuqua, M. R. Parsek, and S. B. Peterson, Bacterial competition: surviving and thriving in the microbial jungle, *Nat. Rev. Microbiol.* **8**, 15 (2010).
- [146] A. Buckling, R. C. Maclean, M. A. Brockhurst, and N. Colegrave, The beagle in a bottle, *Nature* **457**, 824 (2009).
- [147] J. E. Keymer, P. Galajda, C. Muldoon, S. Park, and R. H. Austin, Bacterial metapopulations in nanofabricated landscapes, *Proc. Natl. Acad. Sci. USA* **103**, 17290 (2006).
- [148] J. E. Keymer, P. Galajda, G. Lambert, D. Liao, and R. H. Austin, Computation of mutual fitness by competing bacteria, *Proc. Natl. Acad. Sci. USA* **105**, 20269 (2008).
- [149] J. S. Chuang, O. Rivoire, and S. Leibler, Simpson's paradox in a synthetic microbial system, *Science* **323**, 272 (2009).
- [150] W. H. Krull and C. R. Mapes, Studies on the biology of *Dicrocoelium dendriticum* (Rudolphi, 1819) Looss, 1899 (Trematoda: Dicrocoeliidae), including its relation to the intermediate host, *Cionella lubrica* (Müller). ii. Collection of the snail, *Cionella lubrica*, and its maintenance in the laboratory., *Cornell Vet.* **41**, 433 (1951).
- [151] D. Wilson, How nepotistic is the brain worm?, *Behav. Ecol. Sociobiol.* **2**, 421 (1977).
- [152] M. A. Nowak, Five rules for the evolution of cooperation, *Science* **314**, 1560 (2006).
- [153] S. A. West, A. S. Griffin, and A. Gardner, Social semantics: altruism, cooperation, mutualism, strong reciprocity and group selection, *J. Evol. Biol.* **20**, 415 (2007).
- [154] M. A. Nowak, Evolution of indirect reciprocity, *Nature* **437**, 1291 (2005).
- [155] S. A. West, A. Gardner, D. M. Shuker, T. Reynolds, M. Burton-Chellow, E. M. Sykes, M. A. Guinnee, and A. S. Griffin, Cooperation and the scale of competition in humans, *Curr. Biol.* **16**, 1103 (2006).
- [156] B. Rockenbach and M. Milinski, The efficient interaction of indirect reciprocity and costly punishment, *Nature* **444**, 718 (2006).
- [157] C. Hauert, A. Traulsen, H. Brandt, M. A. Nowak, and K. Sigmund, Via freedom to coercion: The emergence of costly punishment, *Science* **316**, 1905 (2007).
- [158] G. Szabó and G. Fáth, Evolutionary games on graphs, *Phys. Rep.* **446**, 97 (2007).
- [159] C. P. Roca, J. A. Cuesta, and A. Sanchez, Evolutionary game theory: Temporal and spatial effects beyond replicator dynamics, *Phys. Life. Rev.* **6**, 208 (2009).
- [160] M. A. Nowak and R. M. May, Evolutionary games and spatial chaos, *Nature* **359**, 826 (1992).
- [161] M. A. Nowak, S. Bonhoeffer, and R. M. May, Spatial games and the maintenance of cooperation, *Proc. Natl. Acad. Sci. USA* **91**, 4877 (1994).
- [162] C. Hauert and M. Doebeli, Spatial structure often inhibits the evolution of cooperation in the snowdrift game, *Nature* **428**, 643 (2004).

- [163] C. P. Roca, J. A. Cuesta, and A. Sanchez, Effect of spatial structure on the evolution of cooperation, *Phys. Rev. E* **80**, 046106 (2009).
- [164] E. Lieberman, C. Hauert, and M. A. Nowak, Evolutionary dynamics on graphs, *Nature* **433**, 312 (2005).
- [165] H. Ohtsuki, C. Hauert, E. Lieberman, and M. A. Nowak, A simple rule for the evolution of cooperation on graphs and social networks, *Nature* **441**, 502 (2006).
- [166] J. M. Pacheco, A. Traulsen, and M. A. Nowak, Coevolution of strategy and structure in complex networks with dynamical linking, *Phys. Rev. Lett.* **97**, 258103 (2006).
- [167] C. E. Tarnita, T. Antal, H. Ohtsuki, and M. A. Nowak, Evolutionary dynamics in set structured populations, *Proc. Natl. Acad. Sci. USA* **106**, 8601 (2009).
- [168] C. E. Tarnita, H. Ohtsuki, T. Antal, F. Fu, and M. A. Nowak, Strategy selection in structured populations, *J. Theor. Biol.* **259**, 570 (2009).
- [169] D. S. Wilson, Structured demes and the evolution of group-advantageous traits, *Am. Nat.* **111**, 157 (1977).
- [170] A. T. C. Silva and J. F. Fontanari, Deterministic group selection model for the evolution of altruism, *Eur. Phys. J. B* **7**, 385 (1999).
- [171] J. Fletcher and M. Zwick, Strong altruism can evolve in randomly formed groups, *J. Theor. Biol.* **228**, 303 (2004).
- [172] J.-U. Kreft and S. Bonhoeffer, The evolution of groups of cooperating bacteria and the growth rate versus yield trade-off, *Microbiol.* **151**, 637 (2005).
- [173] M. A. Janssen and R. L. Goldstone, Dynamic-persistence of cooperation in public good games when group size is dynamic, *J. Theor. Biol.* **243**, 134 (2006).
- [174] T. Killingback, J. Bieri, and T. Flatt, Evolution in group-structured populations can resolve the tragedy of the commons, *Proc. Roy. Soc. B* **273**, 1477 (2006).
- [175] R. E. Michod, The group covariance effect and fitness trade-offs during evolutionary transitions in individuality, *Proc. Natl. Acad. Sci. USA* **103**, 9113 (2006).
- [176] J. A. Fletcher and M. Zwick, The evolution of altruism: game theory in multilevel selection and inclusive fitness, *J. Theor. Biol.* **245**, 26 (2007).
- [177] R. E. Michod, Evolution of individuality during the transition from unicellular to multicellular life, *Proc. Natl. Acad. Sci. USA* **104**, 8613 (2007).
- [178] E. Szathmary and L. Demeter, Group selection of early replicators and the origin of life, *J. Theor. Biol.* **128**, 463 (1987).
- [179] P. B. Rainey and B. Kerr, Cheats as first propagules: a new hypothesis for the evolution of individuality during the transition from single cells to multicellularity, *Bioessays* **32**, 872 (2010).

- [180] W. Hamilton, *Narrow Roads of Gene Land: Evolution of Social Behaviour*, Oxford University Press, Oxford, 1996.
- [181] V. C. Wynne-Edwards, *Animal Dispersion in Relation to Social Behavior*, Oliver and Boyd, 1962.
- [182] G. C. Williams, *Adaptation and Natural Selection: A Critique of Some Current Evolutionary Thought*, Princeton University Press, 1966.
- [183] J. Maynard Smith, Group selection and kin selection, *Nature* **4924**, 1145 (1964).
- [184] D. Wilson, Altruism in mendelian populations derived from sibling groups: The haystack model revisited, *Evolution* **41**, 1059 (1987).
- [185] S. Okasha, Maynard Smith on the levels of selection question, *Biol. Philos.* **20**, 989 (2005).
- [186] M. J. Wade, A critical review of the models of group selection, *Quart. Rev. Biol.* **53**, 101 (1978).
- [187] D. S. Wilson, A theory of group selection, *Proc. Natl. Acad. Sci. USA* **72**, 143 (1975).
- [188] D. S. Wilson, The group selection controversy: history and current status, *Annu. Rev. Ecol. Syst.* **14**, 159 (1983).
- [189] E. Sober and D. S. Wilson, *Unto Others*, Harvard University Press, 1998.
- [190] A. Traulsen and M. A. Nowak, Evolution of cooperation by multilevel selection, *Proc. Natl. Acad. Sci. USA* **103**, 10952 (2006).
- [191] W. D. Hamilton, The genetical evolution of social behaviour. I+II, *J. Theor. Biol.* **7**, 1 (1964).
- [192] R. E. Michod, The theory of kin selection, *Annu. Rev. Ecol. Syst.* **13**, 23 (1982).
- [193] J. B. S. Haldane, *The Causes of Evolution*, Princeton Univ. Press, reprint edition, 1990.
- [194] A. Buckling and M. A. Brockhurst, Kin selection and the evolution of virulence, *Heredity* **100**, 484 (2008).
- [195] K. R. Foster, T. Wenseleers, and F. L. W. Ratnieks, Kin selection is the key to altruism, *Trends Ecol. Evol.* **21**, 57 (2006).
- [196] J. B. S. Haldane, Population genetics, *New Biology* **18**, 34 (1955).
- [197] M. J. Wade et al., Multilevel and kin selection in a connected world, *Nature* **463**, E8 (2010).
- [198] L. Lehmann, L. Keller, S. West, and D. Roze, Group selection and kin selection: Two concepts but one process, *Proc. Natl. Acad. Sci. USA* **104**, 6736 (2007).
- [199] A. Traulsen, Mathematics of kin- and group-selection: Formally equivalent?, *Evolution* **64**, 316 (2009).

- [200] D. S. Wilson, Social semantics: toward a genuine pluralism in the study of social behaviour, *J. Evol. Biol.* **21**, 368 (2007).
- [201] S. A. West, A. S. Griffin, and A. Gardner, Social semantics: how useful has group selection been?, *J. Evol. Biol.* **21**, 374 (2007).
- [202] E. O. Wilson, Kin selection as the key to altruism: Its rise and fall, *Social Research: An International Quarterly of Social Sciences* **72**, 1 (2005).
- [203] M. A. Nowak, C. E. Tarnita, and E. O. Wilson, The evolution of eusociality, *Nature* **466**, 1057 (2010).
- [204] J. Boomsma et al., Only full-sibling families evolved eusociality, *Nature* **471**, E4 (2011).
- [205] R. Ferriere and R. E. Michod, Inclusive fitness in evolution, *Nature* **471**, E6 (2011).
- [206] J. E. Strassmann et al., Kin selection and eusociality, *Nature* **471**, E5 (2011).
- [207] E. A. Herre and W. T. Wcislo, In defence of inclusive fitness theory, *Nature* **471**, E8 (2011).
- [208] P. Abbot et al., Inclusive fitness theory and eusociality, *Nature* **471**, E1 (2011).
- [209] M. A. Nowak, C. E. Tarnita, and E. O. Wilson, Nowak et al. reply, *Nature* **471**, E9 (2011).
- [210] S. Okasha, Altruism researchers must cooperate, *Nature* **467**, 653 (2010).
- [211] J. W. Costerton, K. J. Cheng, G. G. Geesey, T. I. Ladd, J. C. Nickel, M. Dasgupta, and T. J. Marrie, Bacterial biofilms in nature and disease., *Annual Review Of Microbiology* **41**, 435 (1987).
- [212] G. O'Toole, H. Kaplan, and R. Kolter, Biofilm formation as microbial development, *Annual Review Of Microbiology* **54**, 49 (2000).
- [213] L. Hall-Stoodley, J. W. Costerton, and P. Stoodley, Bacterial biofilms: From the natural environment to infectious diseases, *Nat. Rev. Micro.* **2**, 95 (2004).
- [214] J. B. Xavier, Social interaction in synthetic and natural microbial communities, *Molecular Systems Biology* **7**, 483 (2011).
- [215] D. McDougald, S. A. Rice, N. Barraud, P. D. Steinberg, and S. Kjelleberg, Should we stay or should we go: mechanisms and ecological consequences for biofilm dispersal, *Nature reviews Microbiology* **10**, 39 (2011).
- [216] E. Ben-Jacob, O. Schochet, A. Tenenbaum, I. Cohen, A. Czirok, and T. Vicsek, Generic modeling of cooperative growth patterns in bacterial colonies, *Nature* (1994).
- [217] M. A. Brockhurst, Population bottlenecks promote cooperation in bacterial biofilms, *PLoS ONE* **2**, e634 (2007).
- [218] M. A. Brockhurst, M. G. J. L. Habets, B. Libberton, A. Buckling, and A. Gardner, Ecological drivers of the evolution of public-goods cooperation in bacteria, *Ecology* **91**, 334 (2010).

- [219] M. Cabeen and C. Jacobs-Wagner, The bacterial cytoskeleton, *Annu. Rev. Gen.* **44**, 5486 (2010).
- [220] J. Trent, H. Kagawa, T. Yaoi, E. Olle, and Zaluzec, Chaperonin filaments: The archaeal cytoskeleton?, *Proc. Natl. Acad. Sci. USA* **94**, 5383 (1997).
- [221] L. Luo, Actin cytoskeleton regulation in neuronal morphogenesis and structural plasticity, *Annu. Rev. Cell Dev. Biol.* **18**, 601 (2002).
- [222] T. J. Mitchison and L. Cramer, Actin-based cell motility and cell locomotion, *Cell* **84**, 371 (1996).
- [223] <http://rsb.info.nih.gov/ij/images/FluorescentCells.jpg>.
- [224] <http://publications.nigms.nih.gov/moleculstomeds/images/newtcells.jpg>.
- [225] W. Kabsch and J. Vandekerckhove, Structure and function of actin, *Annu. Rev. Biophys. Biomol. Struct.* **21**, 49 (1992).
- [226] H. Herrmann, H. Bär, L. Kreplak, S. Strelkov, and U. Aebi, Intermediate filaments: from cell architecture to nanomechanics, *Nat. Rev. Mol. Cell Biol.* **8**, 562 (2007).
- [227] A. Akhmanova and C. C. Hoogenraad, Microtubule plus-end-tracking proteins: mechanisms and functions, *Curr. Opin. Cell Biol.* **17**, 47 (2005).
- [228] J. Howard and A. A. Hyman, Growth, fluctuation and switching at microtubule plus ends, *Nat. Rev. Mol. Cell Biol.* **10**, 569 (2009).
- [229] J. Hayles and P. Nurse, A journey into space, *Nat. Rev. Mol. Cell Biol.* **2**, 647 (2001).
- [230] C. Pearson and K. Bloom, Dynamic microtubules lead the way for spindle positioning, *Nat. Rev. Mol. Cell Biol.* **5**, 481 (2004).
- [231] A. Desai and T. Mitchison, Microtubule polymerization dynamics, *Annu. Rev. Cell Dev. Biol.* **13**, 83 (1997).
- [232] T. Mitchison and M. Kirschner, Dynamic instability of microtubule growth, *Nature* **312**, 237 (1984).
- [233] P. Carvalho, J. Tirnauer, and D. Pellman, Surfing on microtubule ends, *Trends Cell Biol.* **13**, 229 (2003).
- [234] A. Dimitrov, M. Quesnoit, S. Moutel, I. Cantaloube, C. Poüs, and F. Perez, Detection of Gtp-tubulin conformation in vivo reveals a role for Gtp remnants in microtubule rescues, *Science* **322**, 1353 (2008).
- [235] H. Flyvbjerg, T. Holy, and S. Leibler, Stochastic dynamics of microtubules: a model for caps and catastrophes, *Phys. Rev. Lett.* **73**, 2372 (1994).
- [236] M. Dogterom and S. Leibler, Physical aspects of the growth and regulation of microtubule structures, *Phys. Rev. Lett.* **70**, 1347 (1993).

- [237] L. Brun, B. Rupp, J. J. Ward, and F. Nedelec, A theory of microtubule catastrophes and their regulation, *Proc. Natl. Acad. Sci. USA* **106**, 21173 (2009).
- [238] C. Tischer, P. R. ten Wolde, and M. Dogterom, Providing positional information with active transport on dynamic microtubules, *Biophys. J.* **99**, 726 (2010).
- [239] I. M. Tolić-Nørrelykke, Force and length regulation in the microtubule cytoskeleton: lessons from fission yeast, *Curr. Opin. Cell Biol.* **22**, 21 (2010).
- [240] J. Howard and A. A. Hyman, Microtubule polymerases and depolymerases, *Curr. Opin. Cell Biol.* **19**, 31 (2007).
- [241] S. Ray, E. Meyhöfer, R. Milligan, and J. Howard, Kinesin follows the microtubule protofilament axis, *J. Cell Biol.* **121**, 1083 (1993).
- [242] R. Vale, T. Funatsu, D. Pierce, L. Romberg, Y. Harada, and T. Yanagida, Direct observation of single kinesin molecules moving along microtubules, *Nature* **380**, 451 (1996).
- [243] K. J. Verhey and J. W. Hammond, Traffic control: regulation of kinesin motors, *Nat. Rev. Mol. Cell Biol.* **10**, 765 (2009).
- [244] R. Vale and R. Milligan, The way things move: Looking under the hood of molecular motor proteins, *Science* **288**, 88 (2000).
- [245] C. Kural, H. Kim, S. Syed, G. Goshima, V. I. Gelfand, and P. R. Selvin, Kinesin and dynein move a peroxisome in vivo: A tug-of-war or coordinated movement?, *Science* **308**, 1469 (2005).
- [246] A. Yildiz, M. Tomishige, R. Vale, and P. Selvin, Kinesin walks hand-over-hand, *Science* **303**, 676 (2004).
- [247] Q. Shao and Y. Gao, On the hand-over-hand mechanism of kinesin, *Proc. Natl. Acad. Sci. USA* **103**, 8072 (2006).
- [248] A. Seitz and T. Surrey, Processive movement of single kinesins on crowded microtubules visualized using quantum dots, *Embo J.* **25**, 267 (2006).
- [249] J. Howard, The movement of kinesin along microtubules, *Annu. Rev. Physiol.* **58**, 703 (1996).
- [250] N. Hirokawa, Y. Noda, Y. Tanaka, and S. Niwa, Cytoskeletal motors: Kinesin superfamily motor proteins and intracellular transport, *Nat. Rev. Mol. Cell Biol.* **10**, 682 (2009).
- [251] A. Hunter and L. Wordeman, How motor proteins influence microtubule polymerization dynamics, *J. Cell Sci.* **113**, 4379 (2000).
- [252] J. R. Cooper, M. Wagenbach, C. L. Asbury, and L. Wordeman, Catalysis of the microtubule on-rate is the major parameter regulating the depolymerase activity of MCAK, *Nat. Struct. Mol. Biol.* **17**, 77 (2010).

- [253] C. A. Moores and R. A. Milligan, Lucky 13 - microtubule depolymerization by kinesin-13 motors, *J. Cell Sci.* **119**, 3905 (2006).
- [254] L. Wordeman, Microtubule-depolymerizing kinesins, *Curr. Opin. Cell Biol.* **17**, 82 (2005).
- [255] M. K. Gardner, D. C. Bouck, L. V. Paliulis, J. B. Meehl, E. T. O'Toole, J. Haase, A. Soubry, A. P. Joglekar, M. Winey, E. D. Salmon, K. Bloom, and D. J. Odde, Chromosome congression by kinesin-5 motor-mediated disassembly of longer kinetochore microtubules, *Cell* **135**, 894 (2008).
- [256] K. Kinoshita, I. Arnal, A. Desai, D. Drechsel, and A. Hyman, Reconstitution of physiological microtubule dynamics using purified components, *Science* **294**, 1340 (2001).
- [257] P. Bieling, L. Laan, H. Schek, E. L. Munteanu, L. Sandblad, M. Dogterom, D. Brunner, and T. Surrey, Reconstitution of a microtubule plus-end tracking system in vitro, *Nature* **450**, 1100 (2007).
- [258] M. Evans, Phase Transitions in one-dimensional nonequilibrium systems, *Braz. J. Phys.* **30**, 42 (2000).
- [259] D. Mukamel, Phase transitions in non-equilibrium systems, in *Soft and Fragile Matter*, edited by M. Cates and M. Evans, Institute of Physics Publishing, Bristol, 2000.
- [260] G. Schütz, Exactly solvable models for many-body systems far from equilibrium, in *Phase Transitions and Critical Phenomena*, edited by C. Domb and J. Lebowitz, volume 19, Academic Press, London, 2001.
- [261] B. Schmittmann and R. Zia, Statistical mechanics of driven diffusive systems, in *Phase Transitions and Critical Phenomena*, edited by C. Domb and J. Lebowitz, volume 17, Academic Press, London, 1995.
- [262] C. MacDonald, J. Gibbs, and A. Pipkin, Kinetics of biopolymerization on nucleic acid templates, *Biopolymers* **6**, 1 (1968).
- [263] E. Frey, A. Parmeggiani, and T. Franosch, Collective phenomena in intracellular processes, *Genome Informatics* **15(1)**, 46 (2004).
- [264] T. Guérin, J. Prost, P. Martin, and J.-F. Joanny, Coordination and collective properties of molecular motors: theory, *Curr. Opin. Cell Biol.* **22**, 14 (2010).
- [265] H. Hinsch, R. Kouyos, and E. Frey, From intracellular traffic to a novel class of driven lattice gas models, in *Traffic and Granular Flow '05*, pages 205–222, Springer, Berlin, 2007.
- [266] A. B. Kolomeisky and M. E. Fisher, Molecular motors: A theorist's perspective, *Annu. Rev. Phys. Chem.* **58**, 675 (2007).
- [267] B. Derrida, E. Domany, and D. Mukamel, An exact solution of a one-dimensional asymmetric exclusion model with open boundaries, *J. Stat. Phys.* **69**, 667 (1992).
- [268] B. Derrida, M. Evans, V. Hakim, and V. Pasquier, Exact solution of a 1d asymmetric exclusion model using a matrix formulation, *J. Phys. A: Math. Gen.* **26**, 1493 (1993).

- [269] B. Derrida and M. Evans, The asymmetric exclusion model: exact results through a matrix approach, in *Nonequilibrium Statistical Mechanics in One Dimension*, edited by V. Privman, page 277, Cambridge University Press, Cambridge, 1997.
- [270] L. Gwa and H. Spohn, Bethe solution for the dynamical-scaling exponent of the noisy Burgers equation, *Phys. Rev. A* (1992).
- [271] J. Krug, Boundary-induced phase transitions in driven diffusive systems, *Phys. Rev. Lett.* **67**, 1882 (1991).
- [272] E. Lieb and D. Mattis, *Mathematical physics in one dimension: Exactly soluble model of interacting particles*, Academic Press, London, 1966.
- [273] N. D. Mermin and H. Wagner, Absence of ferromagnetism or antiferromagnetism in one- or two-dimensional isotropic heisenberg models, *Phys. Rev. Lett.* **17**, 1133 (1966).
- [274] V. Popkov and G. M. Schütz, Steady-state selection in driven diffusive systems with open boundaries, *Europhys. Lett.* **48**, 257 (1999).
- [275] J. S. Hager, J. Krug, V. Popkov, and G. M. Schütz, Minimal current phase and universal boundary layers in driven diffusive systems., *Phys. Rev. E* **63**, 056110 (2001).
- [276] A. Parmeggiani, T. Franosch, and E. Frey, Phase coexistence in driven one-dimensional transport, *Phys. Rev. Lett.* **90**, 086601 (2003).
- [277] A. Parmeggiani, T. Franosch, and E. Frey, Totally asymmetric simple exclusion process with langmuir kinetics, *Phys. Rev. E* **70**, 046101 (2004).
- [278] L. Reese, A. Melbinger, and E. Frey, Crowding of molecular motors determines microtubule depolymerization, submitted.
- [279] K. Nishinari, Y. Okada, A. Schadschneider, and D. Chowdhury, Intracellular transport of single-headed molecular motors kif1a, *Phys. Rev. Lett.* **95**, 118101 (2005).
- [280] P. Greulich, A. Garai, K. Nishinari, A. Schadschneider, and D. Chowdhury, Intracellular transport by single-headed kinesin Kif1a: Effects of single-motor mechanochemistry and steric interactions, *Phys. Rev. E* **75**, 041905 (2007).
- [281] R. Lipowsky, S. Klumpp, and T. Nieuwenhuizen, Random walks of cytoskeletal motors in open and closed compartments, *Phys. Rev. Lett.* **87**, 108101 (2001).
- [282] S. Klumpp and R. Lipowsky, Traffic of molecular motors through tube-like compartments, *J. Stat. Phys.* **113**, 233 (2003).
- [283] E. Frey and A. Vilfan, Anomalous relaxation kinetics of biological lattice-ligand binding models, *Chem. Phys.* **284**, 287 (2002).
- [284] P. Pierobon, M. Mobilia, R. Kouyos, and E. Frey, Bottleneck-induced transitions in a minimal model for intracellular transport, *Phys. Rev. E* **74**, 031906 (2006).
- [285] P. Greulich and A. Schadschneider, Single-bottleneck approximation for driven lattice gases with disorder and open boundary conditions, *J. Stat. Mech.* **2008**, 23pp (2008).

- [286] L. Cook and J. Dong, Power spectra of TASEP with a localized slow site, arXiv (2010).
- [287] L. B. Shaw, R. K. P. Zia, and K. H. Lee, Totally asymmetric exclusion process with extended objects: A model for protein synthesis, *Phys. Rev. E* **68**, 021910 (2003).
- [288] T. Reichenbach, T. Franosch, and E. Frey, Exclusion processes with internal states, *Phys. Rev. Lett.* **97**, 050603 (2006).
- [289] T. Reichenbach, E. Frey, and T. Franosch, Traffic jams induced by rare switching events in two-lane transport, *New J. Phys.* **9**, 159 (2007).
- [290] R. Juhasz, Weakly coupled, antiparallel, totally asymmetric simple exclusion processes, *Phys. Rev. E* **76**, 021117 (2007).
- [291] E. Pronina and A. B. Kolomeisky, Two-channel totally asymmetric simple exclusion processes, *J. Phys. A: Math. Gen.* **37**, 9907 (2004).
- [292] E. Pronina and A. B. Kolomeisky, Asymmetric coupling in two-channel simple exclusion processes, *Physica A* **372**, 12 (2006).
- [293] T. Mitsudo and H. Hayakawa, Synchronization of kinks in the two-lane totally asymmetric simple exclusion process with open boundary conditions, *J. Phys. A: Math. Gen.* **38**, 3087 (2005).
- [294] V. Popkov and I. Peschel, Symmetry breaking and phase coexistence in a driven diffusive two-channel system, *Phys. Rev. E* **64**, 026126 (2001).
- [295] I. T. Georgiev, B. Schmittmann, and R. P. Zia, Anomalous nucleation far from equilibrium, *Phys. Rev. Lett.* **94**, 115701 (2005).
- [296] V. Popkov, Infinite reflections of shock fronts in driven diffusive systems with two species, *J. Phys. A: Math. Gen.* **37**, 1545 (2004).
- [297] V. Popkov and G. M. Schütz, Shocks and excitation dynamics in a driven diffusive two-channel system, *J. Stat. Phys.* **112**, 523 (2003).
- [298] W. Knospe, L. Santen, A. Schadschneider, and M. Schreckenberg, A realistic two-lane traffic model for highway traffic, *J. Phys. A: Math. Gen.* **35**, 3369 (2002).
- [299] M. Evans, Y. Kafri, K. E. P. Sugden, and J. Tailleur, Phase diagram of two-lane driven diffusive systems, arXiv (2011).
- [300] A. Vilfan, E. Frey, F. Schwabl, M. Thormahlen, Y. Song, and E. Mandelkow, Dynamics and cooperativity of microtubule decoration by the motor protein kinesin, *J. Mol. Biol.* **312**, 1011 (2001).
- [301] L. Reese, Regulation of microtubule dynamics: Transport-limited growth, Master's thesis, Ludwig-Maximilians Universität, 2008.
- [302] D. Sharp, G. Rogers, and J. Scholey, Microtubule motors in mitosis, *Nature* **407**, 41 (2000).

- [303] D. Foethke, T. Makushok, D. Brunner, and F. Nédélec, Force- and length-dependent catastrophe activities explain interphase microtubule organization in fission yeast, *Mol. Syst. Biol.* **5**, 241 (2009).
- [304] B. S. Govindan, M. Gopalakrishnan, and D. Chowdhury, Length control of microtubules by depolymerizing motor proteins, *Europhys. Lett.* **83**, 40006 (2008).
- [305] L. E. Hough, A. Schwabe, M. A. Glaser, J. R. McIntosh, and M. D. Betterton, Microtubule depolymerization by the kinesin-8 motor Kip3p: A mathematical model, *Biophys. J.* **96**, 3050 (2009).
- [306] G. A. Klein, K. Kruse, G. Cuniberti, and F. Jülicher, Filament depolymerization by motor molecules, *Phys. Rev. Lett.* **94**, 108102 (2005).
- [307] R. Vasquez, D. Gard, and L. Cassimeris, Xmap from xenopus eggs promotes rapid plus end assembly of microtubules and rapid microtubule polymer turnover, *J. Cell Biol.* **127**, 985 (1994).
- [308] J. Kerssemakers, E. L. Munteanu, L. Laan, T. L. Noetzel, M. Janson, and M. Dogterom, Assembly dynamics of microtubules at molecular resolution, *Nature* **442**, 709 (2006).
- [309] C. Asbury, Xmap215: A tip tracker that really moves, *Cell* **132**, 19 (2008).
- [310] J. Tirnauer, J. Canman, E. D. Salmon, and T. Mitchison, Targets to kinetochores with attached, polymerizing microtubules, *Mol. Biol. Cell* **13**, 4308 (2002).
- [311] P. Grissom, T. Fiedler, E. Grishchuk, D. Nicastro, R. West, and J. R. McIntosh, Kinesin-8 from fission yeast: A heterodimeric, plus-end-directed motor that can couple microtubule depolymerization to cargo movement, *Mol. Biol. Cell* **20**, 963 (2009).
- [312] Y. Du, C. A. English, and R. Ohi, The kinesin-8 Kif18a dampens microtubule plus-end dynamics, *Curr. Biol.* **20**, 374 (2010).
- [313] K. E. P. Sugden, M. R. Evans, W. C. K. Poon, and N. D. Read, Model of hyphal tip growth involving microtubule-based transport, *Phys. Rev. E* **75**, 031909 (2007).
- [314] K. E. P. Sugden and M. R. Evans, A dynamically extending exclusion process, *J. Stat. Mech. Theor. Exp.* **2007**, P11013 (2007).
- [315] K. Thorn, J. Ubersax, and R. Vale, Engineering the processive run length of the kinesin motor, *J. Cell Biol.* **151**, 1093 (2000).

Danksagung

Zuallererst gilt mein Dank meinem Doktorvater Prof. Erwin Frey. Durch sein großes Interesse an physikalischen und biologischen Fragestellungen sowie seine enorme Erfahrung waren unsere Diskussionen immer eine Bereicherung und haben diese Arbeit in großen Schritten vorangetrieben. Auch möchte ich mich für sein Vertrauen in meine Leistungen bedanken, wodurch ich die Möglichkeit hatte, meinen wissenschaftlichen Interessen frei nachzugehen. Des Weiteren verdanke ich ihm die Möglichkeit an zahlreichen Konferenzen teilzunehmen und damit auch die internationale wissenschaftliche Atmosphäre kennenlernen zu können.

Besonders möchte ich mich bei Jonas Cremer bedanken, der mir über die letzten Jahre nicht nur ein treuer Arbeitskollege war sondern auch zu einem guten Freund geworden ist. Dank seines bemerkenswerten Sachverstands und seiner schnellen Auffassungsgabe waren unsere gemeinsamen Projekte nicht nur fruchtbar, sondern haben auch viel Spaß gemacht. Lieber Jonas, es war mir eine Ehre, mit Dir zusammenzuarbeiten!

Mein weiterer Dank gilt Louis Reese. Seine große Begeisterung für biologische Zusammenhänge und sein unerschütterlicher Optimismus haben mir die Zusammenarbeit zu einer Freude gemacht. Aber auch durch Treffen abseits unserer wissenschaftlichen Projekte, bei der ein oder anderen Runde Schafkopf oder Wikingerschach, werde ich die Zeit mit Louis immer in guter Erinnerung behalten.

Daneben gilt mein Dank Thomas Franosch und Tobias Reichenbach, von deren Wissen ich bei meiner Tätigkeit sehr profitieren konnte. Beide haben mir fachlich ungemein weitergeholfen, indem sie mir sowohl mit vielen Ideen zur Seite standen als mir auch die Grundzüge wissenschaftlichen Schreibens beigebracht haben. An dieser Stelle möchte ich auch Philipp Stefani, Matthias Lechner, Johannes Knebel und Karl Wienand danken, mit denen sich sehr ergiebige Zusammenarbeiten entwickelt haben.

Zudem möchte ich mich ganz herzlich bei Jan-Timm Kuhr, der mit Jonas Cremer und mir gute drei Jahre eine Bürogemeinschaft gebildet hat, bedanken. Dank zahlreicher Diskussionen an unserem Whiteboard und auch abends bei einem kollegialen Bier, haben sich mir viele Zusammenhänge erschlossen. Besonders bemerkenswert war unsere gute Büroatmosphäre, die es unglaublich angenehm gemacht hat, jeden Tag in die Arbeit zu kommen und über die Jahre zu einer echten Freundschaft gewachsen ist.

Darüber hinaus danke ich Prof. Kerstin Jung und Prof. Heinrich Jung, an deren Lehrstuhl für Mikrobiologie der Ludwig-Maximilians Universität gerade Experimente zu unseren Modellen entstehen. Ich bin schon sehr gespannt, wie sich dieses Projekt entwickeln wird, und freue mich auf zukünftige Ergebnisse. Ein herzliches Dankeschön geht außerdem an Andrej Vilfan (Fig. 4.6), John Heuser (Fig. 4.3A), Angelika Bentin (Fig.3.1 A) und Silke Meyer-Arndt (Fig.3.1 B), deren Bilder ich in dieser Arbeit verwenden durfte.

Mein Dank gilt außerdem dem kompletten Lehrstuhl, in dem eine freundschaftliche und produktive Atmosphäre herrscht. In besonderen Maße möchte ich mich bei Anton Winkler, Patrick Hillenbrand, Jan-Timm Kuhr, Brendan Osberg, Louis Reese und Jonas Cremer bedanken, die mich beim Korrekturlesen unterstützt haben. Des Weiteren danke ich den derzeitigen und ehemaligen Balkongängern Daniel Schlesinger, Gerald Ryseck, Benjamin Andrae, Hauke Hinsch, Patrick Hillenbrand und Fabienna Arends für viele entspannte Fünfminutenpausen. Ferner gilt mein Dank an dieser Stelle auch den ehemaligen Mitgliedern dieses Lehrstuhls, Karen Alim, Richard Neher und Benedikt Obermayer, mit denen ich eine schöne und prägende Zeit verbracht habe.

Besonders danke ich meinen Eltern Katrin Lietke-Melbinger und Stefan Melbinger. Sie haben mich während meines ganzen Lebens in jeder erdenklichen Art und Weise unterstützt und immer an mich geglaubt. Damit gebührt ihnen ein großer Anteil am Gelingen dieser Arbeit. Danke, Euch beiden, ohne Euch wäre ich nicht da, wo ich jetzt bin. Meinen beiden Schwester Sophie und Sarah Melbinger möchte ich mit einem Verweis auf das Zitat auf Seite 54 dieser Arbeit danken: Liebe Schwestern, auch für nur eine von Euch würde ich jederzeit in einen Fluss springen. An dieser Stelle möchte ich auch meiner lieben Freundin Eva Maier danken, die sich nicht nur durch ihre Hilfe beim Korrekturlesen einen Platz in dieser Danksagung verdient hat. Vielmehr hat sie mich seit der ersten Klasse bis hin zur Promotion begleitet und ist über die Jahre zu einer immer engeren Freundin geworden.

Zuletzt möchte ich mich von ganzem Herzen bei meinem Freund Jan Heyder bedanken. Er hat mich nicht nur mit vielen morgendlichen Tassen Kaffee unterstützt, sondern er konnte mir selbst in Phasen größter Anstrengung immer noch ein Lächeln abringen. Danke Jan, dass es dich gibt!